TECHNICAL REPORT
68-7-CM

STUDY OF YIELDING PHENOMENA

by

D. H. Ender
Massachusetts Institute of Technology
Cambridge, Mass.

Contract No. DA19-129-AMC-930(N)

July 1967

UNITED STATES ARMY
NATICK LABORATORIES
Natick, Massachusetts 01760

Clothing and Organic Materials Laboratory
CEMM-36

225

DISTRIBUTION OF THIS DOCUMENT IS UNLIMITED

The findings in this report are not to be construed as an official Department of the Army position unless so designated by other authorized documents.

Citation of trade names in this report does not constitute an official indorsement or approval of the use of such items.

Destroy this report when no longer needed. Do not return it to the originator.

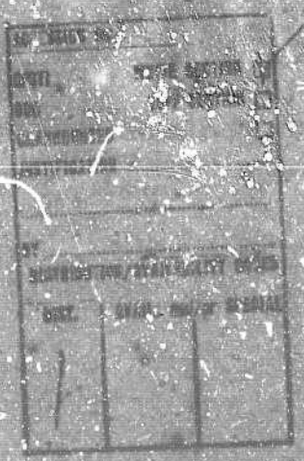

STUDY OF YIELDING PHENOMENA

D.H. Ender

Massachusetts Institute of Technology
Cambridge, Massachusetts

July 1967

Distribution of this
document is unlimited

AD _____

TECHNICAL REPORT
68-7-CM

STUDY OF YIELDING PHENOMENA

by

D. H. Ender

Department of Mechanical Engineering
Massachusetts Institute of Technology
Cambridge, Massachusetts 02139

Contract No. DA19-129-AMC-930(N)

Project Reference:
1C024401A329

Series: C&OM - 36

July 1967

Clothing & Organic Materials Laboratory
U. S. ARMY NATICK LABORATORIES
Natick, Massachusetts 01760

FOREWORD

Glassy amorphous polymers are of ballistic interest because of characteristics such as transparency and in some cases the ability to draw and yield. Knowledge of the factors influencing yielding can be useful in advancing our theoretical knowledgeoof the mechanisms operating. From a more practical point of view this knowledge may allow fabricators to produce transparent polymers which will maintain ductility even at ballistic speeds.

The work covered in this report was conducted by Dr. D. H. Ender over the period from 15 February 1966 to 30 April 1967. The work was concentrated upon two polymers; polymethylmethacrylate and polystyrene. The two most important factors involved in the yielding of polymethylmethacrylate appear to be plasticization by water and quenching.

The U. S. Army Natick Laboratories Project Officer was Mr. Roy C. Laible and the Alternate Project Officer was Mr. Anthony Alesi, both of the Materials Research Division of the Clothing and Organic Materials Laboratory.

S. J. KENNEDY
Director
Clothing & Organic Materials Laboratory

APPROVED:

DALE H. SIELING, Ph.D.
Scientific Director

W. M. MANTZ
Brigadier General, USA
Commanding

TABLE OF CONTENTS

LIST OF TABLES

FIGURE CAPTIONS

ABSTRACT

In yielding under constant tensile load, glassy polymethyl methacrylate (PMMA) and glassy polystyrene (PS) exhibit work softening at small strains, followed by strain hardening at higher strains. In this work, the initial softening has been of most interest. In the constant load experiment, the yield point shows up as a minimum of the deformation velocity vs. elongation curve.

Measurements have been made of the variation of delay time (the time for accelerated elongation to occur under load) with stress and temperature (measured on PS and PMMA) with preorientation birefringence (PS), and with thermal history and water absorption (PMMA). The logarithm of the delay time decreases linearly with increasing stress and temperature. The temperature interval systematically investigated is $T_g - 40 \leq T \leq T_g - 5$ (°C). Several experiments with PMMA were made for $T > T_g$. The polymer response to constant load divides the temperature-stress plane into two regions; one where creep is observed and another in which cold drawing takes place. Specimens deforming by creep do not contain deformation bands.

The stress influence on strain rate under constant load is expressible as a stress shift factor. The same stress shift factor governs the stress influence on delay time and deformation rate changes associated with incremental stress changes. The influence of stress on strain rate is reversible. The stress shift factor is predicted correctly from a free volume theory assuming that Poisson's expansion caused by drawing stress changes contributes entirely to the free volume.

The important contribution to the increase in strain rate under constant load is caused by a true strain softening. The conclusion is drawn that it is a consequence of the disturbance of the annealed positions of the polymer segments. In this picture strain causes the breaking up of the relative order that is brought about in annealing; thus leaving the polymer in a far-from-equilibrium state.

INTRODUCTION

Many long chain polymers have the peculiar ability to undergo extensions of several hundred percent without fracturing. For soft rubbery or viscous polymers this is quite well understood. It is more surprising that hard solid polymers yield under high stress to extensions of a similar order of magnitude.

The present study is an experimental approach to yielding of solid polymers. The most striking observation, often seen in yielding of tensile specimens, is a constriction or neck, which forms early in the deformation. The shoulders of the neck move along the specimen, thereby straining the as yet undrawn portion of it. Carothers, making the first fully synthetic fibers from a polyester, used the term "cold drawing" for this phenomenon, apparently implying a resemblance to phenomenological similarities in the cold drawing of metals.

Cold drawing confers, to polymeric fibers, as Carothers found in the early 1930's, the usage properties required of textile fibers. The technological importance which this process gained subsequently has provided much of the incentive for research on cold drawing. More recently, cold drawing is being investigated as a fast (and thus economical) forming method for plastics. In present hot-forming processes, heat transfer limits the production rate.

Early investigators[1] (1945) ascribed an important part in cold drawing to the crystalline fraction of the polymer. Later it was shown[2] (1952) that amorphous polymers also cold draw. In the present work, normal atactic amorphous polystyrene and polymethyl methacrylate, which have little or no importance as textile fibers, were studied. It was felt that the deformation of a one-phase system can be more easily understood.

In amorphous polymers the neck-down is only observed near or below the glass transition temperature T_g; above it, the polymer stretches uniformly like a rubber. For amorphous polymers cold drawing has the connotation of drawing below T_g.

The hard and brittle appearance of amorphous polymers and the ability to undergo several hundred percent strain are in

spectacular contrast. To obtain drawing, stresses of the order of several percent of the modulus, the magnitude depending largely on temperature, must be applied. As the polymer is strained, the stress-strain behavior becomes highly nonlinear at this stress level. This leads to a gradual softening and a geometrical instability--the neck. As softening is important to initiate cold drawing, the process that saves the situation from rupture is the ability, unique for long chain polymers, to strain-harden, after some strain, to such an extent that the thin region can carry the load required to draw the as yet undrawn section. This strain corresponds to the natural draw ratio, which varies from one type of polymer to the other by several hundred percent.

Strain hardening is the result of the alignment of polymer chains in stretch direction. The strong covalent chain backbone bonds thus contribute most efficiently to the strength in the orientation direction. As this provides mechanical stability to the polymer as it draws, it is at the same time the cause for the industrial importance of the drawing process. The oriented structure has, in stretch direction, greatly enhanced modulus and strength.

The strengthening is, at least qualitatively, understood and will be of secondary importance in this study. The present work is concerned with the initial phase of polymer deformation, which has the appearance of a strain-induced brittle to ductile transition. This effect has been investigated repeatedly and the present research is not prompted by a lack of ideas or experimental data, but by the need to consolidate seemingly divergent ideas on the basis of evidence from very specific experiments.

Several authors have proposed mechanisms, which one way or another, explain the nonlinear stress vs. strain response as the coming about of the glass transition. The adiabatic theory[3,4] (1954) postulated that T_g is reached by heating from mechanical work. Vincent[5] (1960) showed necking to occur in slow isothermal drawing as well; he also pointed out the difficulty of explaining the initiation of cold drawing by the adiabatic theory. According to Vincent, the softening temperature is lowered, by straining, to the environmental temperature, whereas Müller and Engelter[6]

conclude that stress alone softens the polymer.

Very recently Goldstein[7] has developed a model which accounts for stress and strain softening through breakdown of load carrying elements which, after some time, bear load again until a new breakdown follows. This author has not specified the nature of these elements. Andrews[8] has suggested that initially secondary bonds provide strength which, under stress, gradually give way. These bonds could be the load carrying elements of the first mentioned author. Crowet and Homés[9] explain in quite similar fashion the stress-strain curve of polymethyl methacrylate, postulating that there are bound spots of high activation energy, thought to be ordered regions or entanglements, which are freed under stress.

A dislocation analogy for yielding of glassy polymers was proposed by Whitney[10] in which defects, specified to be holes or local ruptures, play the same role as dislocations in crystals.

The principal objective of this work is to study the tensile rheology of glassy polymers under high stresses, one aspect of which, under certain circumstances, is cold drawing in the sense of drawing with a neck. A clear separation of flow behavior as caused by stress, and the changes of it due to strain, seemed especially necessary. When it was realized that straining may well cause a stable glass to attain a less stable state, the investigation of the effect of glass structure, as influenced by pretreatments, on rheological behavior was included.

A description of the drawing mechanism presupposes knowledge of the bulk structure of the polymer. There is, unfortunately, not much known about structure that one could profit from in deciding which of the proposed mechanisms is operative in yielding. It rather appears that research on mechanical properties could contribute to the knowledge of glassy structure.

In nearly all of the experiments in this work yielding was brought about by attaching constant loads to tensile specimens. It will be seen that this test has several advantages over the constant rate of elongation test in interpreting material properties.

On a microscopic scale cold drawing is usually associated

with shear bands. They appear at small strains and lead later to the macroscopic instability, the neck. Little is known about formation, geometry, and propagation of the bands. Methods for their observation have been developed and some results will be reported. Other microscopic features (in particular, crazes) have been studied to detect their relevance to yielding, if any.

This report is divided into eight chapters. Chapter I deals with the constant load drawing test. In a systematic drawing study of polymethyl methacrylate and polystyrene, the effects of temperature and stress on drawing parameters and mode of deformation, in the latter case also that of initial birefringence, were investigated. In Chapter II the connection between the constant load and the constant rate drawing test is established. Furthermore, the softening of the polymer is separated into a contribution due to strain and a superposed softening by stress. Strain rate vs. strain curves is introduced as an equivalent alternative to stress vs. strain curves. Chapters III and IV report the influence of heat treatments and plasticization by water on the drawing behavior of polymethyl methacrylate. Several brief birefringence and polymer density studies are collected in Chapter V. A theory of stress and strain softening, together with a molecular model for it, is given in Chapter VI. This theory utilizes information gained in all previous chapters. Chapter VII discusses the microscopic deformation modes accompanying yielding. Experimental equipment and techniques are described in Chapter VIII. If a few words were sufficient for their explanation, it has been given in the body of each chapter.

CHAPTER I
CONSTANT LOAD DRAWING

Introduction

Near y all data on cold drawing reported in literature are taken from constant rate of extension experiments. A second method to draw polymers is by a+taching a sufficiently high, constant load to the specimen; this test is made use of in the present work.

In the conventional constant rate of extension experiment the test load rises, with extension, to a maximum value at the upper yield point, then drops to a lower, essentially constant level, termed the drawing load. At the maximum, a neck begins to form and, somewhere in the early part of the constant load region, its shoulders have reached their final shape. For the rest of the load plateau the shoulders of the neck move along the specimen and, when they arrive at the ends, the load starts to rise until fracture intervenes.

Drawing under constant load was reported by Kauffman and George[11] for polyamide films and by Bender and Williams[12] for nylon 66 fibers. Experiments on polymethyl methacrylate (PMMA) by Curran and Andrews[13] and on polystyrene (PS) by Morrison[14] showed that constant load drawing is also found in amorphous polymers.

An example of the length vs. time curve which the constant load drawing test yields is presented in Fig. 1.1. After a rapid elastic elongation, further extension under load continues for some time at a slow and decreasing rate. After some time the curve inverts (at point YP) and the deformation starts to accelerate, which continues until the deformation rate has become many times higher than in the vicinity of the inversion point. At a strain of the order of 100% the rapid drawing comes to an end and is followed by creep of the stretched polymer. The geometrical changes of the specimen as it draws will be discussed at the end of the chapter.

The intersection of the straight lines, with which the slow and the rapid part of the curve can be approximated, defines the delay time t_d and the delay strain ε_d. Other parameters, taken from the curves, are $\dot{\varepsilon}_y$ and ε_y, velocity and elongation at the point YP, which is the yield point. Elastic moduli have been calculated from the initial elastic deflection, ε_e.

Temperature has an important influence on yielding. Hence it is necessary to ascertain that isothermal conditions exist during drawing. The environmental temperature being essentially constant, the mechanical work of the draw load dissipated in the polymer will cause the temperature to increase to an extent, depending upon the rate of heat transfer to the ambient air. For the most extreme conditions of interest in this study the estimated adiabatic temperature rise is 3.2°C (Appendix A). To reach the strain producing this temperature rise, required anywhere from one to hundreds of minutes in the experiments to be reported. Only for the very fast experiments is there any possibility to reach a fraction of the calculated temperature rise. Hence, the drawing tests are essentially isothermal.

The constant load drawing test is used extensively throughout this study. This chapter presents the constant load drawing behavior of PS and PMMA by means of a systematic investigation of temperature, load, and for PS, perorientation birefringence.

Drawing of Polystyrene

The occurrence of cold drawing of PS under a constant load has been demonstrated in previous work[14]. The present investigation is concerned with the influence of stress, temperature and pre-orientation on the characteristic parameters of the constant load drawing experiment. The parameters evaluated from recorded length vs. time curves are delay time and delay strain as defined previously. (Fig. 1.1.)

The samples were preoriented in the device of Fig. 8.3 (Chapter VIII) to three levels of birefringence (Δn = 1, 5 and 10 x 10^{-3}). The polymer was commercially available cast sheet (Appendix B). Drawing was carried out above room temperature in a specially built chamber shown in Fig. 8.1 and described, together with details of the sample preparation, in Chapter VIII.

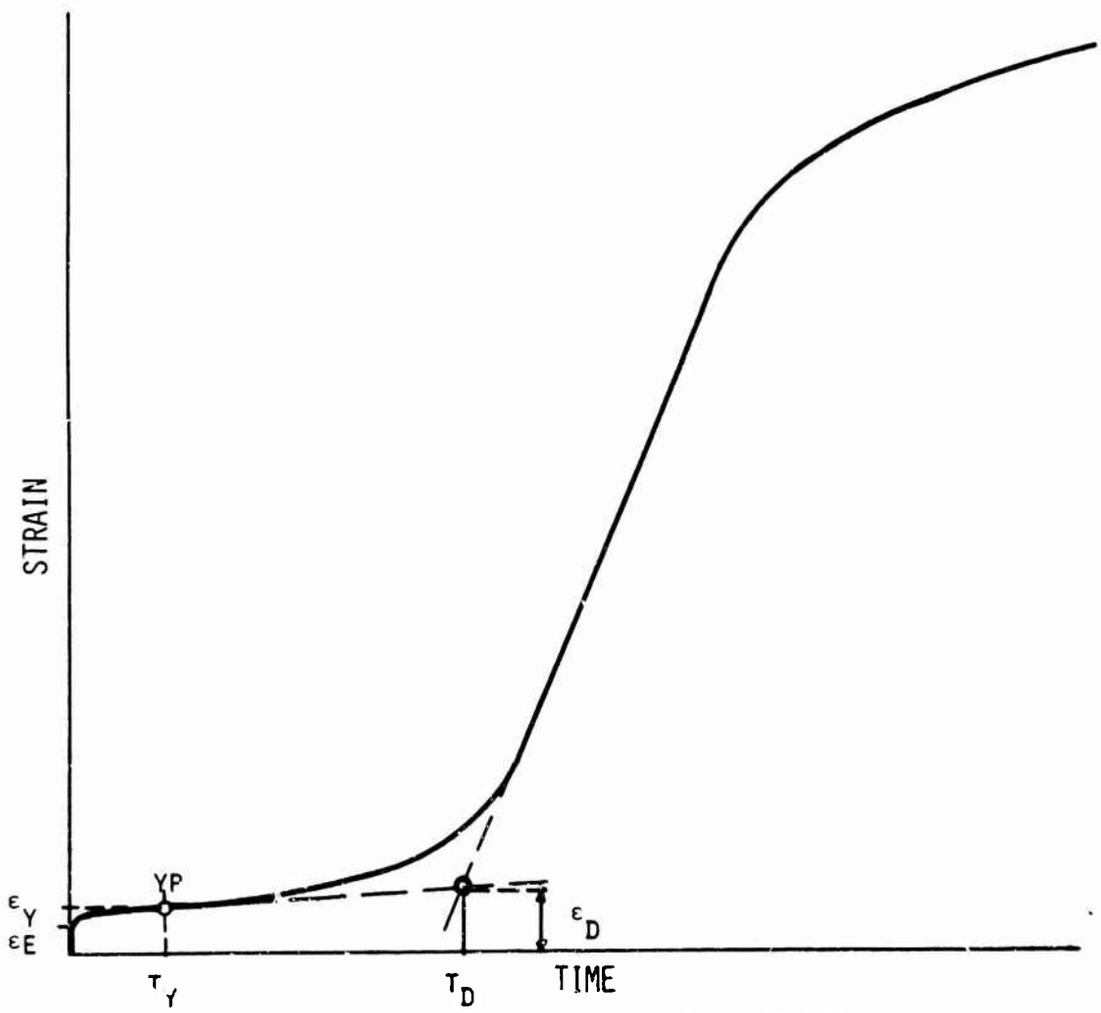

FIG.1.1 DEFINITION OF CONSTANT LOAD DRAWING PARAMETERS

T_Y	TIME TO YIELD	ε_D	DELAY STRAIN
T_D	DELAY TIME	ε_E	ELASTIC STRAIN
		ε_Y	YIELD STRAIN

The specimens were observed between crossed polarizers as drawing proceeded to gain information about the deformation mode. For the same reason partially drawn samples were inspected, after the test, under the polarizing microscope.

Experimental results. Three different types of elongation-time curve were observed (Fig. 1.2). When the specimen drew with a neck [curve (a)], deformation first took place homogeneously for some time and at a slow rate. The rate then increased until a constant rate was reached again, several times higher than the initial one. Simultaneous with the acceleration of deformation rate, the appearance of a constriction somewhere along the specimen was observed. This developed into a neck and when the steeper slope was reached, the neck had formed and the specimen was drawing by propagation of the neck. Once the neck had reached the ends of the specimen, elongation became slow and homogeneous again.

Sometimes deformation remained homogeneous. In some cases high strains were reached after sufficiently long times [Fig. 1.2(b)]; in other cases deformation rate decreased with time and only comparatively small strains were attained even after very long times [see Fig. 1.2(c)]. When the experiments of the type (c) were interrupted, at the times indicated in Figs. 1.3, 1.4, and 1.5, the rate of deformation was steadily decreasing.

Figures 1.3 to 1.7 present the delay-time and delay elongation results in table-graph form. At any particular value of pre-orientation the delay times (Figs. 1.3, 1.4, 1.5) increase with decreasing stress and temperature, as expected. Below a certain critical stress, which decreases with increasing temperature, deformation is homogeneous. The stress-temperature plane is thus divided into two distinct regions, one in which drawing takes place by the formation and propagation of a neck, and another in which the deformation is homogeneous. In the region above the boundary line, type (a) drawing (Fig. 1.2) is obtained; below the boundary line, type (c) takes place. The homogeneous type of drawing [Fig. 1.2(b)] was observed in the vicinity of the boundary line, particularly at higher temperatures. At the lowest degree of preorientation (Fig. 1.5) drawing occurred only in a limited

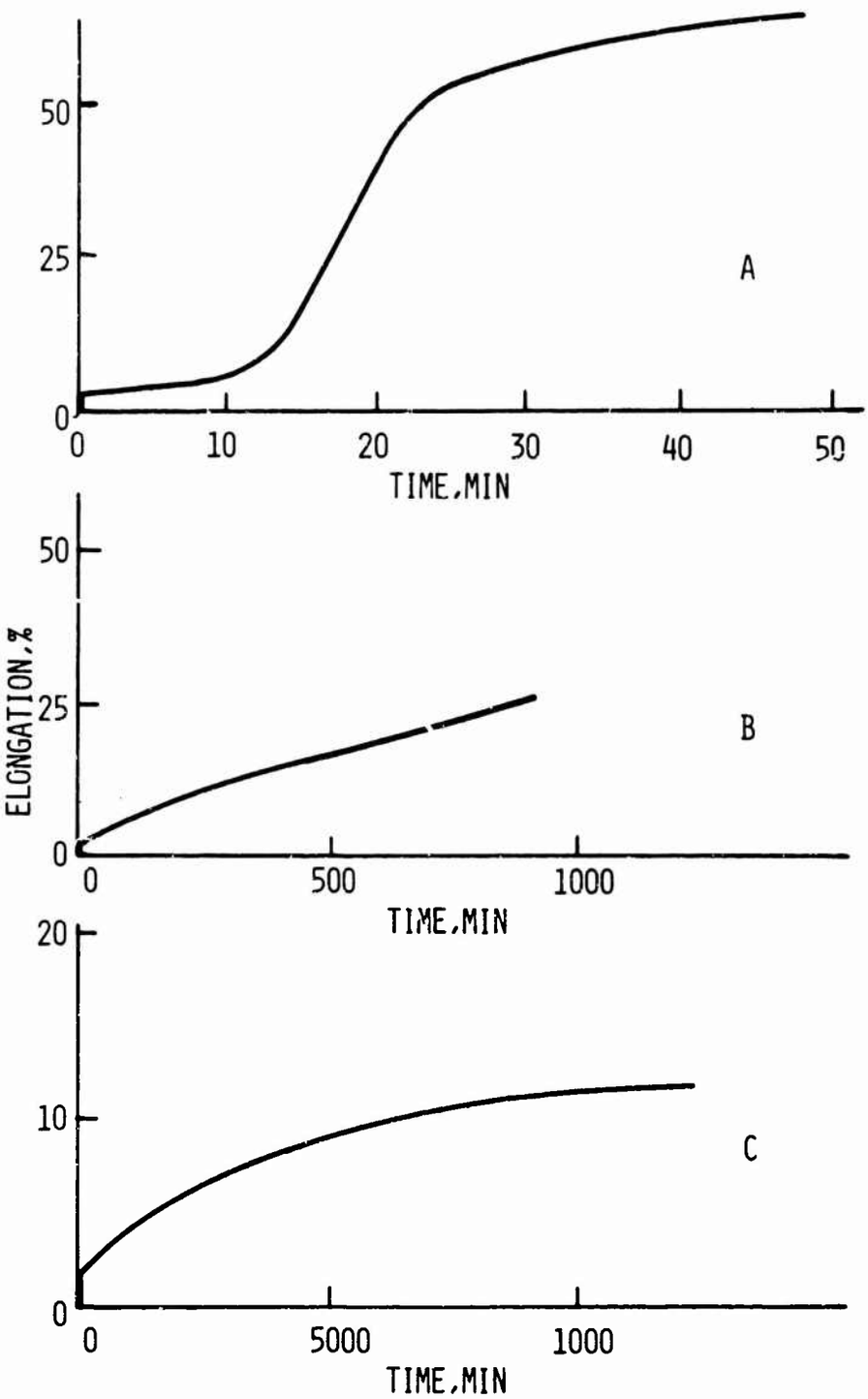

FIG.1.2 TYPES OF ELONGATION VS TIME CURVES OBSERVED FOR CONSTANT LOAD DRAWING

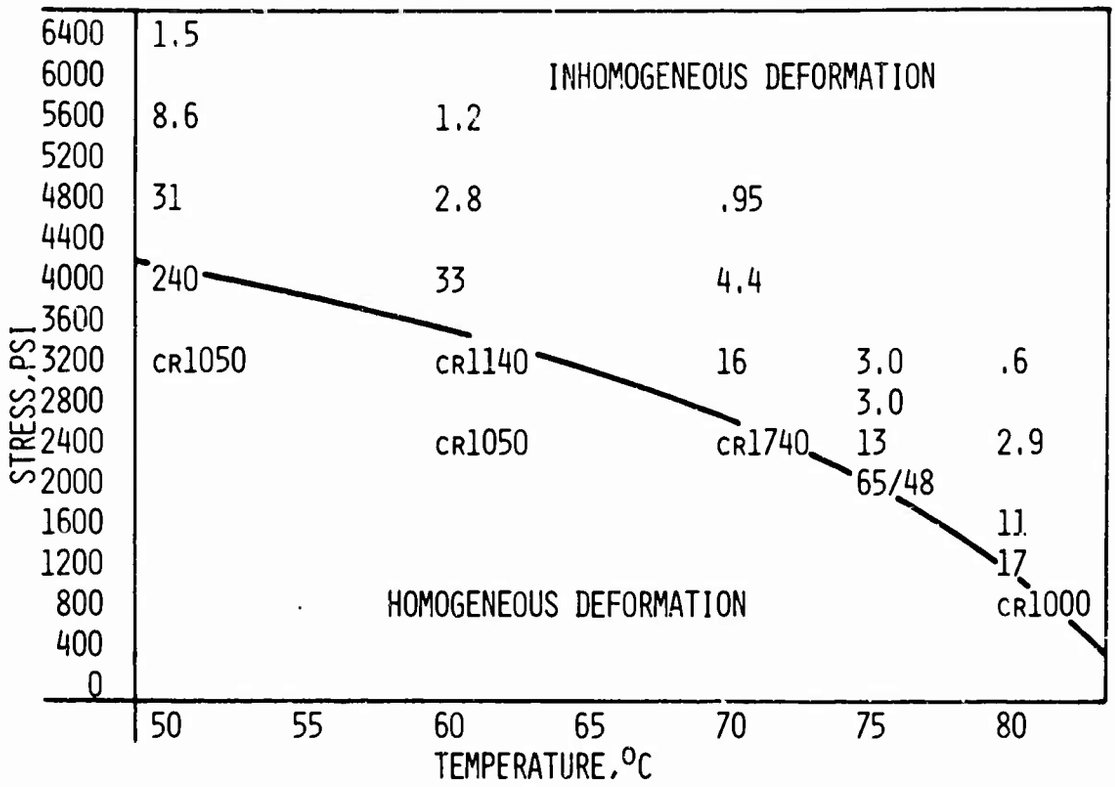

FIG.1.3 DELAY TIMES AND REGIONS OF DEFORMATION TYPE FOR PREORIENTED POLYSTYRENE $\Delta N = 10 \times 10^{-3}$

DELAY TIMES ARE LISTED IN MIN; CR INDICATES HOMOGENEOUS DEFORMATION ONLY WAS OBSERVED FOR THE OBSERVATION TIME INDICATED

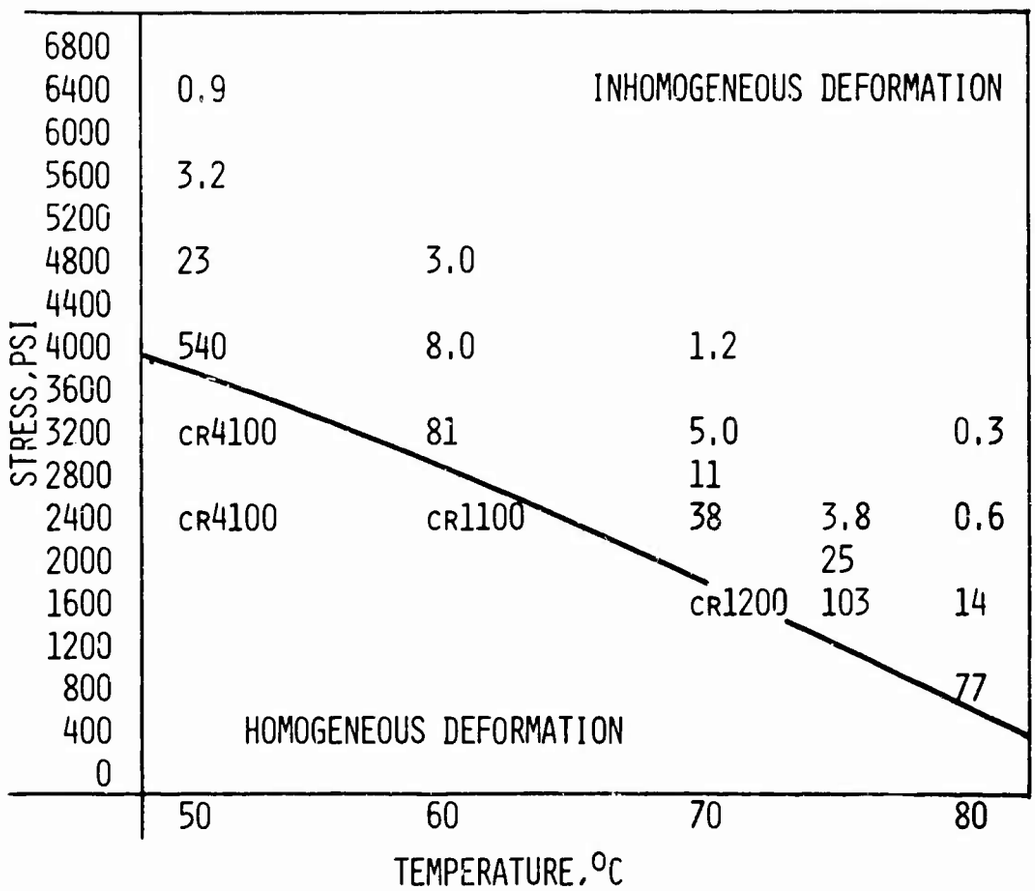

FIG.1.4 DELAY TIMES(MIN) AND REGIONS OF DEFORMATION TYPE FOR PREORIENTED PS(BIREFRINGENCE=5×10^{-3}); CR INDICATES HOMOGENEOUS DEFORMATION ONLY WAS OBSERVED FOR THE TIME OF THE EXPERIMENT GIVEN

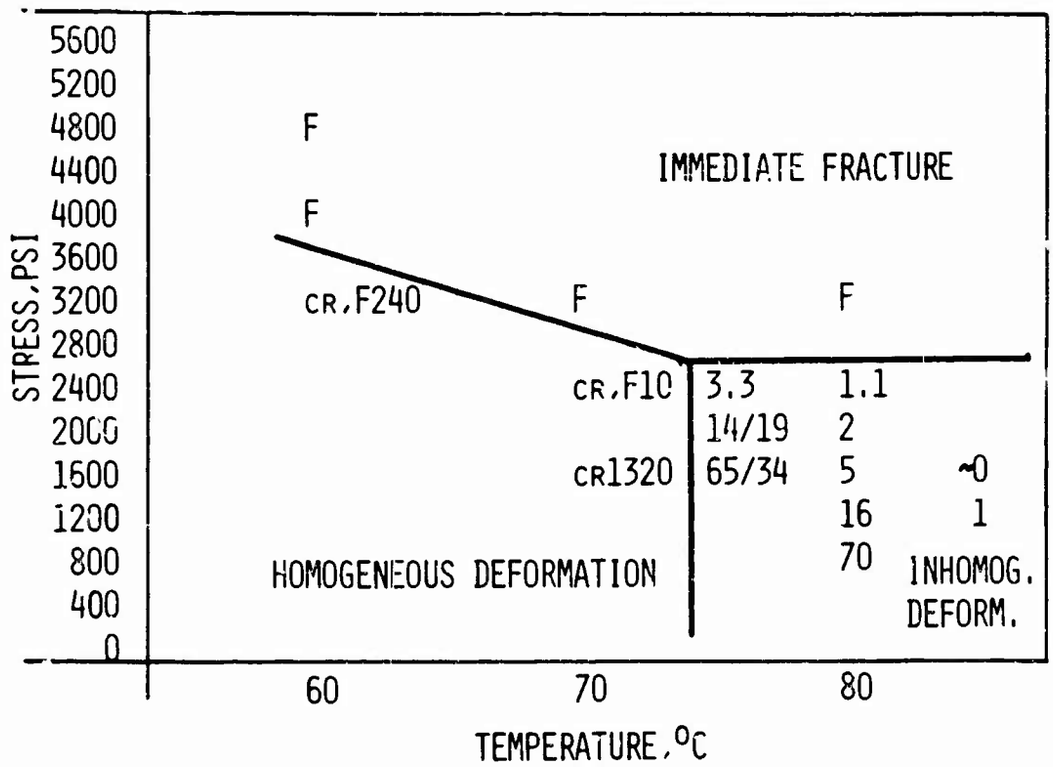

FIG.1.5 DELAY TIMES(MIN) AND REGIONS OF DEFORMATION TYPE FOR PREORIENTED PS(BIREFRINGENCE=$1x10^{-3}$);CR INDICATES HOMOGENEOUS CREEP WAS OBSERVED FOR THE TIME OF THE EXPERIMENT GIVEN;F INDICATES FRACTURE OF THE SPECIMEN

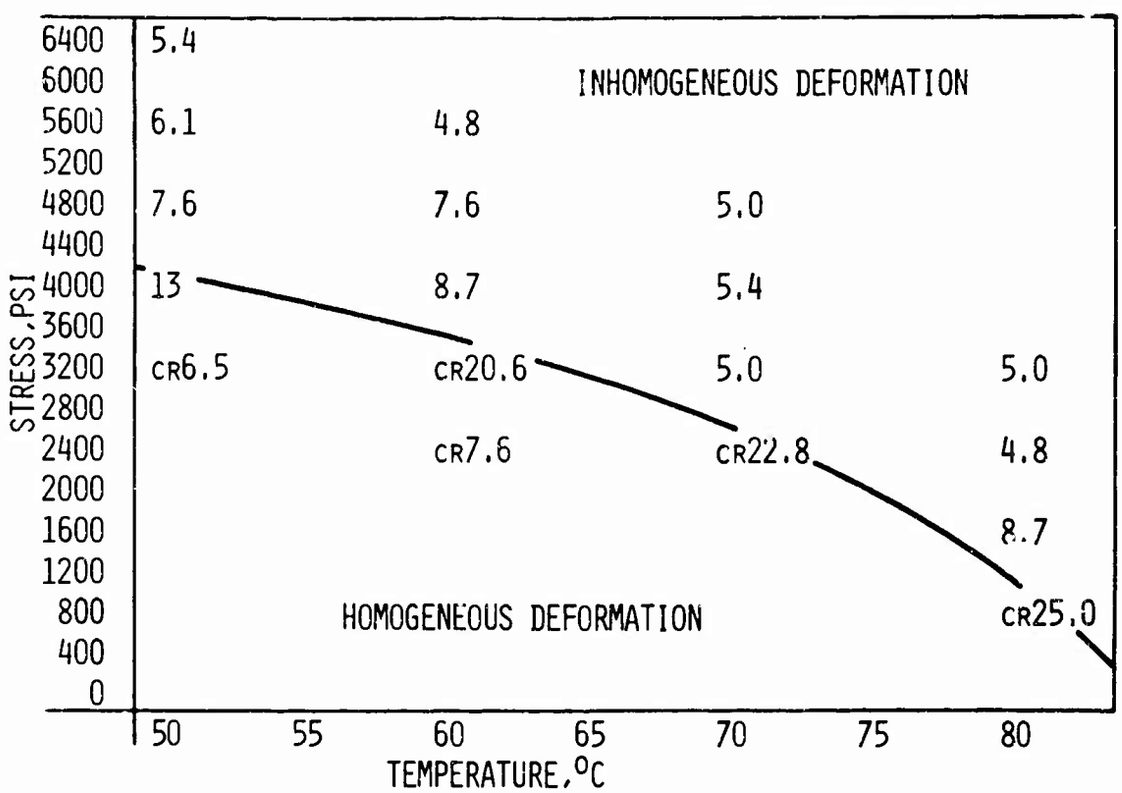

FIG.1.6 DELAY ELONGATIONS(%) AND REGIONS OF DEFORMATION TYPE FOR PREORIENTED POLYSTYRENE $\Delta_N = 10 \times 10^{-3}$

CR INDICATES HOMOGENEOUS DEFORMATION WAS OBSERVED FOR THE OBSERVATION TIME

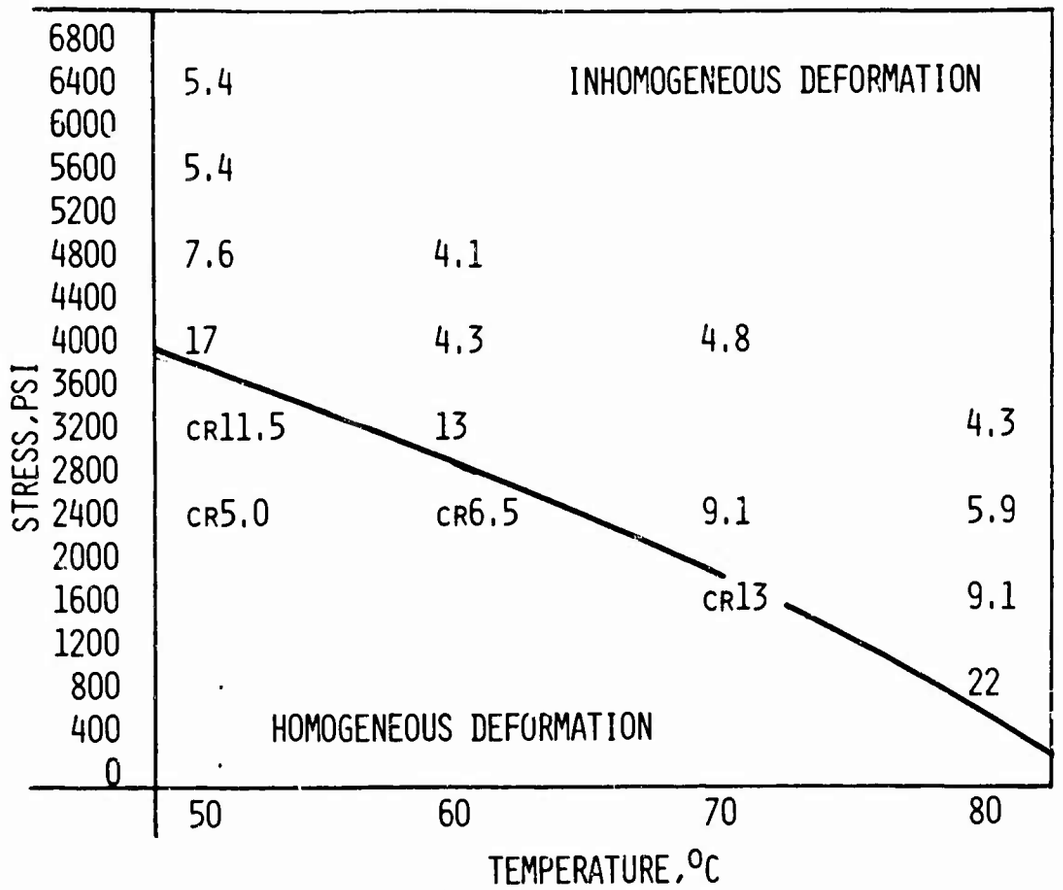

FIG.1.7 DELAY ELONGATIONS(%) AND REGIONS OF DEFORMATION TYPE FOR PREORIENTED PS(BIREFRINGENCE=5×10^{-3});CR INDICATES SPECIMEN ELONGATED TO THE STRAIN GIVEN WITHOUT DRAWING

region at high temperatures and low stresses. Outside this region the specimens failed by fracture, either immediately or after some time, before cold drawing had started. The data were not complete enough to define the boundary line between the drawing modes in this case.

The change in deformation mode is also reflected in the delay elongations (Figs. 1.6 and 1.7). The boundary lines in Figs. 1.6 and 1.7 are, of course, identical with those in Figs. 1.3 and 1.4 since the coordinate plane is the same in all cases. The delay elongation is usually of the order of 5% - 10%. In the region of homogeneous deformation, much higher strains than this can be reached after sufficient time, without the occurrence of necking. This division on the basis of strain seems less clear-cut in Fig. 1.7, where large delay strains have been measured in the region of drawing with a neck, close to the boundary line. These specimens apparently reached the stress necessary for necking only after some reduction in cross section had taken place by homogeneous extension. This borderline case could perhaps be avoided by carrying out the experiments at a strictly constant stress rather than at constant load. This was not done for the sake of experimental simplicity. As a consequence, the stress increases with strain by the factor $(1 + \varepsilon)$.

At the onset of necking, localized areas of high strain were always seen in the samples. These shear deformation bands[10,15,16] ran across the specimen at an angle of approximately 50°. The bands usually formed to some degree along the entire gauge length. The neck would form either where the band density was highest, or where some of the individual bands were particularly pronounced. Sometimes a great number of bands formed simultaneously and so densely that no single neck was formed and drawing took place entirely by proliferation of the band structure. On superficial observation, the specimen appeared to draw homogeneously, but closer inspection revealed a great number of these shear deformation bands.

When the deformation remained truly homogeneous [type (c) drawing, Fig. 1.2], no bands could be observed during the experiment, nor could they be detected by microscopic inspection afterwards.

The origin points of the deformation bands were often imperfections at the edges of the specimen. In all specimens crazes and sometimes internal cracks developed to some degree after load application and these became sources of deformation bands. Band structures could be particularly observed in the neck of the specimens and in the undrawn material close to the neck. In the drawn region of the specimens, over which the neck had passed, the bands had disappeared. Chapter VII will deal with the microdeformation in more detail.

Drawing of Polymethyl Methacrylate

The peculiarity of PS to cold draw only if it is somewhat preoriented by hot stretching, precludes a separate investigation of molecular orientation and thermal history[17]. PMMA does not have this drawback. It yields without preorientation below the glass transition temperature but above room temperature. It was also found that commercial PMMA sheets are superior in uniformity over PS sheets--the nonuniformities of which are further enhanced in the hot stretching step.

Normal PMMA was used (Rohm & Haas Company, Plexiglas II UVA, Appendix B). The polymer had a glass transition temperature of 106°C (Chapter V). The specimens were stored for at least three weeks in air of 65% RH and 22°C prior to drawing. Later a large effect of equilibrium moisture content on the time to draw was found. The polymer contains close to 1.0% water under the conditions given; part of it is lost during the test. When heated, the air of the testing laboratory drops in relative humidity to the values given in Table I.

Table I

Change of Relative Humidity of Testing Laboratory Air at Elevated Temperature

(Calculated from Change of Saturation Vapor Pressure)

T°C	22	70	80	90	100
RH%	65	5.5	3.6	2.5	1.7

During the drawing test, the polymer approaches an equilibrium moisture content corresponding to these humidities. To which extent this occurs depends mainly on the duration of the

experiment. The first data were obtained from such nonequilibrium specimens. They are, nevertheless, reported here as they give some useful information. Figure 4.1 shows the moisture content vs. heating time at 80°C. During the 10 minute equilibrium period, the specimen loses approximately 0.2% water. During the test, the concentration of water is expected to be nonuniform within the sample and changing with time.

Experimental results. Nonequilibrium moisture. The measurements on polymethyl methacrylate revealed two types of behavior under constant load. At low stress the specimens deformed by creep, above a certain stress an instability in the elongation vs. time curve appeared of the nature shown in Fig. 1.2(a). The occurrence of the instability was first indicated by optical inhomogeneities growing bandlike in shape from the specimen edges, oblique to the stress direction, and towards the center of it. They formed before the rapid phase of cold drawing occurred and persisted in the neck or, if the drawing remained uniform, were visible all along the specimen. The typical appearance was, in fact, nearly the same as that found in PS. Nonuniformly distributed bands were indicative of necking which started at the highest band density, uniformly distributed ones for drawing without a neck. For both modes the curve of Fig. 1.2(a) is typical. When only creep was observed, with no acceleration of deformation rate, there was no indication of bands. Tests of this type were only interrupted after a time in excess of the extrapolated delay time if the rate of deformation was decreasing. In all experiments resulting in drawing the acceleration of deformation rate occurred at 1/3 to 1/5 of the time necessary for drawing.

The boundaries between bands and less strained polymer were diffuse as compared to PS. The bands were detectable unambiguously only by schlieren light observation or related methods (Chapter VII). Figure 1.8 contains the delay times from tests at various combinations of stress and temperature. At each temperature there is a stress at which the deformation remains microscopically homogeneous and above which delayed drawing takes place. This critical stress becomes lower with increased temperature.

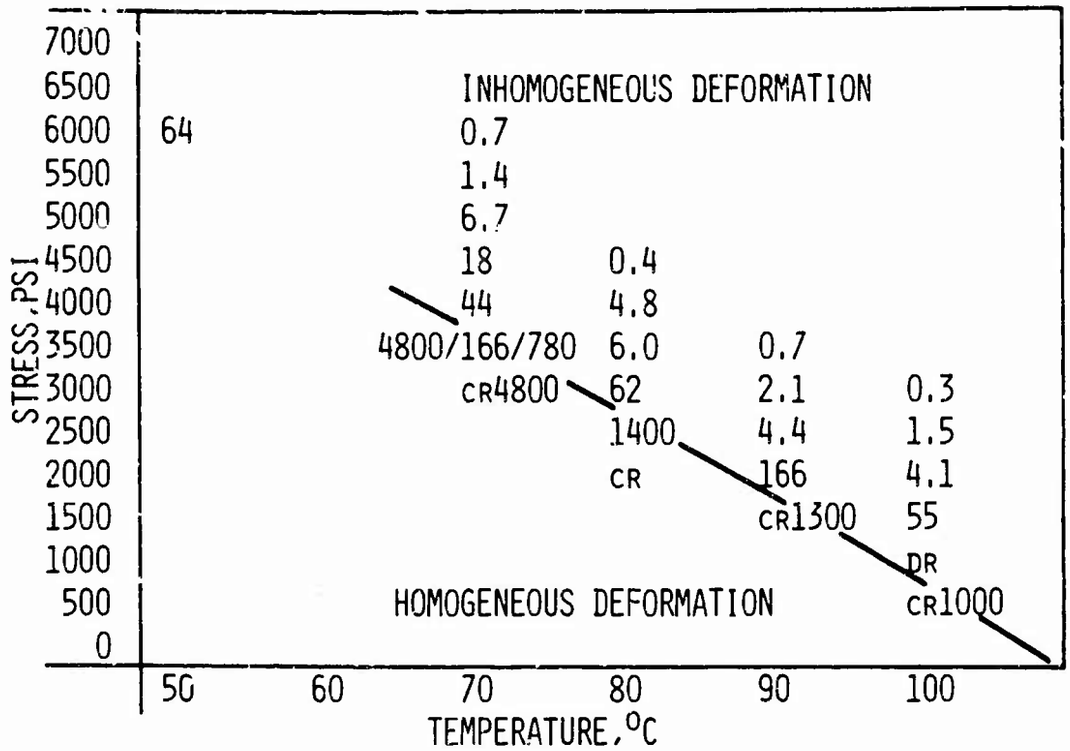

FIG.1.8 DELAY TIMES(MIN) AND REGIONS OF DEFORMATION TYPE FOR PMMA: CR INDICATES HOMOGENEOUS DEFORMATION ONLY WAS OBSERVED FOR THE OBSERVATION TIME INDICATED

Experimental Results. Moisture Equilibrium Specimens. The moisture content of PMMA tensile specimens as a function of time in air of 80°C is shown in Fig. 4.1. Nearly constant moisture is reached after three days. The drying procedure adopted for specimens to be drawn at 70, 80 or 90°C was three days at 80°C. For experiments at 100°C drying was in 100°C air for three days. These treatments, in particular the 100°C exposure, also anneal the polymer, but little influence on properties can be found if the starting material is well annealed already. This will be shown in more detail in Chapter III.

The delay times of the equilibrium moisture content experiments are presented in Fig. 1.9. The delay times are, at equal stress and temperature, ten times higher than the ones of the moist specimens. The slope dlog $t_d/d\sigma$ remains unchanged. The transition from drawing to creep is at much higher times. It can, in fact, only be expected from the upward bending of the delay time curve. One of the dried samples was found to draw after a delay of 7000 minutes. The curve for 100°C is exceptional in that it does not become a straight line at high stresses as the lower temperature isotherms do.

Drying reduced the tendency towards crazing. The crazes formed were smaller than in the moist samples. The mode of deformation was not recognizably changed by drying.

Discussion

Delayed drawing in PS and PMMA appears to occur in three steps:

1. Appearance and growth of oblique deformation bands,
2. Increase of the band density and frequently the simultaneous formation of a neck,
3. Either neck propagation or drawing by shear band proliferation.

Deformation bands have been observed before in tests at constant strain rate and with different polymers[3,10,11,18]. Drawing without a neck by shear bands only has not been reported previous to this work[19].

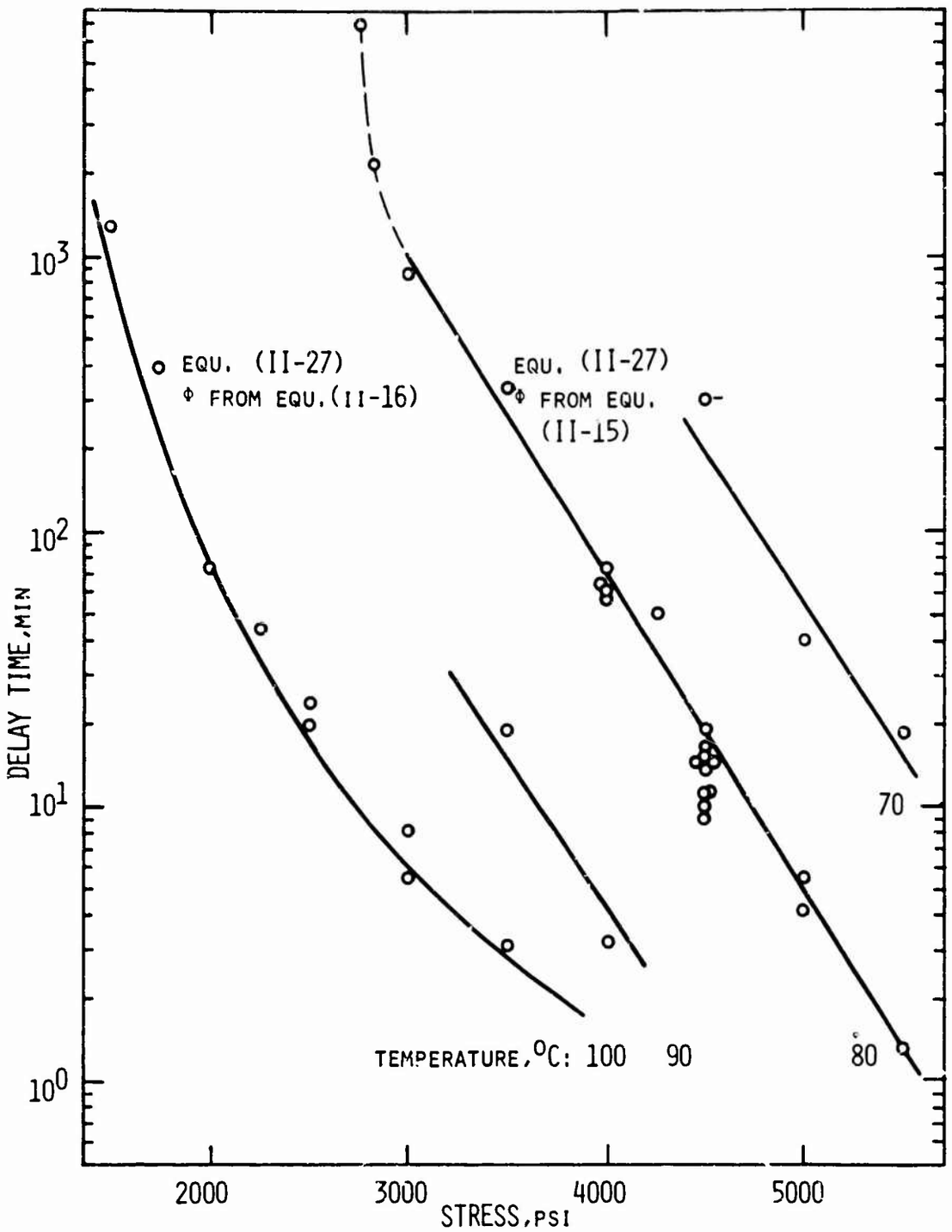

FIG.1.9 DELAY TIME VS STRESS FOR PMMA

The pure shear band drawing is not ordinarily observable in drawing tests at constant strain rate. In this test the load drop after yielding reduces the chance for the formation of further shear bands outside the neck, or the growth of the ones already present. The reason that a neck forms in the constant load drawing at all has to do with imperfections in the sample and probably small temperature gradients as well, since there would otherwise be no tendency for localization of strain at any point.

In both drawing modes the ultimate sample strain attained is the same.

The drawing results obtained up to this point suggest the conclusion that initiation of cold drawing is generally by shear deformation bands. Below some critical stress, which varies with temperature, they do not form and the strain remains homogeneous. There is no known reason to question the correctness of this picture in the case of PS; for PMMA it must be modified. This polymer, when quenched from about T_g, does not reveal deformation bands in subsequent cold drawing, yet the delayed drawing curve is of the same type as that of the original polymer, which is of a well annealed commercial quality (Chapter VII). The high shear strain gradients which exist in banded materials cannot be maintained in the poorly annealed polymer. It behaves in this respect more like a fluid. The microscopic modes of deformation will be discussed in more detail in Chapter VII.

For both polymers, PMMA and PS, a plot of log delay time vs. stress gives, for constant temperature, parallel straight lines (Figs. 1.9, 1.10, 1.11, and 1.12). The 100°C curve of the equilibrium moisture data is an exception. The points drawn in just above the upper border of Figs. 1.10, 1.11, and 1.12 correspond to experiments where only homogeneous creep occurred. It is clear that these points no longer fall on the straight lines for the samples which showed delayed necking and drawing. These specimens contained neither deformation bands nor necks, despite the fact that the elongations attained in some cases greatly exceeded the delay elongations of the samples which drew inhomogeneously.

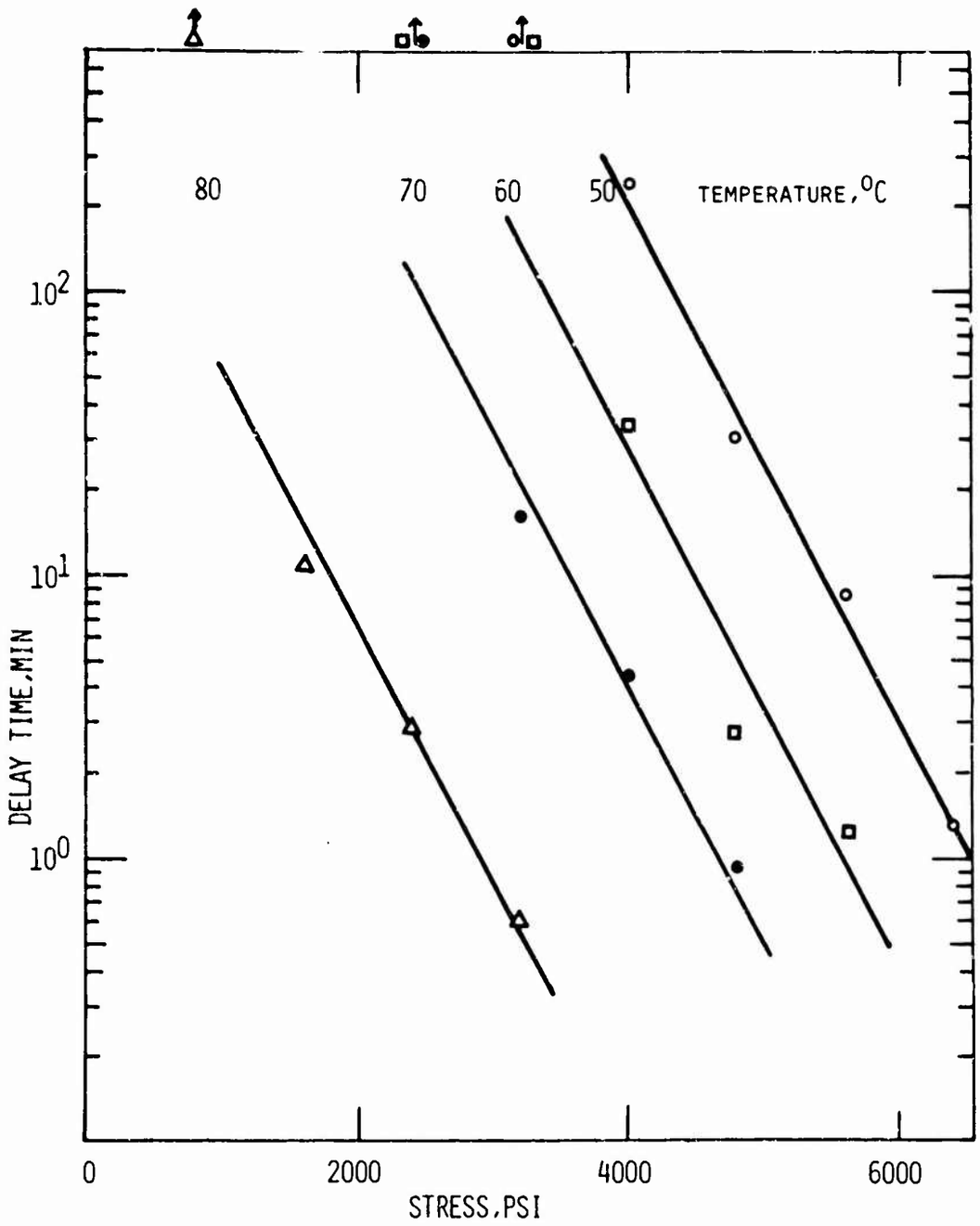

FIG.1.10 DELAY TIME VS STRESS FOR PREORIENTED PS, BIPEFRING.: 10×10^{-3}

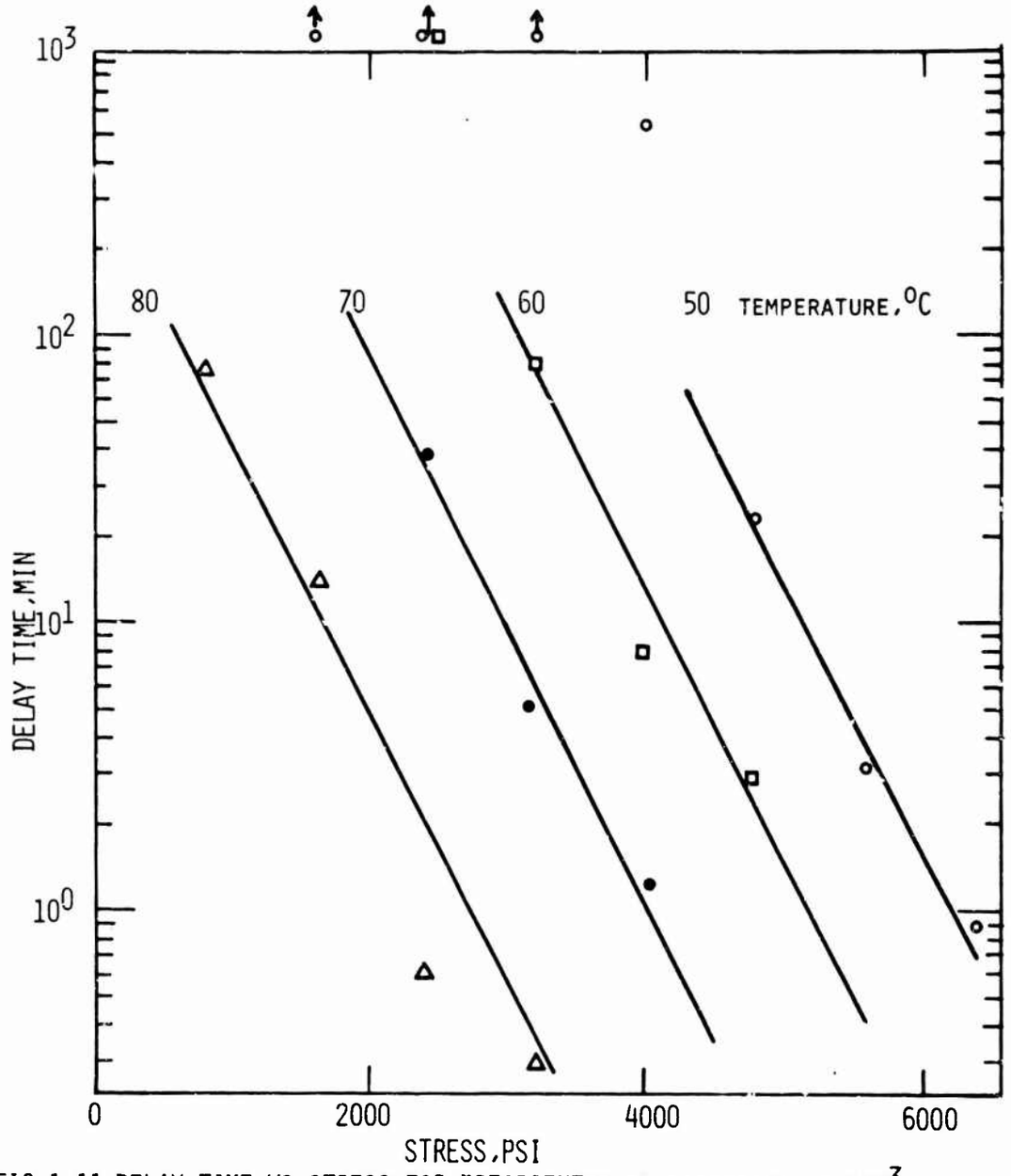

FIG.1.11 DELAY TIME VS STRESS FOR PREORIENTED PS,BIREFRING.:$5x10^{-3}$

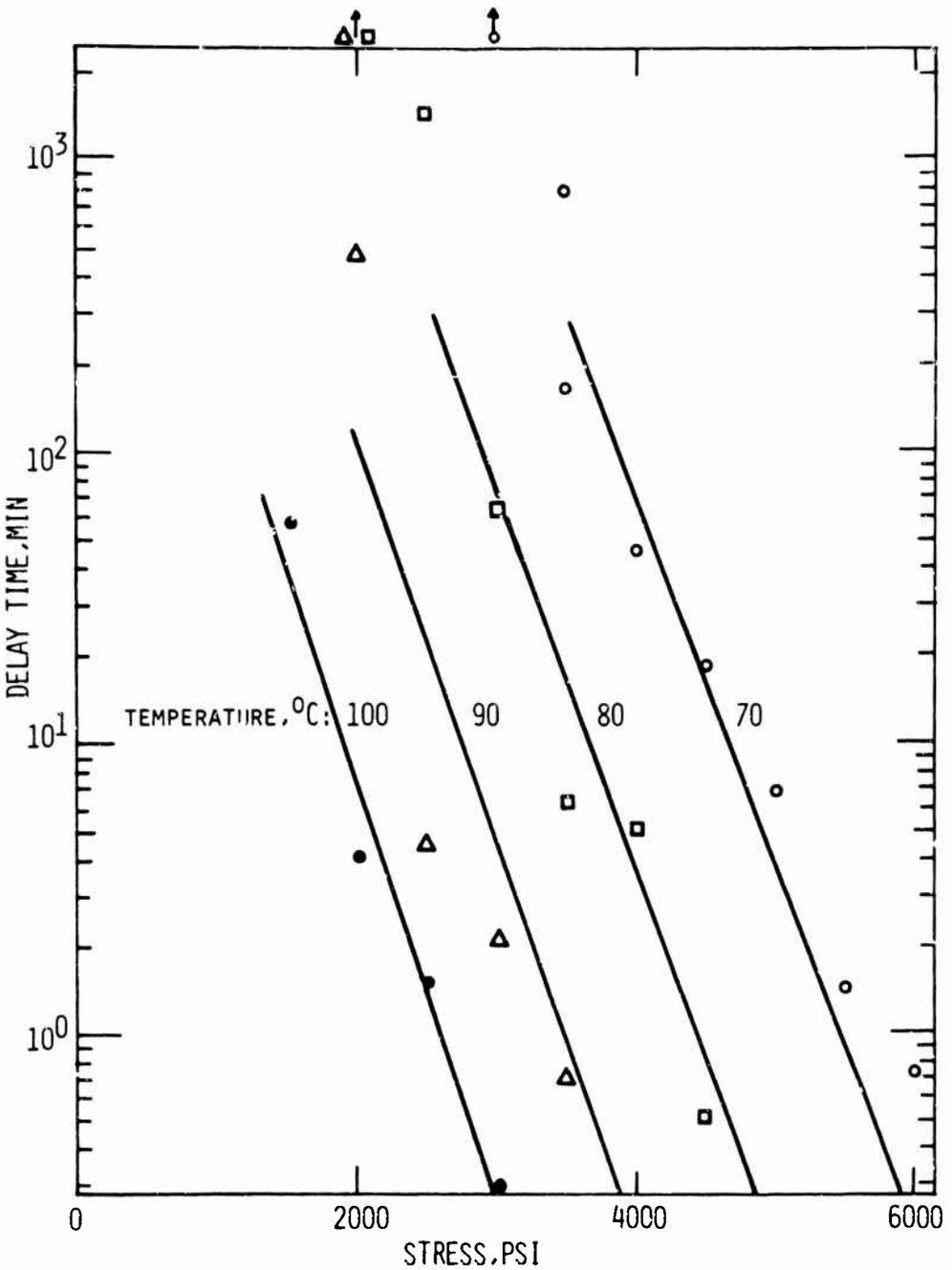

FIG.1.12 DELAY TIME VS STRESS FOR PMMA

Tests with PMMA dried to equilibrium moisture content have not been carried out at low enough stresses to find the deformation mode transition because of prohibitively long experimental times. The upturn of the log delay time vs. stress curve for the equilibrium set of samples (Fig. 1.9, 80°C curve) occurs very close to the transition boundary stress found for the nonequilibrium set. At this point, because of the long delay times near the boundary, the nonequilibrium samples have nearly equilibrated. This is in favor of the existence of a critical stress in PMMA, as these samples have been found not to draw below this stress. Moisture has served to reduce the experimental times for the initial period of the test. This is, admittedly, not very satisfactory evidence, as moisture may be expected to exert other influences, too.

In the nonequilibrium moisture experiments (Fig. 1.12) the enhanced resistance against flow, caused by loss of water, is competing with the process of the deformation. The longer delay time samples have lost more water, and the delay time should approach that of the dried samples (Fig. 1.9). This would result in an increase in slope of the log t_d vs. stress curve. Drying proceeds much faster at 100°C than at 70°C; one would therefore expect a higher slope for the higher temperature. These two influences are not found. This suggests that the water lost in this initial period of 100 minutes, or less, is essentially from a thin outside layer the drawing properties of which, though changed by drying, affect the drawing behavior of the total specimen only little. The much longer times close to the deformation mode transition are sufficient to change the moisture of the bulk of the polymer. This is obviously the reason for the accentuated transition in the nonequilibrium moisture samples as compared to the slow upward bending of the delay time curve found for the equilibrium samples. The large experimental scatter of delay times and elongations near the transition boundary in the nonequilibrium case has its origin in all likelihood in the gradual loss of moisture also.

The question arises if the measurements with PS, for

which the samples have not been dried, are similarly affected by water. This has not been pursued by experiments, nor was a reference on the effect of water on the mechanical properties of PS found in literature. The equilibrium water absorption of this polymer is not reported either. Its 24-hour water absorption is only about one-tenth of that of PMMA[20].

The abnormal shape of the 100°C delay time vs stress curve of PMMA (Fig. 1.9) is believed to be a consequence of the vicinity of the glass transition temperature. Additional experimental evidence (Chapter II) and a proposed explanation (Chapter VI) will follow.

During constant load tests the stress increases with strain and in the course of creep, a stress high enough to bring about drawing may be reached. This has occurred in the experiments near the transition boundary for both PS and PMMA. The delay strain (Figs. 1.6, 1.7, and 1.13) at the transition boundary is much higher than within the region of inhomogeneous stretching. To define more precisely the transition boundary from drawing to creep it becomes necessary to use constant stress tests.

The data of Figs. 1.10, 1.11, and 1.12 have been fitted by the least square method to straight lines; Table II gives the respective slopes.

Table II

Temperature and Stress Coefficients for Log Delay Time
[T, °C; σ, psi]

	$\frac{d\log t_d}{dT}$	$\frac{d\log t_d}{d\sigma}$
PS $\Delta n = 10 \times 10^{-3}$	-0.11	-0.85×10^{-3}
PS $\Delta n = 5 \times 10^{-3}$	-0.13	-0.99×10^{-3}
PMMA $\Delta n = 0$ Nonequilibrium	-0.13	-1.33×10^{-3}

The effect of temperature and stress on $\log t_d$ is nearly independent of preorientation in PS. The delay time does, however, increase slightly with increasing preorientation.

From the PMMA delay time data an activation energy of $Q = 74$ kcal/mole was calculated. The delay times at 3500 psi at different temperatures were used. The 100°C value was

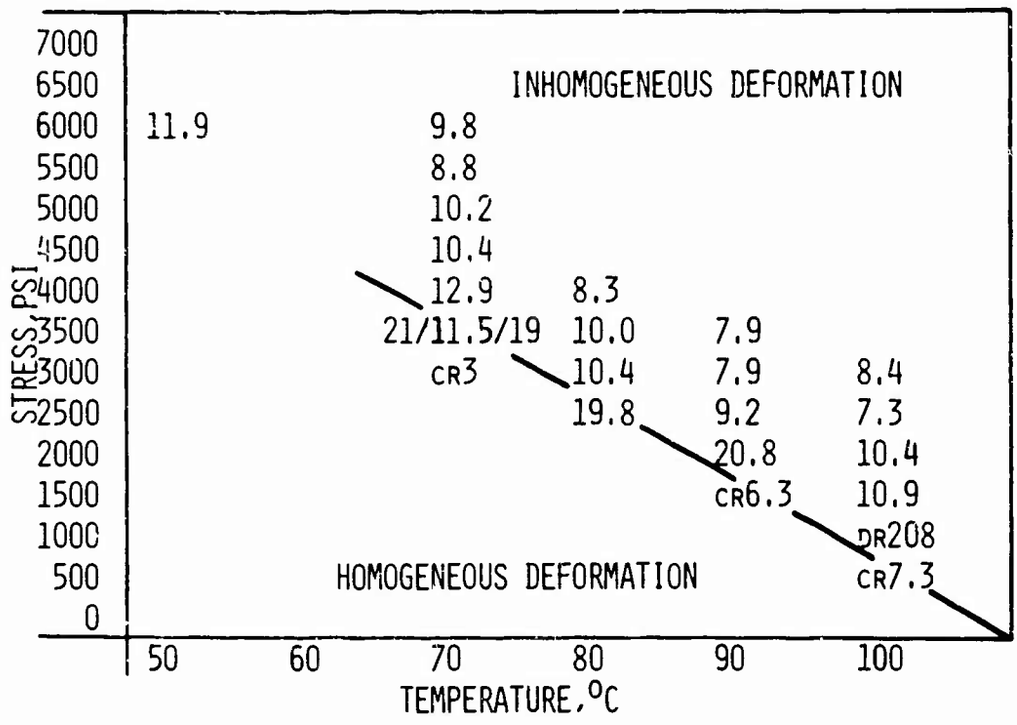

FIG.1.13 DELAY ELONGATIONS(%) AND REGIONS OF DEFORMATION TYPE FOR PMMA; CR INDICATES HOMOGENEOUS DEFORMATION ONLY WAS OBSERVED; DR INDICATES HOMOGENEOUS DRAWING TO THE GIVEN ELONGATION

extrapolated from measured data. Roetling[21] obtained in the region of comparable strain rates Q = 81 kcal/mole. His data were for the upper yield point of constant rate drawing tests. Sherby and Dorn[22] measured small strain creep and report activation energy to be a function of temperature above 50°C. In the temperature region of the present experiments their values increase (Fig. 3.1) from 80 kcal/mole at 70°C to 100 kcal/mole at 100°C.

CHAPTER II
TENSILE RHEOLOGY IN CONSTANT LOAD AND CONSTANT VELOCITY DRAWING TESTS

Introduction

In the previous chapter the constant load test was shown to be useful in investigating cold drawing behavior of glassy polymers. How this test relates to the conventionally used constant velocity test, and what can be learned from it about polymer mechanical properties during drawing will be discussed in this chapter.

The length vs. time curves from constant load experiments contain more information than that extracted from them up to this point. To evaluate parameters which are related in a simple way to parameters of the load vs. elongation curves of constant velocity drawing, the initial part of the length vs. time curve proves of importance. Hence, the recording method for length changes was changed from that used when delay time and strain only were of interest to an electrical method of high resolution described in Chapter VIII.

The precise length vs. time curves are converted to velocity vs. length curves. These contain in principle the same information as load vs. elongation curves. In practice it turns out that they are more useful in interpreting material properties because, under constant load, uniform strain is observed beyond the yield point, whereas at constant velocity the strain is inhomogeneous after yielding.

It becomes necessary to define a yield criterion for the constant load test, which conforms to that of the constant velocity test. To this end, and for the further comparison of the two tests, an assumption concerning the isothermal behavior of the polymer is made, namely that an equation of state exists of the form

$$(F,v,L) = 0, \text{ or } F = F(v,L) \qquad \text{(II-1)}$$

(F = stress with respect to initial cross-section; v = velocity with which specimen ends move with respect to one another;

L = specimen length.)

Equation (1) requires that the three quantities are uniquely related independently of the path by which a momentary state was reached. It is believed that such a relation does not exist in a strict sense; one reason being that the structure of most solid materials depends on the deformation history. Yet, it is useful as a first approximation.

The yield criterion for the constant velocity test is

$$\left(\frac{\partial F}{\partial L}\right)_v \leqq 0 \qquad \text{(II-2)}$$

From Equations (C-1) and (C-2) the yield criterion for the constant load test is derived to be

$$\left(\frac{\partial v}{\partial L}\right)_F \geqq 0 \qquad \text{(II-3)}$$

(Appendix C)

The velocity v is the slope of the length vs. time curves. The minimum of the slope, occurring at the inversion point of the curve, is the equivalent to the upper yield point of the load vs. elongation curve.

From their stress-strain curves, most linear polymers should show delayed drawing. It has been found in nylon 66[11,12]. Other polymers do not appear to have been studied. For polyamids and polyvinylchloride[23] and branched polyethylene[5], drawing has been reported to become uniform at very small strain rates. This implies the disappearance of the upper yield point. In constant load experiments at comparable strain rates delayed drawing should no longer be observed either because $(\partial v/\partial L)_F$ does not become zero. This is found for PS and PMMA as transition from drawing to creep in the latter type of experiment at a strain rate of the order of 10^{-4} 1/min.

Delayed drawing is found in metals also, eg iron and bcc-metals[24,25]. According to Clark and Wood[24] metals show delayed yielding only if they have an upper yield point. Equation (C-1) states this, as $(\partial v/\partial L)_F \geqq 0$ only if $(\partial F/\partial L)_v \leqq 0$. In addition, the force must have a positive strain rate dependence, $(\partial F/\partial v)_L > 0$. Otherwise, the yield stress is reached at once, if the load F is higher than F_{yield}, or not at

all, if it is lower. Delayed drawing is therefore expected in any material for which the last two equations are satisfied.

In this, and the following chapters, the equations have sometimes been written in terms of the symbols F, v, and L. Where uniform strain is included as a possibility, σ, $\dot{\varepsilon}$, and ε (true stress, strain rate, and strain) have been used.

Results and Discussion

Comparison of Drawing Modes in Constant Velocity and Constant Load Drawing. When applied to polymers, the term "cold drawing" has become synonymous with "necking", because a neck begins to form in the constant velocity test at the upper yield point. A new observation is made in constant load drawing. There, often, no neck is observed and if one forms, it does not start at the yield point, $(\partial v/\partial L)_F = 0$, but at higher strains.

Many of the data to be interpreted later have been obtained from that part of the post-yield region where the strain is still uniform. The intention of this section is to examine why uniform straining persists beyond the yield point.

For this discussion, a probability p for neck formation per unit length of undrawn is introduced. In a constant load test it is a function of the length of time for which the load was applied. The maximum probability for a neck to form occurs at the delay time. It is assumed here that the probability changes with stress and temperature in the same way that delay time does. The distribution of p(t) around the maximum is expected to be narrow for good sample uniformity.

The probability of a neck to form in a specimen of length L is

$$P = p.L \qquad \text{(II-4)}$$

For simplicity sharp necks are assumed to form at once (no transient neck shape). Necks form at times t and the shoulders propagate with the velocity

$$V = \frac{v}{2(R-1)} \qquad \text{(II-5)}$$

(R = natural draw ratio = ratio of initial to necked cross-section area.) The length available for more necks to form is

$$L(t) = L_o - 2V \sum_{\nu=1}^{n} (t - t_\nu) \qquad \text{(II-6)}$$

(L_o = initial length.)

Collision and annihilation of shoulders are neglected and thus L(t) is overestimated somewhat. The probability of necks to form in the remaining undrawn polymer is

$$P = p(t)_{\sigma,T}[L_o - 2V \sum_{\nu=1}^{n} (t - t_\nu)] \qquad \text{(II-7)}$$

Examining the constant velocity test first, it is taken for granted that a neck forms at the upper yield point and the load drops by $\Delta\sigma$ to a constant value, the draw load. Under the lower stress the additional time for the as yet undrawn sections to neck is found to be many times higher than the time needed for the originally formed shoulders to move over the total specimen length. A typical numerical example is calculated in Appendix D.

In the constant load test, the appearance of a neck does not reduce the probability p for others to form elsewhere, because the load stays the same in the remaining undrawn polymer. Provided the distribution p(t) is narrow, the necks form simultaneously, or nearly so. The macroscopic deformation mode is uniform and this has been observed frequently with both PMMA and PS. More often, drawing is by single or multiple necks, this is ascribed to nonuniformity of the specimen (Appendix D). In the uniform case isolated necks do not develop, drawing is by shear bands only.

If necking occurs, the spreading of the first neck is often responsible for the total deformation. Under constant load the neck velocity is speeded up by a factor 10 or 100 over the deformation velocity previous to necking. The probability P for other necks is, in this case, reduced by the high velocity of neck propagation (Equation [7]) (Figure 2.1).

When a neck forms under constant load, one cross-section "overtakes" all the others in strain. For this to happen the strain rate must be higher there than anywhere else. Necking under constant load requires, therefore, a weak cross-section. The tendency for this defect to form a local instability (=neck)

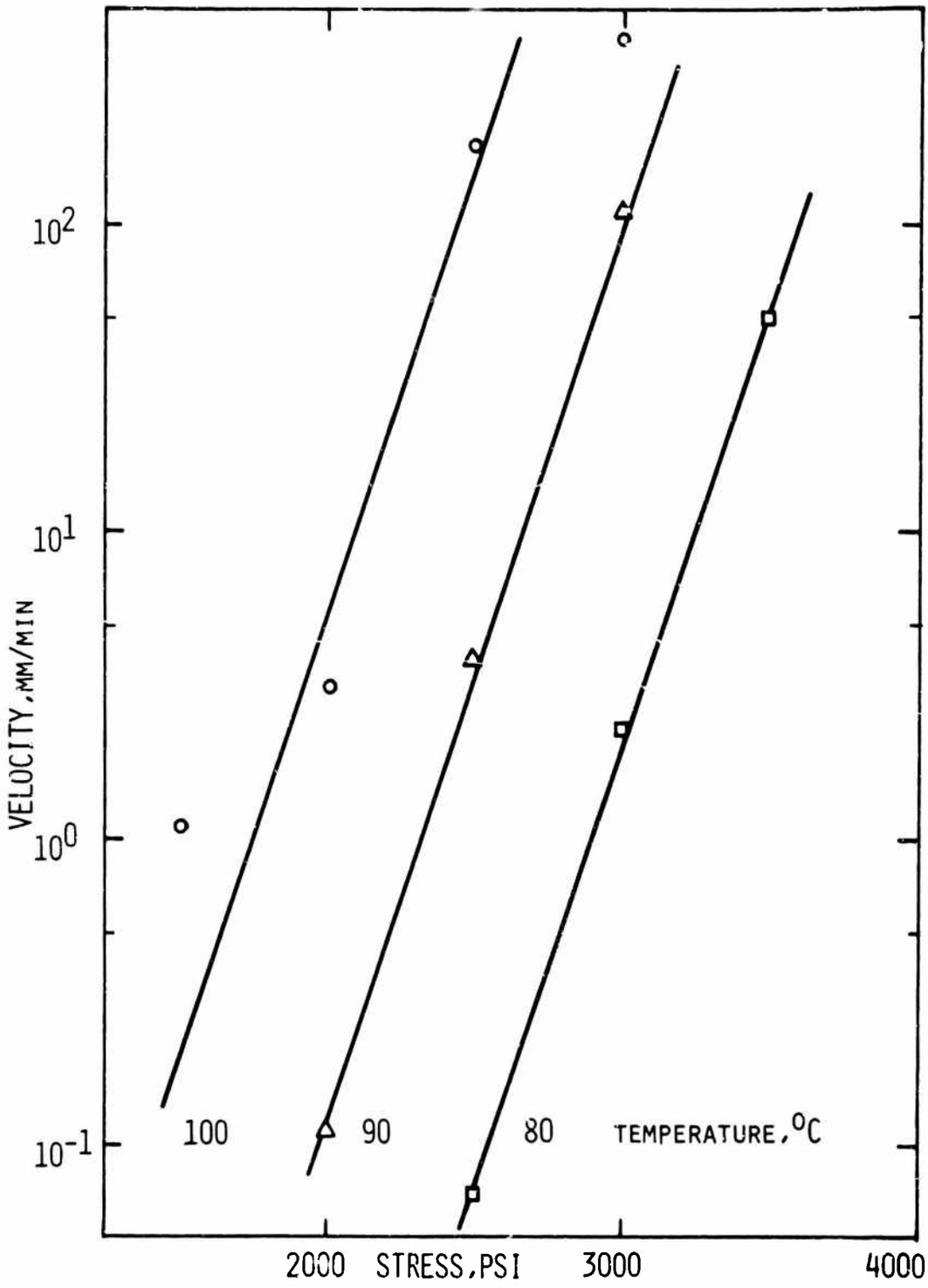

FIG.2.1 EXTENSION VELOCITY IN RAPID PART OF CONST.LOAD DRAWING VS STRESS FOR PMMA. GAUGE LENGTH: 48MM

is expressible by the gain in strain rate due to a small strain increase, $(\partial\dot{\varepsilon}/\partial\varepsilon)_F$. Together with Equation (C-1) and $d\dot{\varepsilon} = d\dot{V}/L$, and $d\varepsilon = dL/L$ this gives

$$\left(\frac{\partial\dot{\varepsilon}}{\partial\varepsilon}\right)_F = \left(\frac{\partial v}{\partial L}\right)_F = -\frac{\left(\frac{\partial F}{\partial L}\right)_v}{\left(\frac{\partial F}{\partial v}\right)_L} \quad . \tag{II-8}$$

Expressing the right hand side in terms of true stress and strain

$$\left(\frac{\partial\dot{\varepsilon}}{\partial\varepsilon}\right)_F = \frac{\sigma - \left(\frac{\partial\sigma}{\partial\varepsilon}\right)_{\dot{\varepsilon}}\dot{\varepsilon}}{\left(\frac{\partial\sigma}{\partial\dot{\varepsilon}}\right)_\varepsilon} \tag{II-9}$$

Instability occurs for $(\partial\dot{\varepsilon}/\partial\varepsilon)_F \geq 0$, that is for

$$\sigma \geq \left(\frac{\partial\sigma}{\partial\varepsilon}\right)_{\dot{\varepsilon}} \tag{II-10}$$

which is the well-known Considére[26] criterion. The strength of the instability is the slope of the velocity vs. length curve in the constant load experiment. The strain rate sensitivity of the draw load acts as a stabilizing factor. Drawing beyond the yield point is an instable situation because $(\partial v/\partial L)_F^{\bullet} > 0$. The fact that one does observe a uniform strain region is explained by the smallness of $(\partial v/\partial L)_F$ near the yield point and the kinetics of forming the neck. From this extended uniform strain region, which is for PMMA usually 10-20%, stress-strain data will be obtained which the constant rate test does not give.

Prediction of Time to Yield from Stress-Strain Curves. The assumption of the existence of an equation of state permits one to derive the results of one type of test, for example constant rate drawing, from those of the other, that is, constant load drawing. This conversion provides a test for the validity of the equation of state.

The curves F(v,L) are useful prior to yielding only because of the complication in specimen geometry afterwards. This strain range is all that is necessary to calculate the time for yielding under constant stress.

Figure 2.2 shows engineering stress-strain curves of PMMA

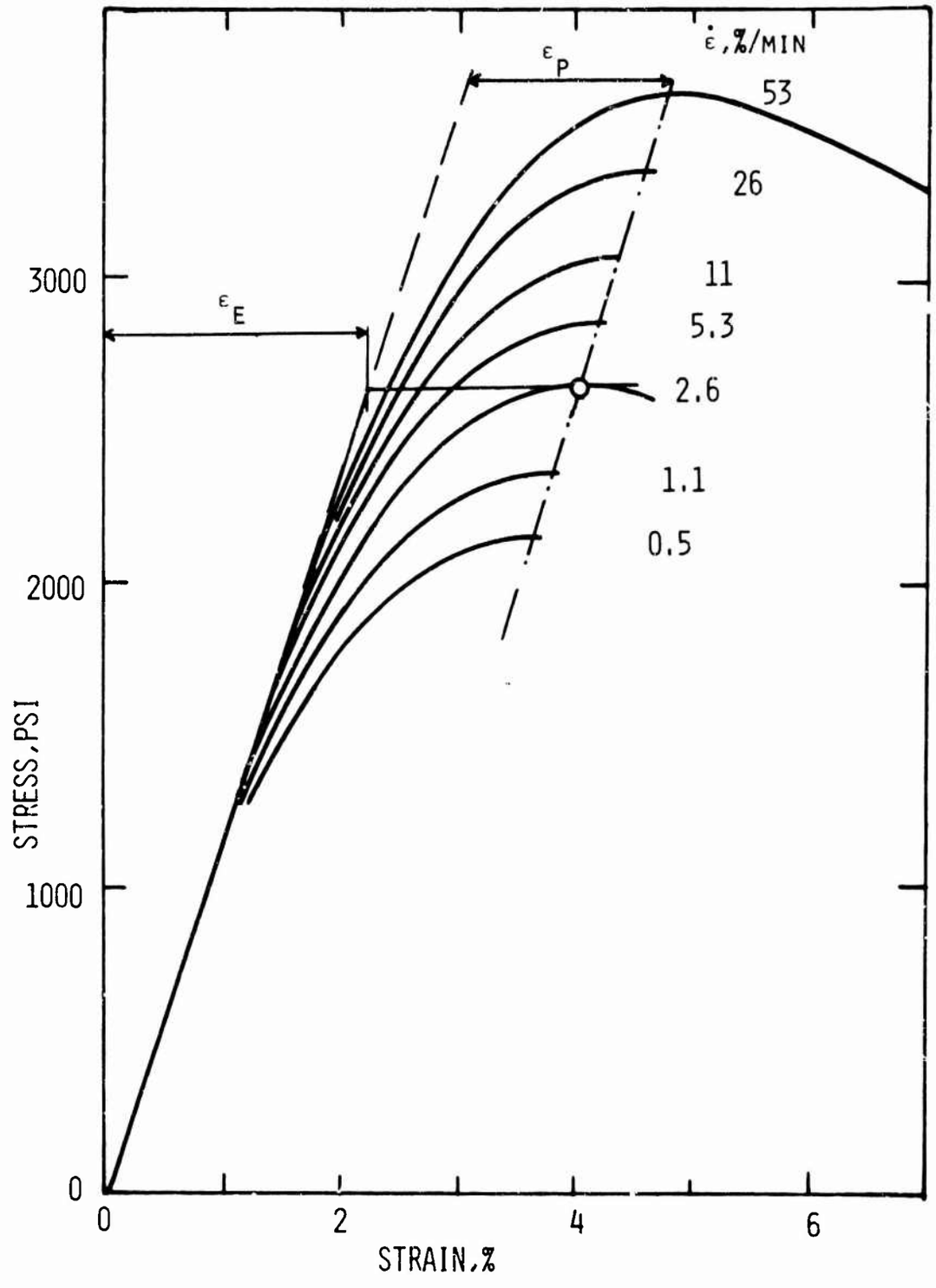

FIG.2.2 STRESS-STRAIN CURVES OF PMMA FOR VARIOUS EXTENSION RATES
TEMPERATURE:100°C;CONDITIONED IN 65%RH

for 100°C at a number of strain rates. The data have been obtained from the same type of specimen as was used in the delayed drawing experiments, which had been equilibrated in a 65% RH, 22°C atmosphere.

To facilitate the conversion, the family of experimental curves has been smoothed out by the following procedure. The upper yield stresses of the measured curves were plotted vs. log v. They followed the linear relation

$$F_y = 3600 + 725 \log v \qquad \text{(II-11)}$$

(F_y = upper yield stress, psi; v in/min.) The yield maximum for each strain rate was then calculated from Equation (II-11) and each curve was redrawn (Fig. 2.2) multiplying all stress values by the ratio of computed to experimental yield stress. From the curves of Fig. (2.2) the time for a specimen to yield in a constant load experiment is calculated by integration of the time intervals $dt = dL/v$ along a line of constant stress from zero to that elongation where the line is tangent to a constant strain rate curve. The contribution of the elastic deformation to the time integral is negligible, compared to the times for yielding. The integration is therefore only over ε_p. The result of the graphical integration is represented for the strain rates of Fig. 2.2 by the equation

$$\log (t_y) = 3.2 - F_y/725 \qquad \text{(II-12)}$$

(t_y, min; F_y, psi.)

From Equation (12) $d\log t/d\sigma = -1.38 \times 10^{-3}$, in good agreement with experimental values (Table II). The calculated time to yield, t_y, is by a factor 4 lower than the delay time t_d. By precise measurements of the initial part of the length vs. time curves, it was found that the yield point occurs at 1/5 to 1/3 of the time which has been defined as delay time. Measurement and prediction are therefore in close agreement.

The Derivation and the Evaluation of Velocity vs. Length Curves of PMMA

From length vs. time curves the velocity vs. length curves are easily derived by plotting the slopes of the former

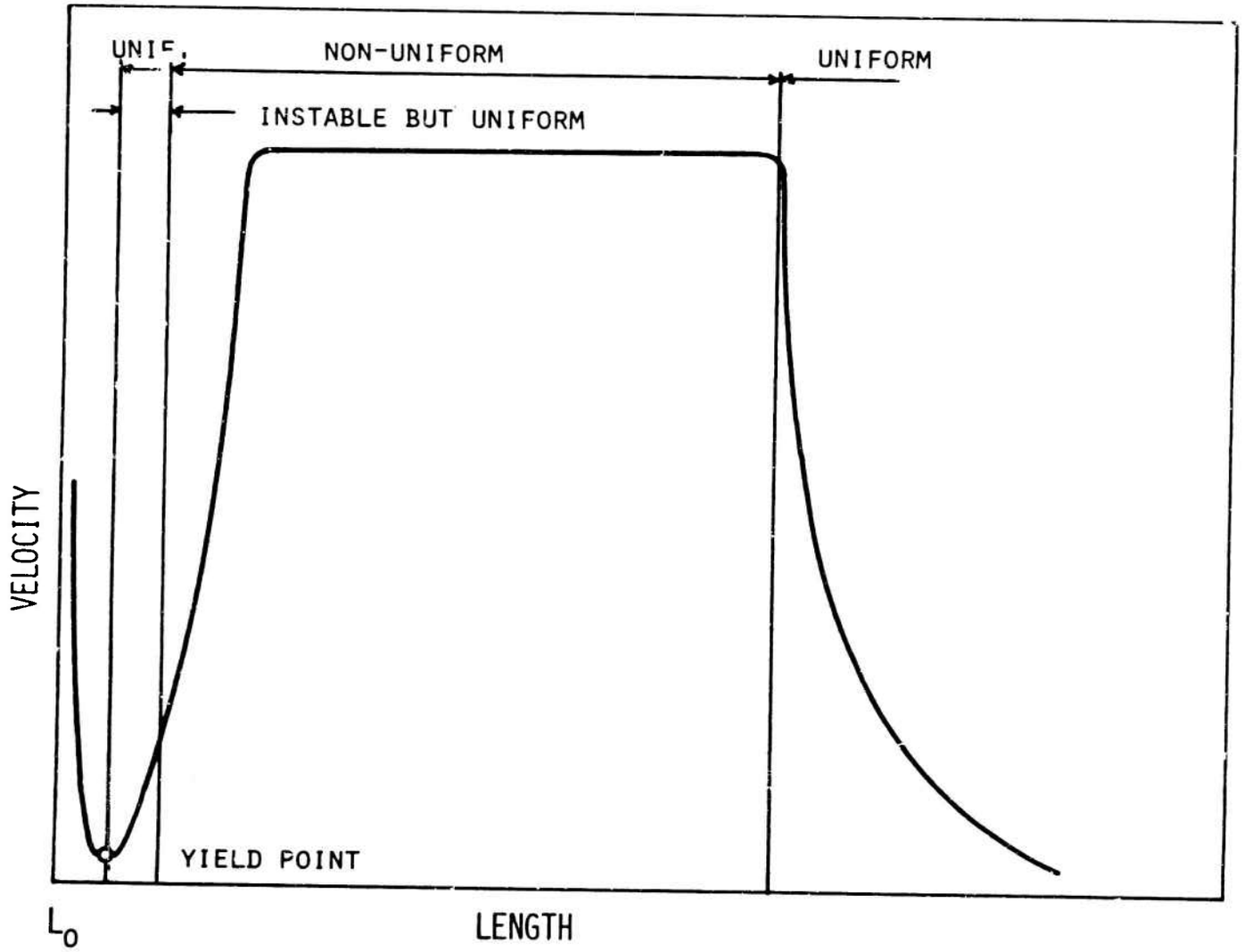

FIG.2.3 VELOCITY VS LENGTH IN CONSTANT LOAD DRAWING

ones vs. length. The character of the resulting curves is shown in Fig. 2.3. The region of most interest as regards initiation of cold drawing is that near the velocity minimum (yield point). From the slope the regions of instability $(\partial v/\partial L)_F > 0$, and stability $(\partial v/\partial L)_F < 0$, are easily recognized.

Experimental Results. The initial part of the L vs. t curves was recorded with an LVDT-amplifier-recorder arrangement (Chapter VIII). The samples were dried to equilibrium moisture content. Other experimental procedures have been described in previous sections and in Chapter VIII.

The families of v vs. L curves derived from L vs. t curves for several stresses are shown in Figs. 2.4 [80°C] and 2.5 [100°C]. The velocities have only been plotted up to length changes at which the strain was uniform. Uniformity of strain was verified by continuous observation of the drawing sample. Table III contains the parameters, which characterize the elastic and plastic behavior. It is apparent that yield strain, elastic modulus and the ratio t_d/t_y are only weakly influenced by stress; delay time, yield time and strain rate at yielding depend exponentially on stress.

Derivation of Stress-Strain Curves. The engineering stress-strain curves of Fig. 2.6 are cross-plots of Figs. 2.4 and 2.5. As they are from uniformly strained specimens, true stress engineering strain curves are derivable assuming thereby that the volume remains constant. The initial parts of the curves have been omitted, as they are not obtainable accurately due to the steep slopes of the v-L curves before yielding.

The 100°C curves derived do not agree well with the measured ones (Fig. 2.2). The latter curves were obtained from non-equilibrium moisture samples. This may explain part of the difference. It may also reflect the poor validity of the equation of state assumption, which has been implied by converting v(L,F = const) to F(L,v = const) data.

Figure (2.3) shows a stability region at high strain $[(\partial v/\partial L)_F < 0]$. This region was not obtainable in many experiments as the samples would fracture when partly drawn. It was also desirable for the study of deformation modes to stop

Table III

Summary of Stress Effects on Constant Load Drawing Parameters of PMMA

Subscripts: e = elastic, y = yield

T °C	σ psi	E x 10^{-5} psi	ε_e %	ε_y %	$\dot{\varepsilon}_y$ %/min	t_y min	t_d min	t_d/t_y	$t_y(\dot{\varepsilon}=\dot{\varepsilon}_y)$ min
80	3750	2.7	1.4		0.023				130
	4000	2.8	1.5	3.4		13.8			
	4000	2.6	1.6	3.3	0.096	13.0	61	4.7	31
	4250	2.6	1.7	4.0	0.104	15.0	50	3.3	29
	4500	2.8	1.6	3.1	0.281	3.7	15.2	4.1	11
	4500	2.5	1.8	3.4	0.35	3.2	13.6	4.3	9
	5000	2.4	2.1	3.7	0.85	1.4	5.5	3.9	3.5
	5500	2.5	2.2	3.7	3.6	0.3	1.3	4.3	0.8
100	1500	2.4	0.6				~1300		
	1750	2.5	0.6	1.6			~390		
	2000	2.4	0.9	1.1	0.054	12.5	75	6.0	39
	2250	2.5	0.9	1.9	0.073	9.6	45	4.7	28
	2500	2.5	1.0	1.9	0.15	4.5	20	4.5	14
	2500	2.4	1.1	1.8	0.102	7.0	24	3.5	20
	3000	2.2	1.3	1.9	0.48	1.5	8.2	5.5	8
	3000	2.4	1.3	2.1	0.25	1.2	5.5	4.6	4
	3500	2.8	1.3	2.4	0.62	0.9	3.3	3.7	3

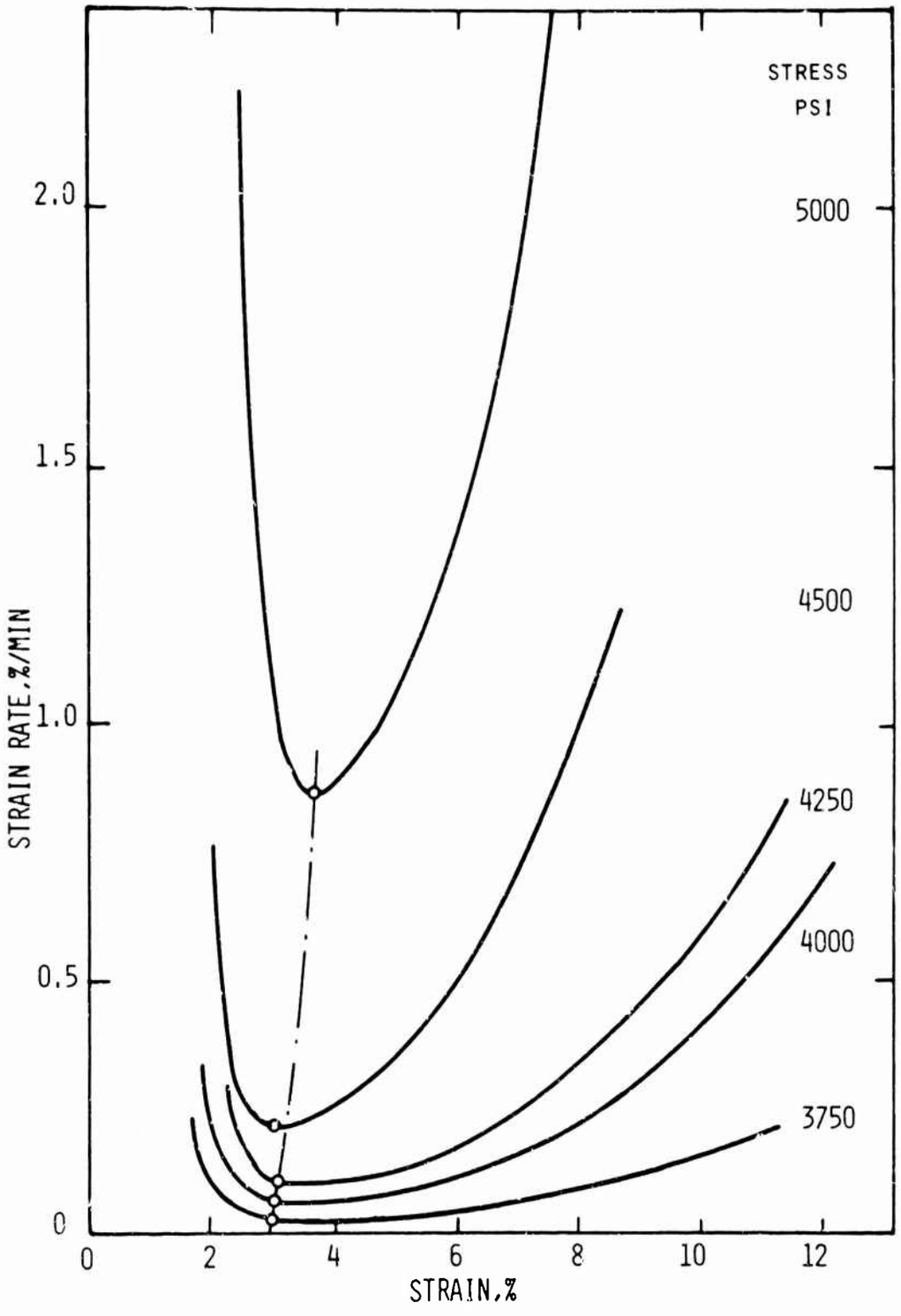

FIG.2.4 STRAIN RATE VS STRAIN IN CONSTANT LOAD DRAWING OF PMMA
TEMPERATURE: 80°C

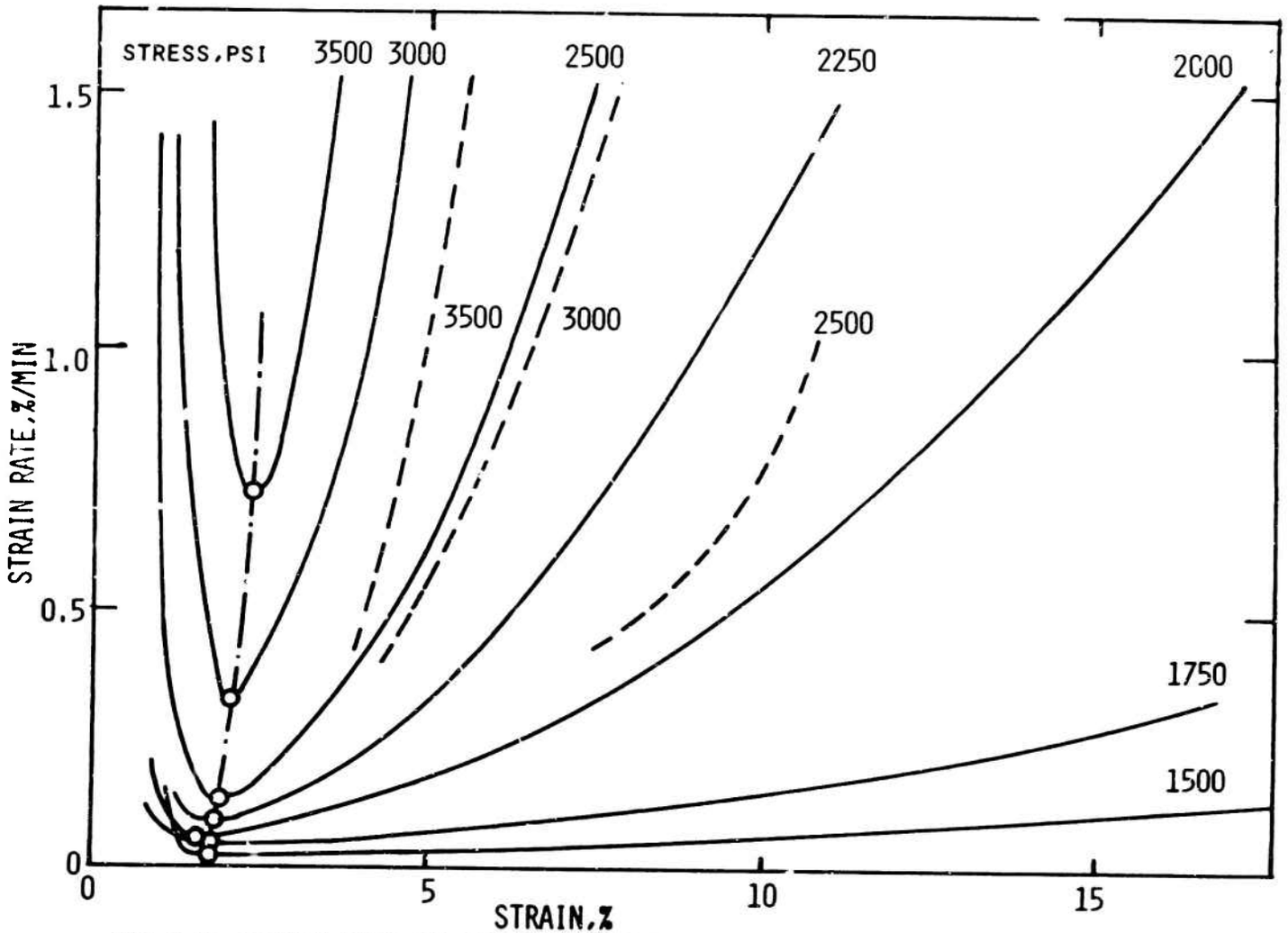

FIG.2.5 STRAIN RATE VS STRAIN FOR PMMA IN CONSTANT LOAD DRAWING
TEMPERATURE: 100°C; BROKEN CURVES: MULTIPLY ORDINATE BY 4

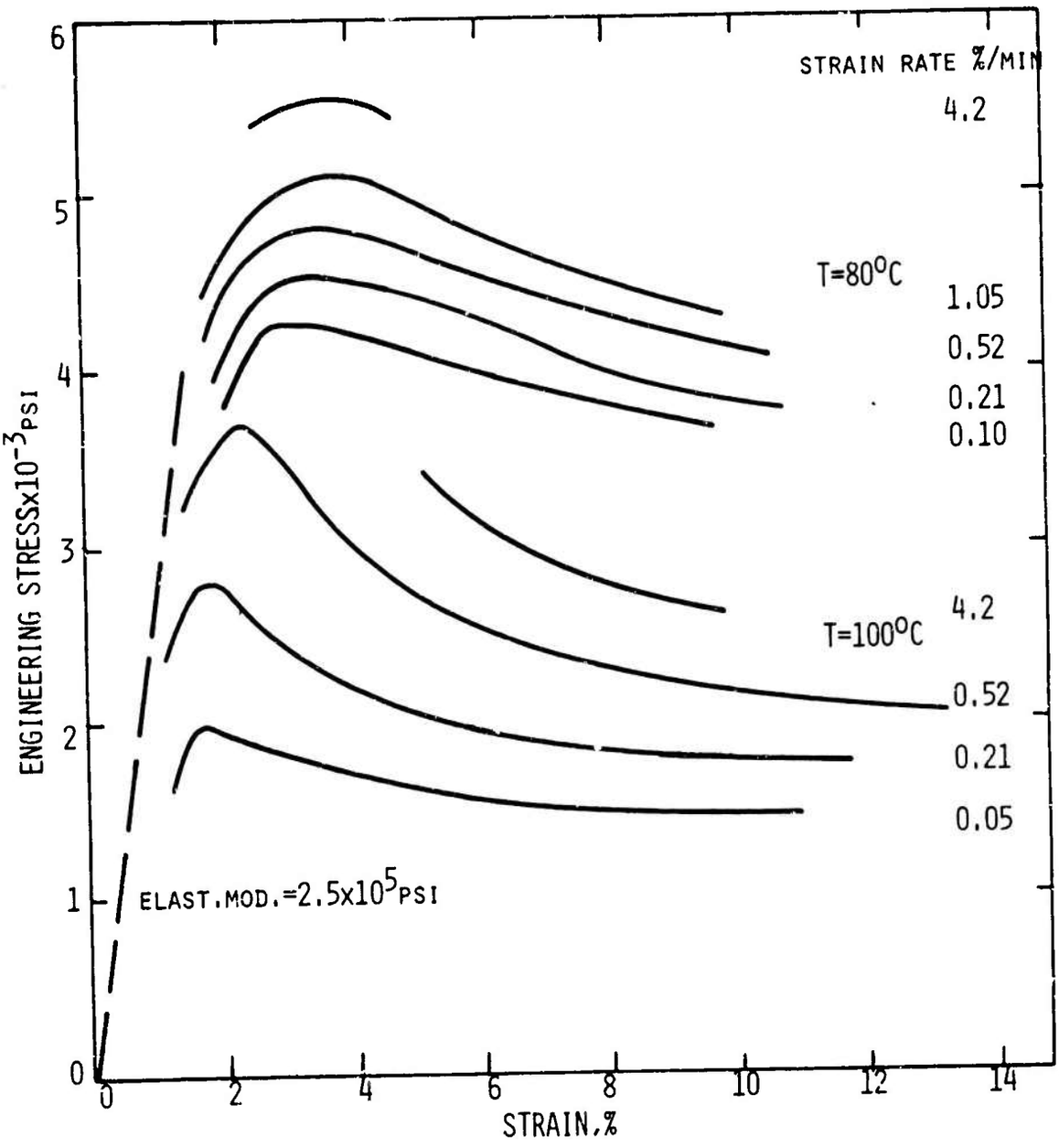

FIG.2.6 ENGINEERING STRESS VS STRAIN CURVES DERIVED FROM VELOCITY VS LENGTH MEASUREMENTS FOR PMMA

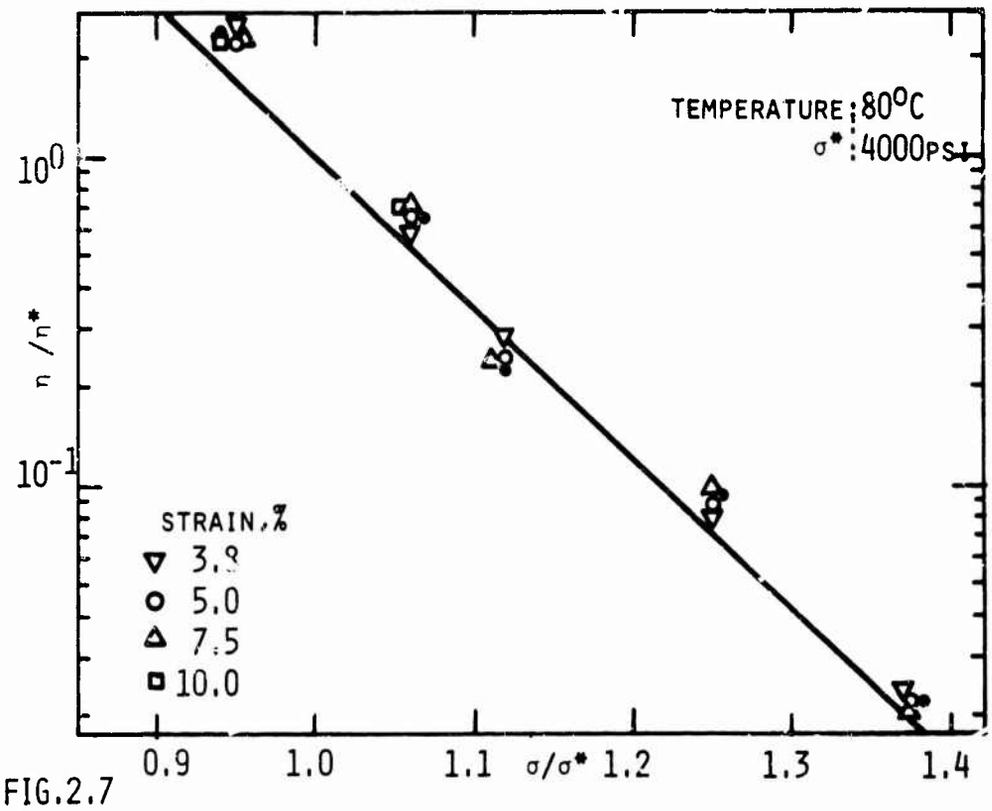

FIG.2.7

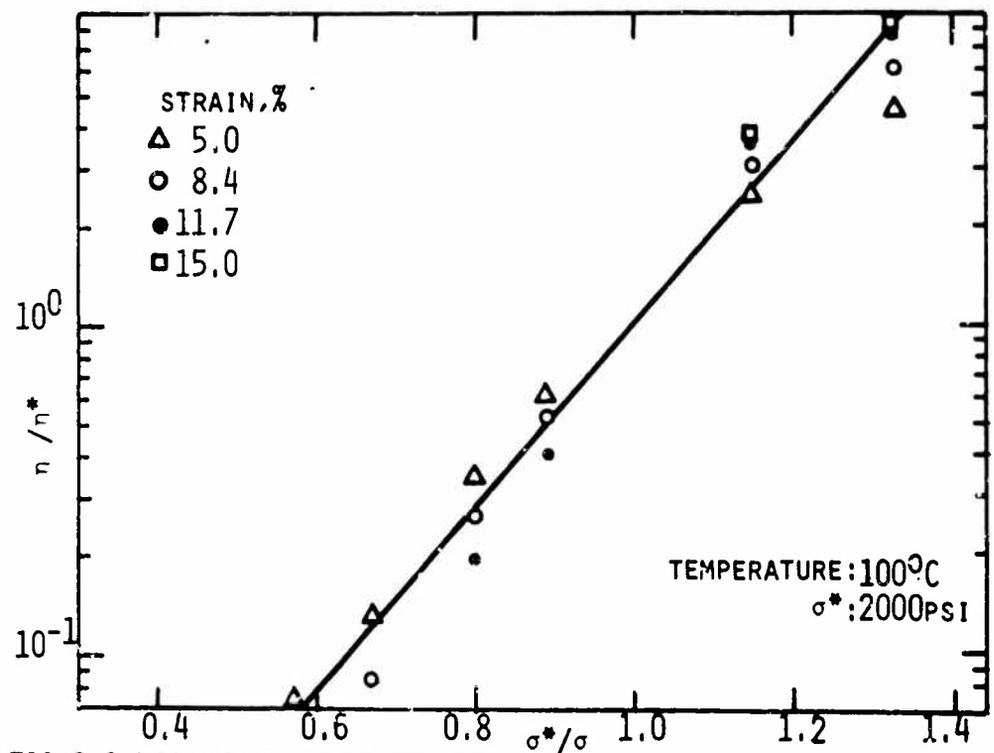

FIG.2.8 VISCOSITY RATIO VS STRESS RATIO FOR PMMA FROM CONSTANT LOAD EXPERIMENTS

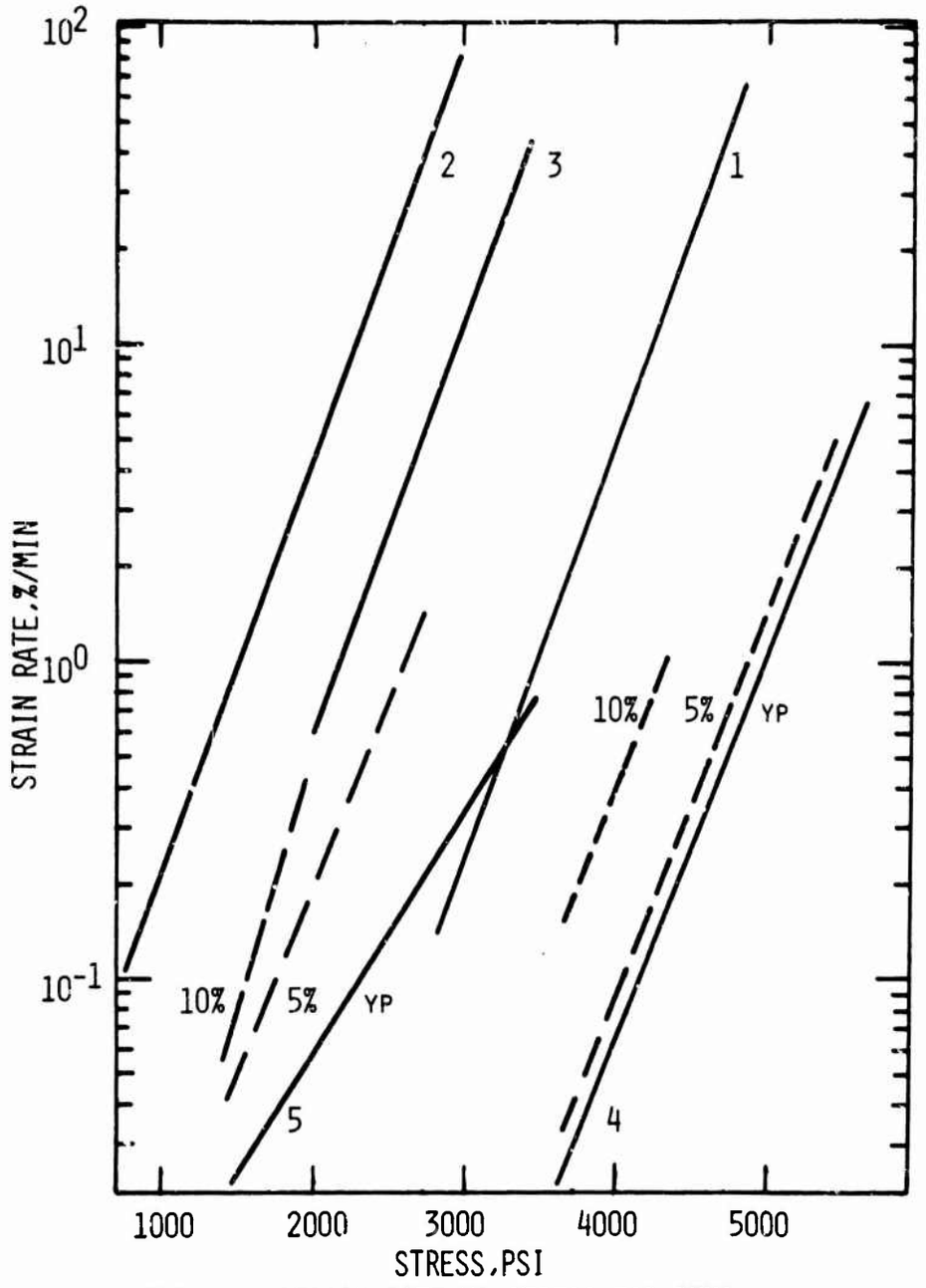

FIG.2.9 STRAIN RATE VS STRESS FOR PMMA

CURVE	TEST	SHOWN	SOURCE	T, °C
1	CONST. STR. RATE	UPPER YIELD STRESS	ROETLING[21]	80
2	" " "	" " "	", EXTRAP.	100
3	" " "	" " "	THIS WORK	100
4	CONST. LOAD	STRAIN RATE AT YP AND 5 AND 10% STR.	" "	80
5	" "		" "	100

the test when a neck was still present. Should the upper stability region be included, a rise in stress-strain curve would ensue for larger strains.

Equations for the Stress Dependence of the v-L Curves. It is attempted to find a mathematical expression to which the experimental data can be fitted. For the time being, strains from zero up to slightly beyond the yield point are excluded. The velocities are converted into viscosities η by the definition of the normal coefficient of viscosity

$$\eta = \frac{\sigma}{\dot{\varepsilon}} \qquad \text{(II-13)}$$

which for uniform strain becomes

$$\eta = \frac{\sigma . L}{v} \qquad \text{(II-14)}$$

Choosing arbitrarily one of the curves, $v^*(L,\sigma^*)$ in each, Fig. 2.4 and Fig. 2.5, the ratio of viscosities of all other curves (η) to that of the chosen curve (η^*) at equal strain is formed.

A plot log (η/η^*) vs. σ/σ^* of the 80° series of curves (Fig. 2.4) reduces all data to a straight line as shown in Fig. 2.7. Log (η/η^*) of the 100°C set of data (Fig. 2.5) is linearized well only if plotted vs. σ^*/σ (Fig. 2.8). In Figure 2.9 this can also be recognized as a divergence of the constant strain lines of the 100°C experiments. This is believed to be a consequence of the vicinity of the glass transition temperature (T_g = 106°C) and will be discussed further in Chapter VI.

The two representations of log (η/η^*), vs. σ/σ^* and vs. σ^*/σ are, for small stress ratios, equally justified for both sets of data.

The two families of curves reduce to

$$T = 80°C: \log \frac{\eta}{\eta^*} = 4.5\left(1 - \frac{\sigma}{4000}\right); \ \sigma^* = 4000 \text{ psi} \qquad \text{(II-15)}$$

$$T = 100°C: \log \frac{\eta}{\eta^*} = 2.8 \left(\frac{2000}{\sigma} - 1\right); \ \sigma^* = 2000 \text{ psi} \qquad \text{(II-16)}$$

The experimental reference stresses had to be different for the two temperatures to obtain easily observable deformation rates.

Combining Equa. 15 or 16 with Equ. 14, one gets,

$$T = 80°C: \frac{v}{v^*} = \frac{\sigma}{4000} \exp.[10.5(\frac{\sigma}{4000} - 1)]; \sigma^* = 4000 \text{ psi} \quad \text{(II-17)}$$

$$T = 100°C: \frac{v}{v^*} = \frac{\sigma}{2000} \exp.[6.4(1 - \frac{2000}{\sigma})]; \sigma^* = 2000 \text{ psi} \quad \text{(II-18)}$$

Equations 17 and 18 will be used in later sections.

Incremental Stress Experiments

As the stress is increased, the polymer becomes less viscous. This is the main content of Equs. 15 and 16. It raises the question if the viscosity drop is a permanent change caused by stress, or if it is reversible on stress removal. Another important question is the influence of time under stress on viscosity.

The following drawing experiments included periods during which load increments were added or subtracted to a constant base load in the region of uniform flow.

The experimental procedures were like the ones described before. The samples were dried at 100°C under vacuum of 0.05 mm Hg for one day. The test temperature was 80°C.

A trace of a recorded length vs. time curve is shown in Fig. 2.10, together with the load step pattern. During one test, a number of different load increments were applied, usually returning to the base load for a period of at least one minute before applying another increment. The immediate deflection upon load change is recovered almost completely after removal of the load increment. The elastic modulus for incremental loading averaged over several experiments is $E_{increm.} - 2 \times 10^5$ psi; that of the unstrained polymer is $E = 2.6 \times 10^5$ psi. The accuracy of $E_{increm.}$ is poor because the small deflections from which this is calculated were not precisely measurable. The new velocity is reached nearly instantaneously. The velocity increases much stronger than proportional to the stress increments. It returns to nearly the value before incremental loading after restoring the initial load. If the additional load is high, or the duration long, the velocity after the

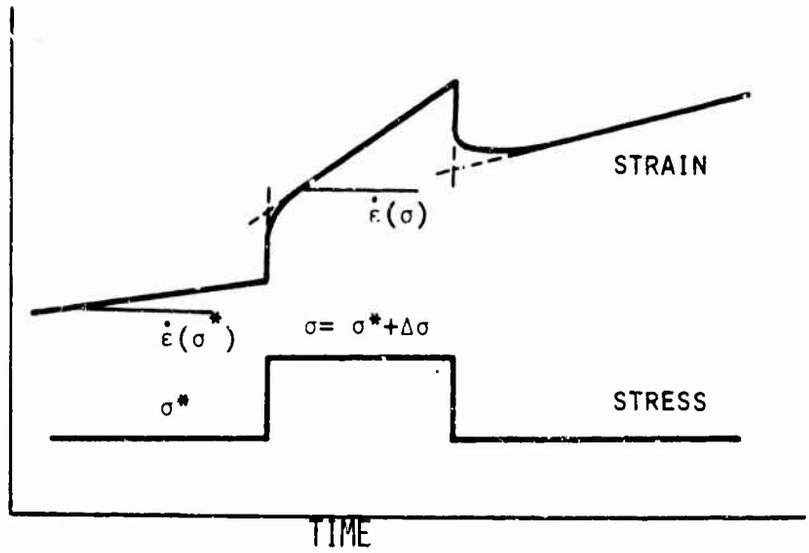

FIG.2.10 CREEP CURVE WITH INCREMENTAL STRESS CHANGE

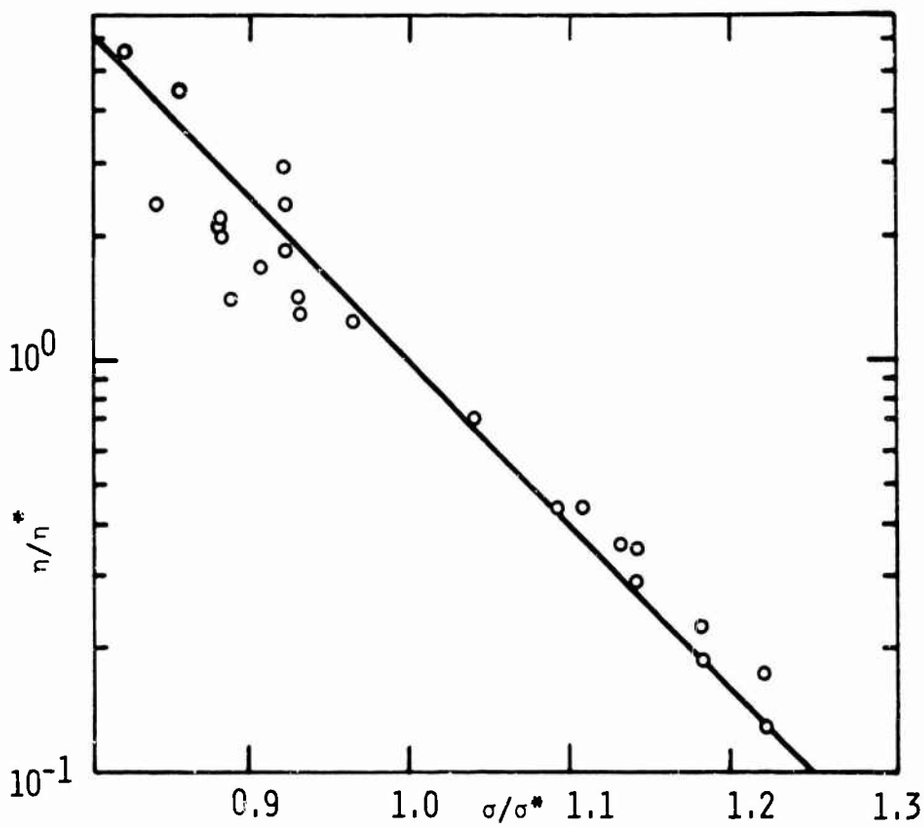

FIG.2.11 VISCOSITY RATIO VS STRESS RATIO FOR PMMA FROM INCREMENTAL STRESS EXPERIMENTS

removal of the increment is higher than before its application. It appears to be approximately that velocity which the sample would have had, had it reached the same strain without the complication in load history.

A plot of viscosity vs. total applied stress gave a very poor correlation. If the viscosity and stress ratios, η/η^*, and σ/σ^*, were used, where η^* is the viscosity when the stress is σ^* immediately before or after the incremental loading, and η is measured during incremental loading under the stress σ, the correlation is quite good (Fig. 2.11). The scatter of points for $\sigma/\sigma^* < 1$ is due to the difficulty in measuring the very small slopes and to time effects, which become relatively more important at slow draw rates. The data are represented by

$$T = 80°C: \log \frac{\eta}{\eta^*} = 3.9\left(1 - \frac{\sigma}{4000}\right); \sigma^* = 4000 \text{ psi} \quad \text{(II-19)}$$

The effect of stress increments is a rapid elastic deflection and an exponential reversible change in viscosity. Transient effects are short and small and have not been evaluated. Stress and viscosity are related through the same function which was found to describe the stress dependence of the v vs. L curves for the same temperature.

Stress and Strain Softening during Yielding.

Müller[23] maintains that cold drawing in constant strain rate tests is a consequence of nonlinear stress-softening. The viscosity of PVC, according to his data, is 10^{14} poise at 30°C under nearly 1000 psi and it drops to 10^{12} poise at several thousand psi. If the viscosity were influenced by stress only, softening of the polymer should be complete right after the stress is applied in the constant load experiment. Yet in this study it is found to drop by 2 or 3 orders of magnitude during straining.

The alternative view, that cold drawing is only due to the straining, is held by Vincent[5]. He explains cold drawing as a reduction of modulus with strain, which at some strain leads to a mechanical instability. The modulus drop is ascribed to breaking of secondary bonds in the polymer, which is thought of as a network of such bonds.

A trivial reason for cold drawing could be the softening of the polymer because of the stress increase alone. Under constant load the stress changes along with the strain by the factor $(1 + \varepsilon)$, constant volume assumed. This possibility is examined below.

Writing Equ. (1) in form of stress and strain, it becomes

$$\dot{\varepsilon} = \dot{\varepsilon}(\varepsilon,\sigma). \qquad \text{(II-20)}$$

By partial differentiation of Equ. 20, holding F constant, one derives

$$\left(\frac{\partial\dot{\varepsilon}}{\partial\varepsilon}\right)_F = \left(\frac{\partial\dot{\varepsilon}}{\partial\sigma}\right)_\varepsilon \cdot \sigma + \left(\frac{\partial\dot{\varepsilon}}{\partial\varepsilon}\right)_\sigma. \qquad \text{(II-21)}$$

For uniform strain $d\dot{\varepsilon} = dv/L$ and $d\varepsilon = dL/L$, and together with Equ. 21

$$\left(\frac{\partial v}{\partial L}\right)_F = \left(\frac{\partial v}{\partial\sigma}\right)_\varepsilon \cdot \frac{\sigma}{L} + \left(\frac{\partial v}{\partial L}\right)_\sigma. \qquad \text{(II-22)}$$

If the supposition that the stress increase by the factor $(1 + \varepsilon)$ causes drawing is to be correct, the second term on the right hand side of the two equations must be zero, or negative. From either one of the two equations and the experimental data of Figs. 2.4, 2.5, or 2.6, it can be seen, by using numerical values, that the first terms of the Equs. 21 and 22 account only for a fraction of the measured velocity or strain rate increase. The assumption that cold drawing is caused by cross-sectional decrease is therefore wrong. In addition, one must conclude that cold drawing also takes place in a constant stress experiment.

At a stress slightly below the deformation mode boundary (eg Figs. 1.3 and 1.8) the stress increase on straining in the constant load case may, nevertheless, be the cause for drawing to set in instead of continued creep.

An important consequence of the above discussion is that the velocity is a function of stress and strain. The stress dependence of the velocity within the uniform strain region beyond the yield point is given by Equs. 17 and 18, which are of the form

$$\frac{v}{v^*} = \frac{\sigma}{\sigma^*}\exp\left[\phi\left(\frac{\sigma}{\sigma^*}\right)\right] \qquad \text{(II-23)}$$

with $\phi = a(\frac{\sigma}{\sigma^*} - 1)$, [Equ.(17)], or $\phi = a(1 - \frac{\sigma^*}{\sigma})$, [Equ.(18)]. The strain function is implicit in the velocity of the arbitrary reference curve $v^*(\varepsilon, F = \text{const.})$. From this velocity v^* the others for stresses different from σ^* can be calculated by multiplying it by the left hand side of Equ. 23. This expression is a function of stress alone and determines the shift of the deformation rate with stress.

v^*, if taken from a constant load experiment, still contains the stress dependence due to cross-section changes. From a constant stress drawing experiment the more distinct $v^*(\varepsilon, \sigma = \text{const.})$ could be obtained.

The validity range for exponential stress softening implied by Equ. 23 has not been determined. The transition boundary from drawing to creep, discussed earlier, is of significance in this respect: stresses below the boundary stress give curves with $(\partial v/\partial L)_F < 0$ everywhere. They cannot, therefore, be derived by Equ. 23 from the higher stress curves, for which $(\partial v/\partial L)_F > 0$ beyond the yield point. The transition stress is thus the lowest possible boundary for the exponential stress softening.

Prediction of the Influence of Stress on Delay Time

The delay time has been a convenient empirical parameter to describe the time dependence of yielding under a constant load. It is a well defined time because of the nearly discontinuous velocity increase which marks the end of the induction period. The time to reach strains in the vicinity of 10% or more is therefore nearly equal to the delay time, because the time consuming part of the deformation is the initial one.

The time required to strain a specimen by ε is calculated by

$$t_\varepsilon = \int_0^{\varepsilon \cdot Lo} \frac{dL}{v} = \int_0^{\varepsilon} \frac{d\varepsilon}{\dot{\varepsilon}} \qquad \text{(II-24)}$$

The elastic strain is disregarded. It is, compared to the plastic strains, small and occurs rapidly, not contributing much to t_ε. Substituting v from Equ. 23 one obtains

$$t_\varepsilon = \int_0^{\varepsilon Lo} \frac{dL}{v^*(\varepsilon,F^*)} \cdot \frac{\sigma^*}{\sigma} \exp\left[-\phi\left(\frac{\sigma}{\sigma^*}\right)\right] \qquad \text{(II-25)}$$

where ϕ is either $a(\frac{\sigma^*}{\sigma} - 1)$ or $a(1 - \frac{\sigma}{\sigma^*})$ as discussed in an earlier section of this chapter.

For the reference curve, one has $\sigma^* = \sigma$ and the stress factor is 1. Therefore

$$t_\varepsilon = \int_0^{\varepsilon Lo} \frac{dL}{v^*(\varepsilon,F^*)} = t^*_\varepsilon \qquad \text{(II-26)}$$

which is the time to reach ε under the stress of the reference curve. For all other stresses the coefficient is $\neq 1$. It is a constant modifying factor with respect to the integrand. The time t_ε for a stress σ is

$$t_\varepsilon = t^*_\varepsilon \cdot \frac{\sigma^*}{\sigma} \exp\left[-\phi\left(\frac{\sigma}{\sigma^*}\right)\right] \qquad \text{(II-27)}$$

The stress ratio enters only, it is therefore of no consequence that the stress increases with strain. It effects, however, the velocity $v^*(\varepsilon,F^*)$. If t^*_ε is determined by experiment, this is of no concern. Equation 27 is only justified in the uniform strain region which extends up to at least 10% strain for PMMA.

Equation 27 requires the stress dependence of the time t_ε to be the same as that of velocity. This has been verified by plotting delay times together with the curves predicted from it (Fig. 1.9). It is worth noticing that the 100°C data are again represented by using $\frac{\sigma^*}{\sigma}$ instead of $\frac{\sigma}{\sigma^*}$ as correlating parameters.

For the integration of Equ. 26 it has been assumed that v^* has the same stress dependence from zero strain on. In the region below the yield point this cannot be investigated. The agreement between prediction and measurement is a point in favor of the correctness of the assumption.

Yielding as Superposition of Two Monotonic Processes

The families of v-L curves for various loads (Figs. 2.4 and 2.5) indicate that the rising branches on the right start

from near the origin and the falling branches to the left of the yield point drop to zero. This suggests the interpretation that the velocity v is the sum of two components

$$v = v_{VE} + v_V \tag{II-28}$$

v_{VE} is mainly responsible for the left hand part and goes to zero at high strains. v_V accounts for the right hand branch and increases with strain. From the definition of the yield point $(\partial v/\partial L)_F = 0$ one gets

$$\left(\frac{\partial v_{VE}}{\partial L}\right)_F = -\left(\frac{\partial v_V}{\partial L}\right)_F \tag{II-29}$$

At the yield point the velocity change of one branch is equal and of opposite sign to that of the other.

The yield point is a singularity in behavior in both constant velocity and constant load test. This singularity is resolved by the interpretation given as a result of the superposition of two monotonic processes. The delayed elastic process (v_{VE}) is expected to be associated with the elastic strain of bonds in much the same way as in creep. At low enough stress it is observed by itself as creep. The second process contributing v_V must be the important one for drawing. For it to occur, the stress must be above some critical value. It prevails beyond the yield point over the other. Its stress dependency is given by the exponential of Equ. 23, v* contains the strain softening function.

Equations 28 and 29 are not sufficient to separate the two branches without further assumptions. Figure 2.12 shows the separation in principle.

Equation 28 is represented by a model of the type shown in Figure 2.13 which, to conform to physical reality must, in all likelihood, be nonlinear in all elements. The spring E_2 accounts for the fast elastic response, the Voigt element (η_1, E_1) represents v_{VE} and the dashpot (η_2) v_V. η_2 is given by Equ. 15 or 16, the strain function is implicit in η^*.

Drawing under constant stress. For simplicity E_1, E_2 and η_1 of Fig. 2.13 are assumed to be linear. Elastic, delayed elastic

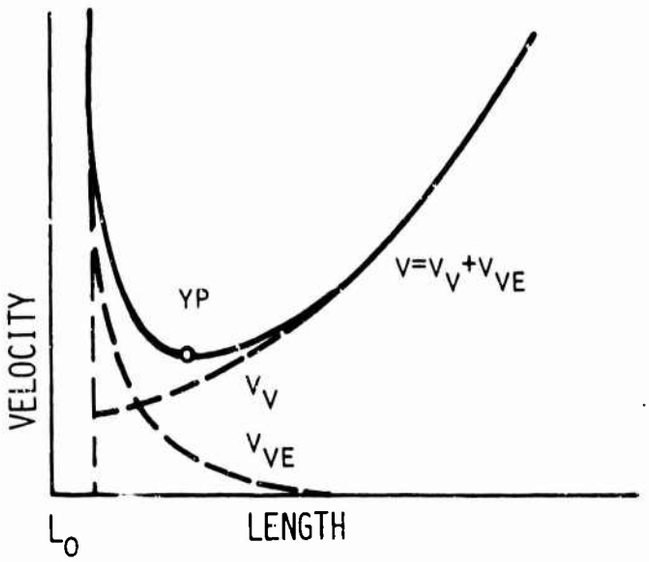

FIG.2.12 SEPARATION OF VELOCITY INTO VISCOELASTIC AND VISCOUS COMPONENT

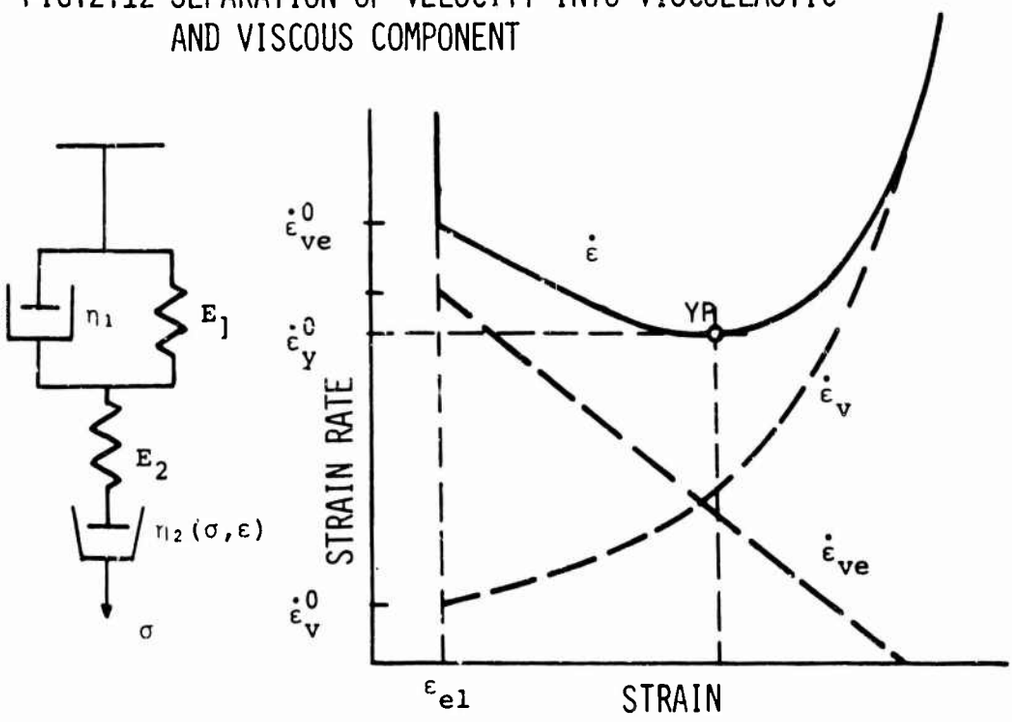

FIG.2.13 MODEL EXPLAINING YIELDING AS SUPERPOSITION OF DELAYED ELASTIC AND VISCOUS PROCESS FOR THE EXAMPLE OF CONSTANT STRESS. THE VISCOSITY OF THE VISCOUS PROCESS DEPENDS ON STRESS AND STRAIN.

and viscous strains are additive and independent of one another under constant stress. A schematic plot of $\dot{\varepsilon}$ vs. ε is shown in Fig. 2.13. The sum of all strains gives an initial slowing down and a subsequent acceleration. The model has a yield point where

$$\frac{d\dot{\varepsilon}}{d\varepsilon} = \frac{d\dot{\varepsilon}_{VE}}{d\varepsilon} + \frac{d\dot{\varepsilon}_{V}}{d\varepsilon} = 0 \qquad \text{(II-30)}$$

For the Voigt element

$$\dot{\varepsilon}_1 = \frac{\sigma - \varepsilon_1 E_1}{\eta_1} \qquad \text{(II-31)}$$

and the dashpot

$$\dot{\varepsilon}_2 = \frac{\sigma}{\eta_2(\varepsilon_2, \sigma)} \qquad \text{(II-32)}$$

By differentiation and observing that $\varepsilon_t = \varepsilon_1 + \varepsilon_2$ Equations 30, 31, and 32 give $d\dot{\varepsilon}/d\varepsilon = - E_1/\eta_1 - d \ln \eta_2/dt$.
With the retardation time $\tau = \eta_1/E_1$, the condition for yielding is

$$- \frac{d \ln \eta_2}{dt} = \frac{1}{\tau} \qquad \text{(II-33)}$$

For yielding to occur, the drop of $\ln \eta_2$ with time must be equal to or greater than the reciprocal retardation time.

From Figure 2.13 it is evident how strain and yield velocity are influenced qualitatively if the viscous or elastic parameters of the model change. Table IV summarizes these trends.

Table IV
Shift of Yield Strain and Strain Rate with
Change in Model Parameters (Fig. 2.13)

Fixed	Increased	ε_y	$\dot{\varepsilon}_y$
τ, $\dot{\varepsilon}^o_{VE}$	$d \ln \eta_2/dt$	↓	↑
τ, $\eta_2(\varepsilon)$	$\dot{\varepsilon}^o_{VE}$	↑	↑
$\eta_2(\varepsilon)$, $\dot{\varepsilon}^o_{VE}$	τ	↑	↑

For constant strain rate the model response is not as straightforward as the strains are now coupled, requiring only that the

sum of all strains is the external strain and both ε and σ, of both of which η is a function, are varying. Provided the viscosity decreases sufficiently with extension, the stress to sustain constant strain rate will begin to drop at some point.

Test of the Permissibility of the Equation of of State Supposition for PMMA

There is, a priori, equal justification to investigate stress-strain behavior of polymers by constant rate or constant load experiments, one yielding $F = F(L,v)$, the other $v = v(L,F)$. One type of test would suffice if the material obeys a relation $(F,v,L) = 0$ (1).

The model of Fig. 2.13 which describes yielding does not follow such an equation. The dashpot can be strained for example by a sequence of stress and stress relaxation periods in such a way that force and velocity are not longer uniquely related to length.

To test the equation of state free from the simplifications implicit in the model, available test results from both tests are compared. One is left with yield point data: from the constant rate test uniform strain data are not obtainable above the yield strain, and the ones from the constant load experiment are not accurate below it (because of the differentiation to get v).

For yielding, $(\partial F/\partial L)_v$ and $(\partial v/\partial L)_F$ must disappear simultaneously if the equation of state exists. By either yield condition one of the variables v, F or L is determined and one gets for the yield point $v_y = v_y(F_y)$ and other analogous equations between two of the variables v_y, F_y and L_y.

Figure 2.9 contains log yield velocity vs. yield stress curves for both types of measurements for PMMA. The drawn out curves are for the yield point, the broken ones for strain rates at strains above the yield strain in constant load tests. The 80°C constant strain rate data (curve 1) have been reproduced from a publication by Roetling[21], one of the 100°C curves (2) has been extrapolated from his data.

Roetling's results are from injection-molded bars from a polymer with $\bar{M}_w = 3.22 \times 10^5$ and with $\bar{M}_n = 1.60 \times 10^5$. The

molecular weight of the cast polymer of this present study is at least by a factor 10 higher. The amount of moisture absorbed, if any, is not reported in Ref. (21). The 100°C constant velocity data of the present work (3) were measured with specimens containing about 1% moisture, the constant force curves (4,5) were from dried polymer. The influence of molecular weight on yield stress of PMMA is not known; that of water has been measured and it accounts for most of the difference between curves 1 and 4 of Fig. 2.9.

Excepting curves 5, the velocity change with stress is the same in all cases. It cannot be decided if the lines of equal temperature also coincide, which is necessary for Equation (1) to be satisfied, because available data are insufficient to adjust for moisture and molecular weight differences.

The 100°C curves (5) diverge for low strains and assume equal slopes for high strain. The increase of yield velocity with stress is less than that of the other curves. The reason is probably the vicinity of the glass transition temperature, near which recovery of a more stable glass structure becomes rapid enough to take place in experimental time.

This leaves the question open why the constant velocity tests at the same temperature do not show anomalous behavior. The discussion of structure recovery will be resumed in Chapter VI.

Equation (1) also requires that the yield strains are the same in both tests at equal strain rate. Figure 2.14 shows the yield strains of 100°C constant load experiments and the ones of the constant strain rate curves of Fig. 2.2 at the same temperatures. Yielding is, in the latter case, clearly at higher strains than under constant load.

The constant load yielding velocity is the minimum velocity of the experiment. Therefore, in the constant velocity test with yield velocity equal for both tests, more time is needed to reach the yield point. This time has been calculated from the Table III data, assuming that the yield strain was that given in the table. The time is about three-fold higher than the time to yield in the constant load test. Taking also into account that the yield strain for constant velocity is 50 to

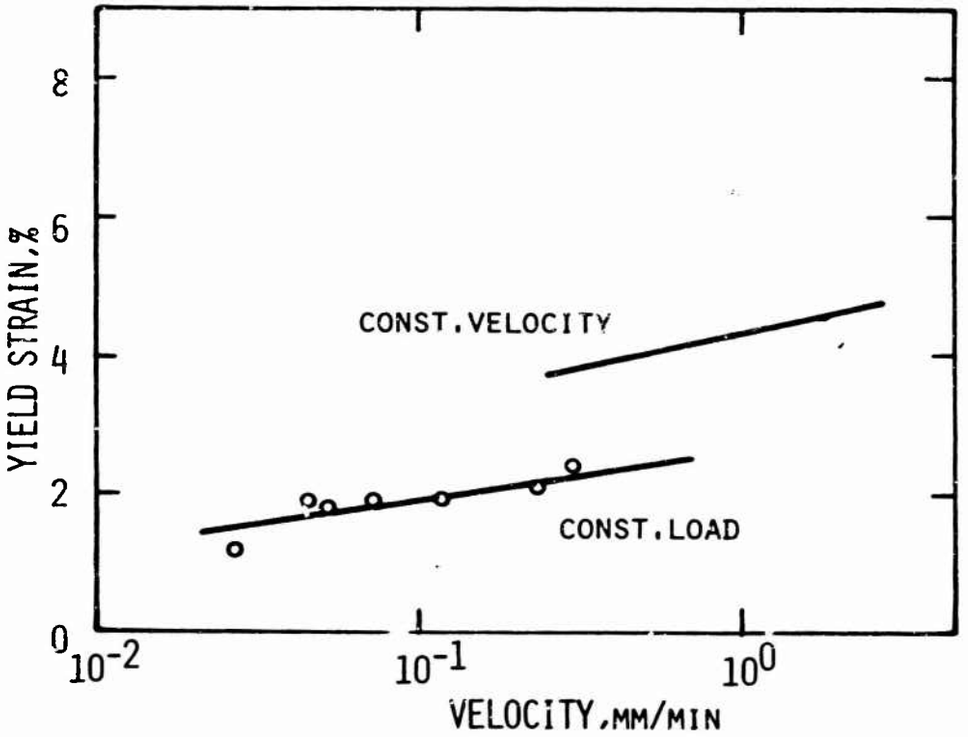

FIG.2.14 YIELD STRAIN VS EXTENSION VELOCITY FOR PMMA AT 100°C IN CONST.VELOCITY AND CONST.LOAD TEST.GAUGE LENGTH:48 MM

100% higher, the time ratio becomes 4 to 6. There is no basis available for judging the influence of this time difference on the yield point variables. From the time dependence of visco-elastic processes in general one should expect that the difference in time to yield also affects yield parameters.

A definitive answer if the equation of state assumption is correct and if it were not how much the predictions, based on it, are in error is not possible from the foregoing. Differences in molecular weight and moisture content and the lack of constant velocity data prevent a conclusive comparison between the different measurements. The data gathered contain evidence for and against the equation of state supposition: The stress dependence of the yield velocity of PMMA is the same in both types of tests and the stress dependence of delay time is predicted correctly from constant velocity results. On the other hand, the yield strains of the two tests disagree.

CHAPTER III

THE INFLUENCE OF THERMAL HISTORY ON THE COLD DRAWING OF GLASSY PMMA

Introduction

Polymer properties in the glassy state depend on the conditions of vitrification. This is evident from published work on creep[22], stress relaxation[27], and loss tangent measurements[28]. In the following section an investigation will be made of the effects that heat treatments near T_g have on the cold drawing properties of glassy PMMA.

A brief review of relevant experimental results and theories will be given first. The transition from the supercooled liquid to the glass is found by measuring properties related to molecular motion. These properties, for example volume or enthalpy, have a rapid, nearly discontinuous change in the derivative with respect to temperature at the transition. The temperature at which the discontinuity occurs is observed to increase when the rate of change of temperature is higher during the experiment.

As an example, one may use volume contraction on cooling. At a characteristic temperature T_g the volume vs. temperature curve changes its slope to a lower value (Fig. 3.1). Increasing the rate of cooling moves T_g up on the temperature scale and a less dense glass is obtained than in the slow experiment. The structural changes necessary for the contraction are associated with a relaxation time, which is larger than the time interval chosen to measure T_g, the glass transition temperature. Below T_g further relaxation towards an equilibrium volume takes place. The derivatives of the properties with respect to time are not zero, the glass is therefore not in a thermodynamic equilibrium. The equilibrium volume is only reached in observable time, if the temperature is in the vicinity of T_g.

Two views have been presented to explain the increase of relaxation times near T_g, a kinetic one and a thermodynamic one. Fox and Flory[29] and Williams, Landel and Ferry[30] maintain that the relaxation time is related to free volume. In a

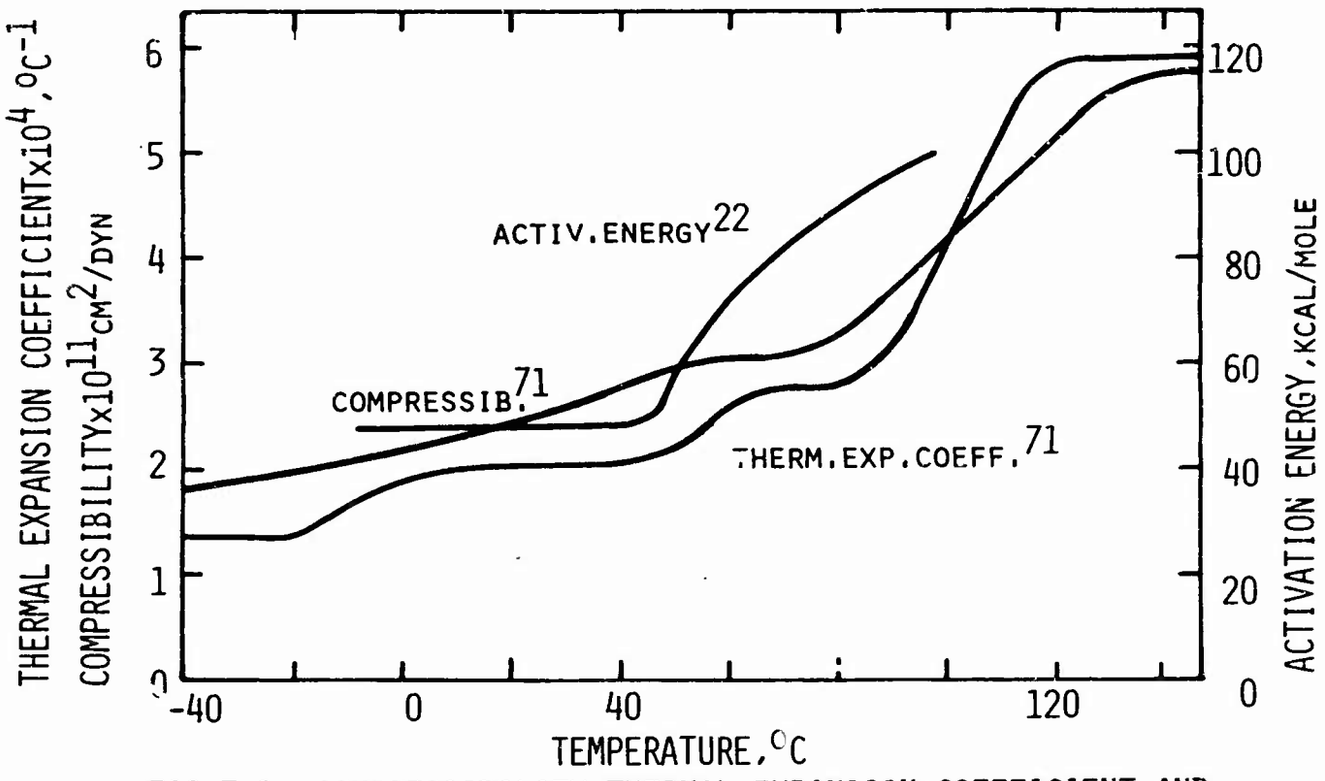

FIG.3.1 COMPRESSIBILITY, THERMAL EXPANSION COEFFICIENT AND ACTIVATION ENERGY FOR VISCOUS FLOW OF PMMA VS TEMPERATURE (REPRODUCED FROM LITERATURE)

second theory, Gibbs and DiMarzio[31,32] state that the glass transition is the consequence of the approach to a thermodynamic transition at which the number of possible chain conformations decreases to one. The present results will be discussed in terms of volume changes.

In the transition region $T_g \leq T \leq T_g + 100°C$, shear viscosity and other related properties of many supercooled liquids and amorphous polymers are determined solely by the free volume, v_f. It is an operational parameter[33(a)] which is not directly measurable and therefore poorly defined. As contrasted to occupied volume, free volume has the physical significance of being the volume available for molecular rearrangements.

The role of free volume in influencing properties below T_g is less clear. Ainbinder et al[34] measured stress-strain curves of PMMA at room temperature under hydrostatic pressure up to 2000 kg/cm^2 and found an increase of flow stress with pressure (by a factor of 2). It is expected that these data cannot be discussed in terms of free volume in a simple manner as the pressure will effect the occupied volume also.

Volume changes during isothermal contraction in the glassy region are entirely due to changes in free volume[35], if they occur at constant pressure and temperature: $(dv)_{P,T} = dv_f$.

The influence of thermal pretreatment on the properties of polymeric glasses has been noted in several publications. The effects were explained in terms of volume changes. McLoughlin and Tobolsky[27] found that the rate of stress relaxation of PMMA below T_g is the higher the faster the polymer is cooled through the transition temperature region. Sherby and Dorn[22] report on creep experiments with the same polymer which manifest higher creep rates for quenched specimens than for annealed ones. Illers and Jenckel[28] measured on glassy polystyrene a higher loss tangent for a sample rapidly quenched from above its T_g than for one slowly cooled.

Kovacs et al[35] have made dynamic shear measurements during isothermal contraction of polyvinyl acetate below T_g and correlated modulus and volume measurements. In this study, the relaxation times were essentially a function of free volume alone.

These reported experiments, with one exception (Ref. 34), were at low strains. In the experiments which follow, a study was undertaken on the effect of the initial stability of the glass, as produced by temperature treatments, on the behavior under cold drawing conditions. Conversely, cold drawing parameters were used as a means of investigating the mechanical stability of the glass with a view towards determining the effectiveness of the annealing conditions.

Two experiments were used to change the volume of the glass by means of thermal treatments:

1. Cooling the polymer from above the T_g at an approximately constant rate to below T_g (Type 1),

2. Cooling the polymer from above T_g rapidly to below T_g and holding it at a temperature at which the relaxation time is still within the experimental time scale (Type 2).

[Kovac's[36] nomenclature includes other types of "stabilization". His type 1a and type 1b correspond here to type 1 and type 2 treatments respectively.]

Experimental and Results

Annealing; Type 1 Experiments. To erase previous history and to effect drying the samples were first kept for several hours in an air oven at 150°C, then cooled at various rates. Milled specimens rather than the polymer sheets were treated. Cooling methods and rates are recorded in Table V.

The dry ice-heptane cooled specimens were observed to be optically anisotropic, when viewed in the thickness direction between crossed polarizers. Inspection of thin sections (1/16 in.) cut perpendicular to the specimen axis, and polished at the new section surfaces, revealed a skin of birefringent material at the circumference of the cross-section and an optically isotropic core. The areas of the core comprised nearly 50% of the total area. Specimens quenched in room temperature heptane were also birefringent, the skin was thinner in this case. Cooling in air at room temperature, with the samples in a vertical position, gave cptically isotropic cross-sections. The quality of the specimen surfaces suffered in the

Table V

Cooling Rates for Type 1 Treatments

Method of Cooling	Rate °C/sec.		Heat Transfer Coefficient h cal/cm^2 sec °C	
Immersion in dry ice-heptane	16	(1)	7.6×10^{-3}	(2)
Exposure to room air, vertical	0.3	(1)	3.8×10^{-4}	(2)
Oven cooled (oven switched off)	0.02	(3)		
Oven cooled with constant rate temperature change	0.008			(4)
Oven cooled with constant rate temperature change	0.0008			(4)

(1) Calculated value for center of specimen when passing through T_g.

(2) Calculated from cooling curves measured under equal conditions by embedding a 0.009 in. thermocouple in the middle of a 0.120 in. PMMA sheet. Cooling rates (1) have been obtained from h and Heisler charts[37] for the center of the specimen.

(3) Measured with thermocouple as (2), uniform T assumed within specimen.

(4) Oven temperature measured.

cases of quenching in liquid. Many wavy lines became visible on the surface, due to small localized changes in thickness.

The different temperature histories were clearly reflected in cold drawing behavior under constant load. The quenched samples had a shorter delay time than the slowly cooled ones.

In these exploratory experiments, the slowly cooled samples were kept for several hours near room conditions. Having been dried initially, they picked up an unknown amount of moisture during annealing. Thus, the property changes measured were not entirely due to thermal history. Treatment of sheets, from which later specimens were milled improved the specimen uniformity, but did not eliminate the moisture problem. For the finished specimens could not be dried, of course, without destroying the previous thermal history.

Because of these various difficulties, the Type 1 experiments were abandoned. The only compelling reason was that the very rapid quench experiments did not give optical isotropy.

Annealing; Type 2 Experiments. The tensile specimens were placed in individual 16 mm Pyrex tubes, sealed on one end and drawn out thin on the other end. Several such tubes were connected at one time to a mechanical vacuum pump. The thick sections of the tubes were placed vertically in a temperature controlled stirred oil bath, thus suspending the specimens in such a way that they would hang without touching the glass walls. The system was repeatedly evacuated and flushed with nitrogen at the beginning of drying. The vacuum was measured with a McLeod gauge. The samples were dried for 24 hours at 140°C under 0.05 mm Hg. or less. After drying, the open ends of the tubes were sealed, still maintaining vacuum. At this point, most of the samples were cooled to room temperature. This constituted the quenching step [indirect quench]. The cooling rate provided by natural convection was low enough to preserve optical isotropy. Later it became desirable to avoid the complication in vitrification inherent in cooling to T_R and keeping the specimens at T_R for some time before they were annealed. Several samples were therefore cooled from 140°C directly to the annealing temperature [direct quench].

During drying, a fine condensate film formed at the thin cool end of the evacuated Pyrex tubes, which appeared to be an oily liquid. It was found from the weight loss to be about 0.8% by polymer weight. The lost substance could have been a plasticizer, or a UV stabilizer; in view of the quantity the first is more probable. The polymer of the annealing series of experiments is therefore not entirely comparable to that of the experiments without 140°C treatment. Drying at 100°C removes essentially only water.

For annealing the sample tubes were placed in a temperature controlled oil bath. The annealing temperatures ranged from 80 to 110°C, and the times were for 0.24, 2.4, 24 and 240 hours. Subsequently, the samples were cooled in room air. The time lag between annealing and testing did not have a recognizable effect on test results. The storage time at room temperature before annealing in the indirect quench experiments was also without influence on the drawing results. There was, however, a difference between indirect and direct quench tests.

The annealed specimens and the unannealed but dried and quenched controls were tested by constant load drawing at 80°C and under 4000 psi. The annealing effect at 80°C is sufficiently small so that no drastic property changes occur in experimental time. The 4000 psi stress was chosen as it gave conveniently measurable times for drawing. The sample tubes were opened immediately before the drawing test. The longest drawing times were below one hour. The relative humidity at 80°C was about 4% (Table 1). Moisture had therefore little, if any, influence on the results.

The length vs. time curves for the 24-hour annealing treatment of the indirect and of the direct quench samples have been reproduced on a reduced scale in Figs. 3.2 and 3.3 respectively. Figure 3.2 also contains the curve of a quenched unannealed specimen and one for a 100°C/240 hour run for comparison. Above 10 minutes, the time scale has been compressed by a factor 10/3. Some duplicate experiments have been included (Fig. 3.2: 80, 100, 105°C). The curves for other annealing times are not shown, but the parameters characterizing drawing

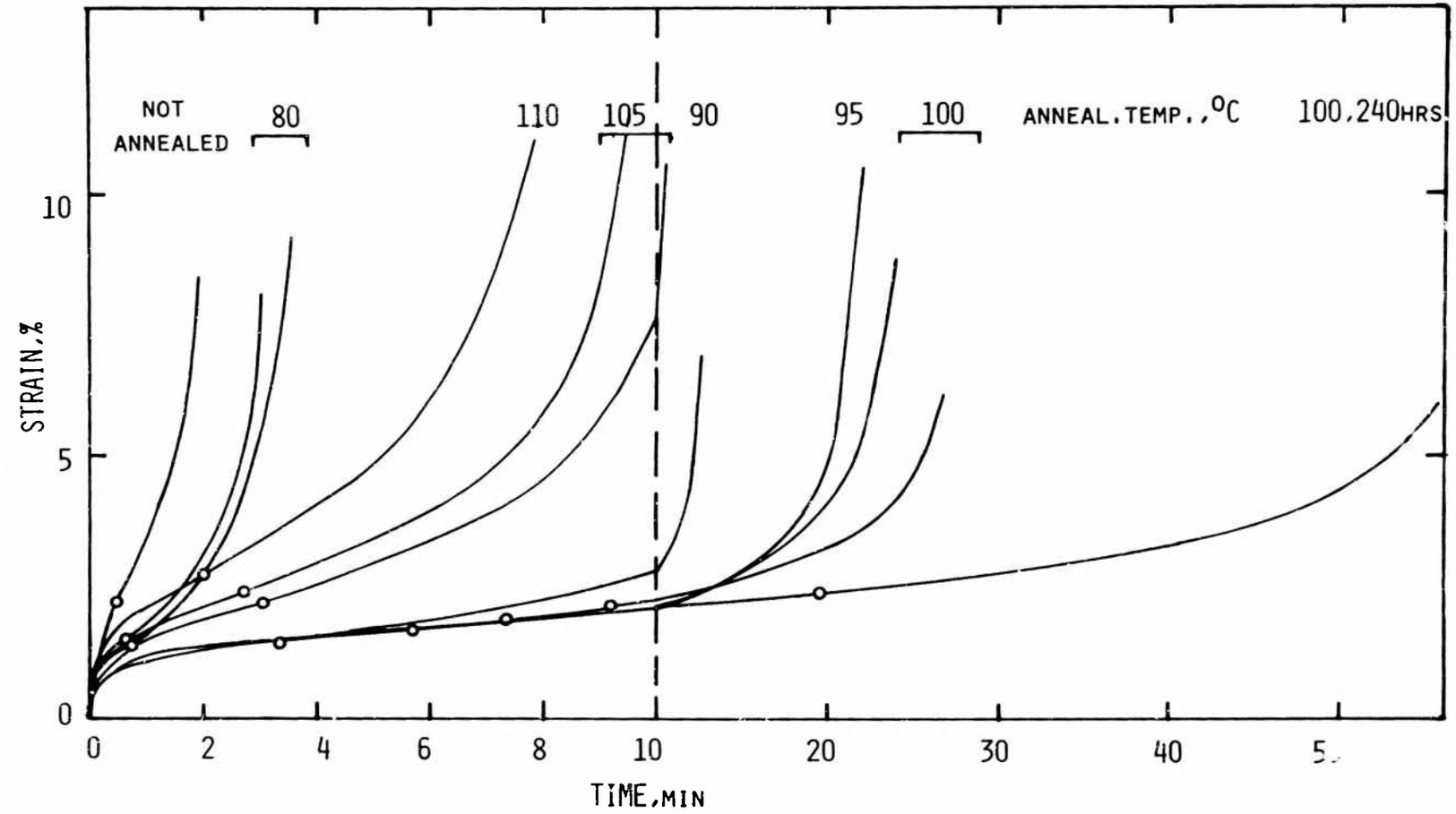

FIG.3.2 STRAIN VS TIME FOR QUENCHED PMMA AFTER ANNEALING FOR 24 HRS
CONST.LOAD TEST:STRESS:4000 PSI;TEMP.:80°C

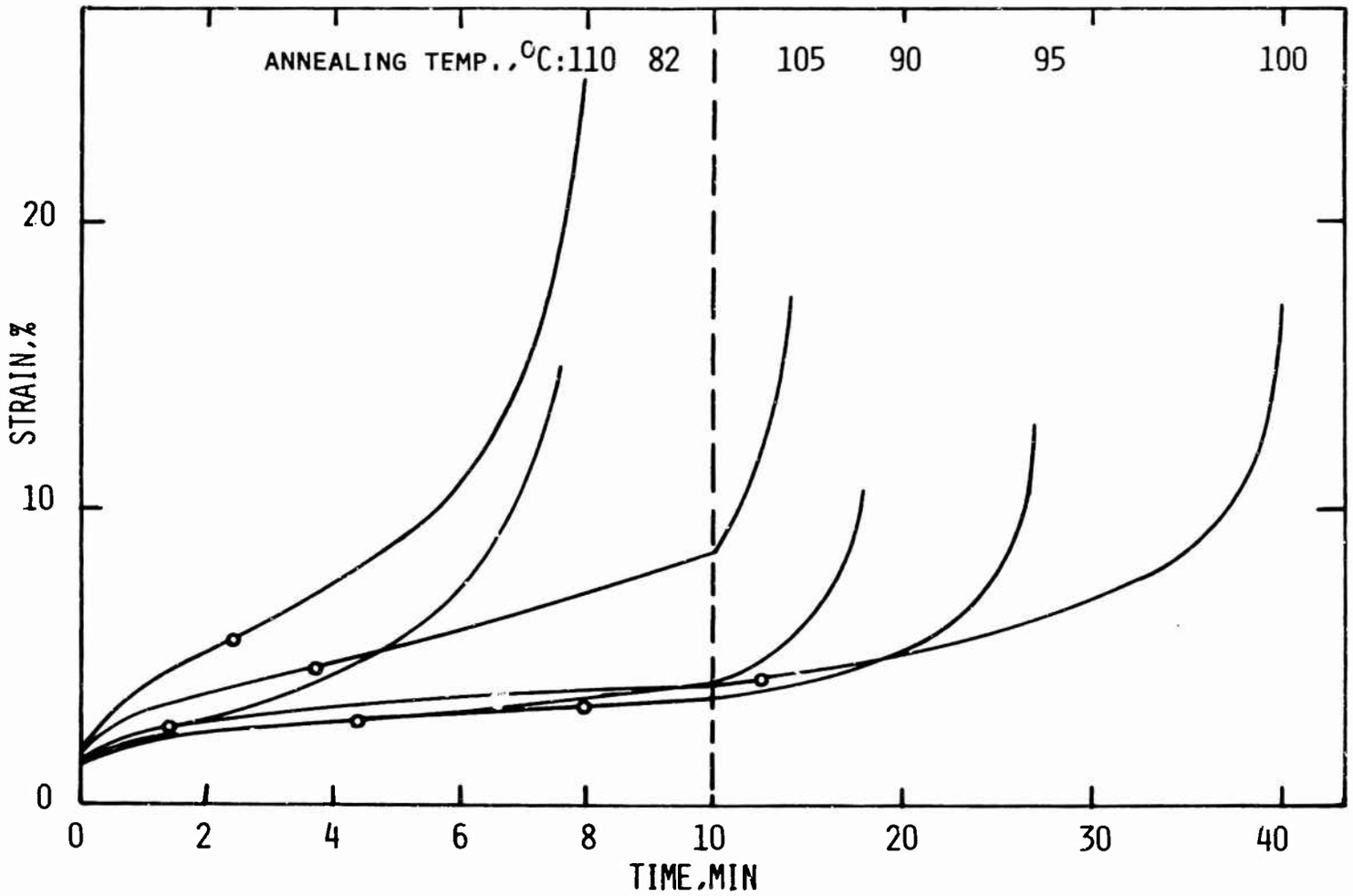

FIG.3.3 STRAIN VS TIME FOR QUENCHED PMMA(DIRECT QUENCH)AFTER ANNEALING FOR 24 HOURS AT SEVERAL TEMPERATURES

Table VI

Yield Strain (%) of PMMA in Constant Load Drawing following Quenching and Annealing

Drawing test: Stress: 4000 psi; Temp. 80°C

t_{ann}, hrs.	T_{ann}, °C 80	85	90	95	100	105	110
0.24					4.0 4.2	3.8	5.1
2.4			3.5		4.5 4.0	3.6	4.6
24	3.1 2.9		3.4	3.5	4.2 4.3	4.9 4.9	5.4
240					4.8 4.3		

Controls (quenched, unannealed): 4.8, 4.3

Table VII

Time to Yield (min) of PMMA in Constant Load Drawing following Quenching and Annealing

Drawing test: Stress: 4000 psi; Temp. 80°C

t_{ann}, hrs.	T_{ann}, °C 80	85	90	95	100	105	110
0.24					1.0 1.8	1.1	1.1
2.4			1.3		3.1 3.2	1.7	1.1
24	0.7		3.3	5.7	7.3 9.2	2.7 3.0	2.0
240					19.5 17.5		

Controls (quenched, unannealed): 0.6, 0.4

Table VIII

Elastic Modulus x 10^{-5} [psi] of PMMA

following Quenching and Annealing

Test conditions: Stress: 4000 psi; Temp. 80°C

t_{ann}, hrs.	T_{ann}, °C 80	85	90	95	100	105	110
0.24					2.5 2.4	2.0	2.2
2.4			2.5		2.6 2.2	2.2	2.3
24	2.3 2.5		2.0		2.3 2.5	1.8 2.0	2.2
240					1.8 2.1		

Controls (quenched, unannealed): 2.3, 2.1

Table IX

Properties of PMMA in Constant Load Drawing

following Direct Quenching and Annealing for 24 hours

Drawing Test: Stress: 4000 psi; Temp. 80°C

T_{ann}	E x 10^{-5}	ε_y	$\dot{\varepsilon}_y$	t_y	t_d
°C	psi	%	%/min.	min.	min.
82.0	2.8	2.6	.50	1.4	7.9
90.3	2.8	2.8	.18	4.4	18.8
94.6	2.7	3.2	.13	8.0	27.5
100.0	2.5	3.4	.12	12.5	40.0
105.0	2.4	4.6	.50	3.7	14.5
110.0	2.2	5.6	1.20	2.4	7.8
Control, quenched only	2.1	4.3	5.7	0.4	1.6

of all tests have either been tabulated [Tables VI, VII, VIII, IX], or are contained in the Figs. 3.4, 3.5, 3.6, and 3.7. The time to reach 10% total strain ($t_{10\%}$) which has been evaluated also, has a similar meaning as the delay time.

From the original length vs. time curves velocity vs. length curves were derived. They will be interpreted in a larger context in Chapter VI.

Density of Annealed PMMA. Small sections of polymer were quenched and annealed under conditions which had produced large changes in drawing properties. The density of the test pieces was measured at room temperature by the "differential expansion method" which was devised for this study. The method utilizes the difference in thermal expansion coefficient between polymer and a non-swelling liquid. It is described in detail in Chapter VIII.

In initial experiments a correlation between treatment and density could not be found. The density was then measured by determining the sample weight in air and in a liquid suspending the specimen on a Pt-wire. The largest source of errors was the surface tension of the liquid-wire interface. The weight measurement in the liquid (sample size approximately one gram) depends on the shape of the liquid meniscus which was either concave or convex upward, depending on the direction of the last motion of the analytical balance. Covering the platinum suspension wire with platinum black[38] reduced the effect, but did not eliminate it. The precision of the improved method was estimated to be $\pm 1 \times 10^{-3}$ g/cm^3.

Two important results were found in these tests:

1. Annealing changes the density by less than 10^{-3} g/cm^3.
2. Moisture alters the density by approximately 10^{-2} g/cm^3 over the total range of absorption. (Density vs. % moisture measurements are reported in Chapter IV.)

Dried polymer absorbs sufficient moisture to conceal the annealing effects when exposed to room air for as short as a second. Through resort to the experimental procedures described

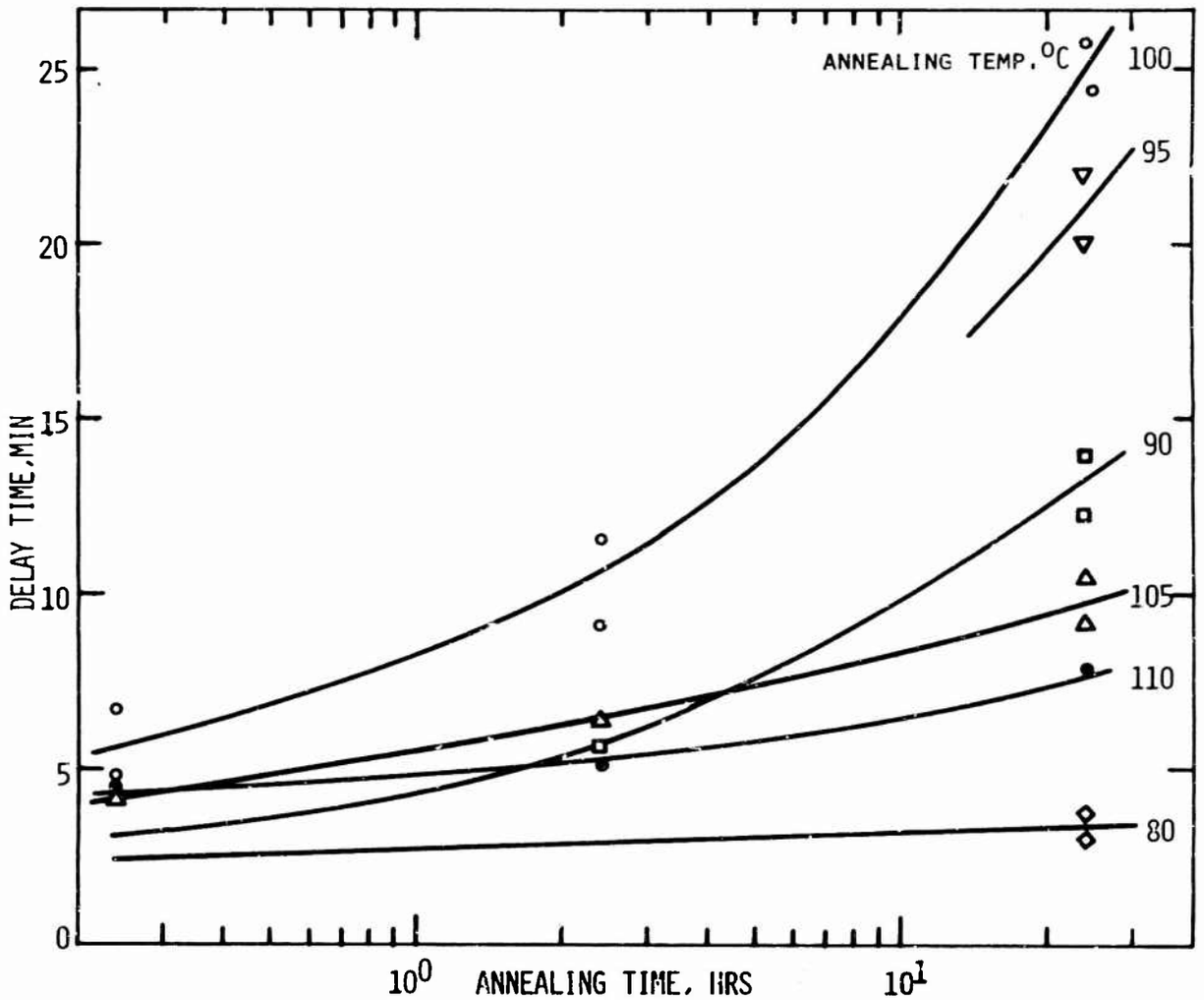

FIG.3.4 DELAY TIME VS ANNEALING TIME FOR QUENCHED PMMA
CONST.LOAD TEST:STRESS:4000 PSI:TEMP.:80°C

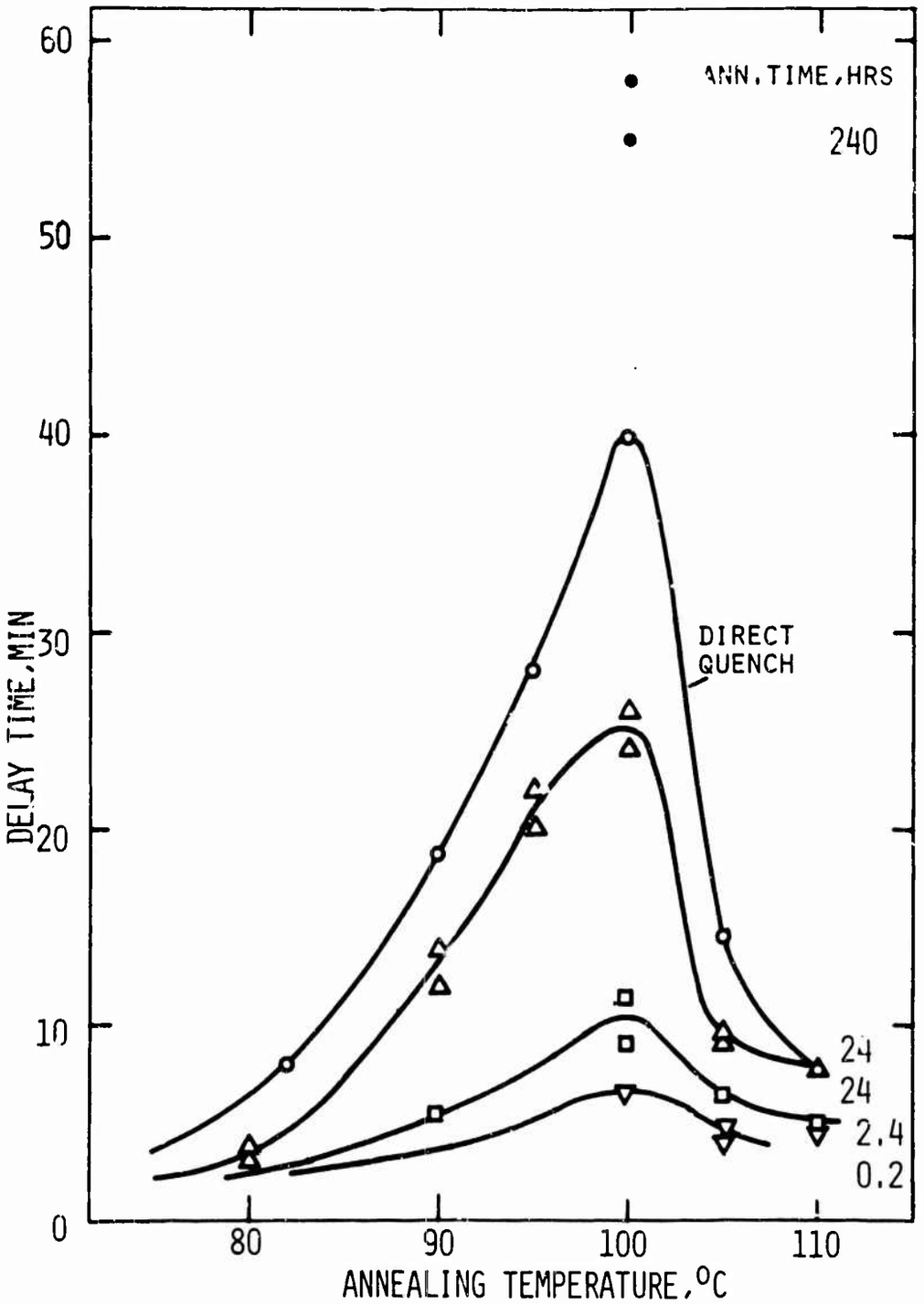

FIG.3.5 DELAY TIME OF QUENCHED PMMA VS ANNEALING TEMPERATURE AFTER VARIOUS ANNEALING TIMES
TEST CONDITIONS:TEMPERATURE:80°C;STRESS:4000 PSI

below contact with air was avoided. The polymer was sectioned in pieces of different shapes for purpose of identification (volume: 50-100 mm^3). The pieces were inserted in a 8 mm Pyrex tube, one end of which was closed. The tube was drawn out in several places, such that a neck separated each piece from the other. Drying, quenching, and annealing was the same as for the tensile specimens of the annealing study. After quenching, the tube sections (each containing a piece of polymer) were melted off and sealed, taking care that the ampoules formed remained evacuated. To provide annealing, the ampoules were immersed in an oil bath. Only indirect quench specimens were made. To measure density, the ampoules were broken under the density liquid.

One group of sections was annealed at 100°C for times from 0.24 to 240 hours; for another group, a 24-hour annealing time and temperatures from 80 to 110°C were used. A quenched, unannealed control was measured with each set. Figs. 3.8 and 3.9 report the results of these tests. The 100°C/24 hr. specimen was damaged and is, therefore, omitted. The 100°C value of Fig. 3.9 was taken from Fig. 3.8.

Discussion

For the discussion of the expected volume changes on annealing use is made of the volume vs. temperature curve of Fig. 3.10. An attempt is made to predict the relation between volume and annealing temperature after rapid direct quenching along A B C to the temperatures T_{ann} along B C, at which isothermal contraction is permitted. The rate of volume contraction is high initially and drops to zero asymptotically as the equilibrium volume on B D is approached[35,39]. The contraction rate decreases with temperature[36] T_{ann} and for practical purposes becomes zero far below T_g. At time t_1, t_2, etc. after annealing started, one may expect the qualitative V vs. T curves of Fig.3.10. After some time the samples annealed near T_g should have reached the equilibrium volume curve B D, at which point the rate is zero. Isothermal volume measurements on PMMA designed to examine these predictions do not seem to have been published. For polyvinyl acetate (PVA_c)[40] the time for reaching equilibrium increases by a factor 10 for each 3°C drop in anneal-

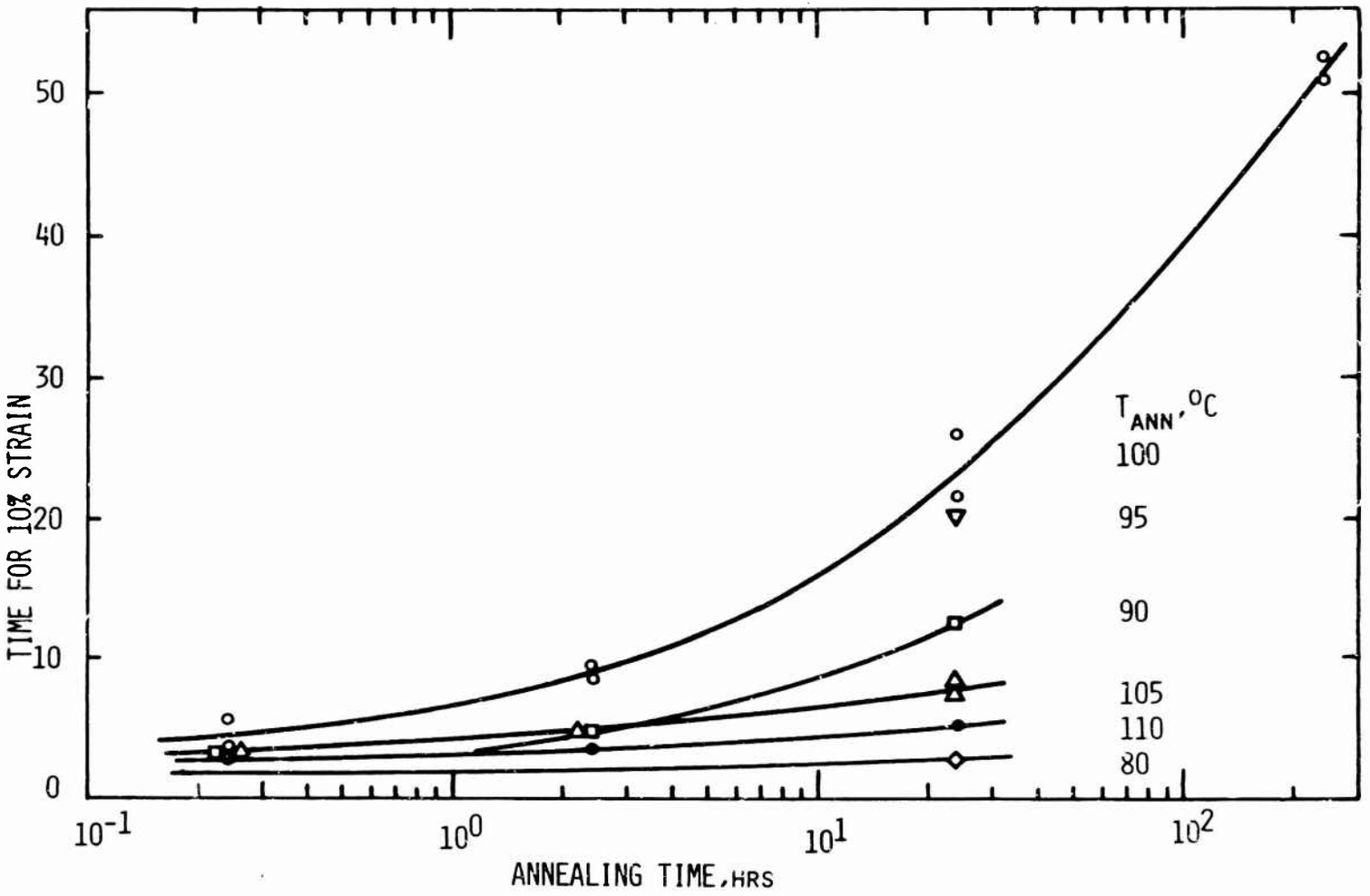

FIG.3.6 TIME FOR 10% STRAIN VS ANNEALING TIME FOR QUENCHED PMMA. STRESS: 4000 PSI
TEMPERATURE: 80°C

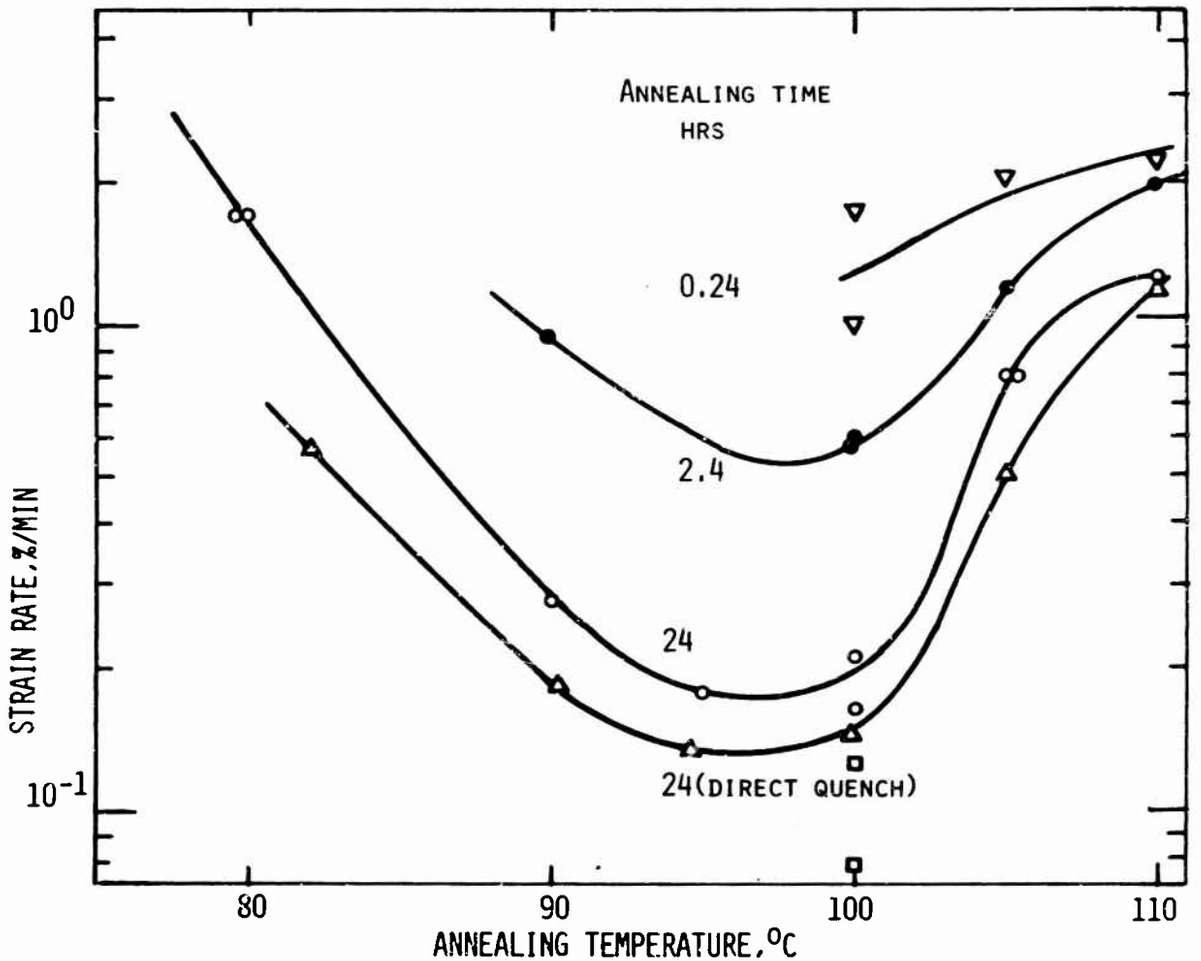

FIG.3.7 STRAIN RATE OF QUENCHED PMMA AT THE YIELD POINT IN CONSTANT LOAD DRAWING AFTER ANNEALING AT VARIOUS TEMPERATURES FOR DIFFERENT TIMES
TEST CONDITIONS:STRESS:4000PSI;TEMP.:80°C

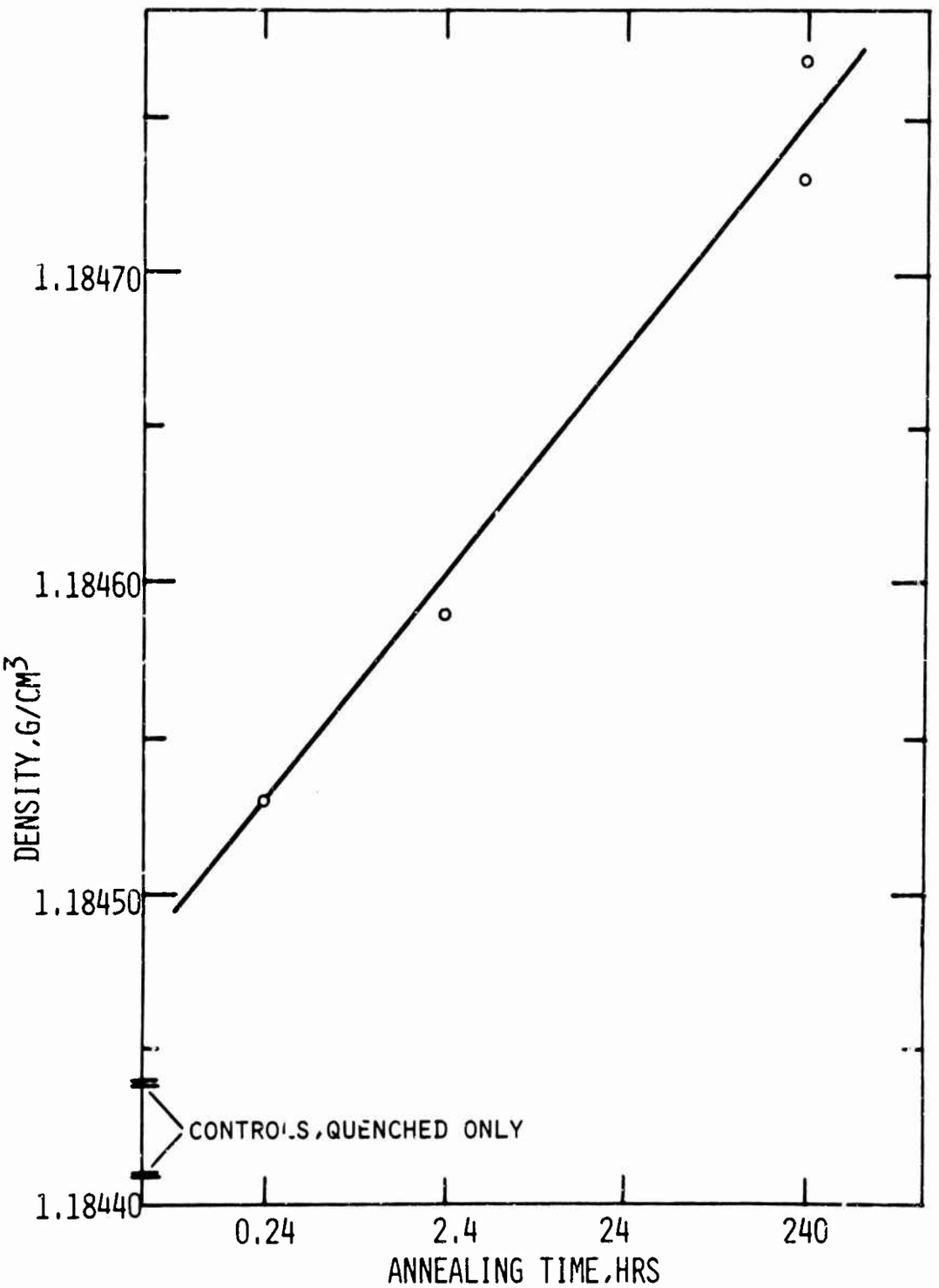

FIG.3.8 DENSITY OF QUENCHED PMMA VS ANNEALING TIME
ANNEALING TEMPERATURE: 100°C

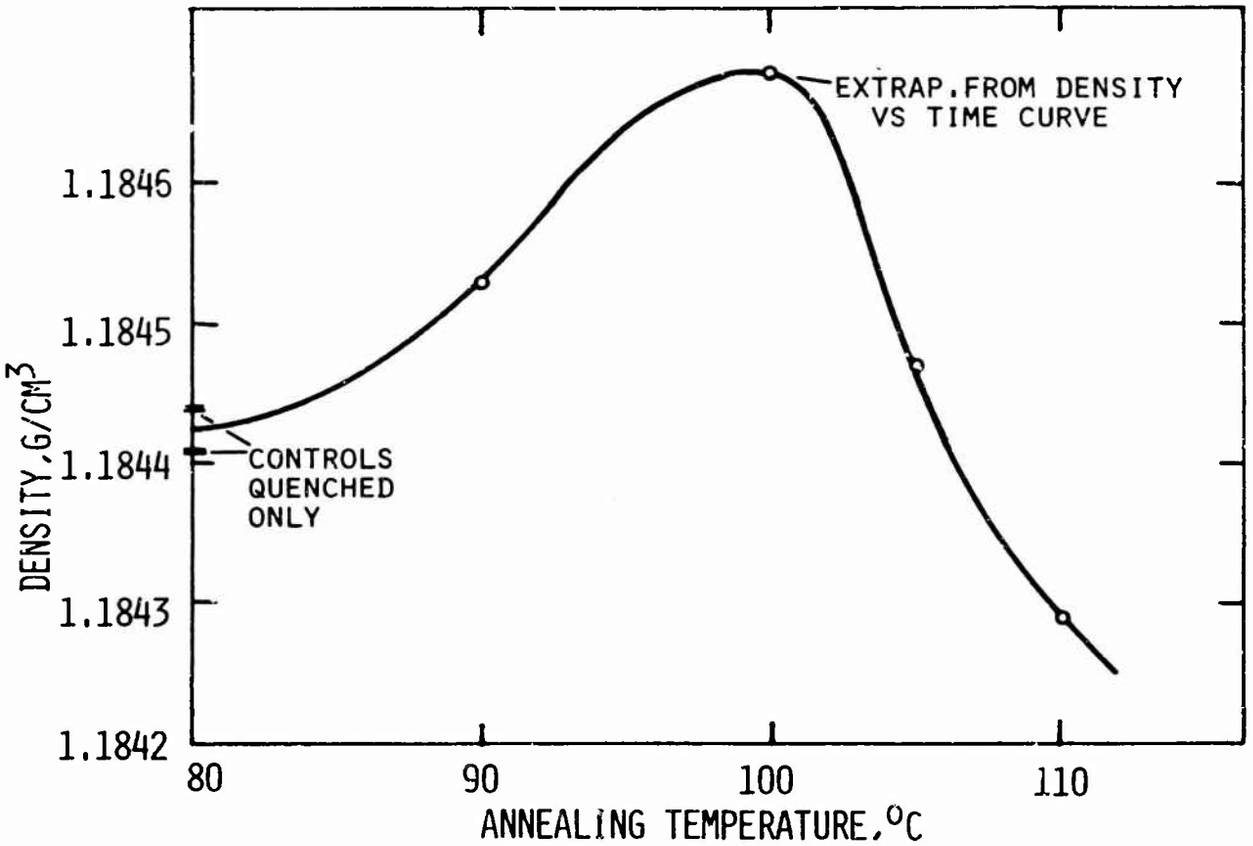

FIG.3.9 DENSITY OF QUENCHED PMMA AFTER A 24-HOUR ANNEALING TREATMENT VS ANNEALING TEMPERATURE

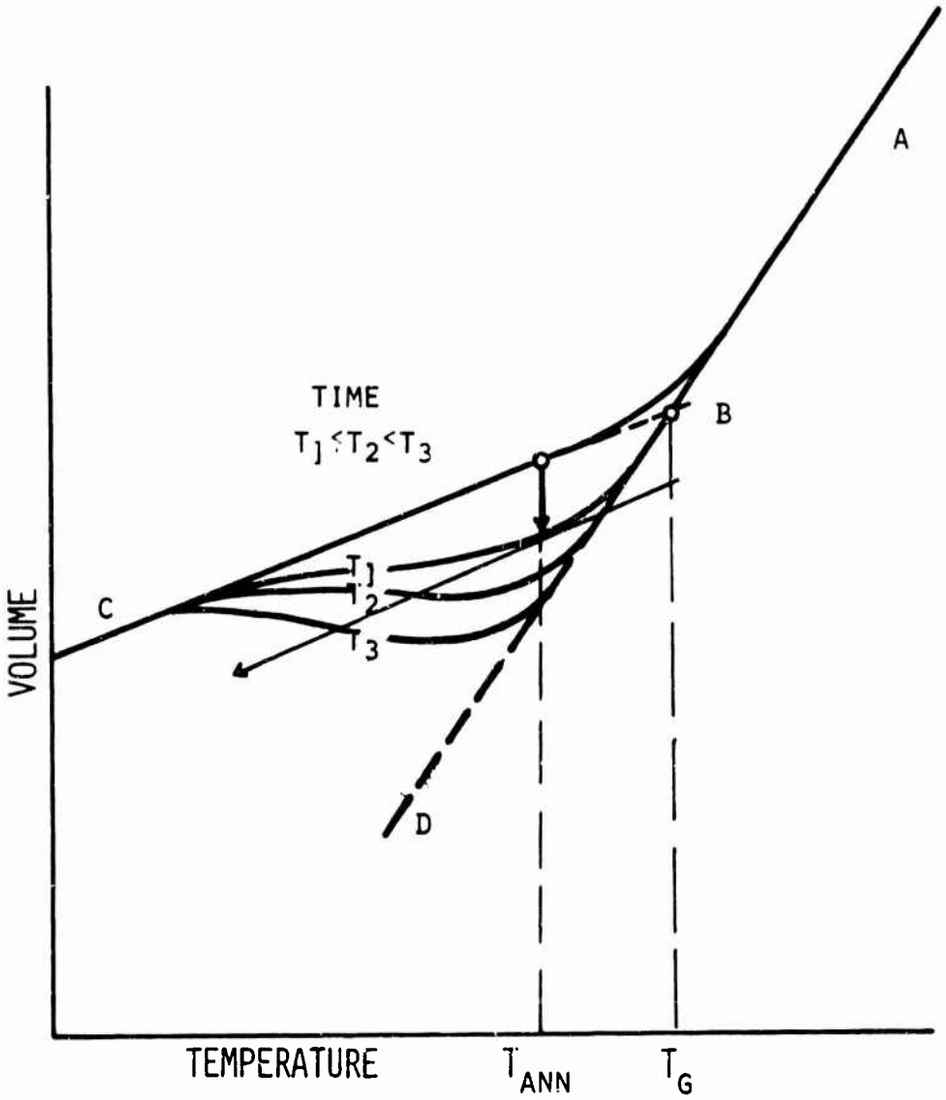

FIG.3.10 VOLUME OF GLASS AFTER COOLING FROM ABOVE T_G TO T_{ANN} AND HOLDING IT THERE FOR VARIOUS LENGTHS OF TIME(SCHEMATIC)

ing temperature in the region T_g to T_g - 15°C.

If the samples, annealing at different temperatures T_{ann} are at some time brought to a common temperature below T_g, the test which lies on the annealing isochronal where it has the slope α_g will manifest the lowest specific volume and therefore the lowest free volume as well (Fig. 3.10). Samples having reached the equilibrium line do not contract further and the free volume minimum point shifts to lower temperatures as the annealing time increases.

Figure 3.9 shows the volume minimum found experimentally (as a density maximum), whereas the shift expected cannot be determined from available data. The densities have been measured at room temperature. One must assume that the density differences are not preserved at higher temperature, for example the drawing temperature (T = 80°C), as the expansion coefficient α_g may depend on the annealing treatment. It is not believed that there are cross-overs of the volume vs. temperature curves, so that at least the order remains the same.

Present annealing times are different by 3 to 4 orders of magnitude, assuming that quenching corresponds to an annealing process of less than 0.024 hours' duration. The 24-hour isochronal should coincide with the equilibrium line B D for about 9°C near T_g as conventionally measured. The density curve of Fig. 3.8 shows that further volume relaxation at 100°C takes place at least up to 240 hours, indicating that the volume contraction of PMMA is more sluggish than that of PVAc.

After annealing, the parameters which characterize the deformation behavior of the glass are either nearly unchanged or changed strongly. The elastic modulus drops somewhat with T_{ann} and t_{ann} (Tables VII and VIII). The yield strain is mainly altered by T_{ann}, increasing over the total range of temperature by about a factor 2 (Tables VI and VIII). t_d, t_y, and $\dot{\varepsilon}_y$ belong to the category of strongly thermal history dependent parameters. Annealing hardly alters the interatomic distances, which mainly account for the elastic behavior. The relative change of the "lattice" parameter of the glass in annealing is $\frac{\Delta a}{a} \approx 10^{-4}$. One therefore would not expect large

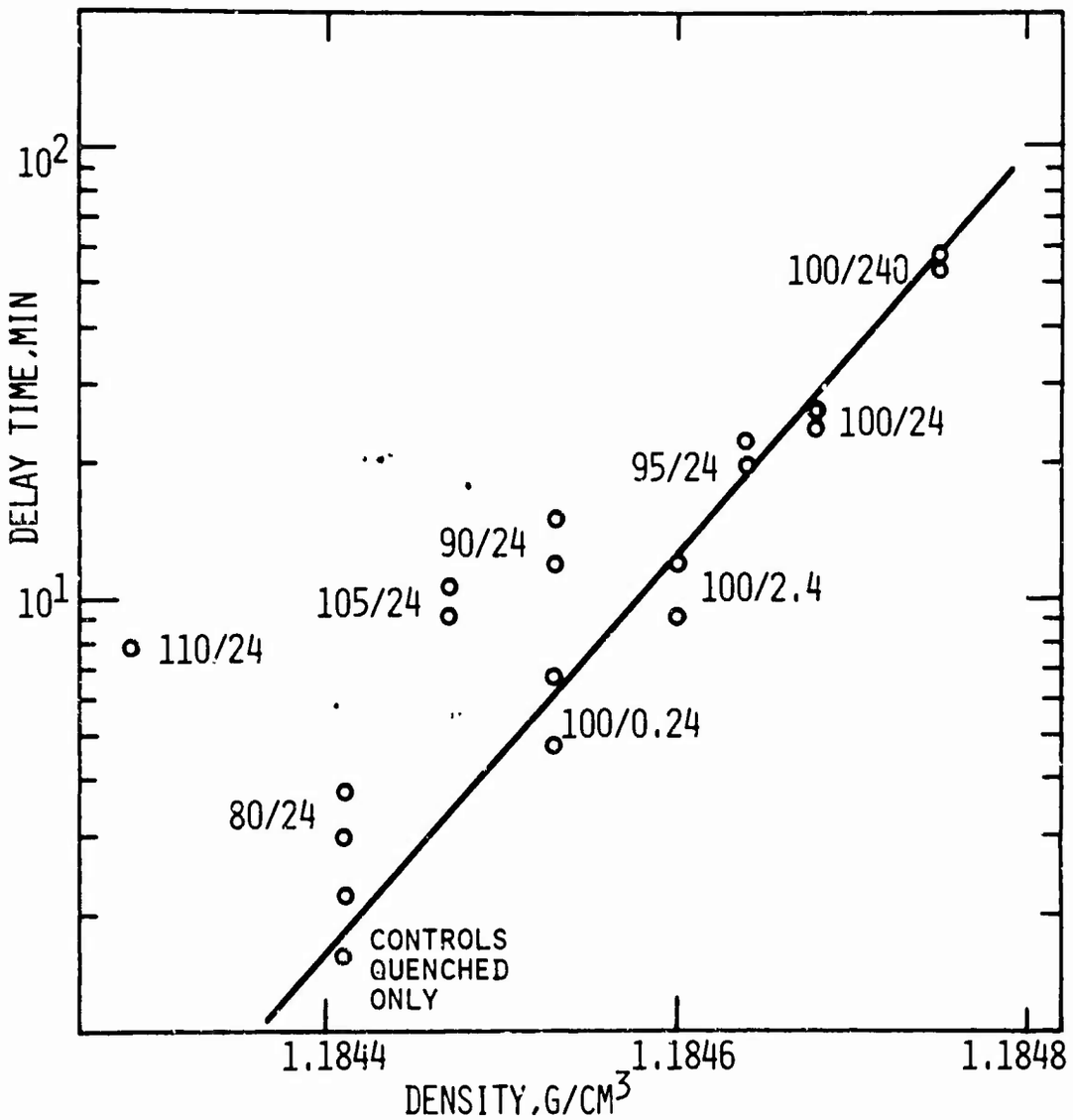

FIG.3.11 DELAY TIME VS DENSITY FOR PMMA AFTER QUENCHING FOLLOWED BY ANNEALING UNDER THE CONDITIONS NOTED, ANNEALING TEMPERATURE/ANNEALING TIME.

modulus changes. By contrast, the great variations of the properties which have to do with the rheological behavior illustrate the importance of available volume for segmental mobility.

From a comparison of the Figs. 3.5 and 3.7 with Fig. 3.9 it is recognized that density maximum and delay time maximum, or yield velocity minimum, appear at the same temperature (100°C). Similarly, as the density increases with annealing time (Fig. 3.8) there is a corresponding increase in delay time (Fig. 3.4) and related parameters. This suggests that the flow properties of PMMA in the glassy region are influenced by free volume.

It is assumed that the density differences between annealing treatments measured at room temperature are at least a qualitative measure of the differences existing at the drawing temperature. Though poor, a correlation does exist between ρ_{TR} and t_d (Fig. 3.11). Only the high temperature annealed specimens deviate seriously from the correlating curve.

One would therefore expect that the delay time results can be discussed analogously with the volume data. Like the volume minimum, the delay time minimum is also expected to shift to lower temperature as annealing time is increased. The data do not resolve this; the step should be of the order of several degrees centigrade.

Near the glass transition temperature (106°C) and especially above it, rate effects in isothermal volume contraction vanish within minutes. In this study the delay time is observed to increase with annealing time at 105 and 110°C, at least up to 24 hours (Figs. 3.4 and 3.6). An explanation for this is suggested further below. Near 80°C the rate of annealing, in terms of regain of flow resistance, becomes quite slow. Hence, an 80°C temperature was chosen for the drawing test.

The top curve (t_{ann} = 24 hrs) of Fig. 3.5 represents data taken with directly quenched specimens. All other measurements were from indirectly quenched samples. The time-temperature histories are represented graphically in Fig. 3.12. The complication in volume relaxation introduced by an intermediate step of low temperature (T_R, Fig. 3.12[a]) has been shown in

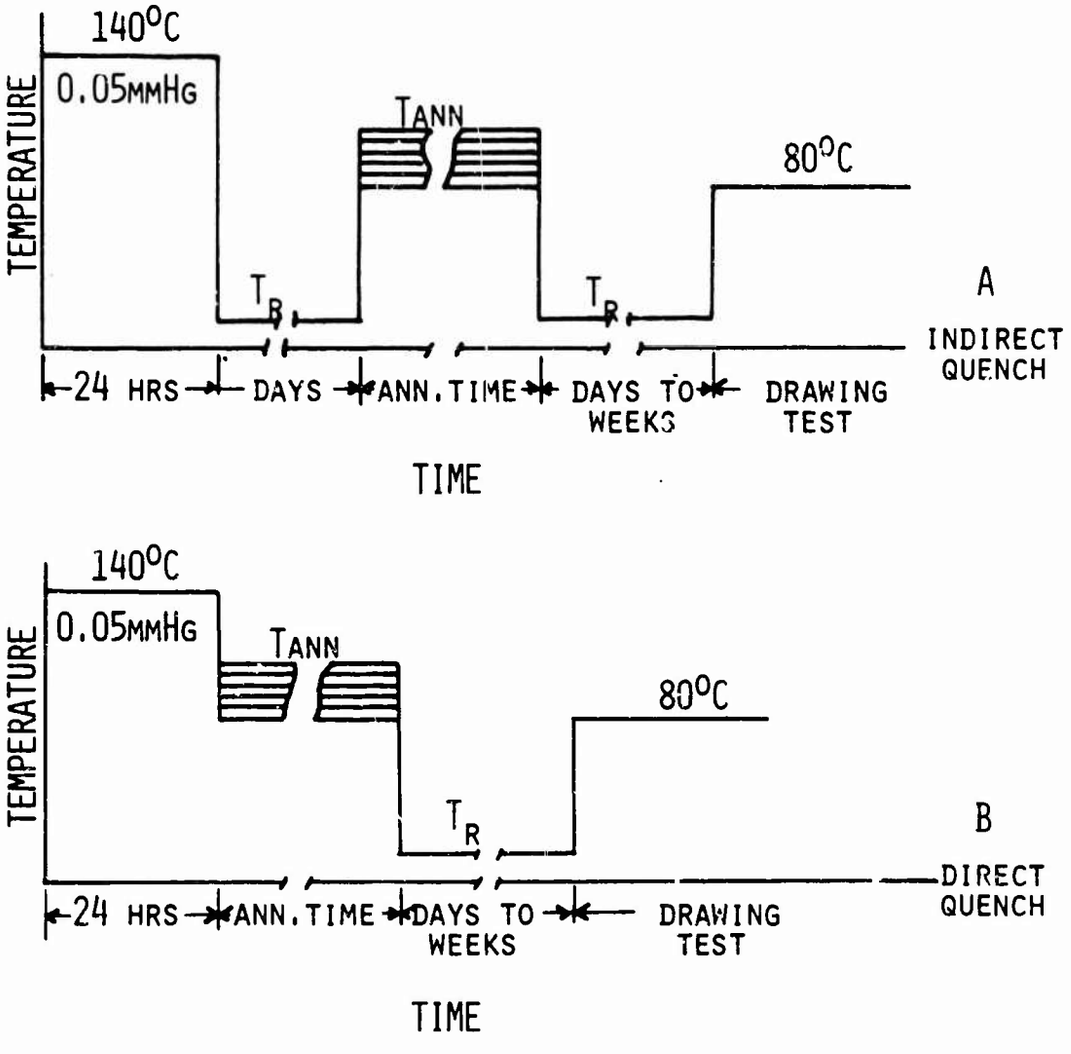

FIG.3.12 QUENCHING AND ANNEALING OF PMMA THERMAL HISTORY

Kovac's[36] experiments. After the temperature has been increased from T_R to T_{ann}, an isothermal transient volume expansion takes place before the V vs. t curve joins that curve which it would have followed isothermally after direct quench to T_{ann}. The time for the transient is the shorter the further the sample is cooled below T_{ann}. During the transient, the volume is always smaller than the one in direct quench. The greater delay time obtained in direct quench is therefore not explainable in a simple way from volume effects. The quench rate near the glass transition in the direct quench is slower than that in the indirect quench as in the first case, the temperature difference is smaller ($140° - T_{ann}$ vs. $140° - T_R$). This may account for the difference in the two 24-hour curves.

The supercooling below T_g, needed to reach the maximum rate of stabilization of the glass, is made plausible by means of the curves of Fig. 3.10. Beyond the maximum, the stabilization is presumably determined by the increasing bulk viscosity. The apparent activation energies for the recovery of t_d and $\dot{\varepsilon}_y$ after quenching, calculated from Fig. 3.13 for the temperatures below 100°C, are as follows:

	Activation Energy k cal/mole
Indirect quench	
From t_d	32
From $\dot{\varepsilon}_y$	39
Direct quench	
From t_d	25
From $\dot{\varepsilon}_y$	32

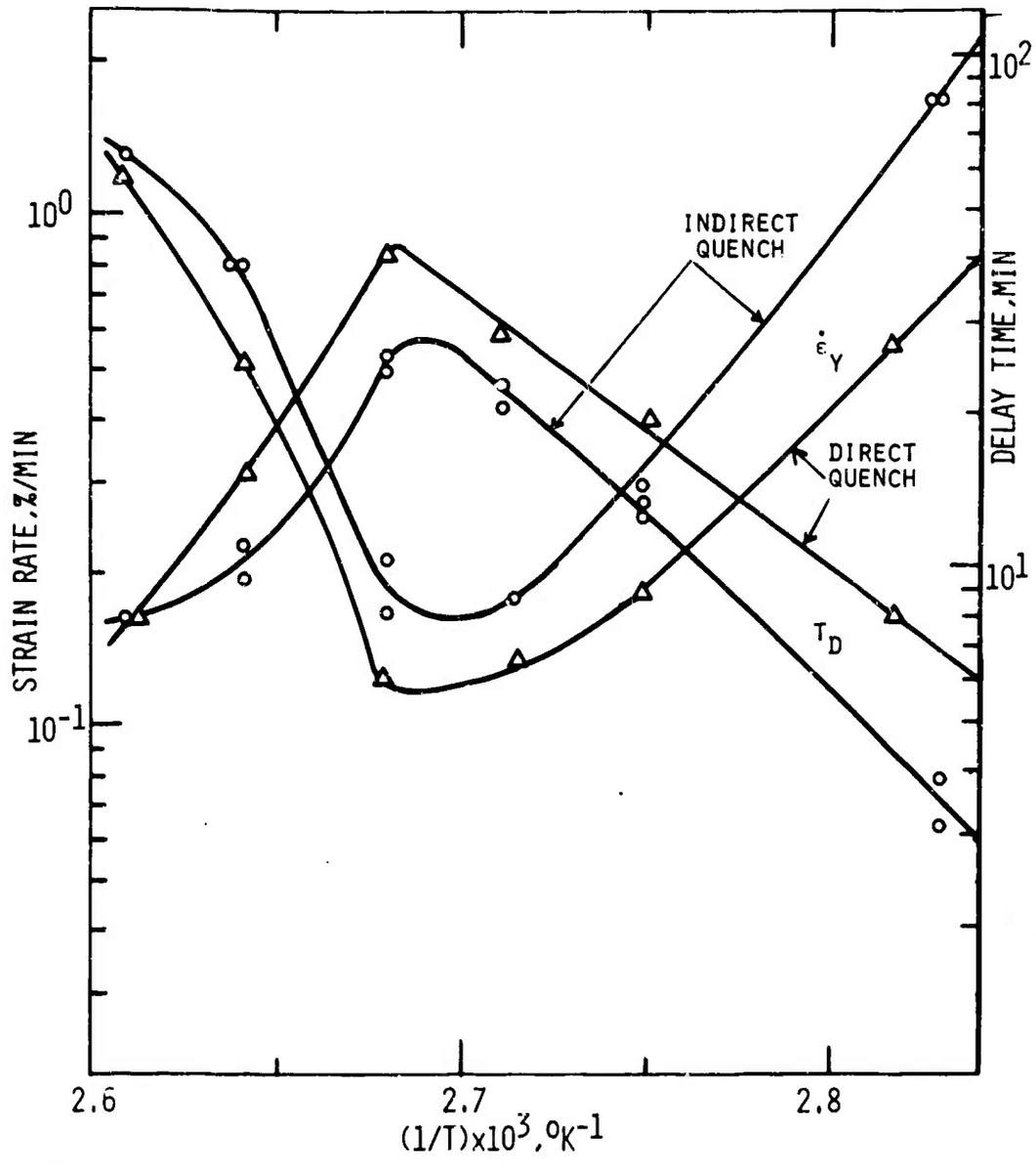

FIG.3.13 STRAIN RATE AND DELAY TIME VS INVERSE ANNEALING TEMPERATURE FOR PMMA AFTER QUENCHING FOLLOWED BY ANNEALING FOR 24 HRS. TESTING CONDITIONS:STRESS:4000 PSI;TEMPERATURE:80°C

The activation energy for shear viscosity for PMMA, as found previously, is 70 to 80 kcal/mole. Litovitz[41] reports near equality of bulk and shear viscosity and the same temperature dependence of both for glass-forming liquids. At the moment, the recovery of properties in annealing is not sufficiently clearcut to attach physical significance to the activation energy listed.

The rearrangement of segments during vitrification, which causes the increased density, could be imagined as a mere closing of intervening gaps, thus eliminating free volume. The density data to be reported in Chapter V suggest an additional possibility. The density of PMMA increases during orientation by about 0.5%. The polymer therefore has the potential to contract by this amount if the molecular segments become fairly well parallel. The glass transition of PMMA could be associated with an ordering reaction of segment directions of close neighbors, favored by the better packing efficiency and the better chance to form association bonds. The presence of associations consequently to prolonged annealing is also manifested in the yielding behavior discussed in Chapter VI.

This proposed ordering would explain the aforementioned annealing rate effect on t_d in the immediate vicinity of T_g where volume relaxation alone is expected to cease within minutes.

The significant result of this chapter, with respect to the theme of this study, is the qualitative showing of the effect of the state of vitrification on the mechanical stability as revealed by cold drawing and the time-temperature requirements to reach stability. The features lending mechanical stability to the well annealed isotropic glass cannot be expected to remain unaffected when the glass is strained. Molecular segments, when forced to leave the position they have in the stabilized polymer so as to follow the external strain, may or may not assume new stable positions, depending on the

time available to do so, and the time necessary to reach such positions. This question will be dealt with further in Chapter VI.

CHAPTER IV

THE INFLUENCE OF MOISTURE ON COLD DRAWING OF PMMA

Introduction

Soluble low molecular weight additives modify polymer properties in a way which manifests enhanced mobility of the polymer molecules. Relaxation spectra are shifted to higher frequencies and the glass transition temperature is lowered. Plasticization over and above that provided intentionally to modify polymer properties is brought about by atmospheric moisture. This is true for many systems, including PMMA.

In Chapter II an increase of 0.8% in water concentration in PMMA was found to lower the delay time just as much as a 10°C increase of temperature. Moisture sensitivity of PMMA properties has been reported before[12,43], yet in much of the published work there is a notable lack of comment on concentration as well as on constancy of moisture during experiments.

Attributing the property shift to the free volume introduced to the system by the plasticizer leads to a successful theory of plasticization[43,44]. Plasticized polymer properties below T_g have apparently been of little interest. The published work on the systems which have been investigated concerns itself primarily with the T_g-shift due to diluent.

This section reports the dependence of the drawing properties and the density of PMMA on water concentration. It is hypothesized that drawing is a strain induced glass transition. If this were to be so, one may suspect that water contained in the drawing polymer shifts the properties to the same extent as an equal water concentration shifts the properties above T_g.

Experimental

Several types of polymer specimens prepared for tensile density and moisture analysis, were conditioned in atmospheres of various humidities for approximately 90 days. To provide the various atmospheres saturated aqueous solutions listed in Appendix E were maintained in desiccator jars. The samples were stored therein. Initially the polymer was in equilibrium

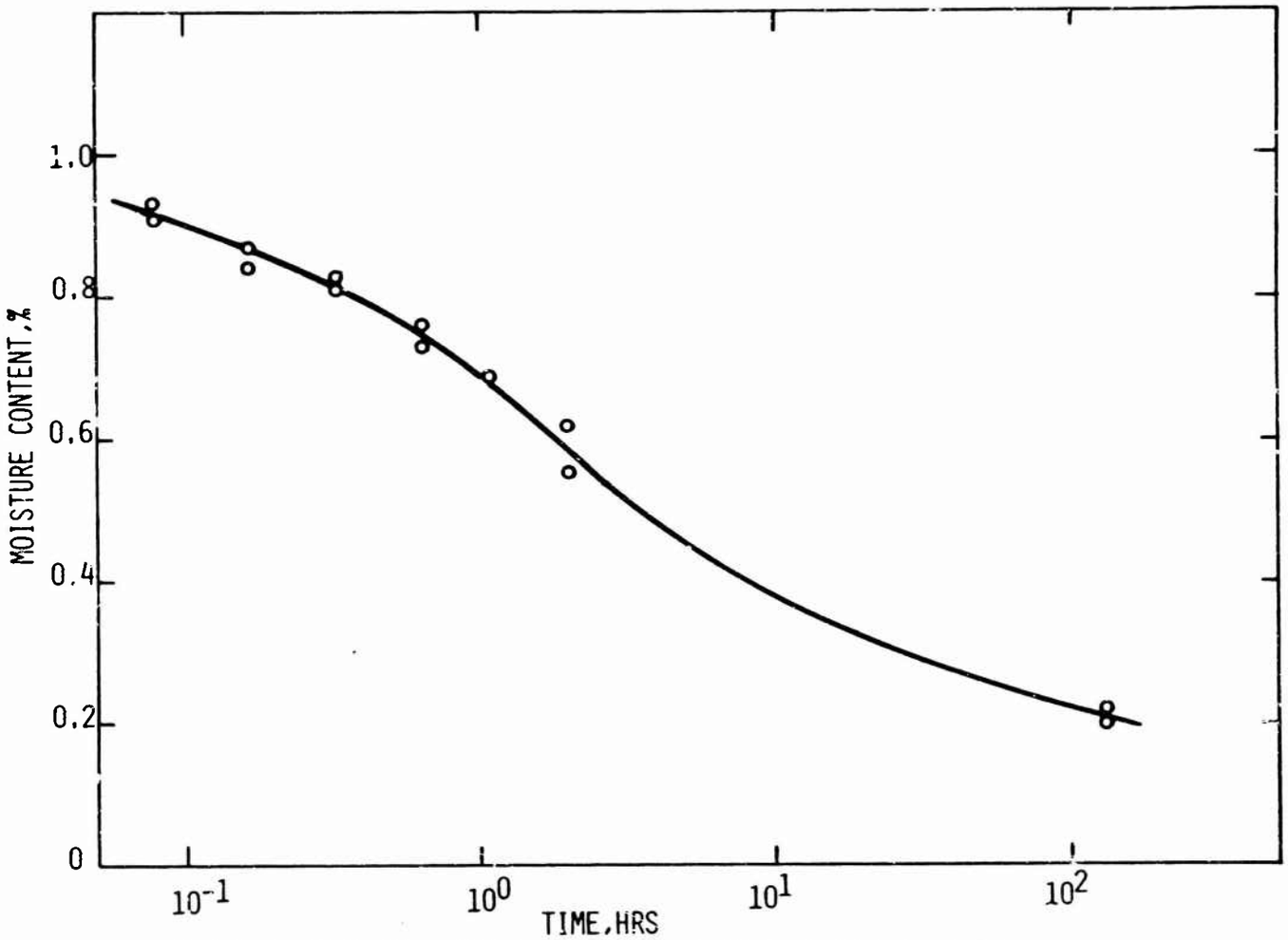

FIG.4.1 MOISTURE CONTENT OF PMMA VS DRYING TIME AT 80°C
SAMPLE CONDITIONED IN 65%RH AT T_R,SAMPLE THICKNESS 1/16 IN

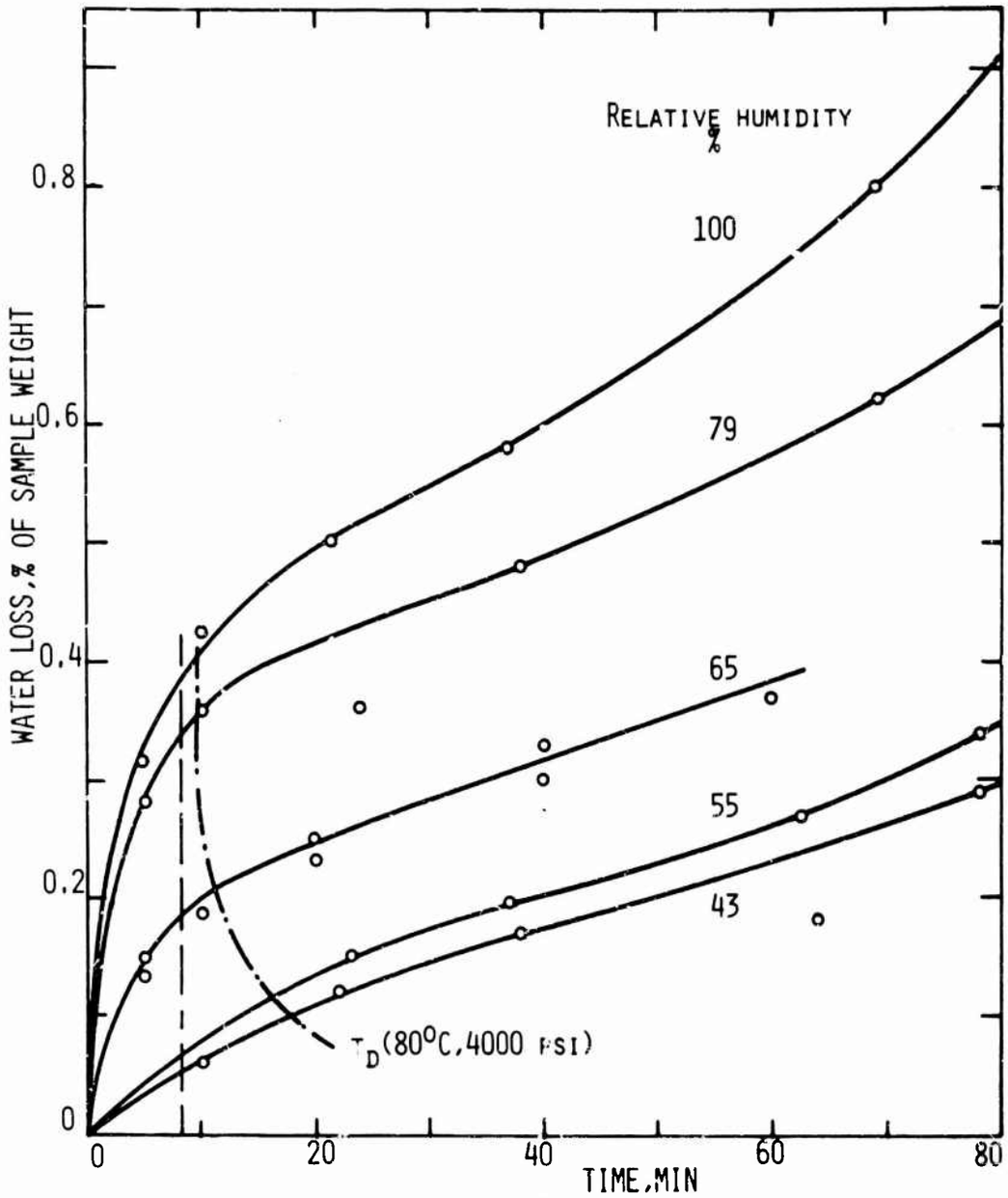

FIG.4.2 WATER LOSS VS HEATING TIME OF PMMA CONDITIONED AT VARIOUS HUMIDITIES.TEMPERATURE:80°C;MAT.THICKN.1/16 IN

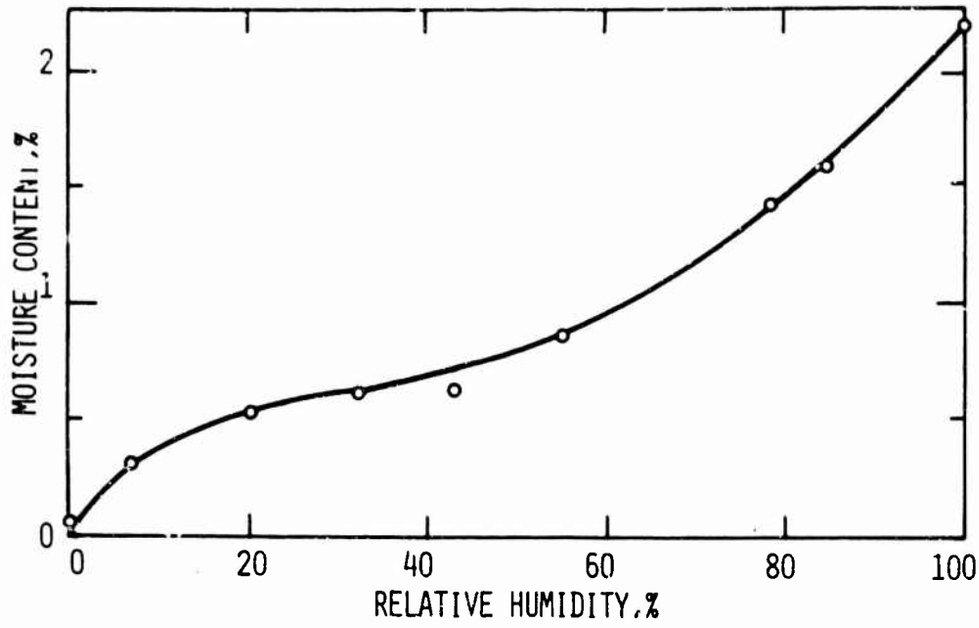

FIG.4.3 MOISTURE CONTENT OF PMMA VS RH OF CONDITIONING ATMOSPHERE

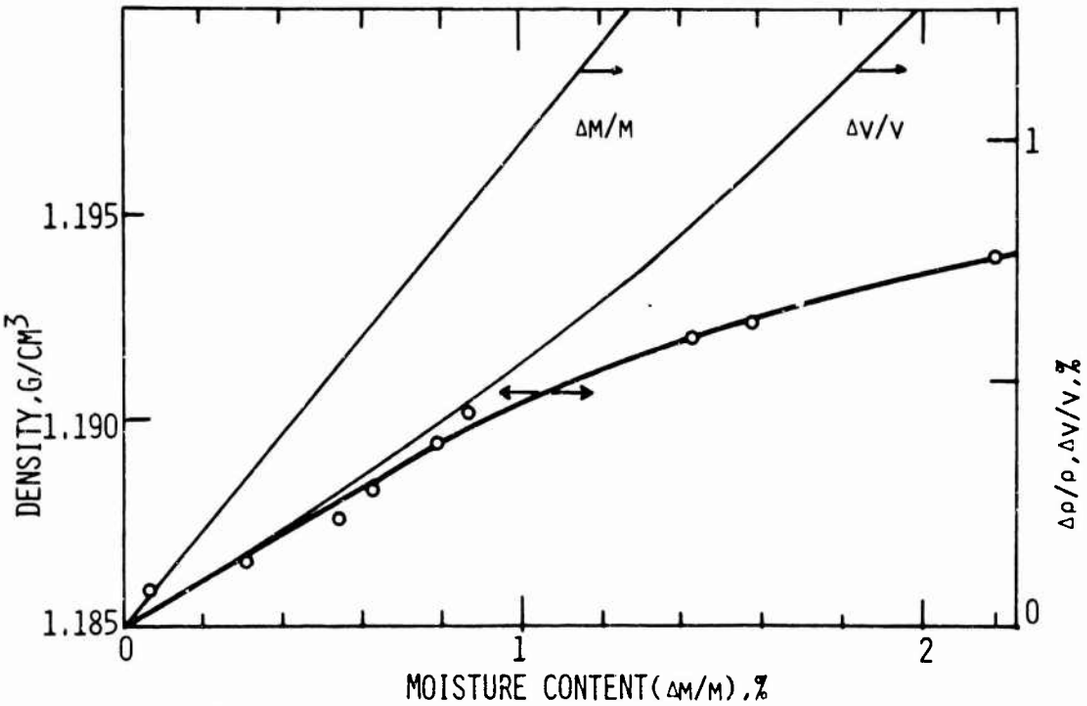

FIG.4.4 DENSITY AND RELATIVE CHANGES OF VOLUME, DENSITY AND WEIGHT VS MOISTURE CONTENT OF PMMA

with 65% RH at room temperature.

The moisture content was found from the weight loss after two days of drying in a circulating air oven at 102°C. In preliminary drying tests at this temperature the sample weight reached a constant value within experimental error after one day of drying. The accuracy of the analysis is estimated to be ±0.07% moisture if, as done in this work, a 1-gram sample is used. The density of the moist specimens was determined by the method described in Chapter VIII.

Subsequent drawing conditions were the same for all samples, σ = 4000 psi, T = 80°C. The specimens were kept in the conditioning atmospheres until immediately before the test.

Results

Provisions to maintain relative humidities in drawing at 80°C equal to the conditioning humidities would have required the construction of a more sophisticated test chamber. Instead, some moisture loss during drawing was tolerated. However, in order to restrict such loss to the surface region, drawing conditions were chosen to give short experimental times. The amount of moisture lost at 80°C was determined in separate tests. Figure 4.1 shows the 80°C drying isotherm for a PMMA tensile specimen previously conditioned in 65% RH. The water loss of PMMA specimens at 80°C conditioned in atmospheres of various relative humidities is presented in Fig. 4.2. The intersecting curve gives the total moisture loss at the end of drawing; the broken line, that at the time of load application. Up to 20% of the water initially present evaporates.

The moisture absorption vs. relative humidity curve (Fig. 4.3) has the sigmoidal shape often seen for polymers. The highest water regain is 2.2%. At laboratory conditions (65% RH) the regain is 1.08%. Drying over P_2O_5 did not completely remove the water. This introduces some uncertainty in the initial part of Figs. 4.3 and 4.4.

Reduced reproductions of the length vs. time curves are shown in Fig. 4.5. The parameters characterizing them are compiled in Table X.

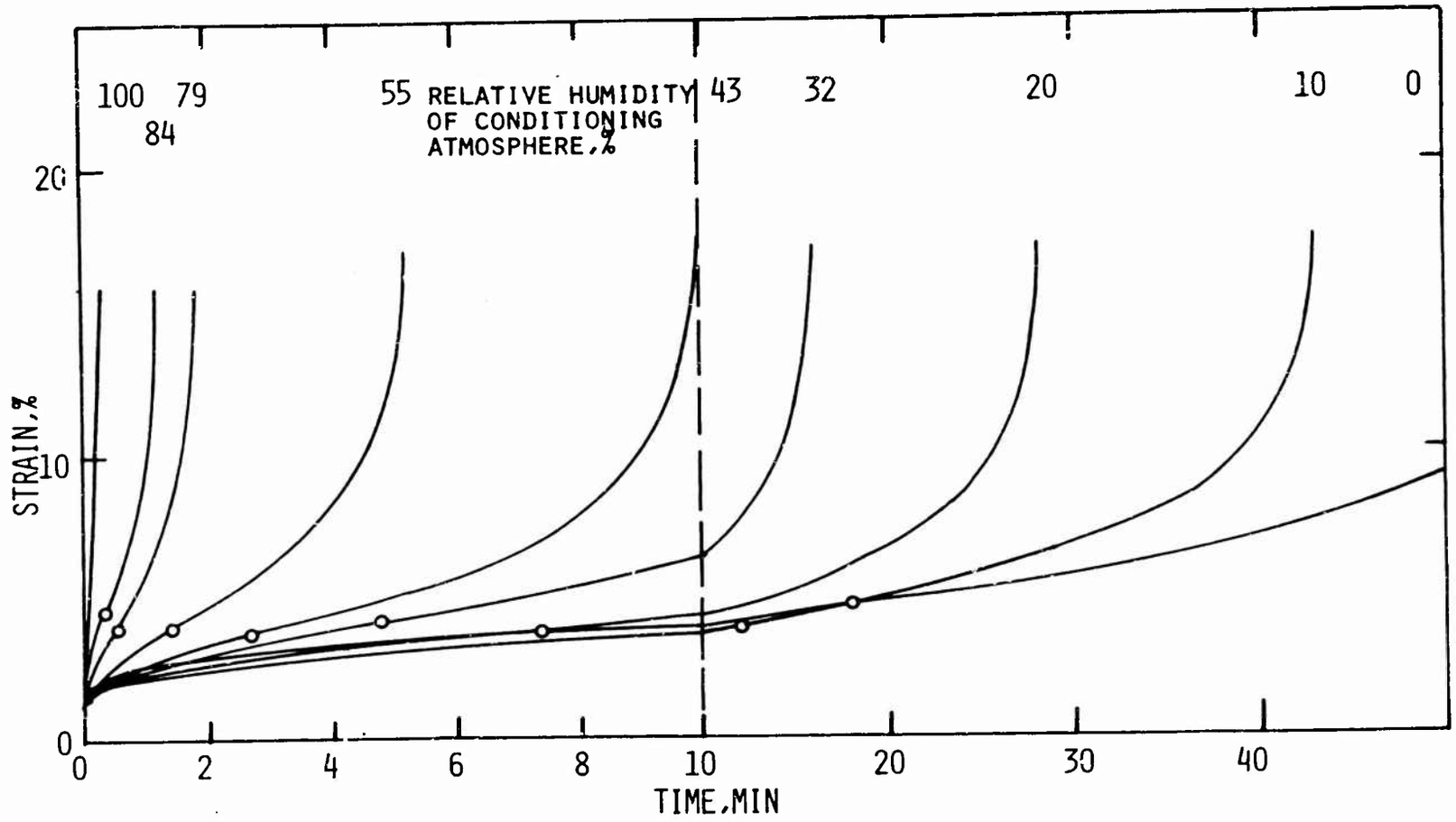

FIG.4.5 STRAIN VS TIME OF PMMA CONDITIONED IN ATMOSPHERES OF VARIOUS RELATIVE HUMIDITIES
TESTING CONDITIONS: STRESS: 4000 PSI; TEMPERATURE: 80°C

Table X

Effect of Moisture on Drawing Parameters

RH %	Moisture %	E x 10^{-5} psi	ε_y %	$\dot{\varepsilon}_y$ %/min.	t_y min.	t_d min.
0	0.07	2.0	4.6	0.09	8.3	58
10	0.32	2.6	4.0	0.12	12	42
20	0.55	2.5	3.8	0.19	7.4	28
32	0.63	2.3	4.1	0.35	4.8	16
43	0.78	2.5	3.7	0.51	2.7	9.7
55	0.86	2.0	3.9	1.1	1.4	5.3
79.5	1.43	(3.0)	3.9	3.2	0.5	1.9
84	1.58	1.6	4.5	5.2	0.3	1.1
100	2.20	*	*	34.5	*	0.2

*Not measurable.

Discussion

The data of Table X confirm further the large effect of absorbed water on drawing of PMMA as discussed in Chapter I. The delay time drops by a factor of nearly 500 as moisture concentration increases from zero to 2.2%; whereas the other rheological parameters show equally large changes, yield strain and modulus remain nearly unaffected.

For constant rate drawing one predicts from these data a drop in yield stress due to moisture of approximately 2000 psi.

Before comparing the concentration shift of delay time with that of viscoelastic properties above T_g, it is worthwhile to note the relation between t_d and viscosity η. The time to reach some strain under constant stress is derived from strain rate by Equ. (II-24) which, after combining it with Equ. (II-13), becomes

$$t_\varepsilon = \frac{1}{C}\int_0^\varepsilon \eta . d\varepsilon = \frac{\bar{\eta}.\varepsilon}{\sigma} \qquad \text{(IV-1)}$$

If two measurements for equal stress are compared and the strain

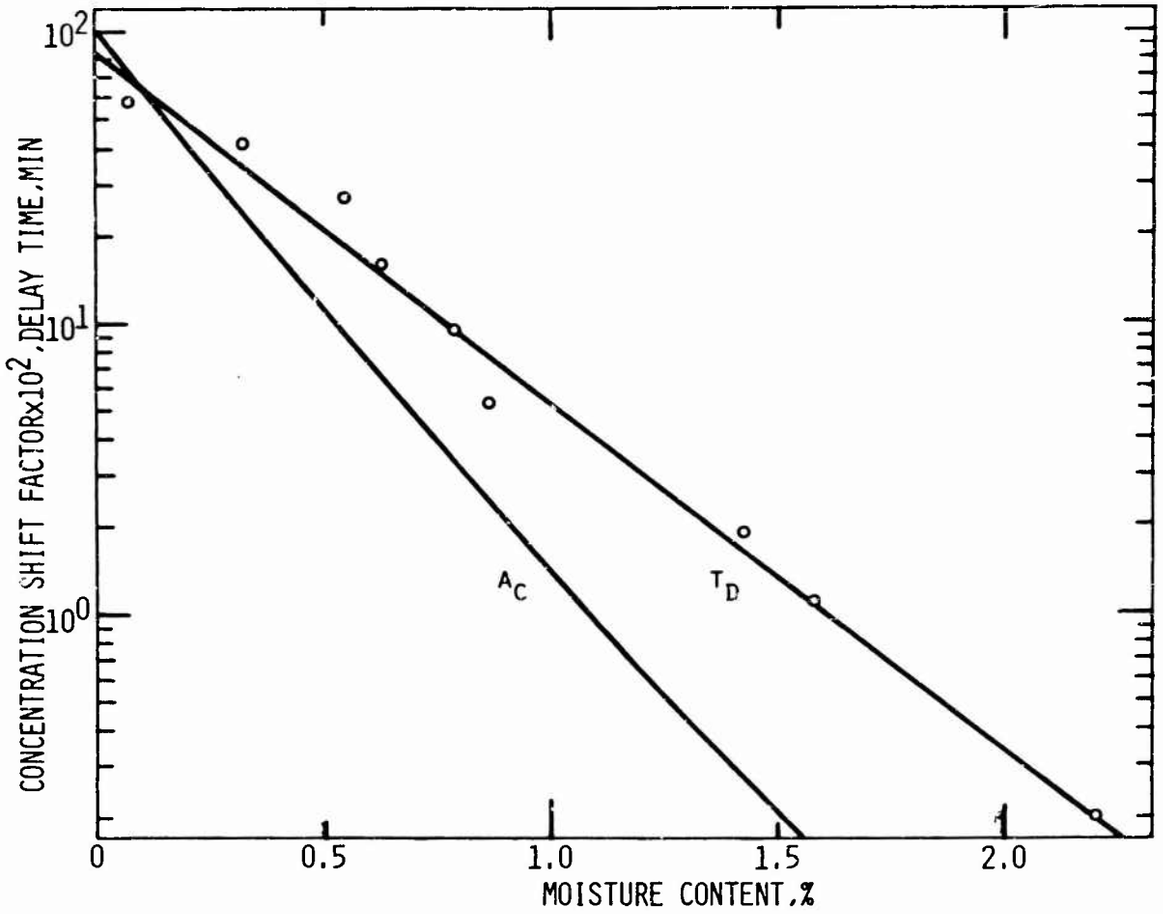

FIG.4.6 DELAY TIME OF PMMA VS MOISTURE CONCENTRATION(STRESS:4000 PSI; TEMPERATURE:80°C) AND CONCENTRATION SHIFT FACTOR(A_c)FOR PMA VS MOISTURE CONCENTRATION FOR TEMPERATURES ABOVE T_G

is chosen to be that at delay it follows that

$$\frac{t_{d1}}{t_{d2}} = \frac{\bar{\eta}_1}{\bar{\eta}_2} \qquad \text{(IV-2)}$$

If the indices stand for two different concentrations or temperatures, these ratios give the respective shift factors. Each viscosity is averaged over the deformation up to the delay strain. It is not certain if these large strain shift factors are the same as the ones commonly calculated for low strain; at a later point it will be assumed that they are.

From the plot $\log(t_d)$ vs. concentration (x) of Fig. 4.6 one calculates $\Delta\log(t_d)/\Delta x = 1.2 \times 10^2$. Comparison with the effect of moisture in the rubbery state is through the concentration shift factor (Ref. 44 or Appendix F).

$$\log a_c = - \frac{[B/(2.3\ f_g)]x}{(f_g/f_1) + x} \qquad \text{(IV-3)}$$

The fractional free volume of the pure diluent, f_1, must be obtained from experimental data. Fujita and Kishimoto[43] have derived an equation for the T_g shift for small concentrations of diluent, and from it f_1 is usually calculated:

$$T_g(x) = T_g(C) - (f_1/\alpha_F)x \qquad \text{(IV-4)}$$

where α_F = difference of the thermal expansion coefficients of liquid and glass, and the "universal" value 4.8×10^{-4} is assumed. [A derivation of an equation by a route different from that of Ref. (43), which reduces to Equ. (4) for small concentration is given in Appendix F.]

The fractional free volume contributed by the water depends on the polymer and f_1 must therefore be calculated from data for the system consisting of PMMA and water. As data for the T_g shift for PMMA were not found in literature, the value for polymethyl acrylate (PMA)-water, $f_1 = 0.30$, was used[43]. For the vicinity of T_g and with B = 1 one has $f_g = 0.025$[33(b)]. The calculated curve [Equ. (3)] is shown in Fig. 4.6 also, arbitrarily

assuming that it goes through $t_d = 100$ for $x = 0$. Water added to the glassy polymer shifts the rheological parameters derived from constant load experiments less than was predicted for the case where the polymer had been strained through its glass transition. One could argue that this transition could be simply a partial softening in view of the fact that the glass transition in PMMA is gradual and over a temperature-interval of at least 20°C. Less of an effect of moisture would be reasonably expected in this case.

The concentration shift below T_g is not known. It is therefore not possible to test if the delay time shifts are, if not as high as in the rubbery region, at least higher than in the glassy region.

Below the glass transition temperature properties are not controlled by free volume alone. Intermolecular associations, sites for which are provided by the ester side groups, should become important. Water interacts with either unbonded groups or by opening associations between ester groups. Unlike the situation existing in a crystalline solid, only a few of the stoichiometrically possible bonds can form in the glass. At the highest absorption one water molecule is shared by eight polymer mer units. There should be an abundance of unassociated side groups for the water to attach to, even without opening of ester-ester links. Still, dissociation by the influence of water remains a possibility.

The density measurements of Fig. 4.4 give some clues to the water absorption in the glass. Each water molecule adds a volume ϕ to the mixture consisting of N_p mer units each of volume ψ. From the relative density change for the system PMMA-water accompanying the absorption the ratio ϕ/ψ is available,

$$\phi/\psi = 1.83\ [1 - d(\Delta\rho/\rho)/dx]. \qquad \text{(IV-5)}$$

Figure 4.4 shows that the volume contribution of each water molecule, expressed as a fraction of the volume of one MMA segment, increases with absorption. Some examples of ϕ/ψ

are given in Table XI.

At low concentrations each water molecule contributes to the mixture only 50% of the volume which it occupies when surrounded by its own species. This increases to 75% for the highest concentration. The proportionality of volume and concentration, which is the basis for the theory concerning the concentration shift factor, is not fulfilled for a glass. This result also suggests that the absorption sites are gradually changing with concentration.

A mere filling of holes, for which $\phi/\psi = 0$, does not appear to occur at any stage of absorption. This affirms that there are not many holes of large size which one could expect to play a role in drawing.

As regards the error caused by moisture traces in density measurements, it is easily recognized, by comparison of Figs. 3.8 and 3.9 with Fig. 4.4, that several hundredths of a percent of water variation completely masks any density changes due to annealing.

Table XI

Relative Volume Contribution of
Watermolecules to the Mixture PMMA-Water

RH	x	
%	g/g	ϕ/ψ
0	0.0	0.10
65	1.1	0.123
100	2.2	0.15
Separate Phases		0.21

CHAPTER V

BIREFRINGENCE AND DENSITY AFTER DRAWING

This chapter is a collection of several birefringence and density studies, each one made with a different objective. They were made at various stages of this work to arrive at or ascertain hypotheses about the chain conformation in drawn or partly drawn polymer. Either birefringence or density measurements characterized the group of experiments.

BIREFRINGENCE AND MOLECULAR ORIENTATION

Introduction

Preferential orientation of polymer chains arising in stretching shows up as an anisotropy of properties in the drawn state. The contribution of a molecular segment to the property is determined by the angle between the segment and the direction in which the property is measured. A possible definition of orientation could be the average angle which the segments include with the stretch direction. More commonly, the anisotropy of a property itself is used, for example that of the refractive index, the birefringence.

In rubbers, where the chains between cross-links move about freely, uniaxial straining causes a difference between the refractive indices parallel ($n_{\parallel}$) and perpendicular ($n_{\perp}$) to the orientation axis as given by

$$n_{\parallel} - n_{\perp} = \Delta n = c.N(\lambda^2 - \frac{1}{\lambda}). \qquad (V\text{-}1)$$

c = constant, specific for chemical structure; N = number of chains; λ = extension ratio = $\frac{L}{L_0}$.

In amorphous uncrosslinked polymers a weak network of secondary bonds or entanglements may be present. This network does not remain intact on straining. Strain itself, or temperature, may break secondary bonds releasing taut short chains between initially present links to form less taut longer chains. A secondary network between oriented chains may form simultaneously with the decay of the first. In general, it is therefore not possible to apply Equ. (1) to glassy polymers. Birefringence

is presently, in this application, a qualitative and empirical measurement.

Chain orientation is also sustained without a network by internal friction in a shear field as, for example, in flow birefringence. Chemically-not-crosslinked amorphous polymers appear to be between crosslinked rubbers and polymeric liquids in that both network and kinetic orientation are operative. The result of external strain with regard to anisotropy is therefore not alone a matter of the magnitude of the strain, but also of the conditions under which it was imposed.

The anisotropy of a property is only then changed by stretching if such stretching alters the anisotropy of segments. This has been demonstrated convincingly by Milagin and Shishkin[45] by correlating PMMA breaking strength with orientation birefringence and stretch ratio. The strength correlates only with birefringence and not with the extension.

The methods to measure birefringence used in this study are described in Chapter VIII.

Results and Discussion

Symmetry of Orientation in a Flat Specimen. If the ratio of original width to original thickness = w_o/t_o of a tensile sample becomes high, the width remains essentially unchanged on straining. The ratio $w_o/$, $\simeq 4$ used here, still gives equal contraction ratios; one finds that along a neck $w/t = w_o/t_o$.

Birefringence measurements were taken in nearly all of this work by viewing in thickness direction. The question was whether lateral symmetry also exists for the optical anisotropy. Thickness and retardation were measured along the necked section (Fig. 5.1) in the center of the surface 1-3. A slice was then cut through the middle of this surface and its faces 1-2 were polished. The retardation was then measured in the 3-direction.

Birefringence and lateral strains in directions 2 and 3 are shown as function of length along the neck in Fig. 5.1. Birefringence is, like strain, equal in both directions and the orientation distribution therefore approximates circular symmetry in spite of the noncircular cross-section.

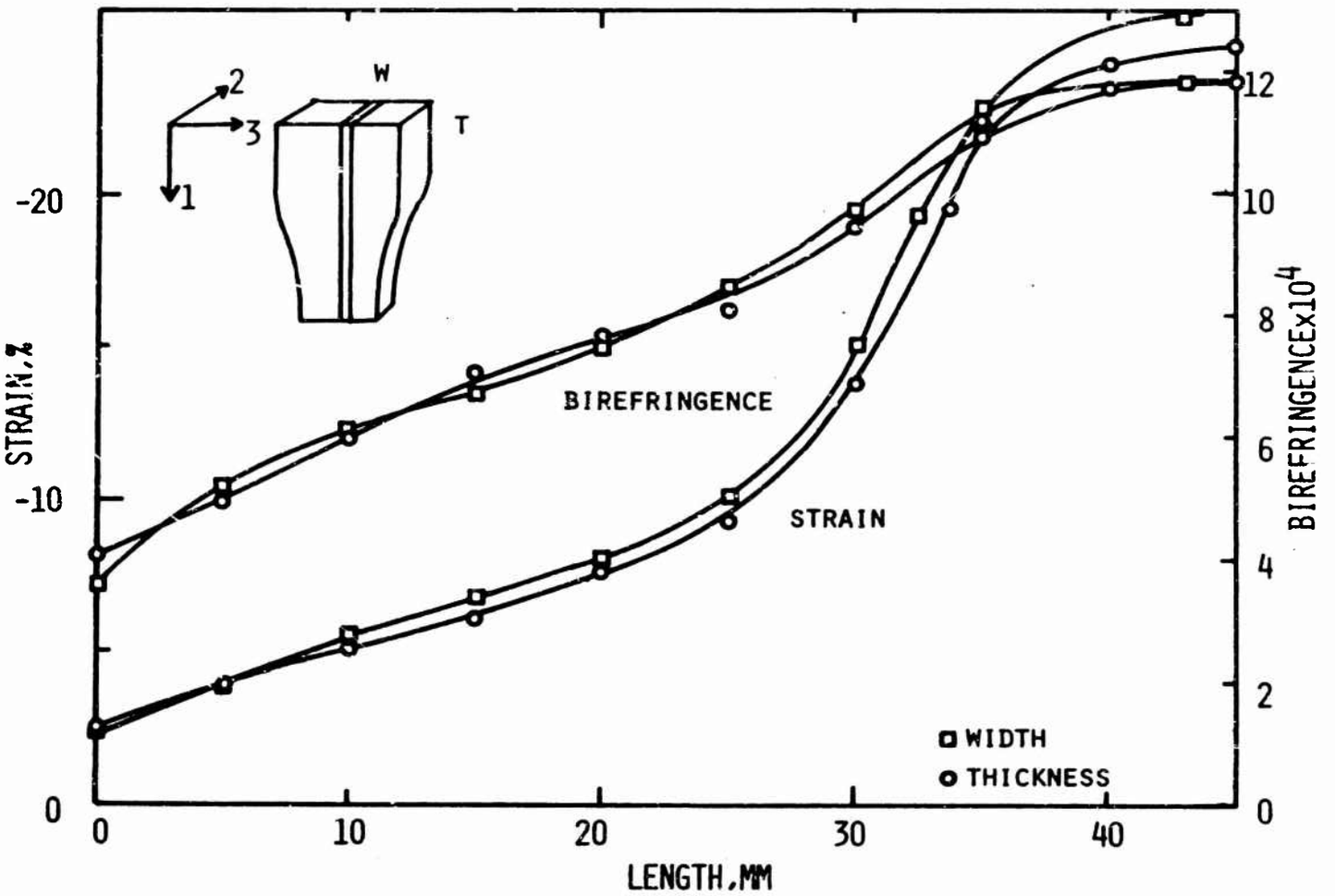

FIG.5.1 LATERAL STRAIN(CONTRACTION OF WIDTH AND THICKNESS)AND BIREFRINGENCE ALONG THE NECK OF A PARTLY DRAWN PMMA SPECIMEN.WIDTH/THICKN.IS APPROX.4

Effect of Stretching Conditions on Birefringence. Stretching PS or PMMA to some given extension produces a much higher optical anisotropy when carried out below the glass transition temperature than above it. Shiskin and Milagin[46] have measured the dependence of birefringence on strain and stretch temperature for PMMA above T_g. Some of their curves have been reproduced in Fig. 5.2 and demonstrate that the orientation birefringence above T_g is a function of both strain and stretch temperature. These authors have shown that the observations are consistent with the presence of an associated bond network, the nodes of which are the ester side groups. These relatively weak bonds dissociate above T_g with increasing temperature and the number of network chains N drops. This accounts, through Equ. (1) for the reduced optical anisotropy.

The orientation birefringence data for PMMA of the present work were measured at room temperature after straining at 140°C and are in acceptable agreement with the data of the above publication (Fig. 5.2). Some points for a crosslinked PMMA modification, Plexiglas P55 (App. B) are also included in the figure.

Birefringence vs. strain data for PS (Fig. 5.3) above its T_g are qualitatively similar to those for PMMA, whereas temperature changes have a clearly larger influence on the birefringence of PS. The molecular structure of PS does not suggest the possibility of association bonding. The temperature dependence is, in this case, probably merely due to the shift of relaxation times, facilitating disorientation of chains more rapidly at higher temperature. The birefringence preserved in glassy PS after hot stretching should, if this is correct, vary with stretch rate and cooling rate. This question has not been further investigated.

Orientation birefringence inserted by drawing below T_g was measured from necked tensile specimens, which had been cooled to room temperature at constant length. Results of such measurements are shown in Figs. 5.2 (PMMA) and 5.3 (PS).

For PMMA the Δn vs. ε curve for drawing below T_g is nonlinear. The birefringence increases strongly to nearly 50%

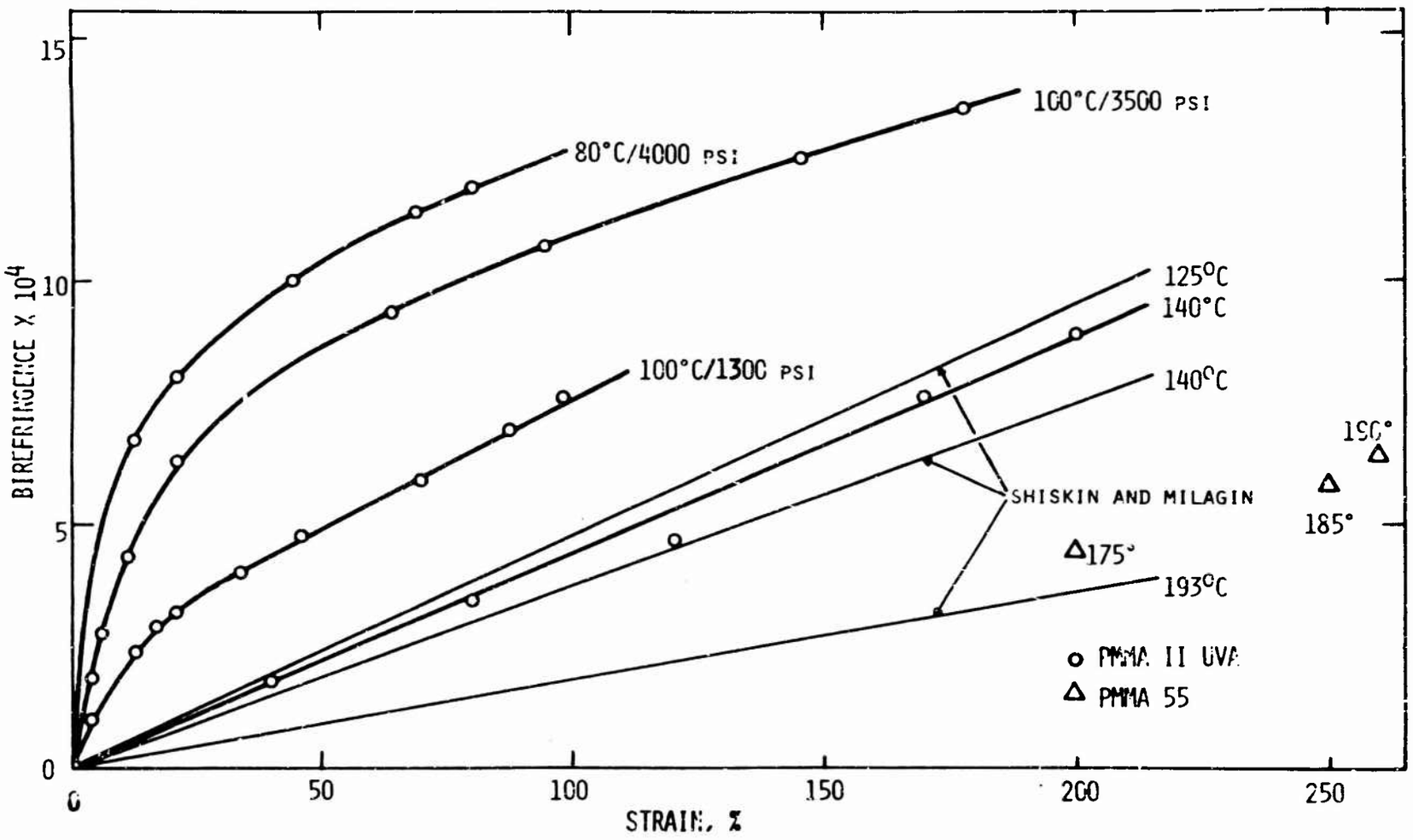

FIG.5.2 BIREFRINGENCE VS STRAIN OF PMMA FOR STRETCHING ABOVE AND BELOW T_G

of that of the fully drawn polymer within the first 10% strain. Beyond 40 to 50% strain the curves run nearly parallel to the linear curves for drawing slightly above T_g.

The observations for PS are quite different (Fig. 5.3). Reducing the drawing temperature to below T_g increases only the slope of the Δn vs. ε curves which remain almost linear.

Turning to the PMMA cold drawing curves again, the following interpretation of the curve shapes is suggested. In the unstrained state physical bonds form a very tight network containing many chains which give rise to the steep increase of birefringence at low strains. As the physical cross-links break down with increasing strain, the effective number of chains is reduced. The parallelism of the 80 and 100°C with the 140°C curves at larger strain may indicate that the number of chains is approximately equal in both cases.

For PS the curves for $T<T_g$ are nearly in the position in which one would expect them to be by extrapolation from the high temperature curves. On closer examination there is some curvature in the cold drawing curves which is too small to give it significance. What has been designated as secondary bond breaking phase in PMMA does not have a counterpart in PS to any comparable extent.

The birefringence reached at some strain varies with the conditions of the drawing experiment as illustrated by Fig. 5.4 for PMMA. The two drawn out curves are typical examples for the curve shapes for drawing below T_g, the straight line represents the 140°C hot orienting results. Each point not connected by curves is from the necked section of one drawn sample. It is believed that the curve passing through a point is approximately parallel to the drawn out curves. The test conditions varied in temperature, stress, and moisture content as noted in the figure. The birefringence is lowered by increased drawing temperature and moisture. For 100°C there is also a clear trend to lower Δn-values as the stress is reduced, that is, as drawing is at a slower rate. This is not found for the 80°C data.

The low birefringence of the very slow drawing experiments

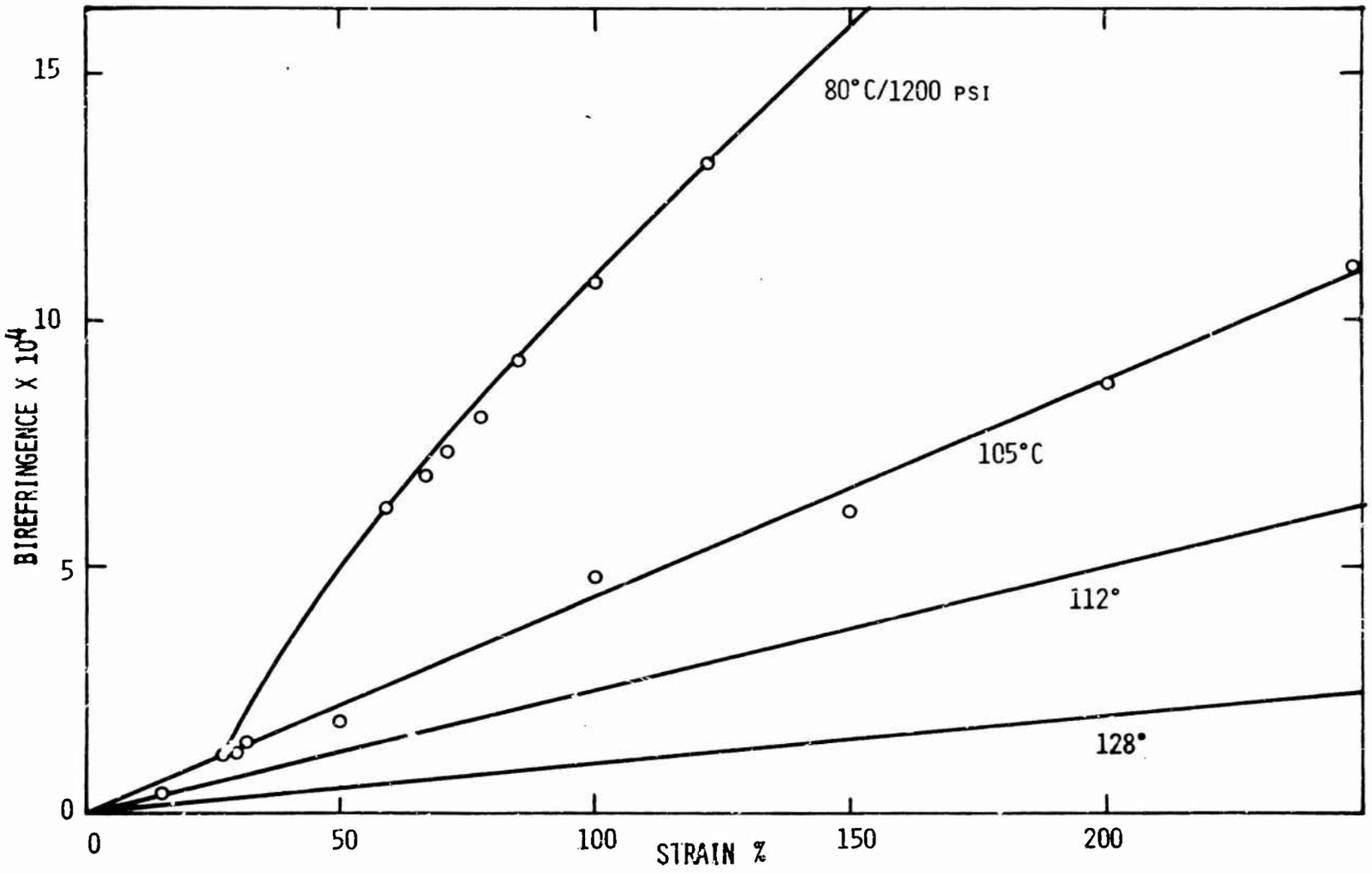

FIG.5.3 BIREFRINGENCE VS STRAIN OF PS FOR STRETCHING ABOVE AND BELOW T_G

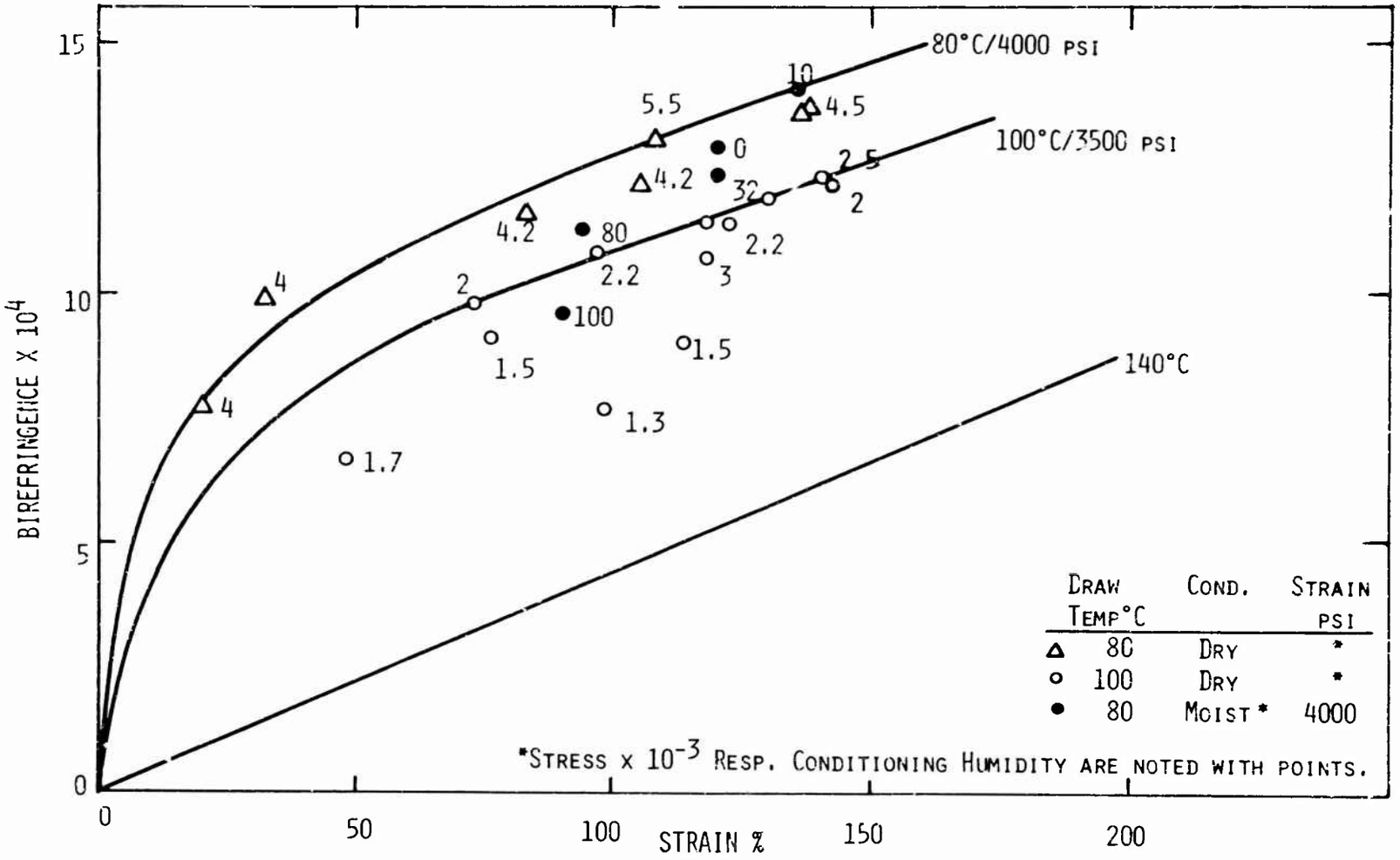

FIG.5.4 BIREFRINGENCE VS STRAIN OF PMMA VARYING DRAWING STRESS, TEMPERATURE AND MOISTURE

(Fig. 5.4) indicates the importance of drawing rate. Given sufficient time, orientation can apparently relax out; presumably, the bond breaking mechanism is of main importance. It is consistent that this is only found at 100°C test temperature where the bond breaking rate should be much higher than at 80°C.

The moisture influence on birefringence is the more remarkable as the 100% test was a factor of 400 faster than the one at 0%. In view of the preceding paragraph the 100% sample, if tested at equal speed as the 0% one, should have an even lower birefringence.

The birefringence changes prior to necking of a sample drawing at 80°C under 3500 psi has been measured also. Specimen dimensions were recorded photographically as direct contact is not possible during the test. The result is shown in Fig. 5.5.

Reversibility of Stretching. It is well known that oriented polymers can, nearly or completely, resume their dimensions before drawing. Crystalline polymers must be heated above the crystalline melting temperature to incur retraction[47]; amorphous polymers[22,46], above T_g. Cheatham and Dietz[48] report PS to shrink to within 10 to 15% of the original length when heated to 145°C after it had been hot stretched 12000%. In PMMA no detectable permanent strain remained after hot stretching at 200°C[46].

The memory for unoriented shape reveals that flow in the sense of complete molecules moving past each other does not take place. Interchain tie points which may be bonds or entanglements persist during drawing. On shrinking, the chains of this network assume a random conformation again. This is more strictly the case for PMMA, whereas in PS some flow is detectable.

The purpose of the following experiment was to test if the shape memory is also preserved after cold drawing and more complicated drawing histories.

PMMA samples were prepared by three different procedures: hot stretching (A), a combination of hot and cold drawing (B), and cold drawing (C). Extension and birefringence values for such a set of PMMA samples are shown in Table XII.

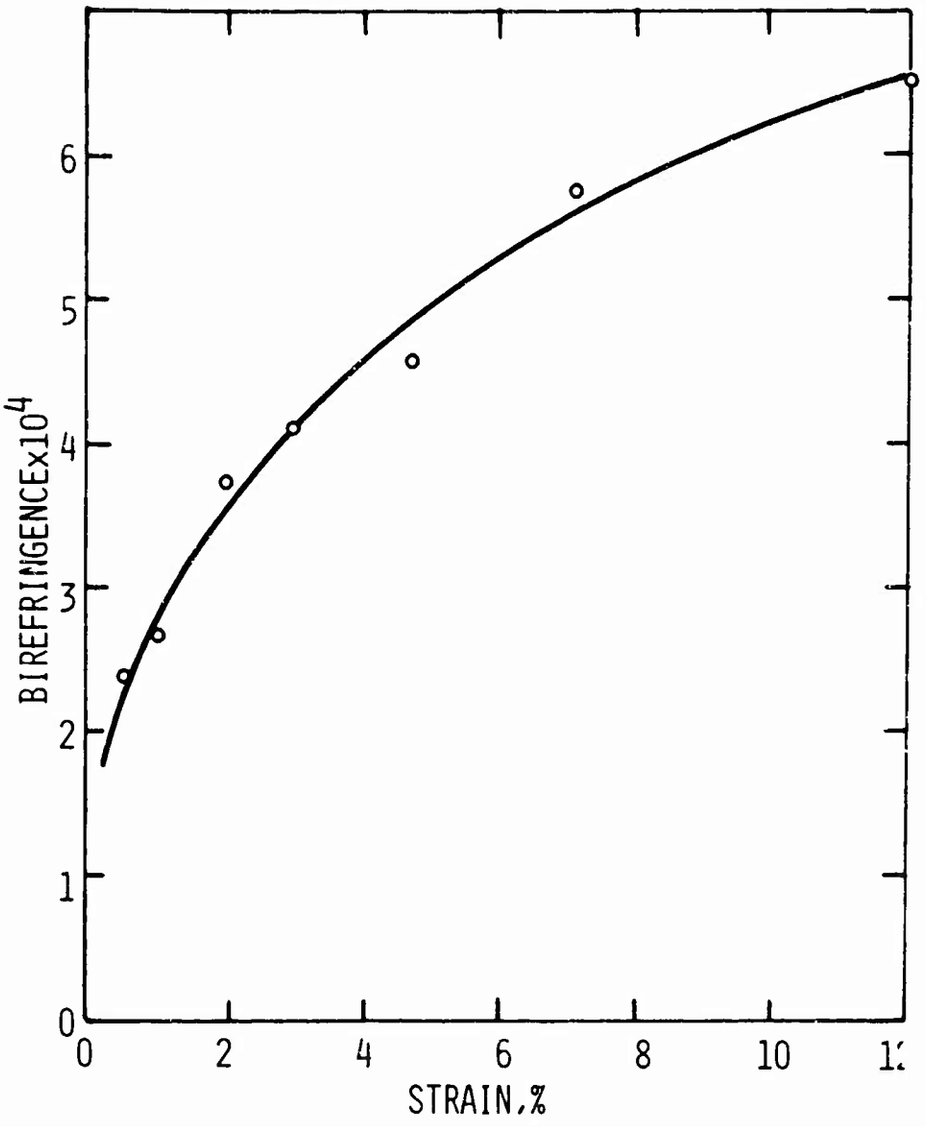

FIG.5.5 BIREFRINGENCE VS STRAIN OF PMMA DURING DRAWING AT 80°C UNDER 3500 PSI FOR THE UNIFORM STRAIN REGION

Table XII

Sample Preparation for the Shrinkage Study

	Elongation (%)*			Birefringence x 10^4	
Sample	Hot	Cold	Total	Hot	Total
A	192	---	192	6.2	6.2
B	115	92	207	4.1	13.0
C	---	120	120	---	12.5

(*The elongation values are based on the original length of the sample)

The elongation possible during cold drawing (C) was set by the natural draw ratio, but the elongation of the hot stretched sample (A) could be matched to the total elongation of the sample (B). The higher birefringence values produced by cold drawing are clearly seen from this table with the combination sample (B) falling in an intermediate position, as expected. When these samples were heated at a temperature well above the glass transition, and permitted to shrink freely, they resumed their original unoriented length, indicating that no molecular flow took place during the orientation process. The birefringence also went to zero in all cases when shrinkage was complete.

A similar series of experiments of PS was not entirely conclusive. It appeared that the hot oriented specimen recovered less than the combined hot and cold drawn one and both did not recover completely.

Birefringence and length recovered during shrinkage at 105°C were measured on freely retracting PMMA after very nearly the same drawing treatments as listed in Table XII. The results are shown in Fig. 5.6, the elongation is based on unstretched length. Initially, length and birefringence decreased too rapidly to measure, towards the end changes occurred very slowly. The curves shown were obtained during about 30 minutes. Strain inserted by cold drawing shrinks out much more readily than that produced in hot stretching.

The recovery of PMMA oriented by hot drawing and by combined hot and cold drawing when the temperature was slowly

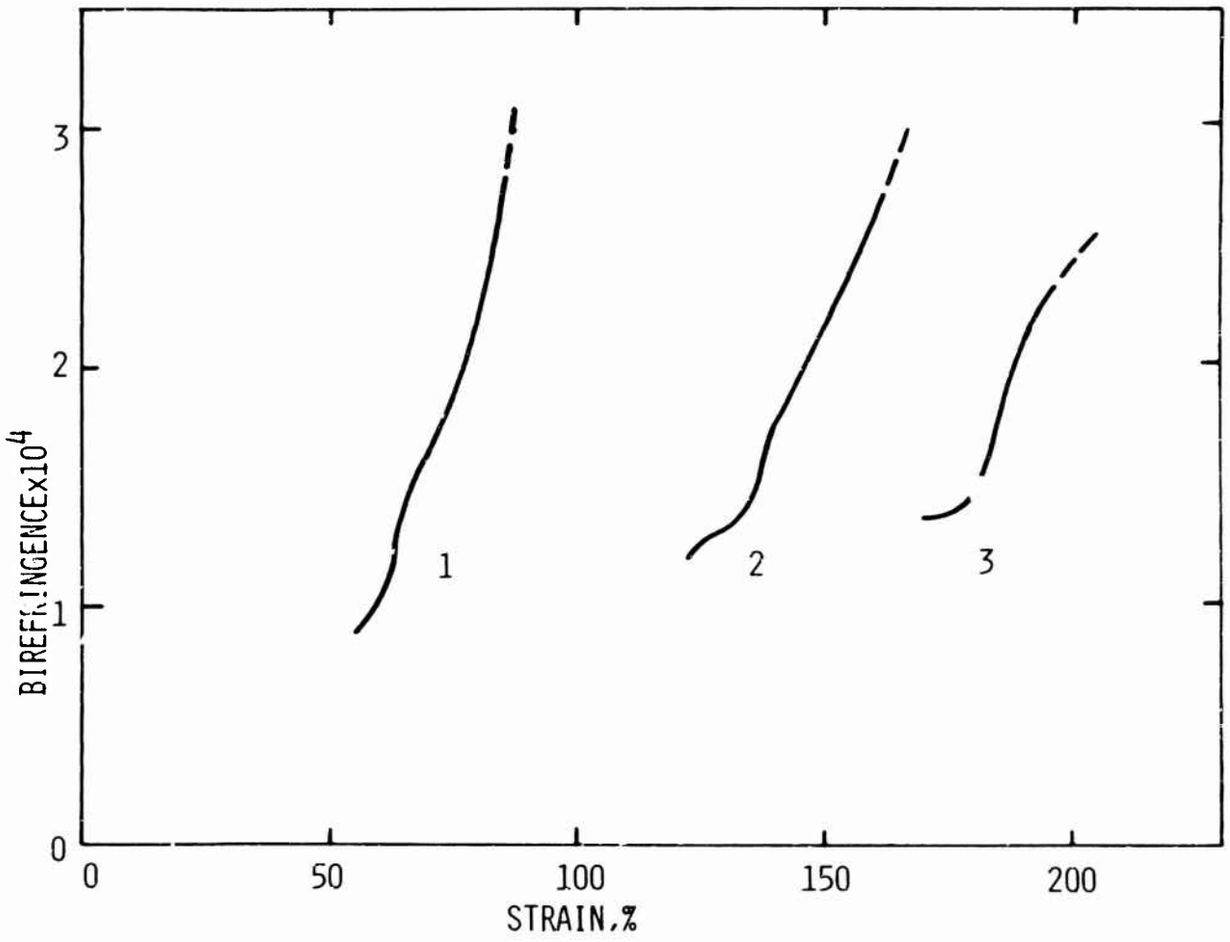

FIG.5.6 BIREFRINGENCE VS STRAIN FOR ORIENTED PMMA DURING SHRINKAGE AT 105°C
SAMPLE 1:110% COLD DRAWN AT 80°C;SAMPLE 2:116% HOT STRETCHED AT 144°C
AND SUBSEQUENTLY COLD DRAWN 89% MORE AT 80°C;SAMPLE 3:205% HOT STRETCHED

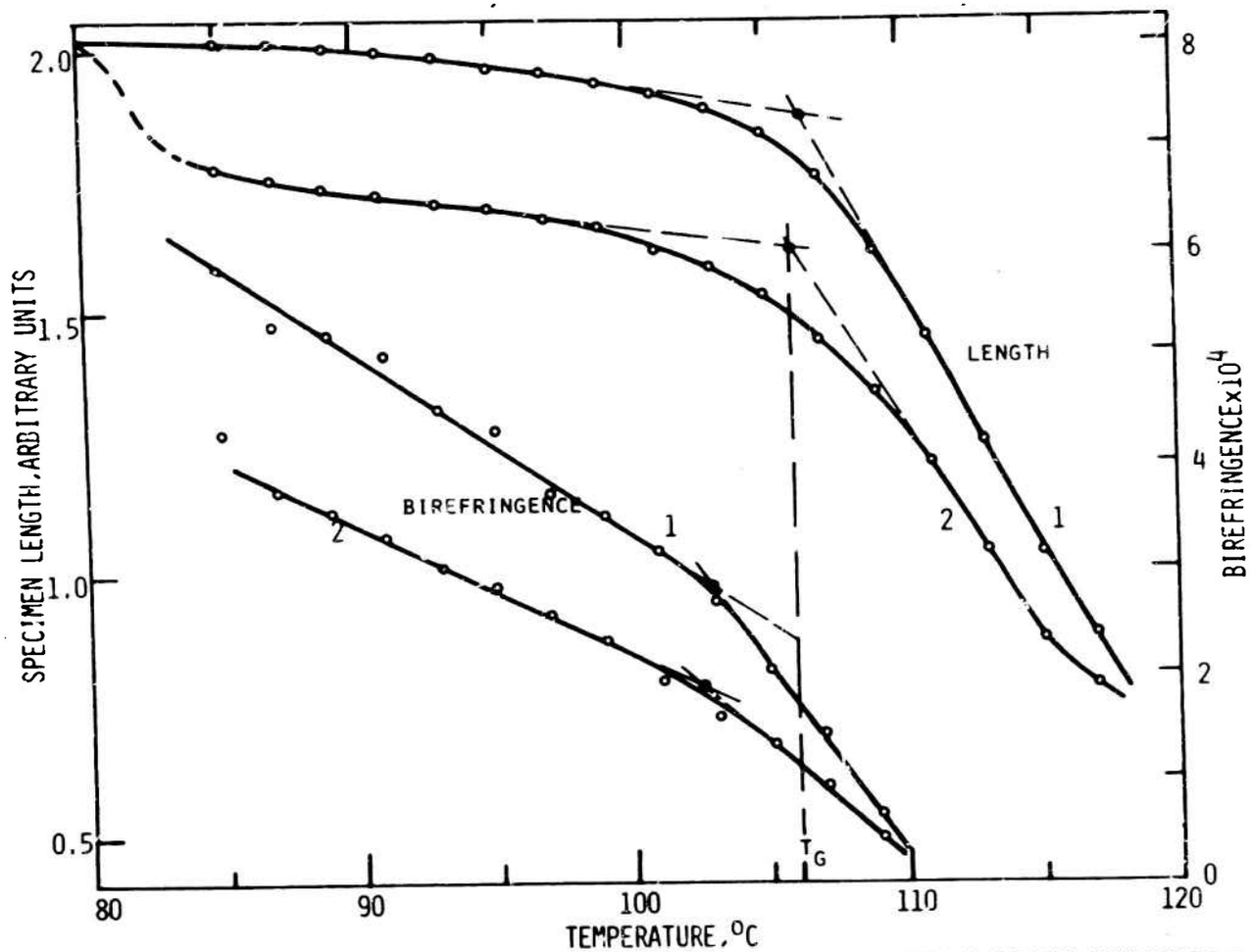

FIG.5.7 SPECIMEN LENGTH AND BIREFRINGENCE OF ORIENTED PMMA VS TEMPERATURE. THE TEMPERATURE WAS RAISED IN 2°C STEPS. MEASUREMENTS WERE TAKEN 15 MIN AFTER REACHING THE NEW TEMPERATURE. SAMPLE 1:200% HOT STRETCHED; SAMPLE 2:180% HOT AND COLD DRAWN

increased is shown in Fig. 5.7. The temperature was changed by 2° followed by 15 minutes at this temperature before the next temperature step followed. Length and retardation were measured at the end of each 15 minute period. The hot and cold drawn sample contracts initially faster than the hot drawn one. At 106°C a break in the length curve occurs, and the rate of length recovery is more rapid than below this temperature. The birefringence shows a change in slope at 103°C. At 110°C the birefringence becomes zero, though the strain is not yet zero. Hammack[49] has found a change of sign of stress optical coefficient in this vicinity. The temperature of slope change of the strain vs. temperature curve drops somewhat with orientation[17]; it has been assumed, based on Fig. 5.7, that the T_g of the PMMA II UVA is approximately 106°C.

DENSITY OF STRAINED PMMA

Introduction

At the end of Chapter III it has been postulated that the mechanical stability of PMMA,which is imparted on it by annealing, may be destroyed by strain. Conditions conducive to losing the mechanical stability would be temperatures below T_g and high strain rates. It should be possible to test this hypothesis by measuring the density of the polymer during straining, because the less stable glass was found to be also less dense (Chapter III).

From observed viscosity changes during drawing, and accepting that they are due to volume changes. one predicts a 10^{-3} g/cm³ (compare Table XIII) density drop. The dilatation caused by the Poisson effect i· tensile drawing tests ($\nu_{PMMA} = 0.35$)[2] corresponds to approximately 5×10^{-3} g/cm³ density decrease. To separate the rapid elastic and the time dependent volume change, a tensile test is suggested in which, after some plastic strain, the stress is suddenly reduced to zero leaving the time dependent or permanent bulk strain, as the case may be, for observation.

Experimental

A less sophisticated experiment than the one mentioned

above was chosen, to avoid the difficult volumetric measurements during a test at elevated temperature. A specimen was cold drawn so that it contained a neck, cooled to T_R and sectioned into pieces of different strain. Prior to drawing a small piece of polymer was cut off the clamping section of some of the specimens. It served as unstrained density control and was tied to the specimen it came from during conditioning and drawing. Equal drying (80°C for 3 days) and moisture absorption conditions for drawn and undrawn were thus provided. The strain of each section was computed from thickness and width changes in drawing. Densities were measured by the differential expansion method (Chapter VIII).

Results

Representative curves for density vs. strain are shown in Fig. 5.8. For small plastic strains the density is below the unstrained value. This drop is recovered on further straining and the drawn density is nearly 0.5% higher than that of the undrawn. Curve 1(b) is a rerun of the sample of curve 1(a), one day after the first measurement, which had been made close to two hours after the drawing of the polymer. The initial dip is now smaller and the density of the strained section has increased with reference to the unstrained polymer.

Curve 2 of Fig. 5.8 shows a similar effect of strain on density. In this case no control had been included and the density at small strains was not measured. The position of the curve with respect to the undrawn material is therefore undetermined. The measurements of Fig. 5.8 were made on normal tensile specimens.

To resolve better the low strain region, the measurements were repeated with tapered specimens. The results in Fig. 5.9 show that the density is lowered already after a few percent of plastic strain.

Discussion

In uniaxial plastic compression the density has been found to decrease in several polymers, including PMMA and PS[10]. The measurements of Ref. (10) were made when stress was applied, where the volume expansion is largely caused by the Poisson

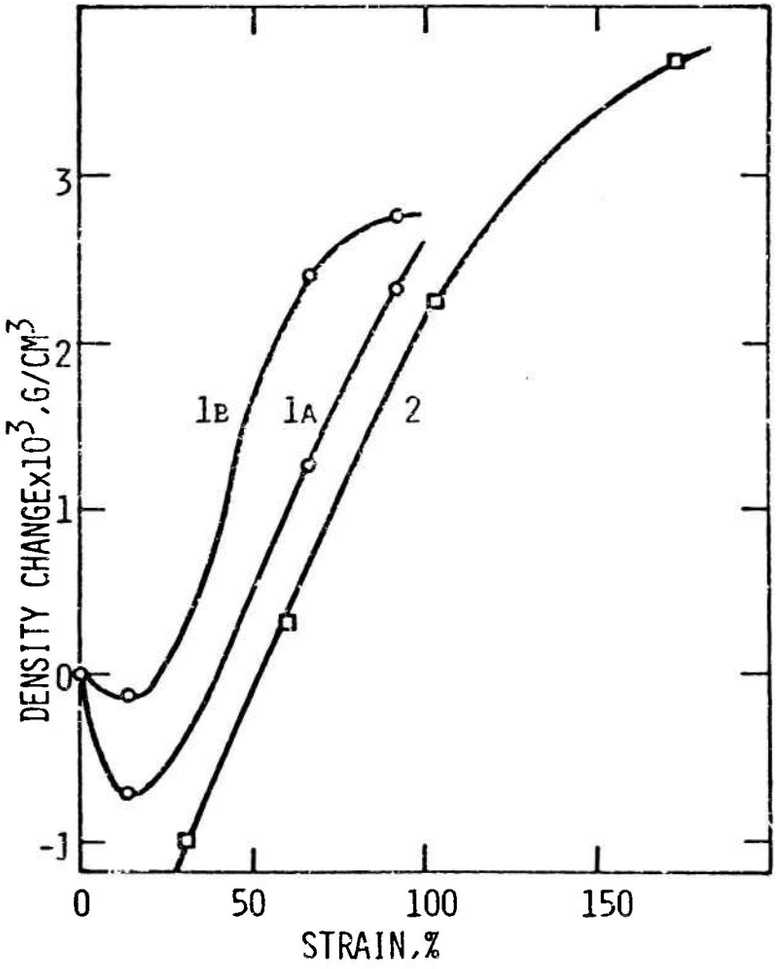

FIG.5.8 DENSITY CHANGE OF PMMA ON STRAINING MEASURED AFTER DRAWING AT T_R

effect. The separation of "plastic volume" change and Poisson volume change is arbitrary insofar as the precise value of the Poisson ratio is not available. The magnitude of the pl stic volume increase reported is several tenths of one percent to one percent, and remains, for the reasons given, quite uncertain.

In tensile straining one observes crazes in many instances which may obscure density measurements. An estimate of the fraction of craze volume v to total polymer volume V gave, for badly crazed samples, $v/V \simeq 0.5 \times 10^{-4}$. The details of this evaluation are incl. d in Chapter VII. If the crazes do not fill at all with the immersion liquid, the relative density measured could be lower or by the given relative amount. The samples used for the density vs strain measurements were only slightly crazed. One section, which showed a density drop, did not contain microscopically visible crazes.

It is concluded that the lowered density reflects a loosening of the glass structure by deformation. The increase of density with time (Fig. 5.8, curve 1[b] vs 1[a]) may be a true change of bulk density, that is, a volume relaxation.

The appreciable density increase by large strains proves the enhanced packing efficiency of parallel chains versus randomly oriented chains. At the end of Chapter III it has been already pointed out that volume contraction during vitrification may be a consequence of directional ordering of next neighbor segments.

If the strained polymer is composed of highly strained and nearly unstrained regions (bands), the former ones being of highly increased, the latter ones of slightly reduced density, the volume change vs strain curve for high strains reflects the relative contribution of both rather than a true density vs strain relation.

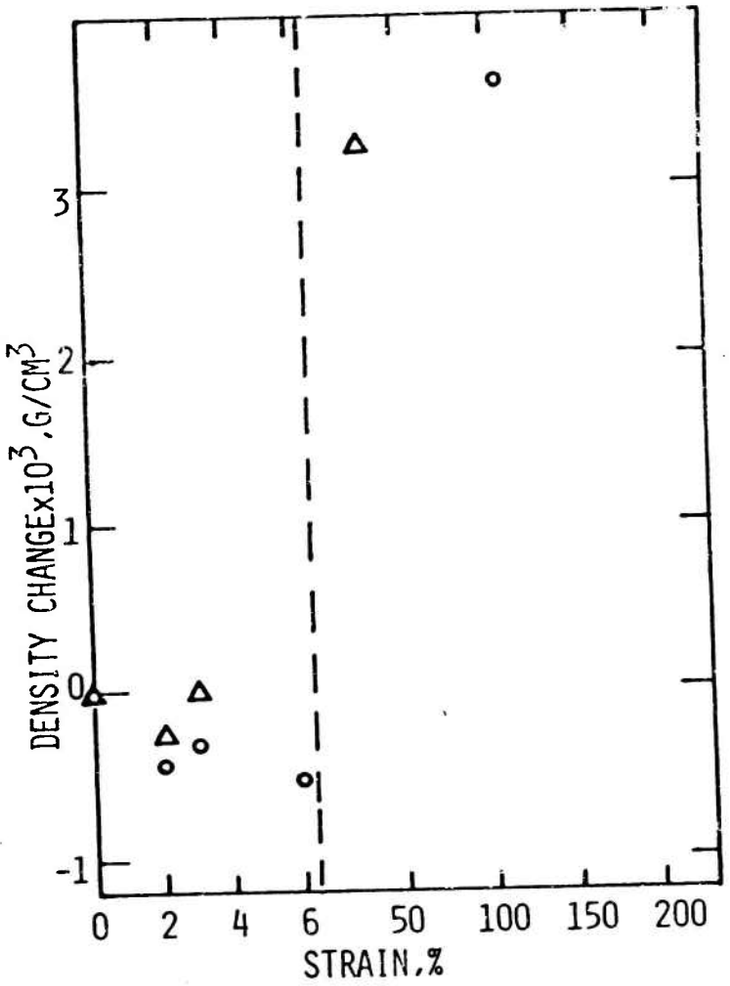

FIG.5.9 DENSITY CHANGE OF PMMA ON STRAINING MEASURED AFTER DRAWING AT T_R

CHAPTER VI

THEORY OF COLD DRAWING

Introduction

The approach to liquid or glassy viscosity in some current theories is from the assumption that the stress biased diffusional jump of a molecule or part thereof requires two events to coincide: the energy must suffice to overcome a potential barrier and there must be free space to jump into. The probability P for the jump is

$$P = p_E \cdot P_v \qquad \text{(VI-1)}$$

(p_E, p_v = probability for availability of energy and volume respectively.)

Mathematical development of this idea leads to equations for viscosity like the hyperbolic sine equation by Eyring[50] or Holzmüller[51] which account for nonlinearity in stress, but somewhat underrate the factor p_v. By contrast, the Doolittle equation[52] takes account only of the volume required for jumps. Recognizing that p_E and p_v may be of similar magnitude, Macedo and Litovitz[53] combined both equations to a hybrid equation, losing thereby the stress dependence of viscosity, as the low stress approximation of Eyring was used.

To succeed, a theory of cold drawing must explain both stress and strain influence on viscosity. Neither one of the above equations contains strain as a variable and does, for this reason among others, not offer a starting point for a cold drawing theory.

Very recently Goldstein[7] developed some new ideas on a cold drawing mechanism. Breakdown of stress carrying elements and redistribution of the stress to neighboring elements explains the effect of stress and strain in this theory. The differential equation of the process has not been solved yet, and therefore it cannot be easily applied to data.

Bond breaking as the cause for structural weakening is also

invoked by Andrews[8] who suggests that cohesive bonds give way under stress and strain thus specifying the molecular origin of the stress carrying elements of Goldstein's theory. But, whereas the latter author suggests that bonds reform to full load carrying capacity after some time, Andrews assumes that the breakdown of bonds results in the unbonded or weakly bonded state characteristic for the glass above T_g.

Yet another new idea is by Robertson[54] who believes that under stress the number of flexed bonds existing in the glass can increase, bringing the chains closer to their conformation above T_g. This author does not include strain in his model.

Equations of dislocation theory have been applied to yielding in polymeric glasses by Whitney[10]. This treatment has merits in that it takes account of structural changes by a strain dependent defect production term. The defects are identified as free volume. Conceptual difficulties arise from the analogy of crystalline and amorphous solid, by which the physics of the problem is temporarily avoided and connection to it is re-established later by adjusting parameters.

Theory of Strain Softening

In a well annealed polymeric glass, the molecular chains have assumed conformations which, for practical purposes, do not change further with time. If it is subjected to shear strain to an extent requiring not only elastic straining of bonds, but also rearrangements of chain segments, the packing of segments, which accounts for the stability, must be destroyed. At least, temporarily so, and unless the conditions are conducive for rapid "healing", recovery will not occur between subsequent rearrangements. For the stability to recover, the ratio of the time for structural stabilization τ_v and the time between two jumps τ_s must be small.

Conformational changes of a molecular segment or part of it are accomplished by rotation of mer units around covalent bonds. The constancy of valence angles requires several segments of the chain to rotate in one process. From the spatial requirements for such chain rearrangements, together with the high packing density of the glass, one must conclude that parts of several

chains move during one process. Each rearrangement process occurs, from the evolving picture, in a volume element of the dimension of several chain segments in each direction. The motion is cooperative like twinning in a crystal, but unlike it in the sense that the displacement of segments is not in one direction. If twinning may be compared with laminar motion, shear straining of the solid amorphous polymer is analogous to turbulent motion. In a single rearrangement jump the annealed coordination of mer units is undone within the volume element participating.

To estimate the time between jumps, during which the glass can regain a dense, stable conformation, the volume element v which participates in a jump is isolated. In one process the element is strained by the shear strain Γ. To deform it to the external shear strain γ it must undergo p such events.

$$\gamma = \Gamma \cdot p \qquad \text{(VI-2)}$$

If the shear rate $\dot{\gamma} = \gamma/\theta$ is imposed, the time to reach this strain is $\theta = \frac{\Gamma \cdot p}{\dot{\gamma}}$. The time available between rearrangements, if the jump requires negligible time, is $\theta/p = \tau = \Gamma/\dot{\gamma}$, independent of the volume of the rearranging unit. Assuming $\Gamma = 1$, the range of τ is 10^2 to 10^6 sec for common tensile test rates, the low value being more typical for cold drawing, the higher one for creep.

The rate of annealing of PMMA was found in this research to have a maximum at 100°C and even there stabilization occurred at least up to 240 hrs ($\simeq 10^6$ sec) annealing time. At 80°C, the temperature used for most of the present drawing experiments, the rate is considerably lower. At this temperature a sample well annealed before drawing does not, even at slow drawing rates, recover its stable glass conformation. During straining, it approaches the state of the poorly annealed glass.

As pointed out above, several investigators have different ideas as to what lends stability to a glass or, putting it another way, as to which structural features which provide mechanical stability initially are lost during straining. Proposed

mechanisms include: breaking of association bonds, straining of primary bonds, and strain-produced free-volume.

Model for the Strain Induced Initiation of Cold Drawing. The model to be developed rests on the hypothesis that the disturbance of the glass structure by strain introduces additional free volume. The treatment is restricted to the low strain region, for which volume expansion on straining has been found experimentally (Chapter V).

The discussion is in terms of fractional free volume

$$f = \frac{v_f}{v - v_f} \simeq \frac{v_f}{v} \qquad \text{(VI-3)}$$

(v_f = specific free volume, v = specific volume) which is, for the present purpose, divided into the free volume f_g at T_g, where T_g is measured at a very slow rate, and a contribution f varying isothermally with strain or time. The total free volume $f_t = f_g + f$.

Free volume is assumed to be generated by strain according to

$$df^+ = \text{const}\, d\varepsilon = a \cdot d\varepsilon. \qquad \text{(VI-4)}$$

Simultaneously, the volume relaxes towards an equilibrium volume. Kovacs[55] has used the equation

$$df^- = -\frac{k}{\eta_v} \cdot f \cdot dt \qquad \text{(VI-5)}$$

for the isothermal bulk contraction of glasses, which has been rewritten in terms of fractional free volume for the present purpose. (k = bulk modulus; η_v = bulk viscosity = viscosity for volume changes; t = time.) The net effect of straining and volume relaxation is

$$df = a \cdot d\varepsilon - \frac{k}{\eta_v} \cdot f \cdot dt. \qquad \text{(VI-6)}$$

By substituting for dt from Equation (II-13), $d\varepsilon/dt = \sigma/\eta$, and

neglecting the difference between shear viscosity η_s and normal viscosity η, Equ. (6) can be rewritten

$$\frac{df}{d\varepsilon} = a - \frac{\eta_s}{\eta_v} \cdot \frac{k \cdot f}{\sigma}, \qquad \text{(VI-7)}$$

provided $d\varepsilon/dt \neq 0$.

For volume changes and shear deformations, molecular rearrangements are required, that is, one would expect η_s and η_v to be related. Associated liquids, which include the glass forming ones, where shown by Litovitz[41] to have $\eta_v/\eta_s \simeq 1$, whereas in nonassociated liquids, the ratio is between 5 and 1000.

If the same molecular mechanism is responsible for shear and volume flow, one might expect, for example, equal temperature dependence of η_v and η_s. Kovacs et al confirmed this on polyvinyl acetate[35]. The difference in apparent activation energy for the recovery of some rheological properties after quenching and the activation energy for the viscosity found in this work shall not be considered to be contradictory evidence; the first one is primarily empirical and not well understood.

Further on it is assumed, following Litovitz, that $\eta_v/\eta_s = 1$. Integrating Equation 7 with σ = constant, and the initial condition $\varepsilon = 0$, $f = f_o$, one obtains

$$f = \frac{a\sigma}{k}\left[1 - \exp\left(-\frac{\varepsilon k}{\sigma}\right)\right] + f_o \exp\left(-\frac{\varepsilon k}{\sigma}\right) \qquad \text{(VI-8)}$$

For constant stress the fractional free volume of the model becomes independent of time.

The limiting fractional free volume, approached asymptotically for high strains is $f_\ell = \frac{a \cdot \sigma}{k}$ (Equ. 8). The decay and generation of free volume are then balanced. Introducing f_ℓ in Equation (8) and rearranging, gives

$$\frac{f - f_o}{f_\ell - f_o} = 1 - \exp\left(-\frac{\varepsilon a}{f_\ell}\right) \qquad \text{(VI-9)}$$

and upon developing the exponential one has

$$\frac{f - f_o}{f_\ell - f_o} = \frac{\varepsilon a}{f_\ell} \left[1 - \frac{1}{2!} \left(\frac{\varepsilon a}{f_\ell}\right) + \frac{1}{3!} \left(\frac{\varepsilon a}{f_\ell}\right)^2 - \ldots\ldots\right] \qquad \text{(VI-10)}$$

It is assumed that the $\frac{\varepsilon a}{f_\ell}$ terms in the brackets are negligible. It will be shown later that this is permissible. With this approximation

$$f - f_o = \left(1 - \frac{f_o}{f_\ell}\right) \varepsilon a. \qquad \text{(VI-11)}$$

The Doolittle equation,

$$\eta = A \exp (B/f), \qquad \text{(VI-12)}$$

provides the connection with viscosity. Using procedures by which the WLF equation can be derived[33c] one arrives at:

$$\ell n \eta_o - \ell n \eta = B\left[\frac{1}{f_g + f_o} - \frac{1}{f_g + f}\right] \qquad \text{(VI-13)}$$

(η_o = viscosity of unstrained glass, η = viscosity of strained glass)

Combining Equations (11) and (13) and changing to base 10 logarithms, one obtains

$$\log (\eta_o/\eta) = \frac{B}{f_g^2 \cdot 2.30} \left(1 - \frac{f_o}{f_\ell}\right) \varepsilon a \qquad \text{(VI-14)}$$

The approximation made in arriving at Equation (14) is that for large viscosity differences f_g is an order of magnitude greater than the terms with which it appears in the denominators of Equ. (13), that is, fairly well annealed samples are assumed. Table XIII shows that this is justified, accepting $f_g = 0.025$[33c].

Combining the Equations (II-13) and (VI-14) the final expression is

$$\log \frac{\dot{\varepsilon}}{\dot{\varepsilon}_o} = \frac{B}{2.30 \quad f_g^2} \left(1 - \frac{f_o}{f_\ell}\right) a \cdot \varepsilon. \qquad \text{(VI-15)}$$

Table XIII

Fractional Free Volume and Viscosity Ratios near T_g

(Calculated from Doolittle Equation [Equ(12)] with f_g=0.025, B=1)

η_g/η	$f_t = f_g + f$	f
	%	%
1	2.5	0.0
10	2.65	0.14
100	2.82	0.32
1000	3.02	0.52
10000	3.25	0.75

Discussion

The final equation [Equ. (15)] derived from the model requires linearity of log $\dot{\varepsilon}$ vs ε plots, with a slope, which decreases as the initial free volume f_o increases. This prediction will now be compared with experimental results.

The strain rate vs strain curves shown in Figs. 6.1, 6.2, and 6.3 have been plotted for strains beyond the yield point in Figs. 6.4, 6.5, and 6.6 respectively. It is implied that these branches of the $\dot{\varepsilon}$ vs ε curves are influenced to a very small degree by delayed elastic effects, and thus they reflect viscosity changes. The strain range available is, unfortunately, very narrow; within it the curves are quite linear in the log $\dot{\varepsilon}$ vs ε plot.

Data from the moisture absorption experiments are shown in Fig. 6.4. The polymer was drawn after exposure of each sample to another moist atmosphere at 80°C under 4000 psi. The curves for different moistures are roughly parallel, the drier samples (= little free volume) reach the velocity of the moister samples after some increase in strain, as expected from the free volume generation of strain. On closer inspection a decrease in slope for the curves of higher velocity is found, predicted by the term $(1 - \frac{f_o}{f_\ell})$.

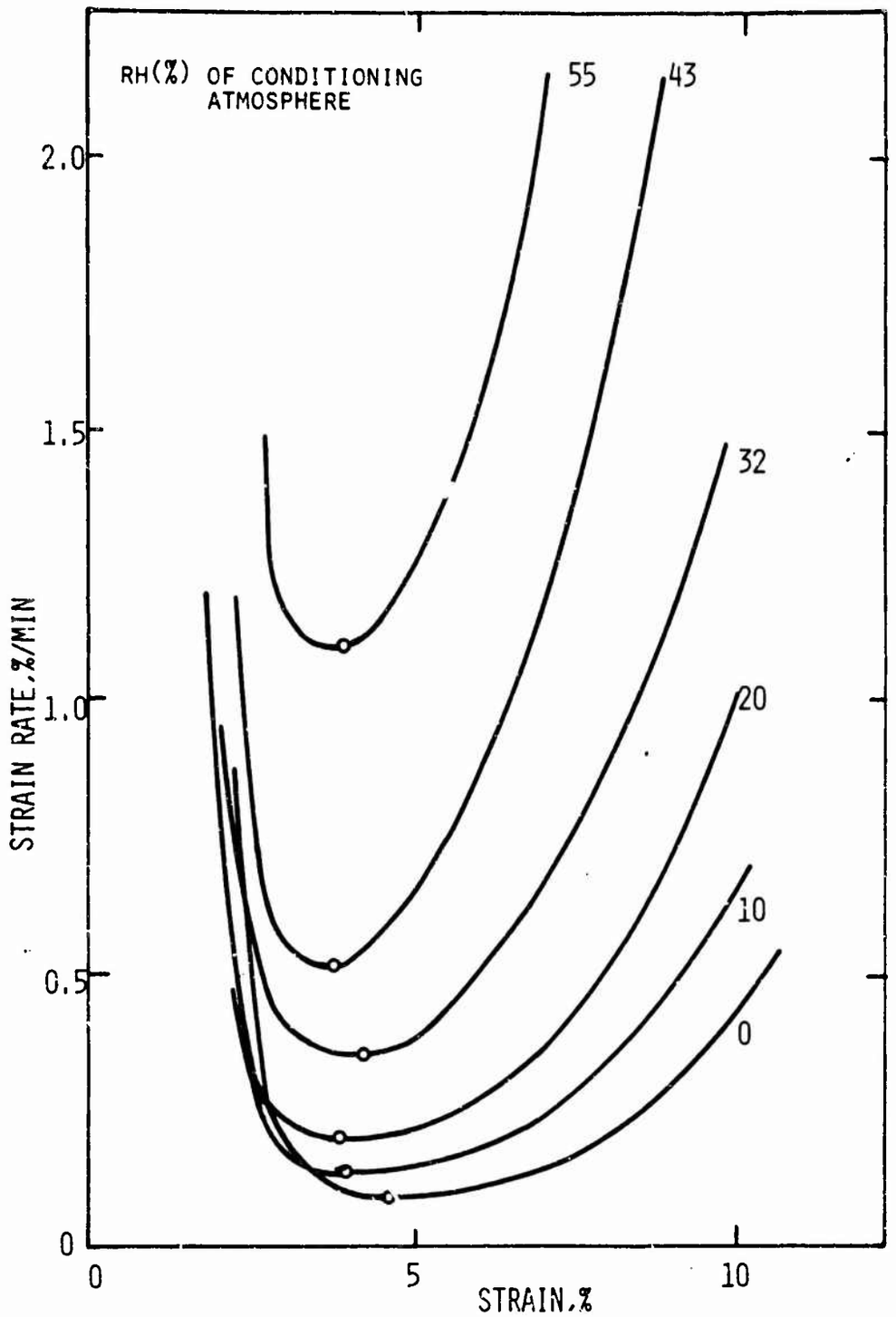

FIG.6.1 STRAIN RATE VS STRAIN FOR PMMA CONDITIONED IN ATMOSPHERES OF VARIOUS HUMIDITIES;CONST.LOAD TEST:STRESS:4000 PSI; TEMPERATURE:80°C

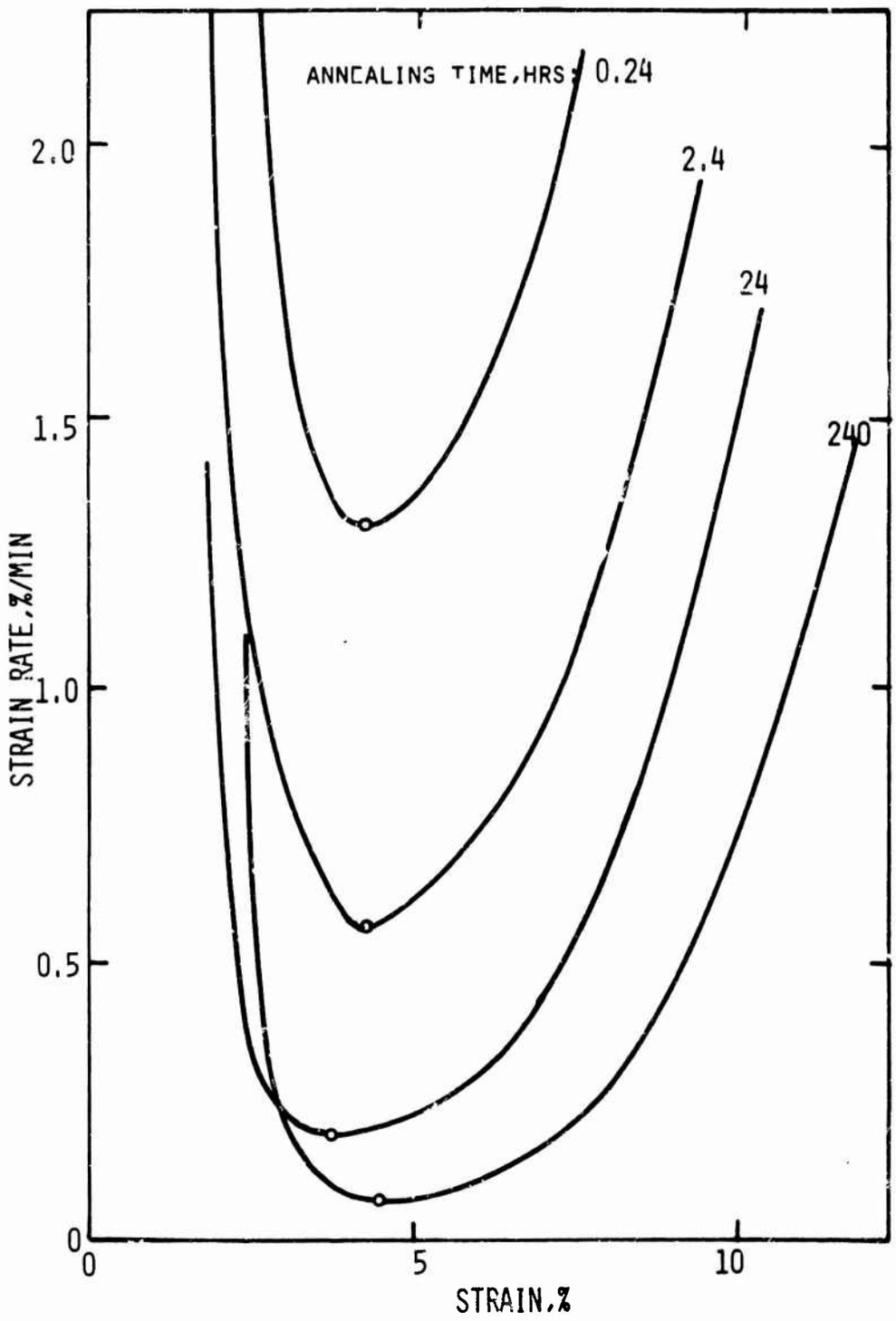

FIG.6.2 STRAIN RATE VS STRAIN FOR QUENCHED PMMA AFTER ANNEALING AT100^{o}C FOR VARIOUS TIMES;CONSTANT LOAD TEST:STRESS: 4000 PSI;TEMPERATURE:80^{o}C

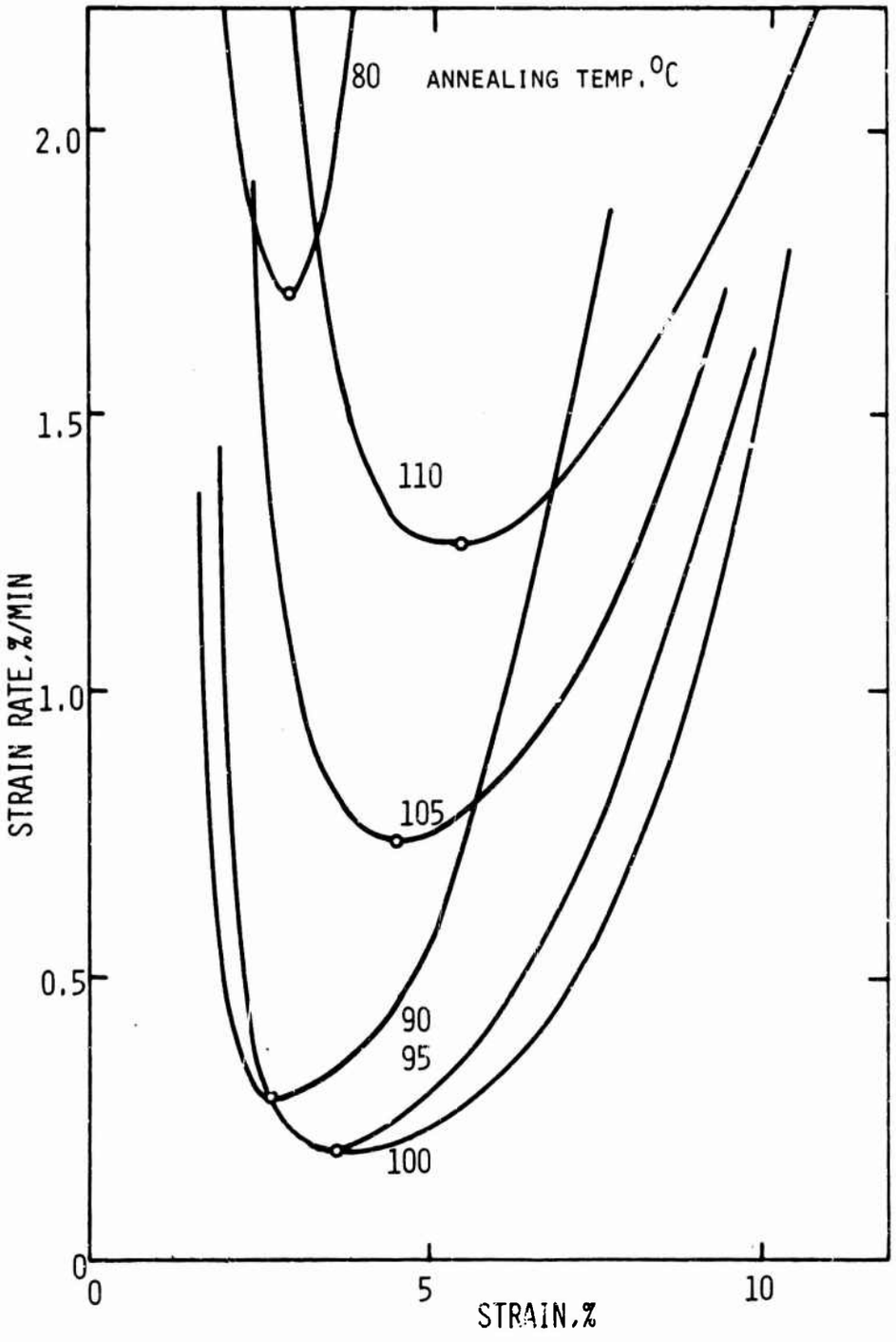

FIG.6.3 STRAIN RATE VS STRAIN FOR QUENCHED PMMA AFTER ANNEALING FOR 24 HRS; CONST. LOAD TEST: STRESS: 4000 PSI; TEMP: 80°C

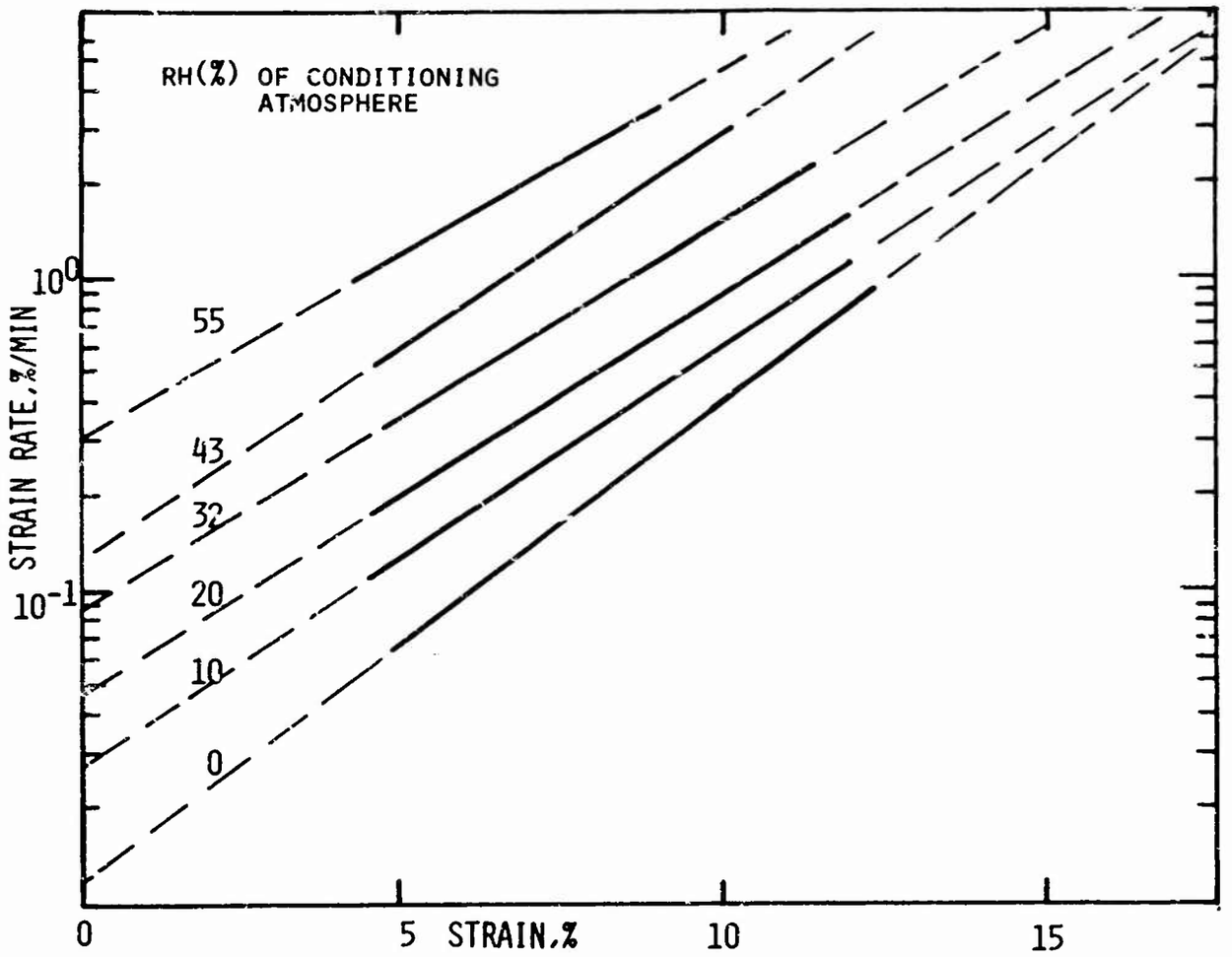

FIG.6.4 STRAIN RATE VS STRAIN FOR PMMA CONDITIONED IN ATMOSPHERES OF VARIOUS HUMIDITIES;CONSTANT LOAD TEST:STRESS:4000 PSI;TEMPERATURE:80°C

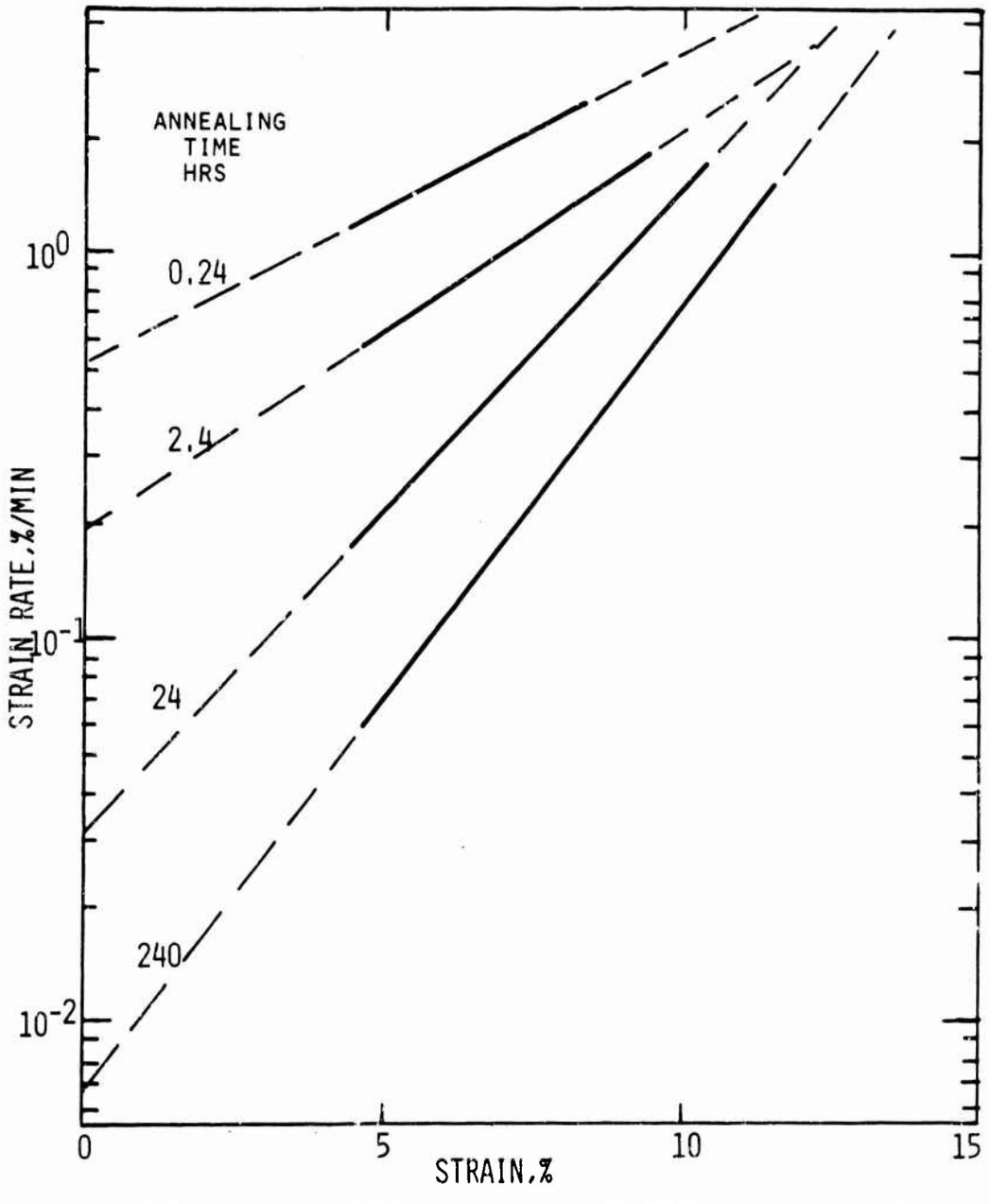

FIG.6.5 STRAIN RATE VS STRAIN FOR QUENCHED PMMA AFTER ANNEALING AT 100°C FOR VARIOUS TIMES; CONSTANT LOAD TEST: STRESS: 4000 PSI; TEMPERATURE: 80°C

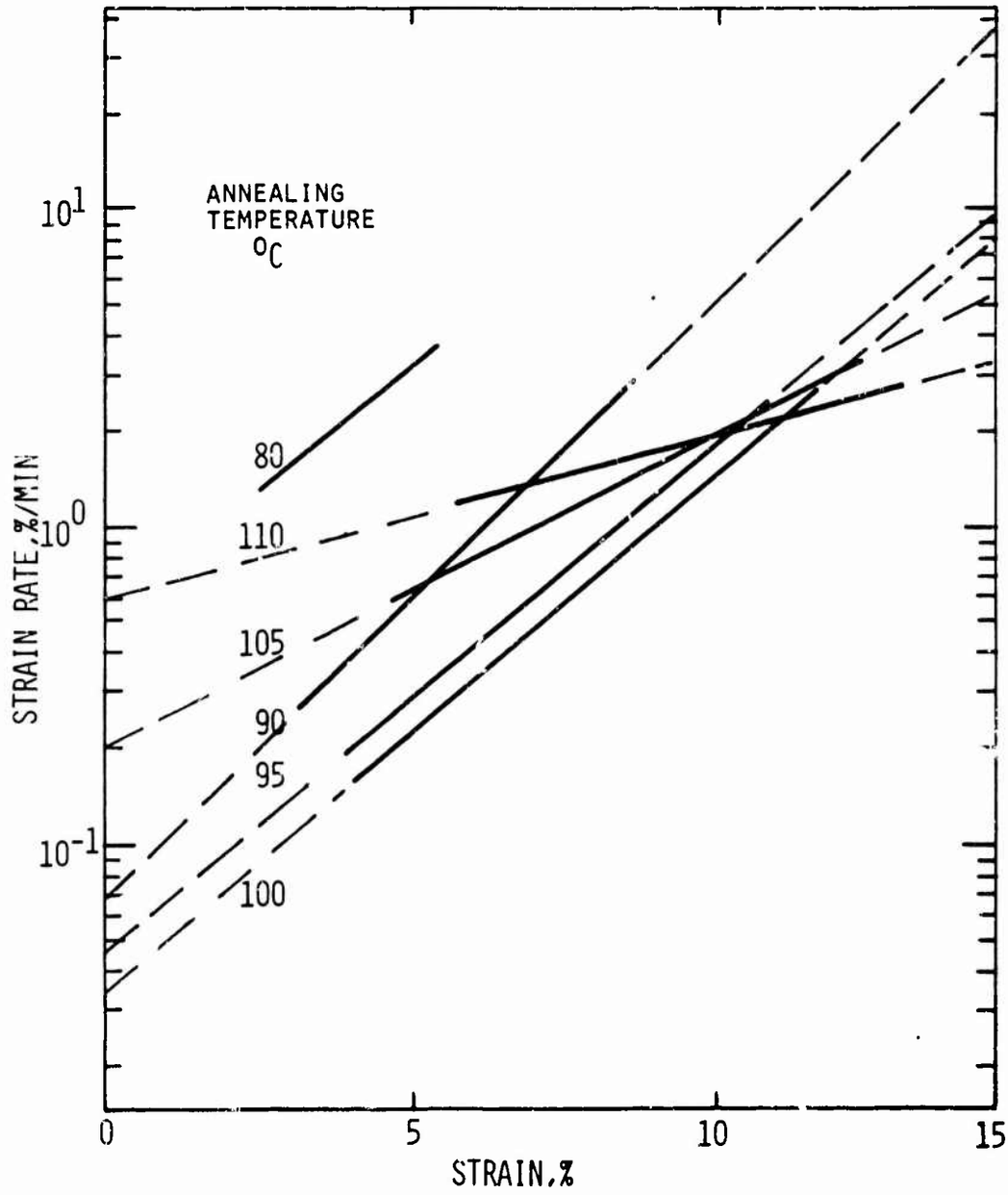

FIG.6.6 STRAIN RATE VS STRAIN FOR QUENCHED PMMA AFTER ANNEALING FOR 24 HOURS AT DIFFERENT TEMPERATURES; CONSTANT LOAD TEST: STRESS: 4000 PSI; TEMPERATURE: 80°C

Figure 6.5 is derived from PMMA annealed for different times at 100°C. In this case the slopes change much more strongly from sample to sample than explainable by the factor $(1 - \frac{f_o}{f_\ell})$. The longer the annealing time, the less rapidly the specimen deforms initially, but the more strongly does it soften with strain.

An even more complicated behavior is found from the plot of results from samples annealed for 24 hours at temperatures from 80 to 110°C (Fig. 6.6). After annealing near T_g, the slopes $d \log \dot{\varepsilon}/d\varepsilon$ are below the ones for low annealing temperature. The curves for 105 and 110°C actually intersect the other curve in contradiction to the predicted model response: Equation (7) states that two samples, which have at any strain equal free volume, continue to have equal free volume on further straining.

Some typical $\log \dot{\varepsilon}$ vs ε slopes, calculated from Figs. 6.4, 6.5, and 6.6 are given in Table XIV.

TABLE XIV

The Influence of Strain on Strain Rate of PMMA under Constant Load

(Computed from Figs. 6.4, 6.5, and 6.6)

(Testing Temperature = 80°C, Stress = 4000 psi)

Sample Preparation	$\Delta(\log \dot{\varepsilon})/\Delta\varepsilon$
Conditioned in 0% RH	15.4
Conditioned in 55% RH	11.8
Annealed at 100°C for 0.24 hours	8.0
Annealed at 100°C for 240 hours	20.4
Annealed at 90°C for 24 hours	18.3
Annealed at 100°C for 24 hours	16.1
Annealed at 105°C for 24 hours	9.5
Annealed at 110°C for 24 hours	5.0

By neglecting f_o/f_ℓ the coefficient "a", which determines the volume increase in the theory is computed to be $7 \times 10^{-3} \leq \leq a \leq 30 \times 10^{-3}$. The lower value is assumed to be more closely correct for the volume generation; it accounts approximately for the experimentally found density drop on straining (Figs. 5.8 and 5.9).

To arrive at Equ. (11) the terms $\varepsilon \cdot a/f_e$ in the brackets of Equ. (10) were neglected. An estimate of the magnitude of

$\varepsilon \cdot a/f_\ell$ is given. The limiting fractional free volume f_ℓ may actually never be reached because the polymer cannot be assumed to conform to the model for high strains as recognized from the density increase measured (Fig. 5.8). The viscosity drops in drawing at least by a factor 10^3. The limiting fractional free volume f_ℓ must therefore be greater than 5×10^{-3} (Table XIII. For the strain range of interest, $\varepsilon \leq 0.1$, the ratio $\varepsilon \cdot a/f_\ell \approx 0.14$, with the smallest value for a from Table XIV.

Should free volume be the only parameter controlling viscosity, cross-overs of the log $\dot{\varepsilon}$ vs ε curves must not occur. The large changes in slope are caused by influences which were not included in the model. Use of the Doolittle free volume equation implies the assumption that the flow in cold drawing is purely volume controlled. It has been suggested in Chapter III that the density increase in annealing (Figs. 3.8 and 3.9) is a consequence of local chain alignment. It is now suggested that this leads to association bonding within these ordered regions. The high density of bonds in the well annealed polymer lends strength when the strain is small, but the higher the bond density, the more rapid is the loss in strength as each strain increment requires more bonds to be broken than in the more densely bonded polymer.

The 110°C/24 hour annealed sample (Fig. 6.6) had little chance for bonding and probably reflects closely the free volume type of structural softening.

A more realistic model of yielding must include a mechanism which accounts for processes other than volume changes. More should be known about the structure of polymeric glasses and its changes during yielding, to include such mechanisms in a theory. A better test of the model which ultimately leads to Equ. (VI-15) would be with a system which, because of its chemical structure, does not form association bonds.

The birefringence vs strain and density vs strain measurements of Chapter V show evidence which can be interpreted as bond breaking and reforming during extension. Doing drawing tests in liquids, Rosenbaum[56] has found that nonsolvents may become

solvents or plasticizers when polyacrylonitrile yields. Although this is explainable as a rate of diffusion or as a free energy effect, it is additional evidence of important changes of the glass structure during straining.

In this section, the polymer has been considered to be an isotropic and homogeneous continuum up to 10 or 20% strain. The isotropy assumption is, of course, incorrect in the exact sense. As regards yielding, it is justified by the near independance of yield stress or delay time on preorientation, as shown in Chapter I for PS.

Above several percent strain, one usually observes non-homogeneities like crazes and shear deformation bands which have been ignored in the discussion. It may well be that in discussing the $\dot{\varepsilon}$ vs ε curves one must take account of the band mode of drawing. In this case, the use of any molecular theory is restricted to small volume elements with the ensuing difficulty to relate the results to the macroscopically observed strains. For the time being, there is too little known about deformation bands which, particularly in PMMA, have been too elusive to allow judgement as to how much they contribute to deformation of the bulk of a specimen. There are also instances where bands do not form at all in PMMA.

Theory of Stress-Softening

At stress levels which are high enough to produce cold drawing the flow rate increases exponentially with increasing stress. The stress influence is expressible as a shift-factor of the rheological properties which is a function of stress alone. The stress shift-factor is in particular independent of strain and temperature in the region studied. An explanation of the influence of stress on the rate of drawing is sought in this section.

Hard polymers experience volume changes under stress, their Poisson's ratio being 0.3 to 0.4[57]. Ferry and Stratton[44] have suggested that volume dilatation under tensile stress contributes to the free volume and have derived a strain shift factor from the Doolittle free volume viscosity equation. An experimental confirmation of the theory has not been given by the authors

and was not found elsewhere. Nielsen[57] attempted to explain the lowering of the stress softening temperature with increasing tensile stress with Poisson's expansion, assuming that it increases the free volume, and found disagreement of theory and data.

As the starting point of the theory to be developed, it is supposed that the stress dilatation is the origin of the flow rate increase. To avoid the low stress region for which stress is known to have less than exponential influence on viscosity, a reference stress σ^* is chosen, which lies within the regime of strong stress dependence of flow rate. The fractional volume change upon elastic incremental loading from σ^* to $\sigma^* + \Delta\sigma$ is

$$\left(\frac{\Delta v}{v^*}\right)_{el} = \frac{\Delta\sigma}{E}(1 - 2\nu). \qquad \text{(VI-16)}$$

It is assumed to contribute exclusively to free volume, $\left(\frac{\Delta v}{v^*}\right)_{el} = \Delta f$. The fractional free volume f is then

$$f = f^* + \frac{\Delta\sigma}{E}(1 - 2\nu). \qquad \text{(VI-17)}$$

(f^* = fractional free volume under the stress σ^*).
Inserting Equ. (15) into (12) and using the same procedure that leads to Equ. (13), one obtains

$$\ln \frac{\eta^*}{\eta} = \frac{B}{(f^*)^2} \frac{\frac{\Delta\sigma}{E}(1 - 2\nu)}{1 + \frac{\frac{\Delta\sigma}{E}(1 - 2\nu)}{f^*}} \qquad \text{(VI-18)}$$

with the assumption $\frac{\Delta\sigma}{E}(1 - 2\nu) << f^*$, which is justified for $\Delta\sigma \leq 1000$ psi ($f^* \approx 2.5 \times 10^{-2}$), and $\sigma = \sigma^* + \Delta\sigma$ Equ. (18) is rewritten, changing to base 10 logarithms, to become

$$\log \frac{\eta}{\eta^*} = \frac{B}{2.3(f^*)^2} \frac{1 - 2\nu}{E} \cdot \sigma^* \left[1 - \frac{\sigma}{\sigma^*}\right] \qquad \text{(VI-19)}$$

Equation (19) is identical with the empirical Equ. (II-15) if

$$\frac{B}{2.3(f^*)^2} \cdot \frac{1 - 2\nu}{E} = \frac{a}{\sigma^*} .$$

The coefficients a/σ^* found by different types of experiments,

are collected in Table XV.

Where the factor a is derived from delay time or velocity data the pre-exponential term σ^*/σ changes the slope of the log (property) vs σ curve from that of the viscosity curve as given by

$$\frac{\Delta \log \eta}{\Delta \sigma} = \frac{a \log (\text{property})}{\Delta \sigma} + \frac{\log e}{\sigma}$$

The term $(\log e)/\sigma = 0.434/\sigma$ has not been applied because the data justify straight lines only in either presentation. This can account for 10% difference among the values of Table XV.

Table XV

Experimental a/σ^* Values

(For Base 10 Logarithms, σ^* [psi])

Temp. °C	From log η/η^*	From v-L curves	t_d From* curves	From incremental stress exp.	Remarks
			PMMA		
70			0.00125 0.00133		(1) (2)
80	0.00113	0.00114	0.00116 0.00133	0.00098	(1) (2)
90			0.00133		(1) (2)
100	0.00078 ÷ 0.0020		0.00065 ÷ 0.00117 0.00133		(3) (1) (2)
			PS		
50 to 80 $\Delta n = 5 \times 10^{-3}$			0.00099		(2)
50 to 80 $\Delta n = 10 \times 10^{-3}$			0.00085		(2)

(1) From non-equilibrium moisture experiments

(2) Same values in Table II

(3) Increasing with strain respectively t_d

*In Table XV the lowest stresses for which drawing was observed have not been included with the exception of the 100°C PMMA data because of uncertainties of results.

Poisson's ratio of PMMA has been reported to be $\nu = 0.35 \pm 0.02$ between -25 to +50°C[2]. Lacking experimental values for higher temperatures ν is assumed to remain unchanged up to the test temperatures used. A further assumption is made, namely that Poisson's ratio for incremental loading is independent of stress and strain. The modulus was found to be $E = 2.5 \times 10^5$ psi and to depend only weakly on temperature. Assuming also, $B = 1$, as is usually done[33c], one calculates from the extreme values of Table XV the free volume of f^* under the reference stress σ^* to be, excluding only the anomalous 100°C values,

$$0.020 \leq f^* \leq 0.023.$$

The free volume at the glass transition temperature is $f_g = 0.025 \pm 0.003$[33b]. The free volume calculated from the stress dependence is in very good agreement with this value.

The correct prediction of the magnitude of the free volume implies the agreement between measured shift factor and that calculated from theory by using independently measured polymer parameters. This result strengthens the basis from which Equ. (19) was derived, namely that the dilatational influence of tensile stress causes the flow ratio to increase by generating additional free volume.

For PS the numerical results are nearly equal to the ones given for PMMA. Modulus and Poisson's ratio of both polymers are almost the same[58] and the result depends only somewhat on which values of these properties reported in literature are adopted.

The stress shift of the 100°C experiments is obviously different from that at all other temperatures. This anomaly may be an apparent one, caused by differences in strain softening. At very small strain rate a recovery of the stable structure of the glass may occur within experimental time. The experiments made do not permit a firm conclusion on this point.

The same stress-shift theory ought to be applicable for

compression, in which case the Poisson effect must increase the resistance of the polymer towards flow. Whitney[10] has found this as an asymmetry of the yield locus. Compression experiments on PMMA (and other polymers) with a superposed hydrostatic pressure as performed by Ainbinder et al[34], also reveal the influence of volume reduction. The upper yield-stress increases with hydrostatic pressure (at T_R) from 20,000 to 40,000 psi by increasing the pressure from atmospheric pressure to 30,000 psi. This is a much weaker than exponential dependence.

To apply the previous equations to Ainbinder's data $\Delta\sigma$ is to be replaced by $-3\Delta P + \Delta\sigma$ (P = hydrostatic pressure, >o for compression). Using the thus modified Equ. (17) indiscriminately one gets for PMMA a physically unacceptable negative free volume. The compressibility of glassy PMMA is almost independent of pressure and the relative volume is reduced by 0.032 when the pressure rises from 0 to 14,000 psi[59]. The fractional free volume at T_g is 0.025 and it can only be kept from zero or negative values if occupied and free volume are compressed. The second right hand term of Equ. (17) must be modified by a factor <1, which is an undetermined function of pressure. Why volume decrease affects both occupied and free volume and, at high stresses, dilatation by tensile stress only free volume remains an interesting question.

It has been reported repeatedly that volume changes from compression are less effective in shifting polymer relaxation times than those which are produced by temperature[60,61]. Only compression has been used in the investigations referred to. In view of the findings in this section, it would be interesting to see if expansive hydrostatic stresses are more effective.

Linear flow behavior at low stress and exponential stress softening at high stress, both must be accounted for by theory. The shift factor derived from volume dilatation predicts an exponential stress influence only, regardless of stress. It must be concluded that one type of response is superseded by the other in different stress regimes. In Chapter II it has been shown that the deformation mode transition is very likely connected with a change of the way in which stress influences viscosity.

The strain rate in constant velocity tests was found to vary with the upper yield stress equally as much as it varies with stress in constant load experiments (Fig. 2.9). This could mean that yielding in the constant rate of extension test occurs primarily because of the dilatational effect of the tensile stress in accordance with the theory developed above. The yield strain in constant rate tests is nearly constant. The extent to which strain softening has taken place up to the yield strain should therefore be essentially the same irrespective of the strain rate. The question if stress dilatation is the important influence in yielding at constant strain rate cannot, nevertheless, be answered at this stage. In the vicinity of the yield point time dependent stress changes are particularly important and their contribution to the total stress cannot be judged on the basis of the present knowledge.

Time Effects in Cold Drawing

Reduction of viscosity by stress may well explain some time effects observed in interrupted drawing reported first by Vincent[5]. If constant rate drawing with a neck is stopped and the sample allowed to relax for some time, a new yield maximum appears when drawing is resumed, without appearance of an additional neck. If, on the other hand, the stress is reduced to zero in the intervening period, no new yield peak is detected. This has been found on PVC[5], nylon, PS and PMMA[10]. The height of the new yield peak increases if more time is permitted for stress relaxation[10].

In yielding, the highly packed stable glass initially present turns temporarily into a less tightly packed unstable glass. The return to the dense glass is accomplished by self diffusion of mer units. It is proposed that the viscosity lowering influence of tensile stress enhances the rate with which the stable glass structure is partly recovered. This influence is only operative with stress relaxation between the drawing periods. Before the shoulders can move again, additional work, appearing in the form of the yield peak, has to be expended to produce the soft, easily deformable shoulder material.

The proposed mechanism could be tested by applying, after initially drawing with a neck, different constant loads instead of permitting stress relaxation. The higher the loads, the more effective in bringing about a new yield maximum this treatment should be. An equivalent influence is expected from temperature increase.

Temperature Effects on Drawing

The strain softening which leads to cold drawing has been interpreted to be a strain induced transition from the glassy to the rubbery regime. The situation suggests that the temperature influence on viscosity during drawing may be that characteristic for $T > T_g$. Confirmation of this suggestion by data would be evidence for the strain induced transition.

The temperature influence on delay time for PS and PMMA is given in Table II by the values $\Delta \log t_d/\Delta T$. They are, within experimental error, the same for both polymers.

It has been shown in Chapter IV that the ratio of delay times measured under different conditions of temperature, for example, is the ratio of the viscosities, each viscosity averaged over strain from zero to the delay strain. The viscosity ratio as a function of temperature is used for a comparison with temperature shift factors from other experiments.

In Figure 6.7 $\log a_T$ vs T is shown; with the value from Table II this gives a straight line (1) for the delayed drawing data. The 80°C value has been taken as a reference point. Two more shift factor curves for PMMA are given; one from replotted data by Tobolsky and McLoughlin[62] who did stress relaxation experiments (2); the other from creep data by Bueche[63] (3). Some caution is necessary as there is no sound basis for the comparison of the large strain data with the small strain data of the authors mentioned. If the temperature effect on t_d were as expected, the slope of curve (1) should agree with that of (2) and (3) above T_g. This is not the case. It remains to test if curve (1) has at least a higher slope than that of the other curves below T_g. Unfortunately, there are large discrepancies between curves (2) and (3) in this region, which permit either one conclusion. What can be said is, therefore, only

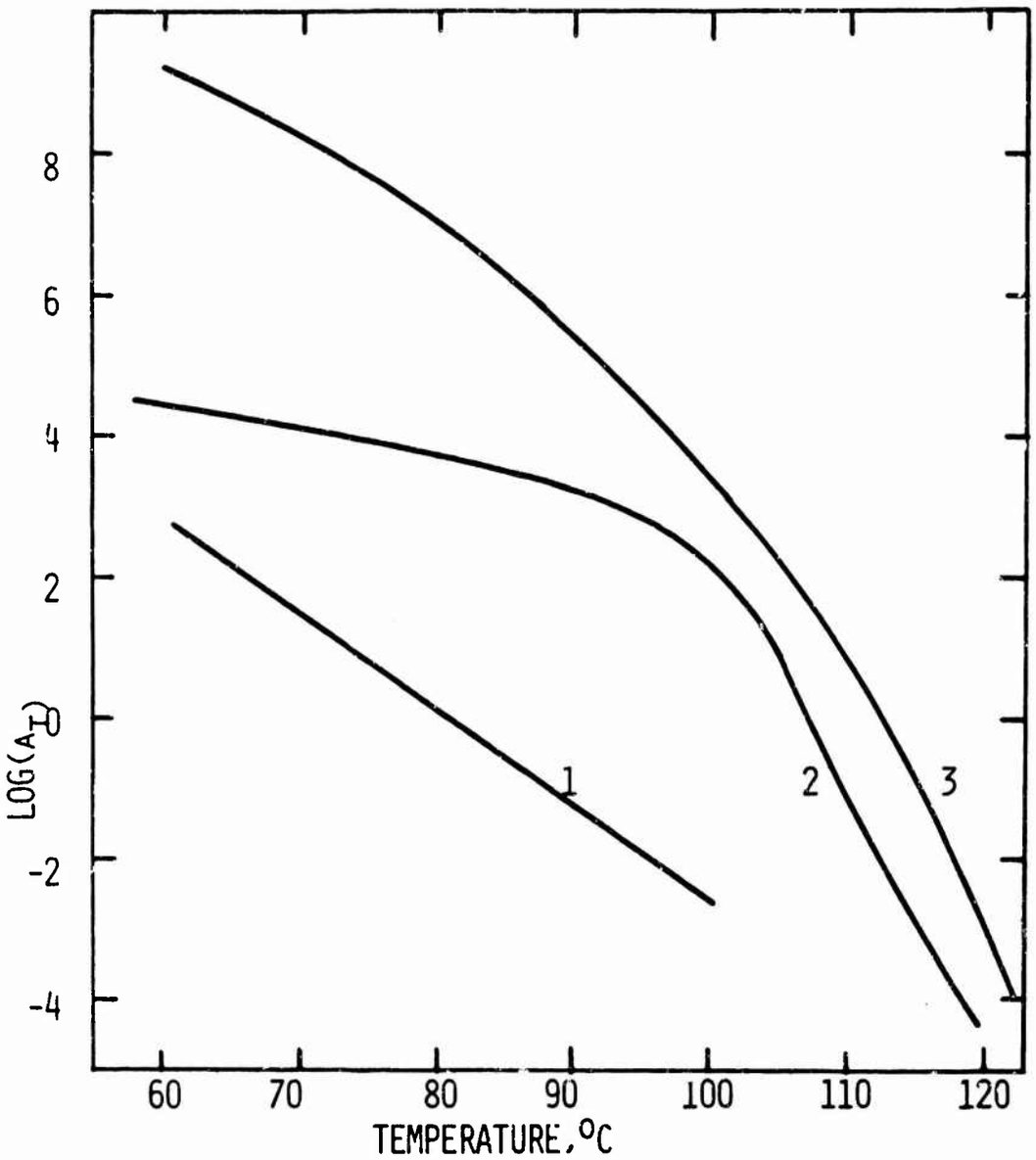

FIG.6.7 TEMPERATURE-SHIFT-FACTOR VS TEMPERATURE FOR PMMA

CURVE	SOURCE	MEASUREMENTS
1	THIS WORK	DELAY TIME IN CONST. LOAD DRAWING
2	TOBOLSKY ET AL[27]	STRESS RELAXATION DATA REPLOTTED
3	BUECHE[63]	CREEP DATA REPLOTTED

that the strained glass does, with respect to temperature changes, not behave like the rubbery polymer, though it may be closer to it than the glass.

The glass transition temperature is, at least for PMMA, not associated with a very abrupt change in behavior. The approach to T_g is recognized in properties 20 to 30°C below it (see, e.g., Fig. 3.1) and cold drawing, usually thought of as being typical for the glass, was found in this work 10°C above T_g. Therefore, one should not expect the strain induced transition to be found as a well defined discontinuity either.

Drawing above T_g

If non-uniform drawing is indeed the result of a loss of the mechanically stable structure, it should disappear at high enough temperatures for the structure to recover rapidly in comparison to the rate of straining. This is, of course, what one observes far enough above T_g. Of more interest is the region where the behavior is rate sensitive, that is, near T_g. One should be able to produce uniform drawing by slow and nonuniformity by rapid extension. Several exploratory experiments of this type were made.

Constant load experiments were carried out as usual. A drawing temperature, at which the flow rates would not be too high to measure them with the available equipment, was established by heating a tensile specimen under 2000 psi at a rate of 1 to 2°C/min, recording its length change. Near 110°C the flow rate increased nearly discontinuously. The tests were carried out at 116°C and stresses below 2000 psi.

The length vs time curves (Figure 6.8) are of the same type as the ones measured below T_g. An immediate elastic deflection is followed by high but decreasing rate of flow which passes through a minimum (yield point) and accelerates thereafter. For low stress experiments (350 and 500 psi) drawing remained homogeneous at all strains in spite of the potential for necking beyond the yield point $[(\frac{\partial V}{\partial L})_F > 0]$. Under higher stress (1000 and 1500 psi) necking started above 10% strain.

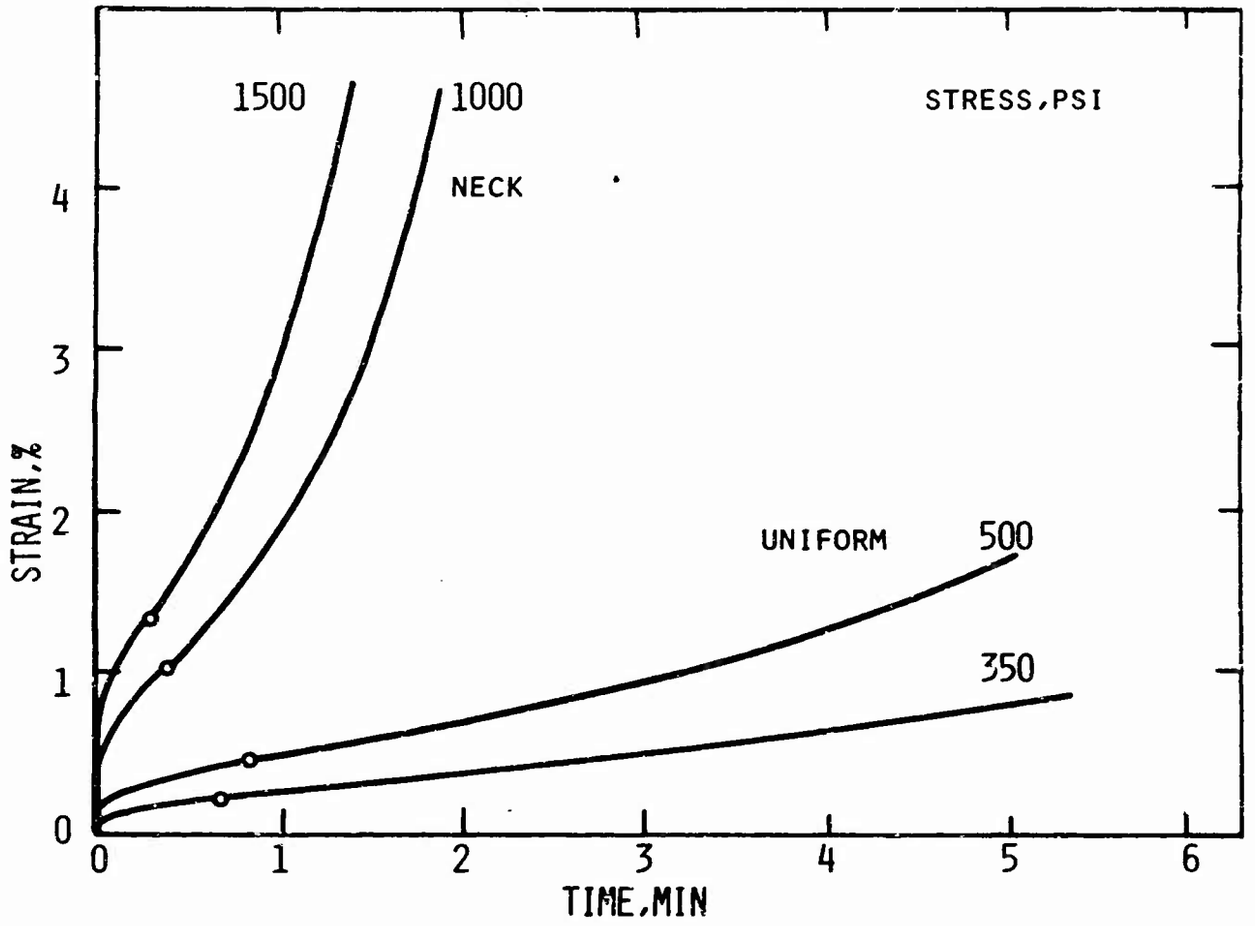

FIG.6.8 STRAIN VS TIME IN CONSTANT LOAD DRAWING ABOVE T_G FOR PMMA
TEMPERATURE:116^{O}C

The characteristic parameters have been collected in Table XVI Precision of strains and moduli is low as the deflections were small. It is surprising that the modulus is still nearly the same as below T_g.

The transition uniform to nonuniform, induced by strain rate increase, supports the hypothesis on which much of the discussion of Chapter VI is based, and which has been restated at the beginning of this section.

Table XVI

Drawing Parameters for Drawing of PMMA Above T_g

Drawing Cond. T	σ	$EMx10^{-5}$	ε_{el}	ε_y	$\dot{\varepsilon}_y$	t_y	t_d
°C	psi	psi	%	%	%/min	min	min
116	350	(3.3)	0.1	0.2	0.09	0.6	uniform Dr.
116	500	2.4	0.2	0.4	0.45	0.8	uniform Dr.
116	1000	1.8	0.6	1.0	1.17	0.3	2.7
116	1500	2.4	0.6	1.3	1.50	0.3	1.9

CHAPTER VII

MICRO-DEFORMATION MODES

Introduction

Drawing is preceded, regardless of whether a neck forms or sample uniformity persists, by the appearance of oblong regions of high shear strain. These become more numerous as the deformation approaches its most rapid phase and they have been referred to as shear deformation bands, though the analogy to bands in crystalline matter is not a good one. In polymers the highly sheared regions are not sharply bounded by the unstrained material-like bands in crystals.

Amorphous polymers have various degrees of confinement of the shear bands; PS develops quite well defined bands, whereas those in PMMA are rather diffuse. Nevertheless, their connection with yielding in these two polymers and in others as well leads one to conclude that sharp shear bands or diffuse zones of high shear are different degrees of the same phenomenon.

Localized shear in polyamid film strips was described by Kauffman and George[11] in 1951. Jaeckel[3] reported in 1954 the observation of localized shear flow regions preceding necking in polyvinyl chloride and Richard and Graube[64] (1956) saw the same effect in polyethylene. These investigators made their observations in connection with tensile tests. Well confined shear bands caused by compression were studied in PS by Whitney[10,15] and by Andrews et al[16] very recently.

Shear bands frequently originate from the edges of crazes, which form under the influence of tensile stress, perpendicular to the stress direction. On first sight, crazes appear to be long, thin surface cracks; but unlike these cracks, they contain craze matter[65], believed to be fiber-like aggregates of oriented polymer connecting the craze walls.

Crazes are easily observable by light and electron microscopy. Though crazing has received much attention, there remain many questions concerning the mechanism of its formation, the structure of the craze matter, and the termination of

craze growth. It seems that termination is reached when the plastic flow at the tip of the craze spreads into the uncrazed polymer[9,65]. One may infer from this, as Crowet and Homès[9] did for PMMA, that crazes, being the origins of severe plastic flow, determine tensile properties. At least, one must concede that crazes may have an influence on cold drawing. The objective of this chapter is to report the microscopic phenomena associated with yielding observed in the course of this study. An essential part of this work was the development of methods by which these surface features were detectable.

Experimental

Light Microscopy. The difficulty one faces in optical microscopy of deformation bands is the lack of changes of light absorption and refractive index or of newly created internal surfaces. The bands are discernible only by use of polarized light as they are birefringent, or by utilizing methods sensitive to the surface unevenness they cause.

In this work, the polarizing microscope has always been tried first. Phase contrast microscopy has often worked quite well also--strangely so, as the great thickness of the sample precludes good phase conditions.

Regardless of which type of microscope was used, the best lighting conditions and other optical adjustments were to be found by trial and error. Even the detection of the features looked for depended often critically on the microscope settings; therefore, the use of methods less subjective became desirable.

Detection of Shear Bands by Light Refraction. Once nonuniform strain has started, the polymer surface is no longer plane. Light passing through it at perpendicular incidence deviates from its original path after passing the surface, if the local surface normal no longer coincides with the beam direction. The methods of shear band detection described below take advantage of this effect.

1. Direct shadow method. The flat tensile specimen is projected by a point light source onto a photographic film or, for direct viewing, onto a ground glass screen. Where the surfaces are not

flat, the light does not arrive at the point of the screen where it would otherwise arrive. Refraction converts the surface texture into differences in light intensity in the projection. This is the most simple form of a schlieren apparatus.

More complicated schlieren optics were difficult to align and offered no advantage in image quality in this application. The point light source is realized by a pin hole in a brass sheet onto which the light of a carbon arc is focused.

2. Light beam refraction method. A light beam, after passing through the structured surfaces of a flat, transparent polymer specimen, forms a figure on a film inserted in its path, which is characteristic for the topography of the specimen. The refraction patterns to be presented were from a nearly parallel beam of white light with circular cross-section, approximately 1.5 mm in diameter, falling at normal incidence on the surface. The apparatus is shown in Fig. 7.1. By letting the undeviated part of the beam pass through a hole in the photographic film, scattered light was eliminated. This clearly improved the definition of the light figures.

The refracted beam lies in the plane formed by the incident beam and the local surface normal. Therefore, when viewing the film in direction of the incident light beam, the refraction effect of parallel surface ripples on the polymer surfaces appears as a light trace radiating out from that point where the unrefracted beam penetrates the film. In this view this light trace runs on the film perpendicular to the ridges on the polymer surfaces.

An example of a typical refraction pattern is given in Figure 7.31(b). The strained PMMA specimen, from which it was obtained, was parallel to the long, black line on the photograph. The oblique lines originate from two sets of surface ripples lying somewhat less than 45° to the stretch direction. These ripples are the consequence of localized shear strain.

The long line parallel to the specimen axis appears only when the surface is crazed. Crazes lying within the beam cross-section scatter or reflect light to the ones outside of it. These, in turn, scatter or reflect light onto the film.

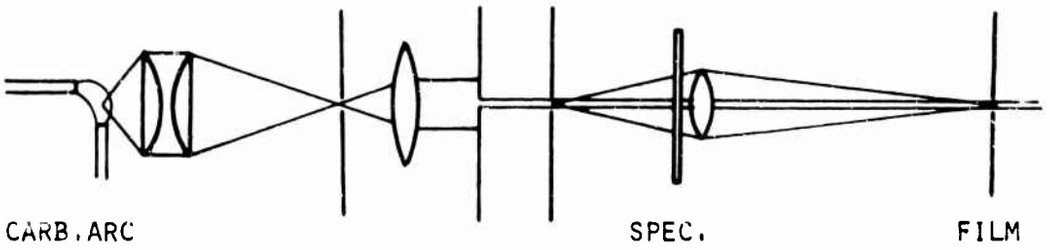

FIG. 7.1 APPARATUS FOR THE DETERMINATION OF LIGHT REFRACTION PATTERNS OF POLYMER SURFACES

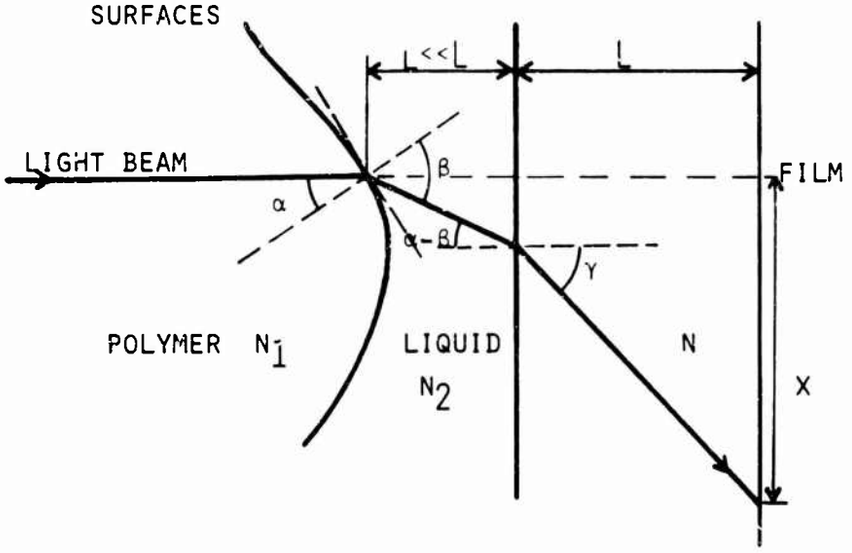

FIG. 7.2 DEFLECTION OF A LIGHT BEAM AT A CURVED INTERFACE BETWEEN MEDIA OF DIFFERENT REFRACTIVE INDEX. THE SPECIAL CASE IS INCLUDED THAT THE SURFACE UNEVENNESS IS FILLED BY A LIQUID OF REFRACTIVE INDEX N_2.

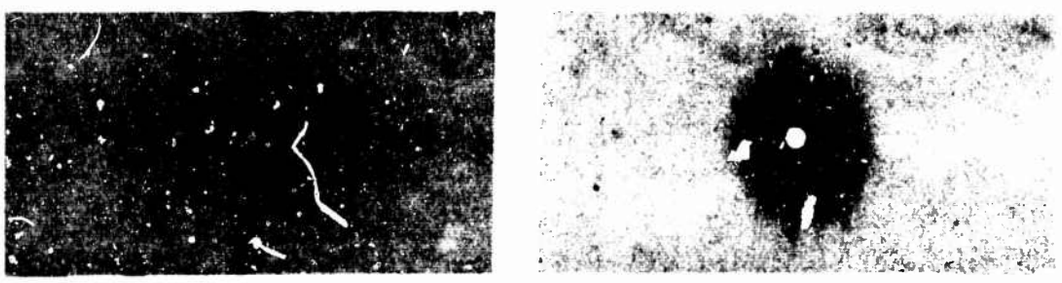

FIG. 7.3 LIGHT REFRACTION PATTERN OF A PARTLY DRAWN PMMA SPECIMEN. LEFT: WITHOUT LIQUID COVER. RIGHT: GLYCEROL FILM APPLIED TO BOTH SURFACES.

The short line perpendicular to this long line appears together with crazes, but not always. It probably comes from the scattering of light at the fibrous craze matter visible in Fig. 26.

How much the light beam is deflected is easily derived with the aid of Fig. 7.2. The resulting equation, the validity of which is restricted to the small angles α found experimentally, is with the symbols of Fig. 2

$$x = L \cdot \alpha \cdot \frac{n_2}{n_1} \left(\frac{n_1}{n_2} - 1 \right) = L \cdot \gamma \qquad \text{(VII-1)}$$

Equation VII-1 takes account of the case where the surface is covered with a thin layer of liquid of refractive index n_2 evening out the surface ripples.

One might suspect that the refraction pattern is, at least partly, caused by internal optical inhomogeneities of the deformed polymer. This is not so, as is easily shown by applying a drop of liquid of refractive index n_2 (see below) to both surfaces, covering it with a cover glass to produce flat surfaces. The refraction figure gets smaller as n_2 approaches n_1 (PMMA n_D = 1.484) and disappears when the two refractive indices are equal (Equ. 1). This would not happen if it were originated by internal schlieren. Therefore, the refraction patterns are caused by surface unevenness.

When $n_2 = n_1$, there remains only a diffuse, non-directional scattering pattern, which has not been studied further. The halo becomes very intense when glycerol is applied to the surface [Fig. 7.3(b)]. The refraction pattern of the same surface, before covering, is shown in Fig. 7.3(a). The long line disappears when glycerol (n_D = 1.469) is used, indicating that the liquid penetrates into the crazes. When water (n_D = 1.331) is applied, the long line becomes more intense. There is no good explanation, at the moment, for this effect of water.

The light beam refraction method has also given firm results in cases where surface features were not detectable by the optical microscopy methods mentioned, over which it has the advantage that critical adjustments of any kind are not

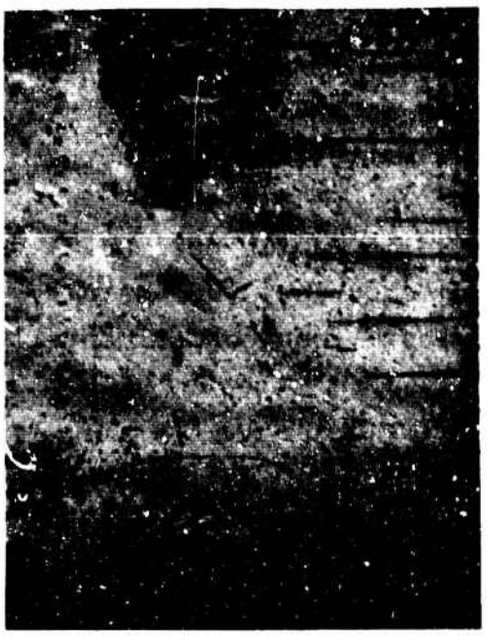

FIG.7.4 SURFACE OF PARTLY DRAWN PMMA. A LAYER OF PT WAS APPLIED IN CIRCULAR AREAS PRIOR TO DRAWING BY SPUTTERING.

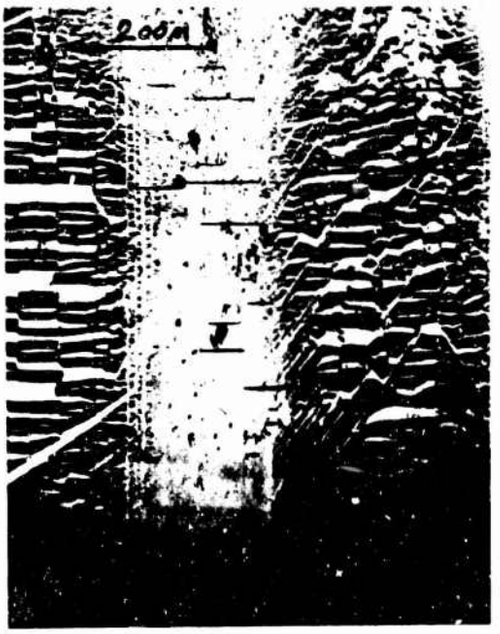

FIG.7.5 SURFACE OF DRAWN PMMA.A LAYER OF PT WAS APPLIED IN CIRCULAR AREAS PRIOR TO DRAWING BY SPUTTERING.

FIG.7.6 SURFACE OF DRAWN PMMA.A CONTINUOUS CR FILM WAS APPLIED PRIOR TO DRAWING BY EVAPORATION.

FIG.7.7 SURFACE OF PMMA PARTLY SHRUNK BY EXPOSURE TO A TEMPERATURE ABOVE T_G.A CONTINUOUS AL FILM WAS APPLIED TO THE DRAWN SURFACE BEFORE SHRINKING.

necessary.

From reflection of the light beam from the polymer surface, one could obtain similar patterns. A thin reflecting film would have to be deposited first.

Deformation Mode Detection by Light Absorbing Films. After application of a light absorbing, well adhering layer to the polymer surface, strains in drawing become visible as cracks in the layer. Films of platinum were applied by sputtering, and films of chromium, aluminum and carbon by evaporation in high vacuum. The layers ranged from semi-transparent to nearly transparent. Neither one of the metals has a particular advantage over the other for the detection of the strain distribution. Layer thickness is the important variable. The metal films crack normal to the stress direction, in addition, there are also oblique cracks if the layer is thin. The Figures 7.4 to 7.7 show some typical results. The surface film studies were made with PMMA II UVA of Lot 1 (Appendix B). In Figures 7.4 and 7.5 the coating metal was restricted to spots, which were initially circular. The layer thickness tapered off towards the periphery. The thin regions show more shear cracks; the thick center, more of the platelet cracking. The oblique metal cracks of Figure 4 continue into a streak of just recognizable bands in the uncoated part of the surface. The streak is bounded on one side by a crazed area and is joined on the other (lower left of photograph) by a group of bands which are initially curved.

Coherent films, if thin, cracked typically like the chromium film of Fig. 7.6.

The carbon layer deformed with the polymer without tensile or shear cracks. It was optically very thin, recognizable only as a brownish tone.

In a complementary experiment the specimen was coated, after partly drawing the polymer. Letting it then shrink by heating to near T_g produced similar cracks as in drawing. The strain recovery is, apparently, along the direction of maximum shear strain (Fig. 7.7). One cannot conclude from the photographs that each oblique crack corresponds to a shear band

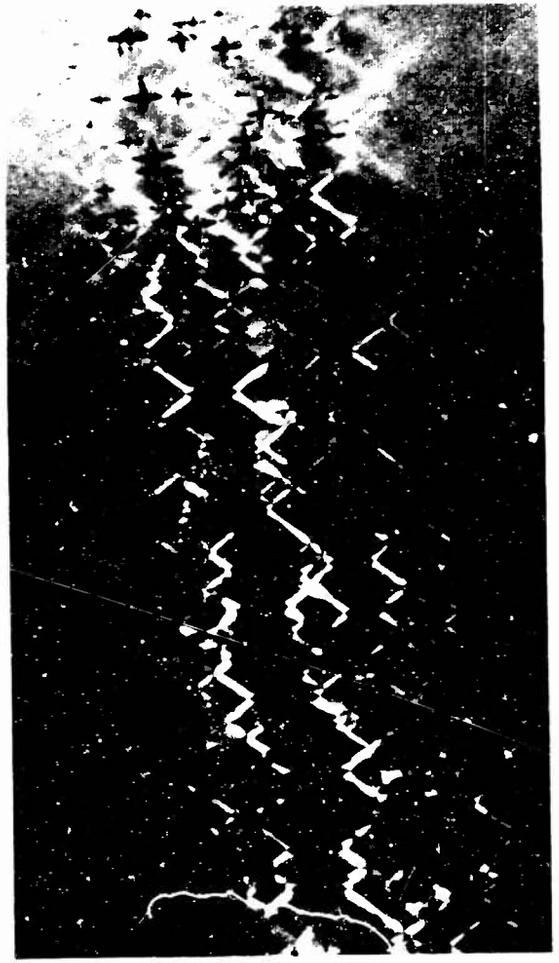

FIG.7.8 INTERNAL CRACKS AND SHEAR BANDS IN PS

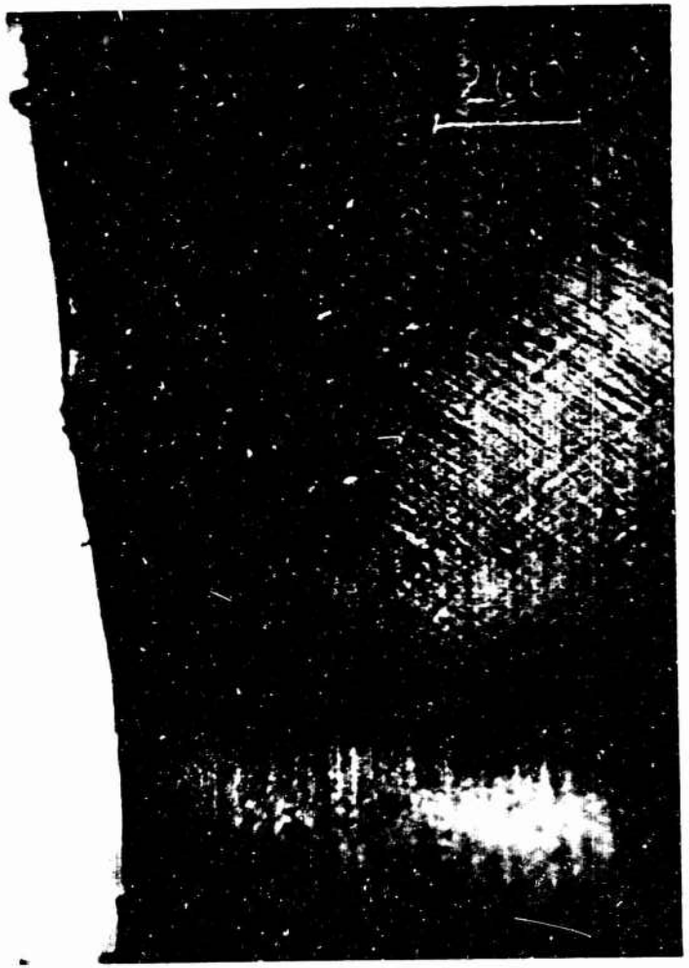

FIG.7.9 SHEAR BANDS IN THE NECK OF A PS SPECIMEN

underneath it, only that the substrate deforms,in the vicinity of the crack,by shear.

Polystyrene

During drawing of PS, a variety of surface defects appears. This has to do, at least in part, with the surface quality of the cast PS sheets. As compared to PMMA, the surfaces of PS are of poor quality before drawing and become even less homogeneous during hot stretching. Beyond that, the deformation of PS appears to lead particularly easily to cracks, crazes and shear deformation bands.

In PS shear bands are always observable in the neck region, starting usually at free surfaces and at the edges of crazes. Nucleation at internal cracks (Fig. 7.8) is not a common observation, but shows well discernible individual bands. Ordinarily, more complicated patterns of bands like those in Fig. 7.9 appear. The vertical lines are tool marks, setting off the oblique shear bands particularly well. The photograph of Figure 7.9 was taken with reflected light. In transmitted polarized light (Fig. 7.10) the bands are brought to view as diagonal streaks of differing light intensity.

Localization of shear strain distorts the crazes into a zig-zag shape, easily observable when the crazes are long (Fig. 7.11). The distortion often persists in the completely drawn polymer (Fig.7.12). At the highest stresses, a single macroscopic band appears sometimes in constant load drawing (Fig. 7.13) as a transient stage before necking occurs. In the case shown, the sample fractured (arrow in Fig. 13) before this had occurred. Interestingly, the fracture propagated through the thick, nearly undrawn section of the band.

Upon drawing, there is often a profusion of surface marks illustrating the complexity of the deformation on a local scale (Fig. 12). Two directions prevail--that of maximum shear stress, and that of the normal stress.

Polymethyl Methacrylate

Drawing of PMMA was studied on two different lots of Plexiglas (Appendix B), type II UVA from Rohm and Haas Company.

FIG.7.10 SHEAR BANDS AND CRAZES IN PS. TRANSMITTED POLARIZED LIGHT

FIG.7.11 DISTORTION OF LONG CRAZES BY SHEAR BANDS IN PS.TRANSMITTED POLARIZED LIGHT

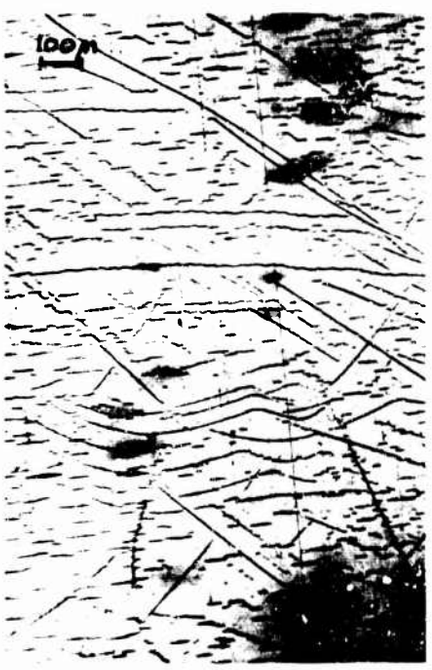

FIG.7.12 INHOMOGENEITIES IN FULLY DRAWN PS

FIG.7.13 NECK INITIATION BY A MACROSCOPIC BAND IN PS.FRACTURE OCCURED BEFORE THE NECK HAD FORMED

FIG.7.14 DEFORMATION BANDS IN PMMA (LOT 1)

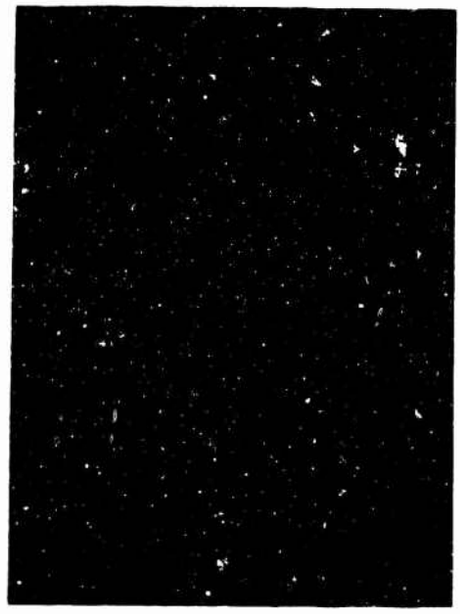

FIG.7.15 COMBINED OCCURENCE OF BANDS AND CRAZES IN PMMA(LOT 1)

FIG.7.16 ELECTRON MICROGRAPH OF A DRAWN PMMA SURFACE SIMILAR TO THAT OF FIG.14,CONTAINING BANDS AND A MICRO-CRAZE(LOT 1)

FIG.7.17 ELECTRON MICROGRAPH OF A DRAWN PMMA SURFACE CONTAINING BANDS AND A CRAZE(LARGELY COVERED BY DEBRIS), THE SPECIMEN IS NEARLY COMPLETELY DRAWN

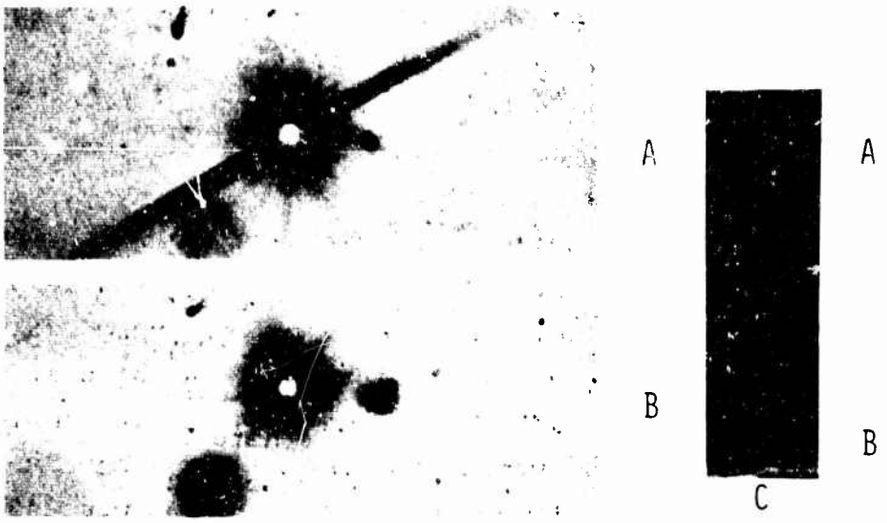

FIG.7.18 A.LIGHT BEAM REFRACTION PATTERN OF A PMMA SPECIMEN IN A REGION CONTAINING BANDS OF THE TYPE SHOWN IN FIG.14.
B.PATTERN OF THE SAME SPECIMEN IN THE FULLY DRAWN PART.
C.SCHLIEREN PHOTOGRAPH OF THE SPECIMEN.THE POSITIONS WERE A.AND B. WERE TAKEN ARE INDICATED(LOT 1)

FIG.7.19 LIGHT BEAM REFRACTION PATTERN OF UNDRAWN PMMA(LOT 1)

FIG.7.20 LIGHT BEAM REFRACTION PATTERN OF PARTLY DRAWN PMMA WITH A MIXED DEFORMATION MODE OF THE TYPE SHOWN IN FIG.15 AND SCHLIEREN PHOTOGRAPH OF THE SAME SAMPLE

On a microscopic scale, the two polymers deformed quite differently, as will be shown below. Yet they were equal in constant load drawing, as judged from the parameters by which drawing was evaluated in this study. There is no explanation for this at present, and the micro-mode of the two lots is therefore discussed separately.

Lot 1. The clearest evidence of what are thought to be Lueder's bands was seen in lot 1. The bands appeared at 2 to 3% plastic strain, probably earlier, under an angle of approximately 55° to the stress axis (Fig. 7.14), turned to an angle of 42° and disappeared as drawing came to an end. A nearly complete absence of crazes was typical for the Lueder's band mode. On the opposite surface, the frequency of shear bands was usually different and most often they ran transversely to one another. The wavy pattern (Figure 14), approximately normal to the well visible bands, is an optical effect caused by the bands of the reverse sample surface. In the presence of crazes the band pattern was less uniform. Figure 7.15 represents what is often seen. Figure 7.16 is an electron micrograph of a banded region. The stress is in the direction of the arrow. The elongated depression has been termed, in this work, a microcraze, believed to be an early stage of crazing. The surface of the electron micrograph of Fig. 7.17 belongs to a nearly drawn region. The bands start to disappear at this stage. The center of the photograph shows a craze, covered for the most part by an unidentified debris.

Pure band deformation (Figure 14) produced the light beam refraction pattern of Fig. 7.18(a) and the corresponding schlieren pattern of Fig. 7.18(c). In the drawn part, the refraction due to bands is no longer seen (Fig. 7.18(b). The undeformed polymer scattered light without directional preference (Fig. 7.19). Uniformly strained polymer produced the same pattern as that of the unstrained polymer. If crazes are present, the symmetrical refraction pattern can be seen, but it sometimes also appears without crazes. Occasionally a mixed mode was observed, a pronounced line, and a symmetrical figure superposed on it (Fig. 7.20(a).

Often, the mode of deformation is different in various

parts of the surface. The metal film cracks in Figure 7.4 show a region with bands and unbanded though highly drawn areas adjoining it. There, the banded area is also free of crazes. The metal film experiments have been made with lot 1 polymer. The type of shear bands of Figure 7.14 were detected only in this lot. One suspects that they are an artifact, probably imprinted on the initial polymer as a consequence of the manufacturing process. The polymer, as received, has been investigated with the same optical means as the drawn one. No traces of initially present defects of this type were found.

A shear band pattern, which is, without doubt, not present in the virgin polymer was discovered near a fracture surface (Fig. 7.21). This was lot 1 polymer containing the type of shear bands discussed above. Before the two sections separated completely, a narrow "bridge" of polymer formed adjoining to which the pattern of bands appeared, superposed to the one often found in this lot.

Conditions conducive to easily visible shear bands were low temperature, low moisture regain, and high stress. The clearest band structures were obtained from experiments with 4500 psi at 80°C with well dried polymer.

Lot 2. Attempts at producing bands like the ones typical for lot 1 polymer (e.g. Fig. 14) in the new polymer were unsuccessful. Under no condition of stress temperature, moisture content, and thermal history studied in this work were they observed in lot 2 polymer. There were merely the type of bands that radiate out from the edges of crazes (Fig. 7.22).

On quenching PMMA from above T_g the polymer no longer crazed. Together with the crazes, the shear bands which had produced the oblique light refraction patterns (for example, in Fig. 31), also disappeared. This was to be expected, as these bands were usually seen to originate at crazes. Nevertheless, typical constant load drawing curves and the neck mode of deformation were also found in these craze and band free samples. The bands are obviously not a necessary stage in cold drawing of PMMA. The quenching experiments were made only with lot 2 polymer.

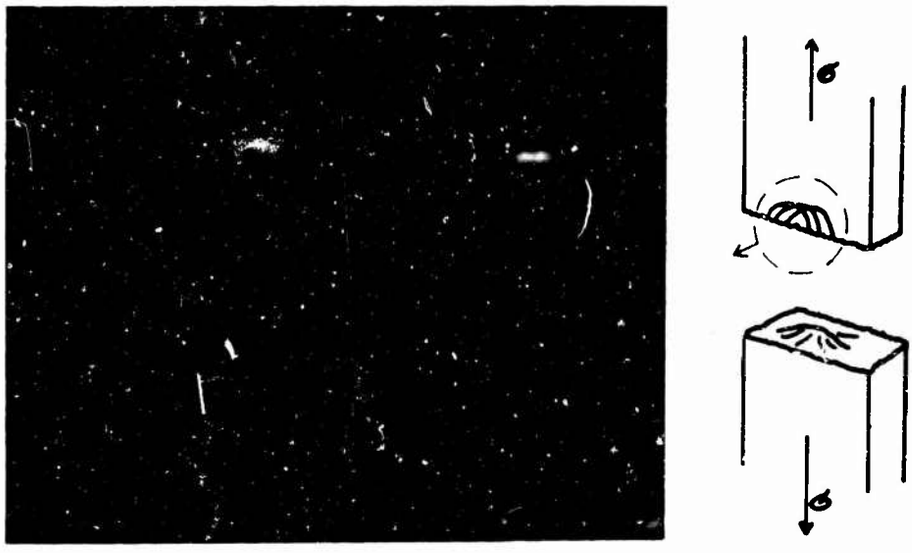

FIG.7.21 SYMMETRICAL SHEAR BAND PATTERN NEAR A FRACTURE SURFACE SUPERPOSED ON THE PATTERN OF BANDS MORE COMMONLY OBSERVED(PMMA,LOT 1)

FIG.22 SHEAR BANDS ORIGINATING AT THE EDGES OF CRAZES IN PMMA(LOT 2)

Internal Shear Strains. Provided the polymer deforms entirely by shear bands, there must be at least two sets of bands with non-parallel slip vectors to account for the observed contraction in two dimensions. Furthermore, they must penetrate the entire bulk of the polymer.

In an attempt to demonstrate the continuation of the surface bands into the polymer interior, a procedure suggested by Argon (see Ref. 16) was put to use. Strain in amorphous polymers is recovered on heating above T_g. A cut through polymer containing shear bands should, after shrinkage, show steps or reversed bands (Fig. 7.23).

PMMA specimens from lot 1, showing surface bands, were cut in the neck region, perpendicular to the specimen axis. The new surfaces were polished (No. 600 paper first, followed by No. 1 and 2 polishing alumina with a finish of No. 3 alumina). Microscopic inspection after shrinking did not reveal the expected bands. To shrink the polymer in steps, either by brief temperature exposures or by successively increasing the temperature also did not give the least evidence of reversed bands at any stage of retraction.

Even if they were present, the fine structures would probably not be preserved after polishing. Thin sections of neck regions of PMMA (also lot 1) were cut on a Porter-Bloom microtome. Some sections were shadowed under 6°, backed with carbon and studied under the electron microscope. There was no feature which would indicate internal bands. Some of the sections were shadowed as before, but remained unbacked. Hoping to see the development of reversed bands under the electron microscope, the intensity of the electron beam was slowly increased until the samples were severely distorted. Again there was no trace of reversed bands found.

One could suspect a differential solubility or swelling of strained and unstrained polymer, but exposure of the polished surfaces to acetone vapor did not reveal localization of such an effect which could point towards localized shear strain.

When the surfaces were brought in direct contact with acetone for several minutes, polishing scratches which had been invisible

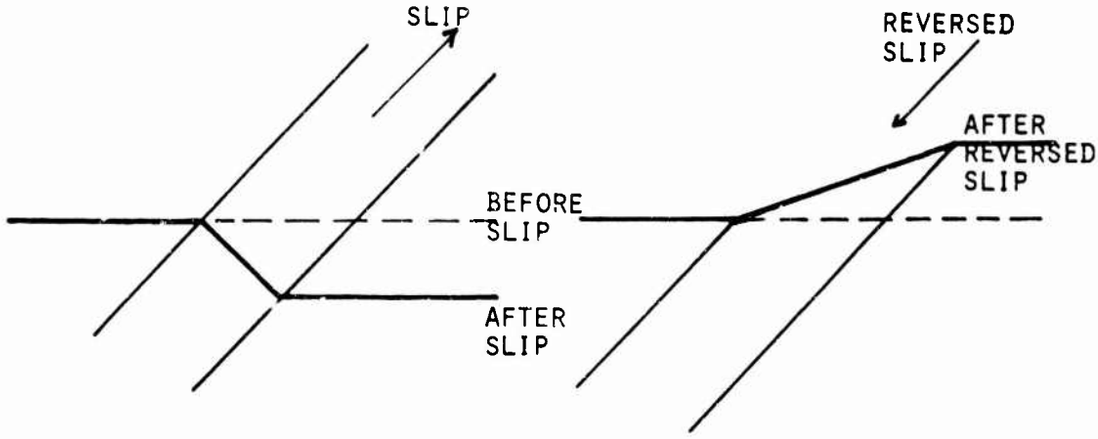

FIG.7.23 DEVELOPMENT OF REVERSED SLIP BANDS EXPECTED IN POLYMER WITH LOCALIZED SHEAR BY SHRINKING ABOVE T_G

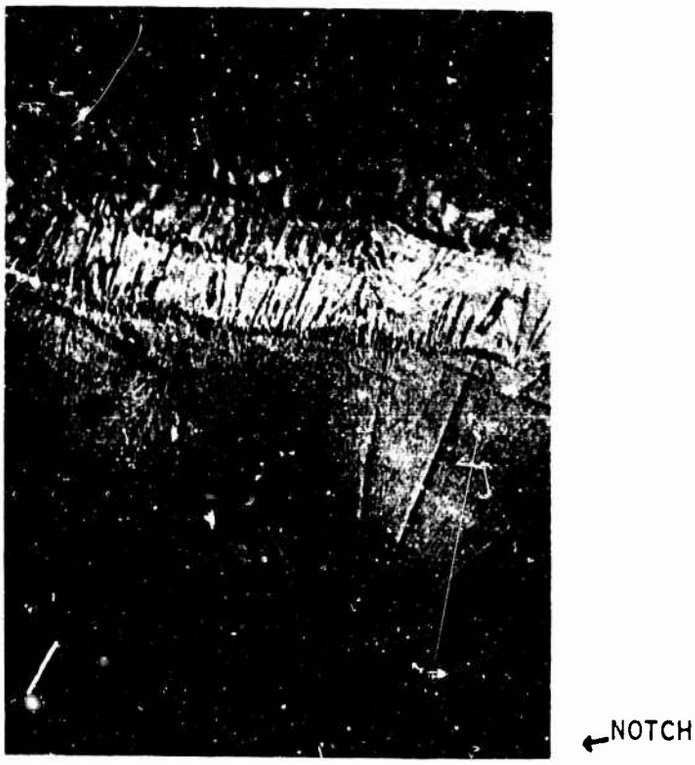

FIG.7.24 FRACTURE SURFACE OF PMMA, FRACTURE WAS PRODUCED BY BENDING AFTER NOTCHING THE SPECIMEN PERPENDICULAR TO ITS AXIS IN AN AREA CONTAINING DEFORMATION BANDS OF THE TYPE SHOWN IN FIG.14

at the end of polishing reappeared. Polishing is therefore not so much of a removal of a surface layer as it is a smearing out of unevenness.

An interesting observation was made on an oriented sample exposed for several days to acetone vapor. The swelling front, clearly visible under polarized light, moved approximately three times faster perpendicular to the orientation direction than in it.

Fracture surfaces in regions showing surface bands (lot 1) were thought possibly to contain features indicative of shear bands. Necked specimens were notched in partly drawn regions and broken by bending. The fracture surface appearance (Fig. 7.24) is quite similar to that of unoriented PMMA and features indicative of bands were not found.

Crazing of PMMA

Though crazing has been incidental to these studies, a brief account will be given here of those observations which appear to be new.

It has been reported that surface contaminations, present before straining, may be sites for crazes[65,66]. Optical microscopy shows, in fact, that in some samples crazes are often associated with small particles.

Observations in this work suggest strongly that the contaminant may, in some instances, be ejected from the polymer in the early stage of crazing. The electron micrograph of Fig. 7.25 shows an example. One reason for believing that the matter, visible on the bottom of the depression which the craze forms in its early stage of development, is not present initially is the direction in which it is lying. The craze forms perpendicular to the stress and there is no known reason why surface impurities should be aligned as they are. The debris often covers much of the craze. This could well be a further accumulation of the ejected matter (Figs. 7.17 and 7.26).

The PMMA of lot 1, in which crazes were particularly often associated with surface particles, showed small regions like that of Fig. 7.27, where groups of crazes occurred together with rather large surface particles. These particles are of a

FIG.7.25 ELECTRON MICROGRAPH OF DEBRIS ASSOCIATED WITH A CRAZE IN PMMA(LOT 1)

FIG.7.26 ELECTRON MICROGRAPH OF A CRAZE PARTLY COVERED WITH DEBRIS

FIG.7.27 OPTICAL MICROGRAPH OF A PMMA SURFACE CONTAINING A CLUSTER OF SPHERULITIC STRUCTURES

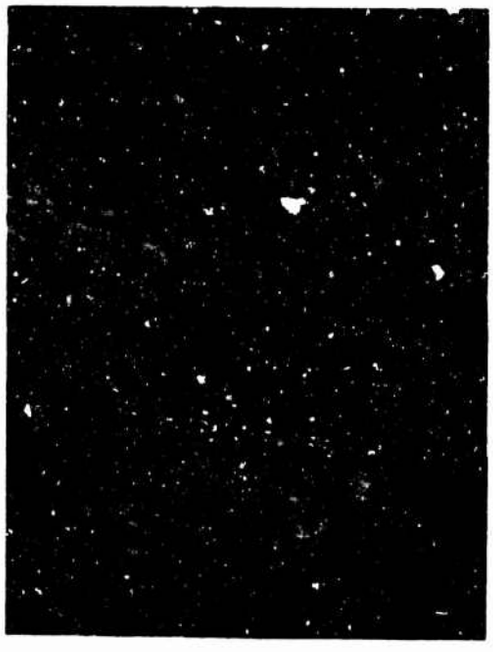

FIG.7.28 ELECTRON MICROGRAPH OF ONE SPHERULITE OUT OF A CLUSTER SUCH AS THE ONE SHOWN IN FIG.27

spherulitic structure (Fig. 7.28). The unstrained polymer did not contain them. It is concluded that they are formed from some substance initially contained in the polymer. The crazes (Fig. 27) have the usual orientation to the stress direction.

In the PMMA of lot 1, very short crazes, termed microcrazes. (Fig. 16) tended to align normal to the stress direction (Fig. 7.29).

Upon quenching from above T_g the polymer remained craze-free in drawing. The ability to form crazes reappeared only after annealing. A qualitative evaluation of the appearance of crazed surfaces after various annealing treatments is recorded in Table XVII .

Table XVII
Crazing After Quenching Followed by
Different Annealing Treatments

T_{ann}, °C	t_{ann}, hrs. 0.24	2.4	24		240
			Direct Quench	Indirect Quench	
80			0	1	
90			0	1	
95			1	0	
100	0	1	3	2	4
105			3	1	
110			2	1	

Control, quenched only: 0

(0 = no crazes; 1 = some isolated crazes or few patches of crazes; 2 = some uniformly distributed crazes; 3 = many small crazes; 4 = many crazes).

Figures 7.30(a)(b) show part of the crazed surface of the 100°C, 240 hrs. annealed sample, and its light refraction pattern. The craze pattern is more irregular than that of the original polymer, with many open crazes appearing in regions which contain a surface film of undetermined origin.

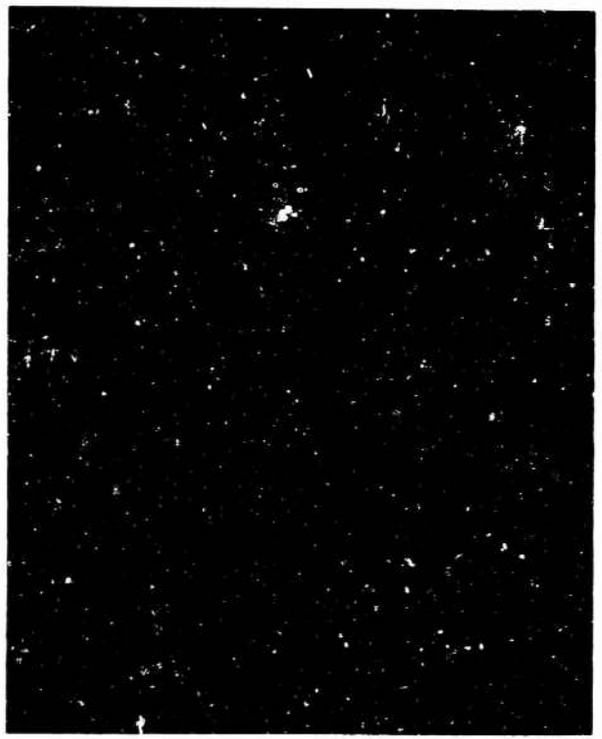

FIG.7.29 ALIGNED MICRO-CRAZES IN STRAINED PMMA(LOT 1)

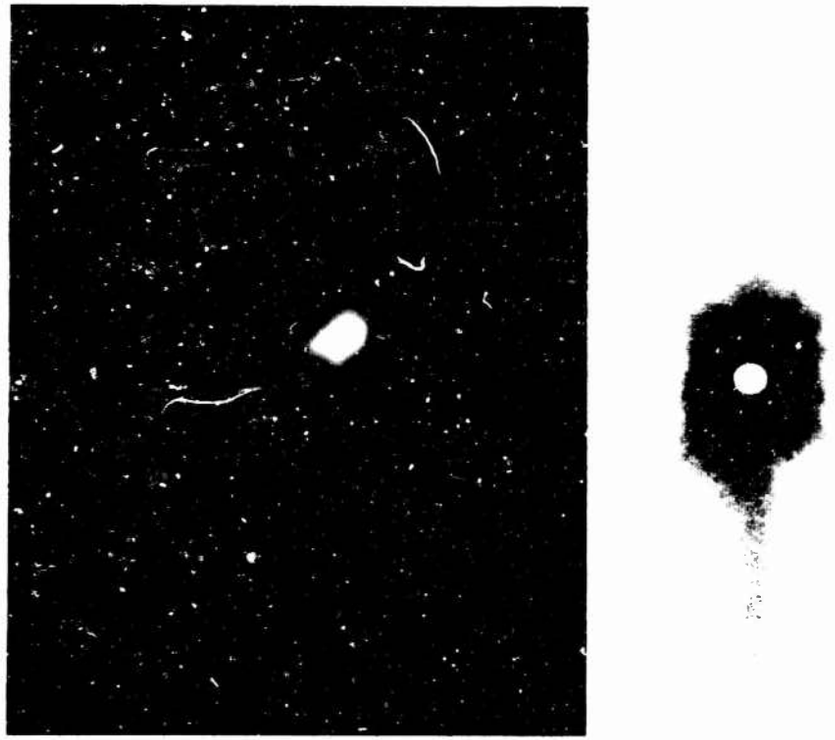

FIG.7.30 IRREGULAR CRAZE PATTERN ON A DRAWN PMMA SURFACE AND THE CORRESPONDING LIGHT REFRACTION PATTERN. THE SAMPLE WAS QUENCHED FROM ABOVE T_g THEN ANNEALED (ANN.TIME:240 HRS,ANN.TEMP.100°C) AND DRAWN

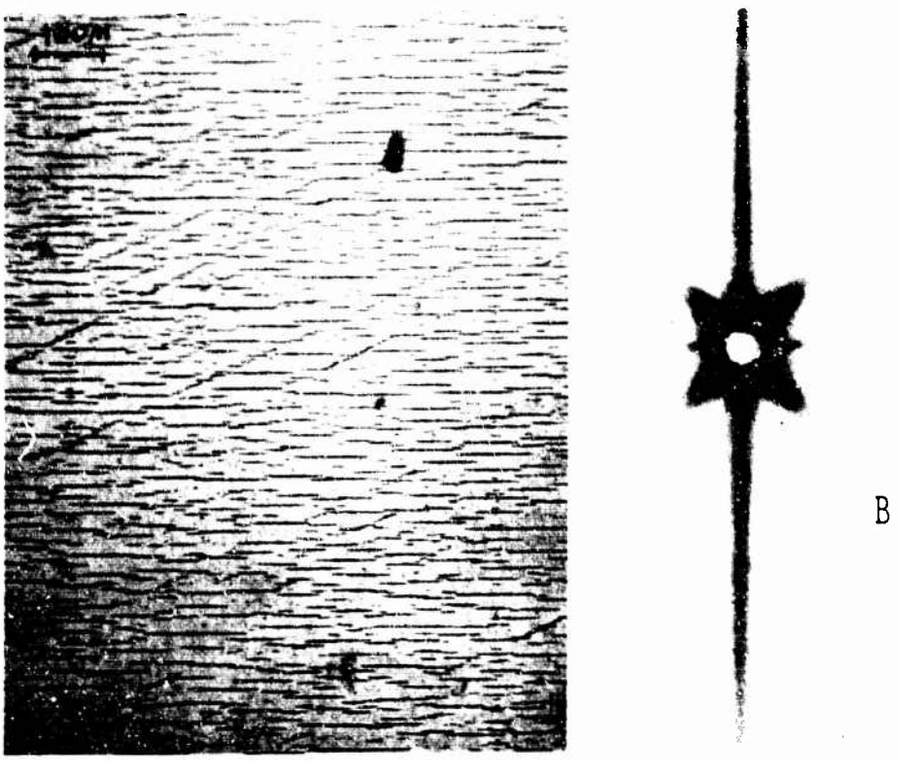

FIG.7.31 A.CRAZES ON A PARTLY DRAWN PMMA SURFACE.THE SAMPLE WAS CONDITIONED IN 100%RH BEFORE DRAWING
B.LIGHT REFRACTION PATTERN OF THE SAME SURFACE

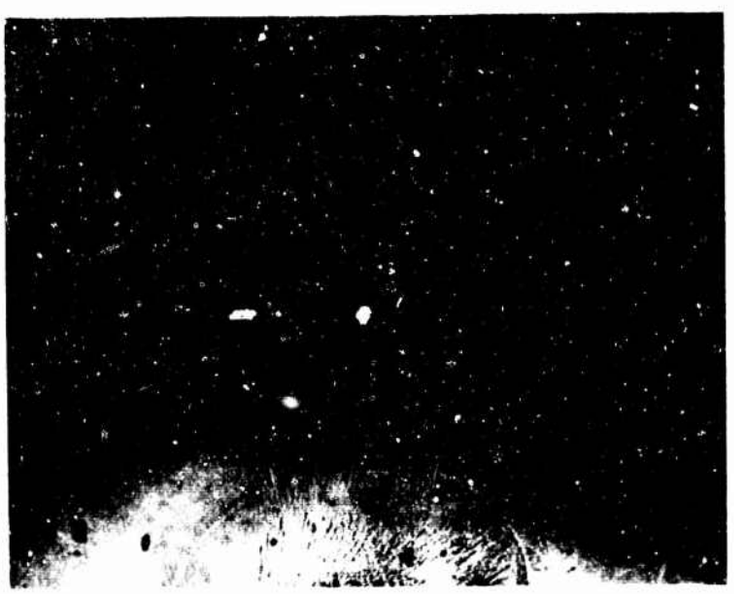

FIG.7.32 FRACTURE SURFACE OF PMMA.FRACTURE WAS CAUSED BY TENSILE STRESS AND ORIGINATED FROM THE SEMI-CIRCULAR REGION WHICH IS A CRAZE

While PMMA usually does craze, it hardly ever shows the long and dense crazes of PS (Fig. 10 and Fig. 11). The most severely crazed PMMA sample obtained was the one drawn with 2.2% moisture absorbed (Chapter IV). It is believed that a dry outside layer forms which causes, as the inside polymer is still swollen, a high tensile stress in this layer superposed on the testing stress. Figure 7.31(a) is a microphotograph of the specimen surface with the corresponding light refraction pattern shown in Fig. 31(b).

Craze Dimensions and Total Craze Volume. If filled incompletely by the density liquid crazes are a source of error in the density determinations, the possible magnitude of which is estimated below. Furthermore, the quantitative characterization of crazed PMMA surfaces, which were carried out to arrive at the estimate, elucidates the craze pattern and its changes during drawing.

The craze length per unit area L and the number of crazes per unit area N were evaluated for badly crazed specimens with widely differing craze patterns (Appendix G). Necked, incompletely drawn samples were used and measurements were taken outside and inside the neck. The fractional empty craze volume (v/V = Empty volume of crazes/sample volume) was calculated from Equ. (G-1) of Appendix G. The results are summarized in Table XVIII.

Table XVIII

Quantitative Evaluation of Crazed PMMA Surfaces

Specimen #	L mm^{-1}	N mm^{-2}	L /N	v/V x 10^5	L/N	R(w)	R(L/N)	Drawing Condition T,°C	σ, psi
N-7 undrawn	3.75	24	0.59	4	0.16	2.1	3.0	80	3000
drawn	1.56	17	0.14		0.092				
N-9 undrawn	2.81	49	0.16	1	0.057	2.0	2.1	80	3000
drawn	1.15	30	0.04		0.039				
N-10 undrawn	25.2	1760	0.35	2	0.015	2.2	1.9	80	4500
drawn	8.42	773	0.09		0.011				

In a badly crazed specimen, the volume fraction of voids due to crazes is of the order 1 to 5 x 10^{-5}. By the same relative amount the density would be in error if the density liquid

did not penetrate into the crazes. It was concluded, however, from the changes of the light refraction pattern when a liquid of equal or nearly equal refractive index as that of PMMA was applied to the surface, that the crazes are penetrated quite well by liquids. The error introduced in density results by the presence of crazes is thus beyond the resolution of the density methods commonly used.

From the figures of Table XVIII it is possible to conclude as to the behavior of crazes during drawing. The draw ratios R derived from average craze length $R(L/N) = [(L/N)_o/(L/N)_n]^2$ and sample width $R(w) = (w_o/w_n)^2$ have been recorded in the table (indices: c = undrawn, n = necked). The two ratios are approximately equal. Crazes deform, in necking, like the surrounding matrix. In particular, they do not grow further on drawing. An exact agreement between R(w) and R(L/N) is not to be expected, because the craze patterns vary somewhat along a sample even before necking.

CHAPTER VIII
EXPERIMENTAL EQUIPMENT AND TECHNIQUES

Drawing Apparatus

Drawing was carried out above room temperature in a specially built chamber shown in Fig. 8.1. Air is forced by a centrifugal blower to circulate through the chamber and the external duct containing heating elements. It enters the chamber through an opening above each sample. The air is directed along the specimen by honeycomb metal discs inserted in the openings. After leaving the chamber, the air passes a battery of electric heating elements. One group of elements is on-off controlled by a bimetal temperature sensor located in the air distribution channel above the test chamber. A second group supplies the base load and is always on. The supply voltages of both groups are independently variable and are adjusted to values designed to minimize temperature fluctuations due to the control cycle. Before entering the distribution channel, the air passes through a space filled with copper chips serving as a heat exchanger and providing inertia against short term temperature variations.

The air temperatures are measured with copper-constantan thermocouples in up to six locations. A multiple position switch serves to select the output of one of the thermocouples at a time. It was measured with a Leeds and Northrup Millivolt Potentiometer, using ice water as a reference. The air temperature variation along the specimen is smaller than $\pm 0.5°C$.

Sample length changes under load are recorded on drums (circumference: 30 cm) wrapped with millimeter paper and driven by synchronous motors. Motors of different speed are used (1/4, 1, 4 rph) depending upon the expected time scale of the test. A ball point pen, attached to the weight carrying rod (Fig. 8.1), produces a continuous trace of the specimen length change on the recording drum.

When details of the initial part of the length vs. time curves were to be resolved, the above method was considered no longer accurate enough. The apparatus shown in Fig. 8.2 was

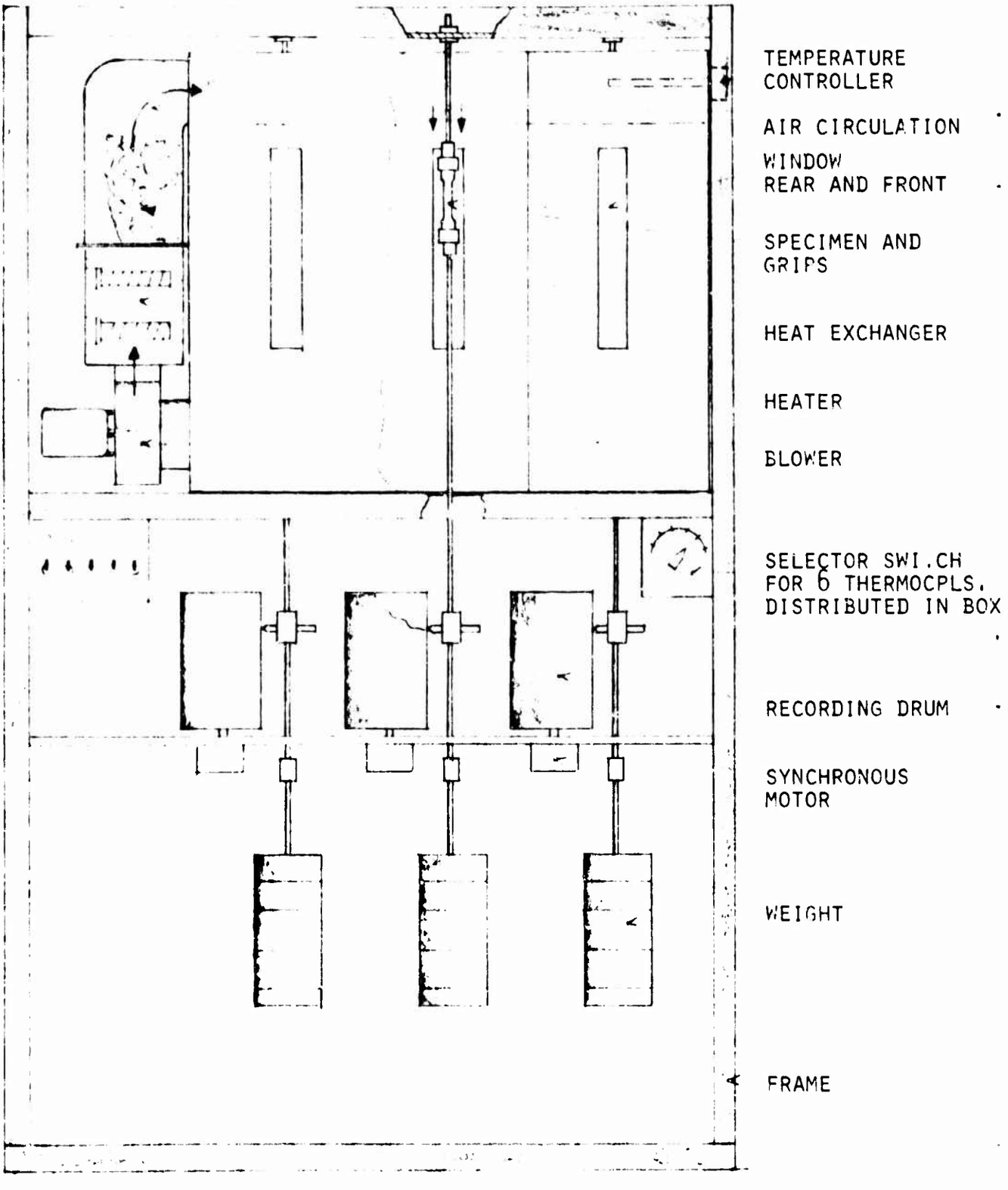

FIG.8.1 APPARATUS FOR CREEP MEASUREMENT UNDER CONTROLLED TEMPERATURE

used instead. It utilizes a linearly variable differential transformer (LVDT), type 1000 SS-L (Schaevitz Engineering, Camden, New Jersey), to pick up the length changes. The LVDT coil assembly is attached to the frame of the creep apparatus. Its core moves with the load-carrying rod. A Sanborn Model 311A Transducer-Amplifier-Indicator supplies the primary voltage and amplifies the signal. The output is a dc-voltage proportional to the distance of core displacement from its mechanical zero position. It is recorded by means of a Leeds and Northrup "Speedomax" Recorder.

The combination LVDT-311A-Speedomax is calibrated by moving the weight-carrying rod through known distances by means of a micrometer screw, clamping the micrometer body to the frame of the creep apparatus for this purpose (Fig. 8.2). After proper setting of the amplification, the recorder chart divisions are readable in even millimeters sample elongation. The internal calibration check device of the 311A permits resetting or correcting of the amplification. This is, however, rarely required if the equipment is left powered overnight, or after it has warmed up for several hours. At the 20x setting of the "sensitivity" step switch, 20 divisions of the recorder chart corresponded to 1 mm length change. Chart speeds of 1, 2, 5, and 10 in/min are available.

The cross beam of the creep apparatus, to which the upper clamp rods are attached, deflects up to 0.3 mm under the higher testing loads. The deflection was measured once and the length changes of the polymer specimens were corrected. When the initial length changes were to be recorded precisely, only the center testing position was used.

The test chamber contains windows in back and in front of each sample. The deforming samples were observed either between crossed polarizers, or by means of a schlieren method (Chapter VII). In some instances the optical retardation was measured during drawing tests, either by means of a calibrated birefringent polymer wedge, or a Senarmont compensator.

The specimen clamp surfaces were covered with No. 120 emery paper. This proved an effective way to prevent slippage of the specimens. The clamps hooked onto the anchoring rod

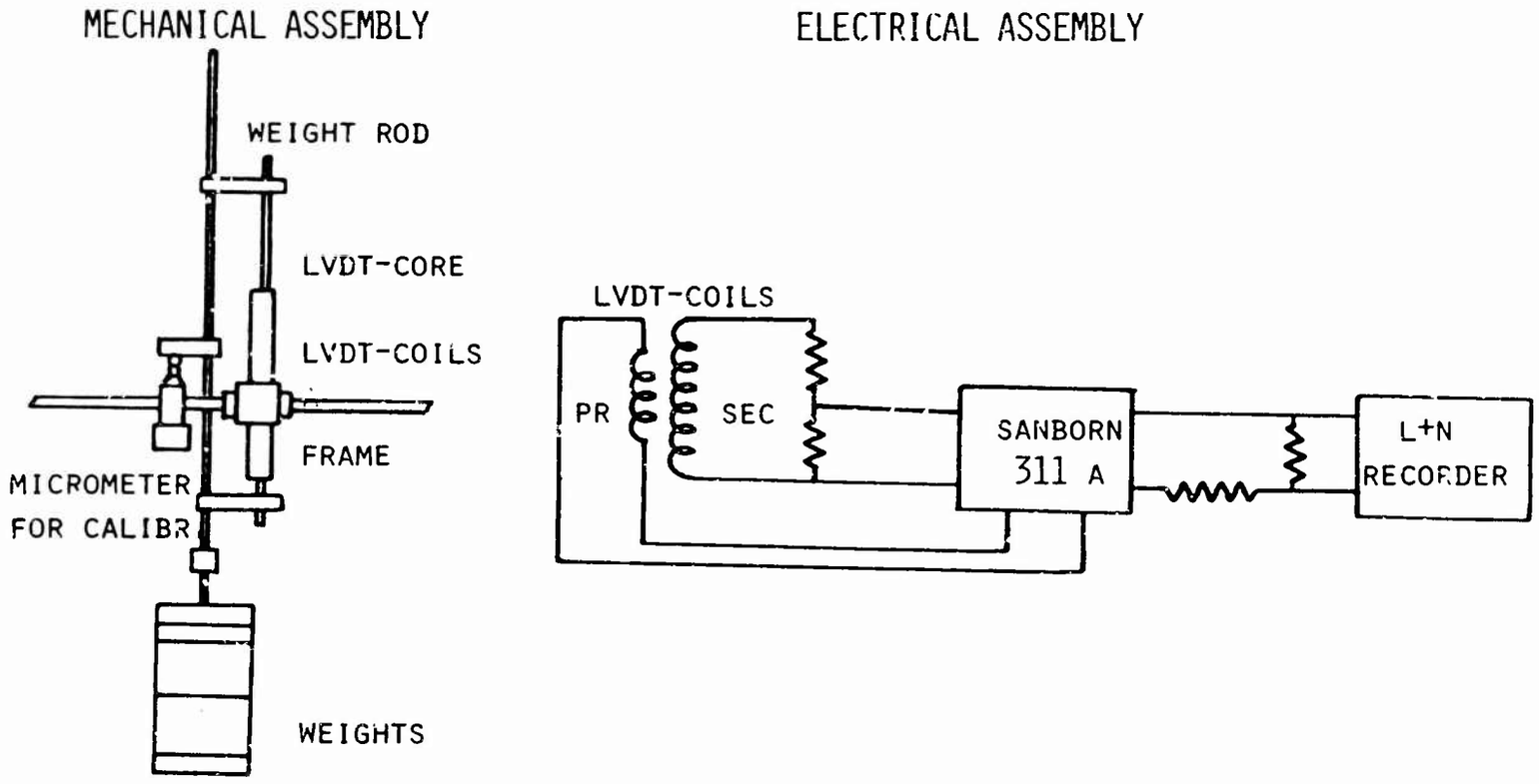

FIG.8.2 CREEP RECORDING APPARATUS

attached to the apparatus frame on one side, and the load-carrying rod on the other (Fig. 8.1).

The load was applied by hand. This had to be done gently, otherwise the craze patterns observed were in part due to impact loading.

Specimen Preparation

Tensile specimens were milled from commercial cast polymer sheets 1/16 in.thick, with 7/16 in.fillet radius and a parallel gauge section of 1.88 in.length and 0.26 in.width.

In the case of PS, some preorientation in the direction of load application was necessary; otherwise, fracture occurred at stresses below the yield stress[48]. Preorientation was introduced by hot stretching at 105°C, followed by rapid cooling. The glass transition of the polymer was approximately 90°C. In carrying out the hot stretching, strips of dimensions 12 x 1-1/2 in.were heated between two aluminum plates, the temperature of which was held constant at the desired value (Fig. 8.3). Convection of outside air into the space between the plates was prevented by felt strips. After a heating time of the order of ten minutes, the plates were removed and the strip was extended to the desired length. The birefringence thus produced was used as the index of the degree of preorientation. In these specimens, the thickness varied with preorientation, as more stretch was required at a given stretch temperature to obtain a higher birefringence.

The highly oriented PS was extremely difficult to machine, as it tended to split in the direction of orientation. For birefringence values of 5×10^{-3} and higher the cutting edge had to be run towards the specimen rather than away from it as in conventional milling. Drilling presented the same problem. To avoid splitting of the fillets, the fillet hole was made with the tip of a hot soldering iron instead of by drilling.

The temperature used for preorientation and the temperature equilibration time before the application of the load were kept constant as nearly as possible in all experiments so as to minimize sample variations due to thermal history and annealing effects. Instances where thermal or other pretreatments were

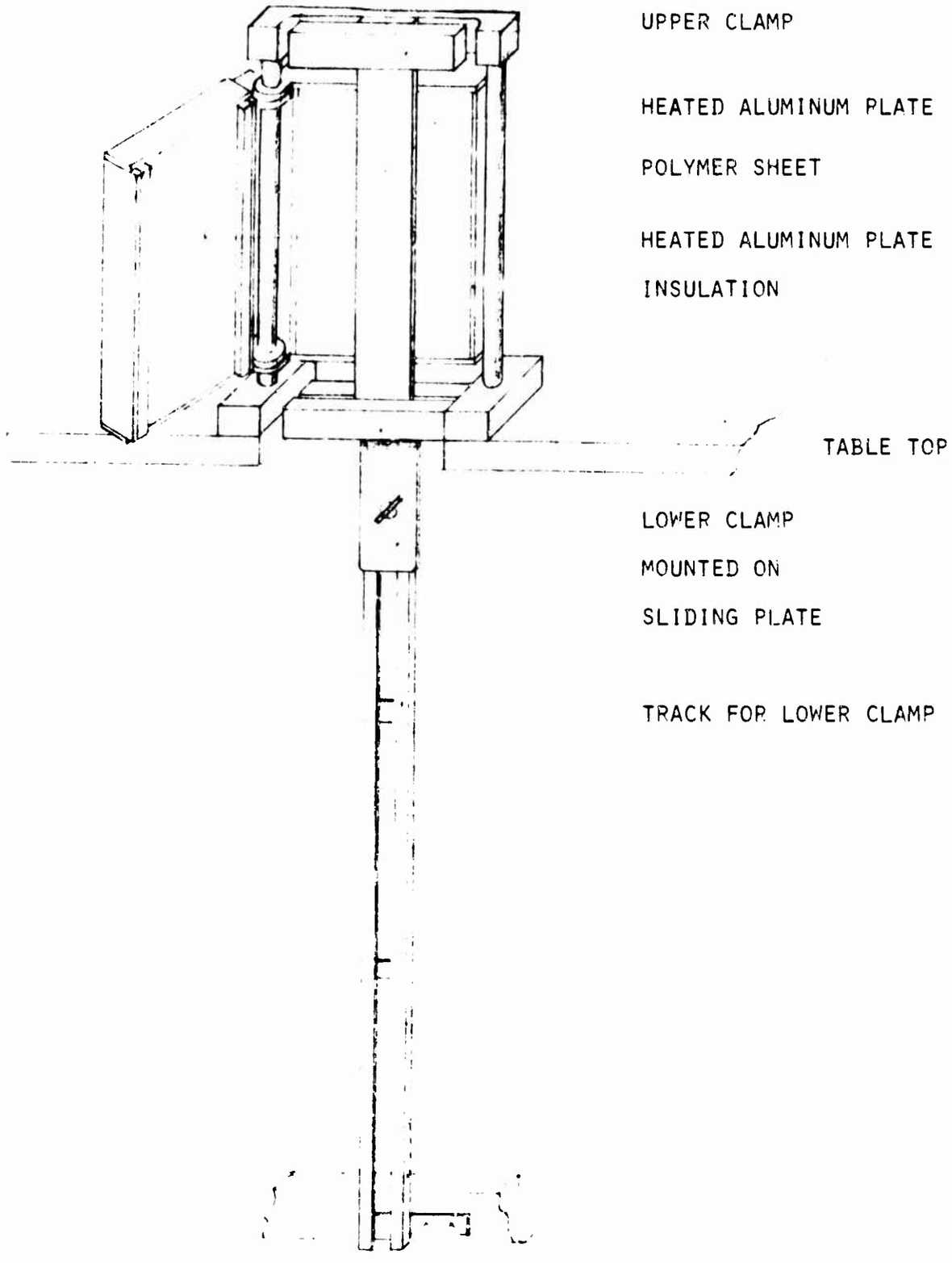

FIG.8.3 APPARATUS FOR ORIENTING POLYMER SHEETS

an important part of the sample preparation have been discussed in the appropriate sections.

Determination of Orientation Birefringence

Measurement of optical retardation was undertaken by three different methods, wedge compensator, Senarmont compensator, or fringe counting. Retardation range and precision required usually determined which method to use.

The wedges were milled from oriented polymer bars having retardation ranges of 0 to 2, 1 to 6, and 3 to 23 orders of green Hg-light (λ = 5461 Å). Specimens to be measured were placed between crossed polaroid sheets in front of a white light source with the orientation axis under 45° to the polarization direction (Fig. 8.4). The wedge was moved between the polaroids across the specimen, wedge orientation at right angle to the sample orientation, until both retardations were cancelled, a state recognized by the appearance of a black area on the sample. The birefringence is calculated from

$$\Delta n = k \cdot \lambda / t \qquad \text{(VIII-1)}$$

(k = wedge reading for compensation in orders of λ = 5461 Å;
t = sample thickness.)

In cold drawn PS (≈0.050" thick) many fringes were available and fringe counting was usually precise enough. The order of one of the fringes was determined with a wedge.

Small retardations, of the order of fractions of one wavelength, were measured with the Senarmont compensator[67]. The birefringence was computed from

$$\Delta n = \phi / 180 \cdot \lambda \cdot t \qquad \text{(VIII-2)}$$

(ϕ = compensation angle = 1/2 [retardation angle].

During drawing the samples were not accessible for direct measurement of the dimensions. The thickness t was then determined either by photographing the sample, or it was calculated from the length, assuming constant volume by

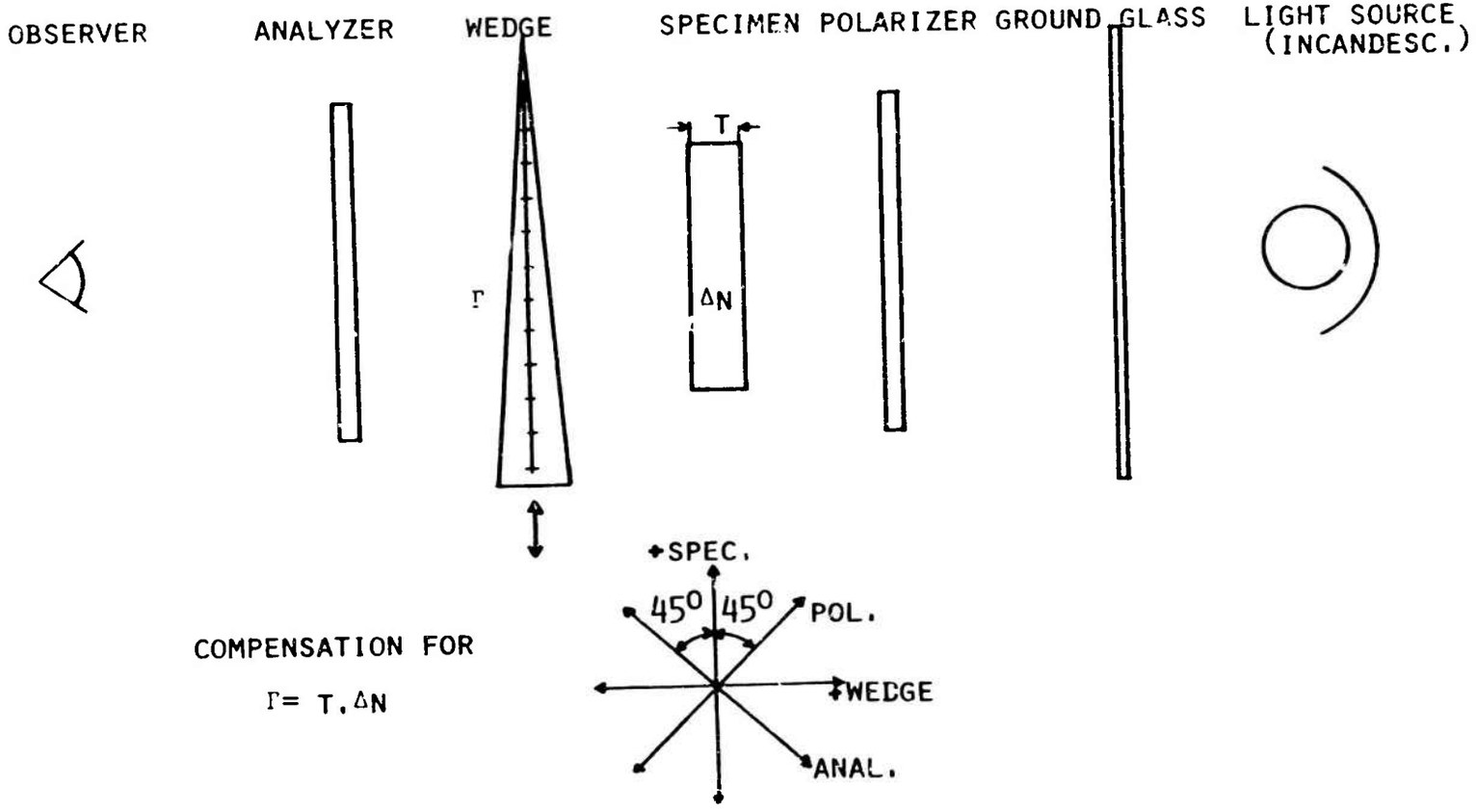

FIG.8.4 BIREFRINGENCE MEASUREMENT BY WEDGE-COMPENSATION

$$t = t_o \cdot (Lo/L)^{1/2} \qquad \text{(VIII-3)}$$

(t_o, Lo unstrained thickness and length)

For birefringence vs strain measurements after cold drawing, drawing was interrupted before completion of neck propagation along the sample. As long as the neck was not abrupt, a complete Δn vs ε curve was obtainable from one sample. Birefringence vs hot stretch strain data were obtained from strips drawn to various extensions in the device described in section 2 of this chapter.

Differential Expansion Method for the Determination of Polymer Density

A density measuring method with the flexibility in density range and resolution required in exploratory work has been developed. The polymer densities reported in the present study were determined with it.

The difference in thermal expansion coefficients between the polymer and a nonabsorbed liquid of a density similar to that of the polymer is utilized. The cubic expansion coefficient of organic liquids is of the order 1×10^{-3} 1/°C, that of glassy polymer of the order 2×10^{-4} 1/°C. If the densities of liquid and polymer are not too different initially, they can be made equal by proper adjustment of the temperature.

A mixture of carbon tetrachloride and n-heptane was found suitable. It is adjustable in density from 0.68 to 1.59 g/cm^3. A 1-gram PMMA sample (1/16 in. thick) after contact with a mixture of the liquids (ρ = 1.18 g/cm^3) for three days did not alter its weight detectably.

The apparatus for the density measurement is shown in Figure 8.5. A flask, containing polymer samples and liquid, is immersed in a stirred water bath which is initially at room temperature. The liquid density is adjusted such that the samples rest on the bottom of the flask. One or more calibrated glass spheres are added as density reference points. They are identified by their colors. The bath is cooled by dripping ice water into it at such a rate as to produce a temperature drift of -0.01 to -0.03°C/min. A sample starts to rise as soon as

the equation (VIII-4) is satisfied

$$\rho_{T_o L}(1 - \alpha_L \Delta T) = \rho_{T_o P}(1 - \alpha_p \Delta T) \qquad \text{(VIII-4)}$$

(ρ_{T_o} density at temperature T_o; α cubic expansion coefficient; ΔT temperature change $T-T_o$ necessary for buoyancy; P, L index for polymer respectively liquid.)
When specimen buoyancy is reached, a temperature reading of the Beckman thermometer is taken.

Equation 4 reduces, for $\alpha_p \Delta T << 1$ to

$$\frac{\rho_{T_o P} - \rho_{T_o L}}{\rho_{T_o L}} = (\alpha_P - \alpha_L)\Delta T$$

or

(VIII-5)

$$\frac{\Delta \rho}{\Delta T} = (\alpha_P - \alpha_L)\rho_{T_o L}$$

With α_p(PMMA) = $0.20 \times 10^{-3}°C^{-1}$ and $\alpha_L = 1.21 \times 10^{-3}°C^{-1}$ for a mixture of 1.186 g/cm³, which is very close to the PMMA density, the last equation becomes

$$\frac{\Delta \rho}{\Delta T} = -1.197 \times 10^{-3} \qquad \text{(VIII-6)}$$

The density changes expected are of the order 10^{-5} to 10^{-3}. The equivalent temperature changes are therefore of the order of 0.01 to 1°C.

The thermal expansion coefficient of the liquid was measured in a pycnometer with a calibrated capillary by immersing the filled pycnometer in a bath the temperature of which was altered in steps of several degrees around room temperature. The expansion coefficient of the polymer was taken from Fig. 3.1. If several density floats are used, the expansion coefficients are not required.

The density liquid was stored over activated alumina to eliminate water.

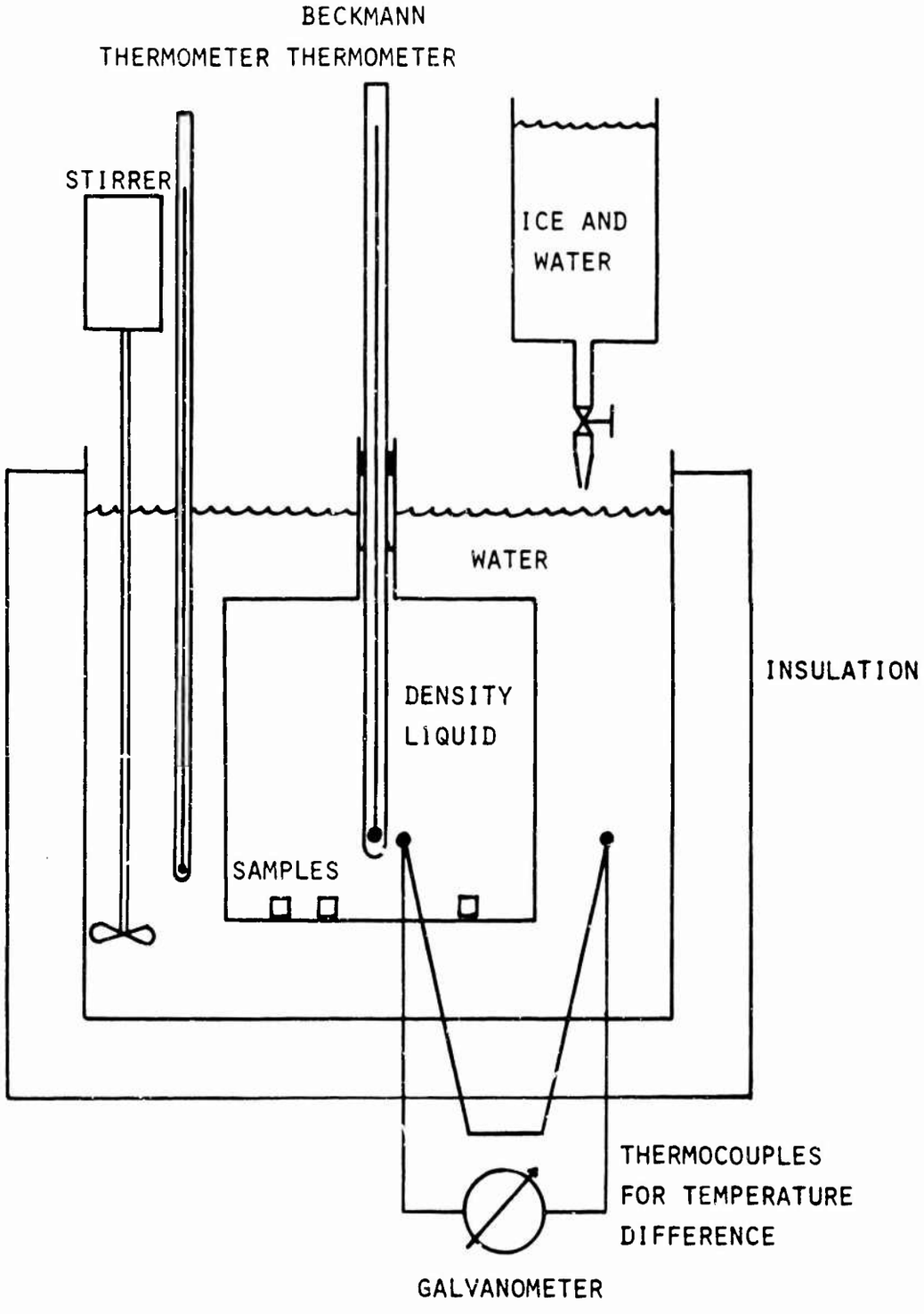

FIG.8.5 APPARATUS TO MEASURE POLYMER DENSITY

The precision of the method is, for a temperature rise of 0.01°C/min, estimated to be $\pm 2 \times 10^{-5}$ g/cm^3 and poorer for faster rates.

Usually polymer density is measured in density gradient columns. Preparation of a column requires previous knowledge of the density range to be measured and much practice in producing the desired range with fair linearity. Once the column is set up, the range cannot be altered. The differential expansion method is flexible as addition of one of the liquids permits large shifts of range. The advantages of the new method are best realized in exploratory work.

Replication of Polymer Surfaces for Electron Microscopy

The method to be described is a modification of the one given by Grube and Rouze[68]. For polymer surfaces this method is particularly useful, as no organic solvents are needed. A water soluble layer of Victawet (Victawet 35B, Victor Chemical Works, Chicago, Illinois), ideally of molecular thickness, is applied to the surface as a parting layer before depositing the replica material.

Preparation of the replica includes vacuum deposition of three substances in the order given:

1. Victawet
2. Shadowing metal (chromium was used in this work)
3. Replica (Silicone monoxide was used in this work).

The evaporations follow one another without intermediately breaking the vacuum. The two baskets and the spiral (sketch) are made of 20 mil tungsten wire and are arranged as shown in the sketch below.

The Victawet is melted onto the spiral initially. Under vacuum it is slowly evaporated with 2 to 3 amperes, followed by a period of 1 to 2 seconds with 20 to 25 amperes. This constitutes a heat treatment of the layer.

Shadowing was under 45°. The replica thickness is controlled by a test plate of polished steel, which is protected from the chromium during shadowing. When depositing the replicating

substance, the plate is moved next to the specimen. When it reaches a bright blue interference color, the evaporation of SiO is stopped.

The replica is divided into small sections after interesting areas have been chosen under the microscope. The sections are floated off by dipping the sample under a slight angle slowly into distilled water. From the water surface they are lifted onto screens.

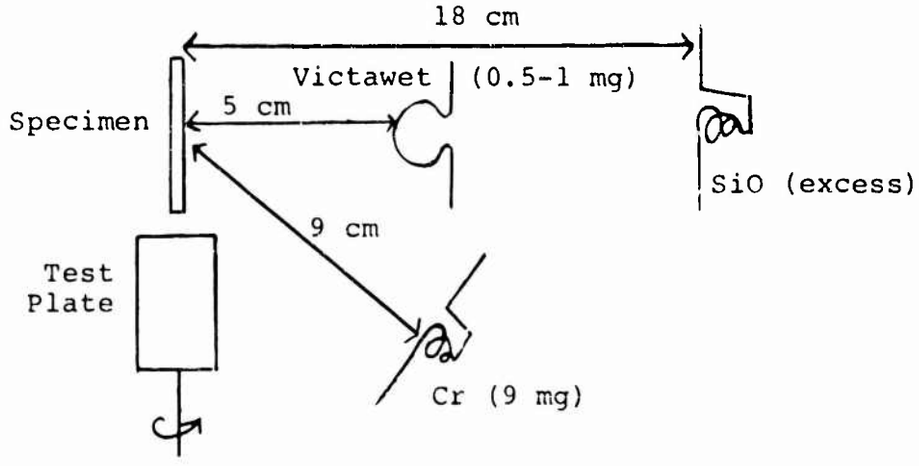
18 cm
Victawet
(0.5-1 mg)
Specimen
5 cm
SiO (excess)
9 cm
Test
Plate
Cr (9 mg)

SUMMARY

This study has been undertaken to investigate the yield phenomenon in glassy amorphous polymers. Polystyrene and polymethyl methacrylate (PMMA) were chosen as representative of this class of polymers. Yielding in polymers proceeds by necking and cold drawing. The main interest of this study centers on the initiation of the cold drawing process, describable as a pronounced work softening.

Whereas nearly all previous investigators have used constant rate of extension experiments, cold drawing in the present work is initiated by attaching a constant load to the sample. The phenomenon of drawing under constant load can be shown to be a consequence of the strain rate sensitivity of tensile properties and the existence of an upper yield point (Chapter II).

The constant load drawing experiment offers an unexpected advantage over the constant rate of extension test for in it the strain remains uniform beyond the yield point. As a consequence, one can evaluate the stress-strain properties from a uniformly strained specimen in the strain region in which, in the constant rate test, a neck has already formed (Chapter II).

Drawing with constant extension velocity proceeds by the spreading of a neck. In constant load drawing one finds a uniform and, from the yield point on, an accelerating deformation. Nonetheless, necking is also seen in this test, but it tends to occur in the later stages of drawing (Chapter I). Necking is, in this experiment, caused by nonuniformity of the sample or the test conditions, as contrasted to the necking in the constant rate of extension test where the deformation localizes because of a drop in stress accompanying yielding. Necking is therefore a consequence of the stress-strain properties of the material and the boundary conditions of the test as well (Chapter II).

Both drawing modes, necking and uniform drawing are usually preceded by the appearance of shear deformation bands. These bands are thought to be more fundamentally connected with

cold drawing than the neck which forms where they are particularly dense. The bands persist in the shoulders of the neck, but disappear in the drawn polymer. In uniform drawing the band density remains uniform all along the specimen length. There, too, the bands disappear upon completion of drawing (Chapters I and VII). Yet the strong localization of strain documented by bands is not necessary for cold drawing, at least not for PMMA. This polymer, when previously quenched from above T_g, does not exhibit shear bands during drawing and still shows the typical elongation vs time behavior characteristic for constant load drawing (Chapter VII). In PS cold drawing was always observed to be accompanied by bands (Chapter I).

The constant load test yields extension vs time curves (Fig. 1.2). One parameter easily evaluated from these curves is the delay time (Fig. 1.1) which has been extensively used to characterize drawing behavior under constant load. This research has devoted considerable effort to the determination of the influence of stress and temperature on the delay time of PS and PMMA (Chapter I), as well as the influence of PS preorientation (Chapter I) and of PMMA moisture content (Chapter IV) and thermal history (Chapter III) on delay times. Below some critical stress, drawing under constant load no longer takes place and shear deformation bands are no longer present. Instead, one observes only creep. Above the critical stress, temperature and stress have a large influence on constant load drawing. The delay time drops exponentially with stress and temperature (Figs. 1.9 to 1.12). Preorientation appears to have little influence on delay time.

The constant load length vs time curves are convertible into extension velocity vs length curves (v vs L-curves) (Fig. 2.3). These derived curves are in principle equivalent in information content to the load elongation curves of the constant rate of extension test. In practice they offer more information because of the wide uniform strain region which occurs only in the constant load test. Most of the results of this work have been derived from the v vs L-curves or strain rate vs strain curves.

If the three variables, stress, strain and strain rate, were uniquely related, that is, if an equation of state were to exist of the form $(F,v,L) = 0$, one could convert results of one type of drawing test to that of the other. From the few data available which can be directly compared, it appears that the equation of state is at the most a first approximation (Chapter II). If, in spite of these reservations, one cross plots the uniform strain parts of v vs L-curves of PMMA, one obtains stress vs strain curves which have a yield stress maximum (Fig. 2.6). Conversely, starting from measured load vs elongation curves for several strain rates, one predicts the stress dependence of delay time correctly (Equ. II-12).

The yield point appears in the v vs L-curves as a velocity minimum, for which $(\partial v/\partial L)_F = 0$ (App. C, Chapt. II). The rising branches of the curves reflect the softening of the polymer fundamental for drawing. It is hypothesized that the velocity is made up of two components, $v = v_{ve} + v_v$. The first component accounts for the declining branch, responsible for the initially high velocity which decreases to zero in the vicinity of the yield point. The second component rising with strain is the more interesting one in the context of cold drawing. This model explains yielding without further assumptions as the condition for which $(\partial v_{ve}/\partial L)_F = -(\partial v_v/\partial L)_F$. The yield point is, in this interpretation, a consequence of two monotonically changing velocities, an increasing one and a decreasing one with strain. The velocity v_{vE} is observed in creep also.

In the uniform strain region beyond the yield point, the velocity v is found experimentally to be shifted by stress in such a way that one can derive the rising branches of the v vs L-curves measured under different stresses from one of the curves by multiplying the velocity by a stress shift factor. The stress shift factor is independent of strain and temperature within the accuracy of the experimental results. The velocity beyond the yield point is therefore presentable as a pure strain function v^* measured under the

stress σ^* and a pure stress function, the stress shift factor:

$$v = v^*(\varepsilon,\sigma^*) \cdot \frac{\sigma}{\sigma^*} \cdot \exp[\phi(\frac{\sigma}{\sigma^*})] \qquad \text{(II-23)}$$

Experiments in which small stress increments were intermittently applied to the polymer when uniformly strained under a high stress, showed that the stress shift of velocity follows stress changes nearly immediately and reversibly.

The stress shift factor derived from the incremental loading experiment agrees with that from v vs L-curves. The change of delay time with stress was found by experiment to be governed by the same stress shift factor also (Chapter II).

The magnitude and functional form of the stress shift is correctly predicted by a theory which presumes that the volume dilatation due to the drawing stress contributes entirely to the free volume. It is applicable for tensile stresses only, which are high enough to cause cold drawing. For yielding in compression one must conclude that free and occupied volume are changing (Chapter VI).

The lower stress limit of the applicability of the exponential stress softening is the drawing mode boundary. The curves measured for stresses below the boundary are not derivable from the ones above, as they do not exhibit a rising branch of the v vs L-curves.

The work softening of the drawing polymer is thus shown to be separable into two contributions, one a stress effect, the other a strain softening influence. Stress changes the deformation rate rapidly and reversibly. Deformation rate increases due to strain are irreversible under the conditions of cold drawing.

For the strain softening, the initial structure of the glass and its changes in straining prove to be of importance. The flow resistance of PMMA varies significantly with the previous thermal treatments as a result of the effect of such treatments on glass structure.

After quenching from above T_g, PMMA becomes more easily deformable as compared to the well annealed polymer. By

exposure to a temperature slightly below T_g the quenched polymer regains its original resistance towards deformation. Annealing times up to many hours effectively increase the resistance. The density change due to annealing of quenched PMMA is only about 4×10^{-4} g/cm^3. (Figures 3.8 and 3.9.) Nevertheless, annealing changes the delay time and related flow properties by a factor of about 50 (Fig. 3.5). The structure of the glass is thus shown to be of great importance (Chapter III).

The initial structure of the polymer is believed to be drastically modified in straining. Mer units must leave the positions assumed in annealing to accommodate the external strain. Density measurements confirm this hypotnesis. The density initially decreases when the polymer is strained by approximately 10^{-3} g/cm^3. Though this initial drop in density is followed at large strains by a density increase of 0.5%, the initial change is believed to be important in reducing the flow resistance (Chapter V).

It is believed that the well annealed glass, when strained, assumes the structure of a poorly annealed or quenched glass. It is postulated that the displacement of segments from the positions they take during annealing introduces free volume into the glass. A theory which takes account of this free volume generation and a viscosity dependent free volume relaxation is developed. It predicts an exponential softening with strain (Chapter VI). Some of the observations on strain rate vs strain curves of PMMA of various annealing histories cannot be explained by this simple theory. The observed behavior is consistent with the presence of association bonds formed during annealing, which must be broken in the subsequent drawing process. Other observations concerned with the annealing process itself may be interpreted as secondary bond formation (Chapter III). As straining proceeds, an increasing number of such bonds are broken. The rate of their reformation depends on the temperature of the experiment. Appreciable strengthening by newly formed bonds can only be expected near 100°C. There, the rate of annealing is found to be appreciably

higher than above or below this temperature. Healing of the association bond network during drawing is believed to be absent below 100°C for practical purposes.

In drawing at 100°C, the stress shift factor appears to assume different values from those at lower temperatures. This apparent anomaly of stress influence is more probably an anomaly in strain softening as structural recovery may occur near T_g. At 100°C, where the annealing rate is high enough for a partial healing out of the strain effects on the glass structure within experimental time (at least for the slow drawing experiments) the strained polymer recovers part of its mechanical stability during drawing.

Drawing above T_g is shown to lead to necking also if done not too far above T_g. If the deformation rate impressed on the polymer is high enough, the recovery of a mechanically stable structure may not be accomplished rapidly enough to prevent the mechanical instability which leads to the accelerated extension.

Chain orientation in cold drawing PMMA, as determined by birefringence, is affected by temperature, drawing rate, and water content. PMMA initially shows a very steep increase of birefringence with strain. At higher strains the curve bends towards the strain axis. This is interpreted as the breaking of the initial tight network of association bonds. PS does not show such a behavior. Its birefringence vs strain curve is comparatively straight.

The dimensions of PMMA are completely recovered after cold drawing if the polymer is heated to above T_g. Flow of molecules past each other does apparently not take place in drawing. Some interchain links remain intact and serve as a memory for the unstrained positions of the segments with respect to one another. In PS some molecular flow does apparently take place in cold drawing (Chapter V).

In the experiments of this research, drawing was practically isothermal (App. A), hence the observed phenomena are not explainable as an adiabatic heating, as an older theory of polymer yielding postulates. The adiabatic theory has been

shown before to have a limited applicability, if any[5].

More recently, cold drawing has been ascribed to the breaking of secondary bonds[8], stress softening[6] and lowering of the softening temperature by strain[5]. The nature of the present experiments, allows (because of the near constancy of stress) a better separation of the influence of stress and of strain than does the constant rate of extension experiments. It is found that the softening of the polymer is caused by strain. It is very probable that such a strain produces free volume as well as breaking of secondary bonds, and these are important mechanisms contributing to the work-softening. The relative importance of either one in the drawing process must be expected to depend on the chemical structure of the polymer and the arrangement of chains in the glass. The effect of stress is merely to modify the rate of deformation.

The condition temporarily produced in the drawing of polymer has often been likened to that existing above T_g. The polymer above T_g is in a metastable equilibrium. The glassy polymer is, before straining, in a thermodynamic nonequilibrium state, which varies with its history. By drawing it is removed further from equilibrium by straining. It appears to be a more correct viewpoint to consider the straining glass as being in a highly nonequilibrium state.

CONCLUSIONS

Drawing under constant load as observed in the present experiments for PMMA and PS, can be expected to occur for all materials exhibiting strain rate sensitivity of stress and an upper yield point. For drawing under constant load to occur in PS and PMMA a characteristic minimal stress must be applied. This stress requirement decreases with increasing temperature. For any given temperature uniform creep takes place under loads below the characteristic minimal load.

The drawing by neck generally observed in constant rate of extension tests is a consequence of the load drop at the upper yield point. Under constant load, deformation often remains quite uniform without a neck. In the latter case, drawing occurs via uniformly distributed shear bands, whereas in the former test the bands always localize with an ensuing neck. Shear deformation bands are, nevertheless, not necessary for cold drawing. In quenched PMMA, drawing is observed without bands. Crazes which appear under the high stresses of cold drawing have very little, or no influence on drawing.

Thermal pretreatment strongly affects the resistance of PMMA against flow under tensile stress. Upon quenching from above T_g the flow rate increases by a factor 50. On material annealing, the properties are recovered to an extent depending on annealing time and temperature. Thermal treatments alter the free volume and are also believed to influence the state of secondary bonding in PMMA.

The flow rate during uniform drawing under constant load can be separated into a pure stress and a pure strain effect. Stress shifts the flow rate of the rising branches of the strain rate vs strain curves exponentially and reversibly. The stress shift of flow rate is considered to be a consequence of Poisson's expansion, which under cold drawing conditions, contributes exclusively to the free volume. The observed stress shift is correctly predicted on the basis of this assumption.

In the constant load drawing experiment, initiation of

drawing corresponds to softening due to strain. The polymer is believed to assume a far-from-equilibrium structure which is comparable to that obtained by quenching from above to below T_g as characterized by an increase in free volume and also a decrease in the number of association bonds from that of the well annealed polymer.

Suggestions for Further Work

1. Constant load drawing is accompanied by a stress increase with strain. It is suggested that constant stress instead of constant load drawing experiments be made in the vicinity of the deformation mode transition from creep to drawing . This eliminates the possibility of reaching the stress necessary for drawing merely by cross-section reduction. The main purpose of such experiments would be to confirm the existence of the critical stress found in this work which must be exceeded for drawing. Another objective would be the quantitative determination of the effect of stress on creep rate below the critical drawing stress. It has been concluded in this work that the exponential influence of stress on drawing rate does not hold for the region in which creep occurs.

2. The increase in polymer volume in the small strain region is believed to contribute to its free volume and thus to play an important role in the work softening. The exploratory density measurements reported here should be supplemented by dilatometric measurements during extension to obtain volume vs strain rate data. Density measurements in the low strain uniform strain region should be of most interest. The strong influence of volume on viscosity requires density changes of less than 10^{-4} g/cm^3 to be measurable.

3. Association bonding has here been ascribed an important part in the deformation behavior of PMMA in this work. Drawing experiments are proposed of the type performed in the present work on polymers (other than PMMA) which should be extremely different in their ability to form association bonds. Quenching and annealing can be used to produce different states of bonding in each polymer. Simultaneous birefringence and cold drawing strain measurements are expected to provide much insight as to state of bonding and drawing mechanism.

4. The anomalously long annealing times found for PMMA near T_g possibly reflect the change in bonding apart from the classically expected volume contraction. A dilatometric investigation of

volume changes during annealing of previously quenched polymer in the vicinity of T_g should clarify this point and possibly permit a separation of volume relaxation and volume changes due to bonding. These experiments would be particularly useful in combination with the ones suggested under suggestion 3 above.

For the purpose of assessing the influence of volume on mechanical properties the time dependent absolute volume must be known. Reported volume relaxation data usually give only the difference between the volumes at some time and that extrapolated for infinite time.

5. The experimentally found and theoretically explained reversible stress shift of flow rates in PMMA and PS should not be observable in pure shear, as Poisson's dilatation is here zero. It is suggested the yielding behavior be tested under pure shear and other stress fields to provide a basis for a more inclusive theory of stress effects.

6. An interesting radiation effect on creep rate of polymers has been found recently. When a polymer is subjected to irradiation with electrons, its creep rate increases by a large factor (see Ref. 72, which also gives additional references concerning the original observations of the effect). If the creep rate increase were due to structural changes, like those caused by heating above T_g and quenching, one would expect a remnant part of these changes after irradiation. And these should be reversible on annealing. It is suggested that this phenomenon be investigated by cold drawing experiments.

7. Deformation bands appear under many conditions of yielding in amorphous polymers. A theoretical study of the factors of test conditions and stress-strain-strain rate behavior which promote the concentration of shear strain in an isotropic continuum would be of interest in this context.

8. Finally, a combined theoretical and experimental study is proposed with a view towards investigating the parameters which account for birefringence of an initially optically isotropic polymer upon rapid quenching from above T_g.

APPENDIX A

ADIABATIC TEMPERATURE RISE IN DRAWING

In drawing under the constant load P the mechanical work $P \cdot \Delta L$ is absorbed when the sample is deformed by ΔL. If conformational energy and entropy changes may be disregarded, which is assumed, this work appears as an equivalent temperature rise. Therefore, one can write

$$P \cdot \Delta L = c \cdot L_o \cdot A \cdot \rho \cdot a \cdot \Delta T. \qquad (A\text{-}1)$$

With $\varepsilon = \Delta L / L_o$ and $\sigma = P/A$ this becomes

$$\Delta T = \frac{\varepsilon \cdot \sigma}{c \cdot \rho \cdot a} \qquad (A\text{-}2)$$

L_o = initial sample length; a = thermomechanical equivalent = $= 4.184 \times 10^7$ erg/cal; c = specific heat, $c_{PMMA} = 0.5$ cal/g°C; ρ = polymer density, $\rho_{PMMA} = 1.18$ g/cm³.

With the quantities given, it is

$$\Delta T = \frac{\varepsilon \cdot \sigma\,[\text{psi}]}{c\,[\text{cal/g°C}] \cdot \rho\,[\text{g/cm}^3]} \cdot 1.65 \times 10^{-3}\ [°\text{C}] \qquad (A\text{-}3)$$

The strain region, for which material properties were evaluated was below $\varepsilon = 0.2$; the highest drawing stress used was 6000 psi. The adiabatic temperature rise is therefore smaller than 3.2°C in any of the experiments of this work (Equ. [3]). Actually, the experimental conditions are far from adiabatic; between one and several hundred minutes are required to reach $\varepsilon = 0.2$. The real temperature increase is with certainty only a small fraction of the temperature rise calculated.

APPENDIX B

POLYMER SOURCES AND SPECIFICATIONS

Polystyrene

Supplier: Transplastic Corp., Cambridge, Mass.

Producer: Unknown

Form: Cast sheet, 1/16 in. thick

$\bar{M}_v$: 230,000

Polymethyl methacrylate

1. Plexiglas II UVA (lot 1 and 2)

Supplier: Forest Products, Inc.

Producer: Rohm and Haas Co., Bristol, Pennsylvania

Form: Cast sheet, 0.060 in. thick

$\bar{M}_v$: $> 10^6$

Additives: U V Stabilizer (amount unknown)

0.8% (per weight) of a substance volatile at 140°C, which is believed to be a plasticizer

2. Plexiglas P55

Supplier: Rohm and Haas Co., Bristol, Pennsylvania

Producer: Same

Form: Cast sheet, 0.080 in. thick

Additives: Chemically cross-linked

APPENDIX C

THE YIELD CRITERION FOR CONSTANT LOAD DRAWING

By forming the total differential of the equation of state, $F = F(v,L)$ (II-1), setting $dF = 0$ and dividing by dL, one obtains

$$\left(\frac{\partial F}{\partial L}\right)_v + \left(\frac{\partial F}{\partial v}\right)_L \left(\frac{\partial v}{\partial L}\right)_F = 0. \qquad \text{(C-1)}$$

The strain rate dependence of stress for polymers found by experiment to be

$$\left(\frac{\partial F}{\partial v}\right)_L > 0, \qquad \text{(C-2)}$$

fixes the sign of one of the terms.

The yield criteria for the constant velocity test are

$$\left(\frac{\partial F}{\partial L}\right)_v \leqq 0; \qquad \text{(C-3)}$$

and

$$\left(\frac{\partial^2 F}{\partial L^2}\right)_v < 0; \qquad \text{(C-4)}$$

Yielding in a constant load test requires therefore

$$\left(\frac{\partial v}{\partial L}\right)_F \geqq 0 \qquad \text{(II-3)}$$

and

$$\left(\frac{\partial^2 v}{\partial L^2}\right)_F > 0 \qquad \text{(C-5)}$$

Equation (II-3) is derived from Equation (C-1) and the conditions (2) and (3). Equation (5) follows from differentiation of (C-1) with respect to L and considering (2), (II-3), and (4).

APPENDIX D
FORMING OF ADDITIONAL NECKS AFTER DRAWING HAS STARTED.

The possibility of two or more necks forming in a tensile specimen is reduced as the shoulders of the first neck formed move along the specimen. Further necks form only if the stress is high enough for them to start before the initial neck has caused complete drawing.

1. Constant Strain Rate Test. A neck forms at the upper yield point. It is accompanied by a stress drop by $\Delta\sigma$ to a constant value, the draw stress. Under this lower stress the time for another neck to form (assumed to be equally influenced by stress as is delay time) is computed for a typical experimental condition for PMMA:

The most probable time for additional necks to appear is given by the stress dependence of t_d (Table II):

$$t_{d_2} = t_{d_1} \cdot 10^{-1.3\ 10^{-3}\ \Delta\sigma} \qquad \text{(D-1)}$$

From Allison's thesis[69] for drawing of PMMA at 80°C:

$v = 0.2$ in/min; $L_o = 1.0$ in; $R = 2.4$; $\sigma_y = 4600$ psi/
$\Delta\sigma = -1600$ psi

From this work for PMMA at 80°C (Fig. 1.12):

$$t_{d_1}(4600 \text{ psi}; 80°C) = 1 \text{ min.}$$

with these data [Equ. (D-1)]: $t_{d_2} = 120$ min.

The time for the shoulders to pass over the specimen is

$$t = \frac{L_o(R-1)}{v} = \frac{1 \times (2.4-1)}{0.2} = 14 \text{ min.}$$

In this example, which is representative for many conditions, a second neck would form after 120 minutes. There is no chance for this to happen as the original neck covers the specimen within 14 minutes.

An important simplification was made in neglecting the effect of the upper yield stress period on the yielding tendency of that polymer which did not neck. Transient load peaks reduce the time to yield the more the higher the stress, and the longer the duration.

2. Constant Load Test. As an example, a PMMA tensile specimen is assumed to vary along its gauge section by 2% in cross-sectional area and by 1°C in temperature. For a uniform specimen t_d = 62 min at 80°C and 3000 psi. If the variations are such as to increase t_d, the cross-section deviation will change t_d by +12 min, the temperature by +21.5 min (Fig. 1.12 or Table II). The shoulders of the neck, assuming it forms in the middle, travel over the 48 mm gauge section in $t = L_o(R-1)/v$ = 29 min. (v = 2.3 mm/min; Fig. 2.1). In each case, the sample would probably form a second neck, but it would not draw uniformly. If both variations occur combined and in the same sense, the delay time increase would be 39 minutes and another neck would not form. These numerical values illustrate the large variations in delay time and related parameters one must expect from small errors in stress and temperature.

APPENDIX E

HUMID ATMOSPHERES USED FOR CONDITIONING PMMA TENSILE SPECIMENS

In a confined space over saturated aqueous salt solutions, the partial pressure of water vapor is such as to result in the relative humidities listed below:

Salt	T, °C	% RH
Zinc chloride	20	10
Potassium acetate	20	20
Calcium chloride	20	32
Potassium carbonate	20	43
Calcium nitrate	20	55
Ammonium chloride	20	79.5
Potassium bromide	20	84

Source: Handbook of Chemistry and Physics, 39th Edition, p. 2317

0% RH and 100% RH were produced by phosphorous pentoxide and pure water respectively.

APPENDIX F

TEMPERATURE SHIFT OF RELAXATION TIMES CAUSED BY DILUENT

Suppose the viscosity is first changed by temperature from η_1 to η, than by diluent from η to η_2. The shift factors are $\eta_1/\eta = a_T$ and $\eta/\eta_2 = a_c$, for the total shift it is $a_T \cdot a_c = \frac{\eta_1}{\eta} \cdot \frac{\eta}{\eta_2}$. Provided the concentration change is chosen to annihilate the temperature effect, it is

$$a_T \cdot a_c = 1 \tag{D-1}$$

and

$$\log a_T + \log a_c = 0 \tag{D-2}$$

$$\log a_T = - \frac{[B/2.303\ f_g] \cdot (T - T_g)}{f_g/\alpha_F + T - T_g} \tag{D-3}$$

$$\log a_c = - \frac{[B/2.303\ f_2]\ (1 - c_2/\rho_2)}{f_2/f_1 + 1 - c_2/\rho_2} \tag{D-4}$$

[For Equations (3) and (4) see Ferry and Stratton, Ref. (44).] From Equations (2), (3), and (4),

$$- \frac{1/f_g\ (T - T_g)}{f_g/\alpha_F + T - T_g} - \frac{1/f_2\ (1 - c_2/\rho_2)}{f_2/f_1 + 1 - c_2/\rho_2} = 0 \tag{D-5}$$

f_g = fractional free volume of polymer at T_g

f = fractional free volume of pure species

α_F = difference of thermal expansion coefficient of liquid and glass

c = concentration g/cm^3 solution

ρ = density

1,2 = index for diluent and polymer respectively

x = weight fraction of diluent

With $1 - c_2/\rho_2 = c_1/\rho_2 \simeq x$ and for $f_2 \simeq f_g$, that is restricting the application to the vicinity of T_g, one gets from Equ. (5)

$$T - T_g = - \frac{x \cdot f_1/\alpha F}{1 + 2\ x\ f_1/f_g} \tag{D-6}$$

and for small x

$$T - T_g = \Delta T = - x \cdot f_1/\alpha_F. \qquad \text{(IV-1)}$$

APPENDIX G

DETERMINATION OF CRAZE VOLUME

A test line of length l is laid over a crazed surface normal to the crazes. It intersects n_i crazes and passes therefore, when moved by Δx perpendicular to itself, over the total length $n_i \Delta x$ of crazes, sweeping out the area $l \cdot \Delta x$. The length of crazes per unit area is therefore $L = n_i/l$. Including both sides of a polymer sheet of area A the craze volume is $V_{cr} = L \cdot A \cdot h \cdot d \cdot 2$. (h = height of craze; d = depth of craze.)

The volume fraction of crazed polymer is

$$\frac{V_{cr}}{V} = \frac{L \cdot h \cdot d \cdot 2}{t}$$

(t = thickness of sheet.)

The depth of one craze is assumed to be one-half of its visible length. This assumption is suggested by observations made on fracture surfaces, in cases where a craze caused the fracture. The original craze is found to form a semicircular region (as shown in Fig. 7.32). From the number of crazes per unit area N, the average length of one craze is $\bar{l} = L/N$. Including also that the crazes are approximately 50% filled with craze matter[70], the fractional empty space associated with crazes is

$$\frac{v}{V} = \frac{L^2}{N} \cdot \frac{h}{2t} \qquad \text{(G-1)}$$

The height of crazes has been measured from electron micrographs. There are individual differences; no attempt has been made to measure the height change with strain of the surrounding matrix. The crazes observed were from partly drawn regions. With this limitation $h \approx 2 \times 10^{-4}$ mm.

BIBLIOGRAPHY

1. C. W. Bunn and T. C. Alcock, The Texture of Polythene, Trans. Faraday Soc. 41, 317 (1945)

2. E. A. W. Hoff, Some Mechanical Properties of Commercial Polymethyl Methacrylate. J. Appl. Chem. 2, 441 (1952)

3. K. Jäckel, Ein Beitrag zur Kaltverstreckung der Hochpolymeren, Kolloid-Z. 137, 130 (1954)

4. I. Marshall and A. B. Thompson, The Cold Drawing of High Polymers, Proc. Roy. Soc. A221, 541 (1954)

5. P. I. Vincent, The Necking and Cold-Drawing of Rigid Plastics. Polymer 1, 7 (1960)

6. F. H. Müller and C. Engelter, Zur Spannungsabhängigkeit des Fliessens Polymerer. Kolloid-Z. u. Zschr. f. Pol. 184, 36 (1962)

7. M. Goldstein, A Model for Cold Flow in Amorphous Polymers. J. Pol. Sci. B 4, 87 (1966)

8. R. D. Andrews, Jr., S. W. Allison, D. H. Ender, R. M. Kimmel and W. Whitney, Final Summary Report on "Research Study on Cold Drawing Phenomena in High Polymers", Fibers and Polymers Div., Mechanical Engineering Department., M.I.T., DSR No. 5043

9. C. Crowet and G. A. Homès, Interpretation of the Load-Elongation Curve of Polymethyl Methacrylate. Appl. Mat. Res. 3, 1 (1964)

10. W. Whitney, Yielding Behavior of Glassy Amorphous Polymers, Sc.D. Thesis, Dept. of Civil Engineering, M.I.T., November (1964)

11. J. W. Kauffman and W. George, Delayed Plastic Flowing in Certain Polyamid Films. J. Colloid Sc. 6, 450 (1951)

12. M. F. Bender and M. L. Williams, Extension of Unoriented Nylon 66 Filaments. J. Appl. Phys. 34, 3329 (1963)

13. R. J. Curran and R. D. Andrews, Dead-Load Creep Rupture of Poly (Methyl Methacrylate), Dept. of Civil Engineering,

M.I.T., DSR No. 9545

14. D. W. Morrison, Cold-Drawing of Oriented Polystyrene in Constant Load Creep. S.B. Thesis, Dept. of Metallurgy, M.I.T. (May 1964)

15. W. Whitney, Observation of Deformation Bands in Amorphous Polymers. J. Appl. Phys. 34, 3633 (1963)

16. R. D. Andrews, A. S. Argon, J. A. Godrick and W. Whitney, Plastic Deformation Bands in Amorphous Atactic Polystyrene. To be submitted to Phil. Mag.

17. L. E. Nielsen and R. Buchdahl, Mechanical Properties of Oriented Polystyrene Film. J. Appl. Phys 21, 488 (1950)

18. R. E. Robertson, The Natural Draw Ratio and the Shape of the Neck in the Cold-Drawing of Polymers. General Electric Research Laboratory, Rep. No. 64-RL-3794C (October 1964)

19. D. H. Ender and R. D. Andrews, Cold Drawing of Glassy Polystyrene under Dead Load. J. Appl. Phys. 36, 3057 (1965)

20. J. Brandup and E. H. Immergut (Editors), Polymer Handbook Interscience Publishers 1966

21. J. A. Roetling, Yield Stress Behaviour of Polymethyl Methacrylate Polymer 6, 311 (1965)

22. O. D. Sherby and J. E. Dorn, Anelastic Creep of Polymethyl Methacrylate. J. of the Mech. and Phys. of Solids 6, 145 (1958)

23. F. H. Müller, Cold Stretching of Plastics (in German) Materialprüfung 5, 336 (1963)

24. D. S. Clark and D. S. Wood, The Time Delay for the Initiation of Plastic Deformation at Rapidly Applied Constant Street. ASTM Proc. 49, 717 (1949)

25. G. T. Hahn, A Model for Yielding with Special Reference to the Yield-Point Phenomena of Iron and Related BCC Metals. Acta Metallurgica 10, 727 (1962)

26. e.g. A. Nadai, Theory of Flow and Fracture of Solids. McGraw-Hill, New York, 1950, p. 71

27. J. R. McLoughlin and A. V. Tobolsky, Effect of Rate of Cooling on Stress Relaxation of Polymethyl Methacrylate. J. Pol. Sci. 7, 658 (1951)

28. K. H. Illers and E. Jenckel, Der Einfluss der Thermischen und Mechanischen Vorgeschichte auf innere Dämpfung von Polystyrol. Kolloid-Z. 165, 73 (1959)

29. T. G. Fox, Jr. and P. J. Flory, Second-Order Transition Temperatures and Related Properties of Polystyrene. I Influence of Molecular Weight. J. Appl. Phys. 21, 581 (1950)

30. M. L. Williams, R. F. Landel and J. D. Ferry, The Temperature Dependence of Relaxation Mechanisms in Amorphous Polymers and other Glass Forming Liquids. J. Am. Chem. Soc. 77, 3701 (1955)

31. J. H. Gibbs and E. A. DiMarzio, Nature of the Glass Transition and the Glassy State. J. Chem. Phys. 28, 373 (1958)

32. E. A. DiMarzio and J. H. Gibbs, Chain Stiffness and the Lattice Theory of Polymer Phases. J. Chem. Phys. 28, 807 (1958)

33. J. D. Ferry, Viscoelastic Properties of Polymers (Wiley 1961) a (p. 218); b (p. 226); c (p. 221-225)

34. S. B. Ainbinder, M. G. Laka and I. Yu Maiors, Effect of Hydrostatic Pressure on Mechanical Properties of Plastics. Polymer Mech. 1, 50 (1965)

35. A. J. Kovacs, R. A. Stratton and J. D. Ferry, Dynamic Mechanical Properties of Polyvinyl Acetate in Shear in the Glass Transition Temperature Range. J. Phys. Chem. 67, 152 (1963)

36. A. J. Kovacs, Transition Vitreuse dans le Polymères Amorphes. Etude Phenomenologique. Fortschr. Hochpol. Forschg. 3, 394 (1963)

37. P. J. Schneider, Conduction Heat Transfer, Addison Wesley, (1957)

38. E. V. Angerer, Technische Kunstgriffe bei Physikalischen

Untersuchungen. Friedrich Vieweg and Sons, Braunschweig.

39. T. Alprey, G. Goldfinger and H. Mark, The Apparent Second-Order Transition Point of Polystyrene. J. Appl. Phys. 14, 700 (1943).

40. A. Kovacs, La Contraction Isotherme du Volume des Polymères Amorphes. J. Pol. Sci. 30, 131 (1958).

41. T. A. Litovitz, Liquid Relaxation Phenomena and the Glassy State. Non-Crystalline Solids, (Wiley 1960) p. 252.

42. J. R. McLoughlin and A. V. Tobolsky, The Viscoelastic Behavior of Polymethyl Methacrylate. J. Coll. Sci. 7, 555 (1952).

43. H. Fujita and A. Kishimoto, Diffusion Controlled Stress Relaxation in Polymers, II. Stress Relaxation in Swollen Polymers. J. Pol. Sci. 28, 547 (1958).

44. J. D. Ferry and R. A. Stratton, The Free Volume Interpretation of the Dependence of Viscosities and Viscoelastic Relaxation Times on Concentration, Pressure, and Tensile Strain. Kolloid-Z. 171, 107 (1960).

45. M. F. Milagin and N. I. Shishkin, Breaking Strength and Double Refraction of Stretched (Oriented) Polymethyl Methacrylate, Sov. Phys.-Solid St. 4, 1973 (1963).

46. N. I. Shishkin and M. F. Milagin, Double Refraction of Light and Stretching of Polymethyl Methacrylate, Sov. Phys.-Solid St. 4, 1967 (1963).

47. D. Prevorsek and A. V. Tobolsky, Determination of Non-Flow Shrinkage Ratio in Oriented Fibers, Text. Res. J. 33, 795 (1963).

48. R. G. Cheatham and A. G. H. Dietz, Effect of Orientation on the Mechanical Properties of Polystyrene, Trans. ASME 74, 31 (1952).

49. T. J. Hammack, Optical-Mechanical Studies of Molecular Orientation in Polymers, Sc.D. Thesis, Department of Civil Engineering, M.I.T., (July 1966).

50. H. Eyring, Viscosity, Plasticity, and Diffusion as Examples of Absolute Reaction Rates, J. Chem. Phys. 4, 283 (1936).

51. W. Holzmüller, Die Deutung von Fliesserscheinungen durch moleculare Platzwechsel, Kolloid-Z. .Z.f. Pol 203, 8 (1965).

52. A. K. Doolittle and D. B. Doolittle, Studies in Newtonian Flow. V. Further Verification of the Free-Space Viscosity Equation, J. Appl. Phys. 28, 901 (1957).

53. P. B. Macedo and T. A. Litovitz, On the Relative Roles of Free Volume and Activation Energy in the Viscosity of Liquids, J. of Chem. Phys. 42, 245 (1965).

54. R. E. Robertson, Theory of the Plasticity of Glassy Polymers, J. of Chem. Phys. 44, 3950 (1966).

55. A. J. Kovacs, Bulk Creep and Recovery in Systems with Viscosity Dependent upon Free Volume, Trans. Soc. Rheol. 5, 285 (1961).

56. S. Rosenbaum, Polyacrylonitrile Fiber Behavior. II. Dependence on Structure and Environment, J. of Appl. Pol. Sci. 9, 2085 (1965).

57. L. E. Nielsen, Stress Dependence of Poisson's Ratio and the Softening Temperature of Plastics, Trans. Soc. Rheol. 9, 243 (1965).

58. L. E. Nielsen, Mechanical Properties of Polymers, Reinhold Publishing Corporation, 2nd Print, 1963, p. 7.

59. K. H. Hellwege, W. Knappe and P. Lehmann, Die isotherme Kompressibilität einiger amorpher und teilkristalliner Hochpolymerer im Temperaturbereich von 20 - 250°C und bei Drucken bis zu 2000 kp/cm^2, Kolloid-Z.u.Z.F., Pol.183, 110 (1962)

60. A. Zosel, Der Schubmodul von Hochpolymeren als Funktion von Druck and Temperature, Kolloid-Z. u. Z. f. Pol. 199, 113 (1964).

61. D. Heydemann, Dielectric Relaxation of PMMA as Function of Pressure, Temperature, and Frequency, Kolloid-Z. u. Z. f. Pol. 195, 122 (1964).

62. A. V. Tobolsky and J. R. McLoughlin, Elastoviscous Properties of Polyisobutylene. V. The Transition Region, J. Pol. Sci. 8, 543 (1952).

63. F. Rueche, Viscoelasticity of Poly Methacrylates, J. Appl. Phys. 26, 738 (1955).

64. K. Richard and E. Graube, Die Kaltverstreckung bei Niederdruckpolyäthylen, Kunststoffe 46, 262 (1956).

65. O. K. Spurr, Jr. and W. D. Niegisch, Stress Crazing of Some Amorphous Thermoplastics, J. of Appl. Pol. Sci. 6, 585 (1962).

66. S. B. Newman, Microscopical Studies of Failure in Polymers, Symposium on Microscopy, ASTM Spec. Tech. Publ., No. 257, p. 132.

67. H. T. Jessop, On the Tardy and Sénarmont methods of measuring fractional relative retardations, Brit. J. of Appl. Phys. 4, 138 (1953).

68. W. L. Grube and S. R. Rouze, Pre-Shadowed Replicas for Electron Metallography, ASTM Proceedings 52, 573 (1952).

69. S. W. Allison, The Necking and Drawing of Amorphous Polymers, M.S. Thesis, Department of Civil Engineering, M.I.T. (1964).

70. R. P. Kambour, Refractive Indices and Composition of Crazes in Several Glassy Polymers, J. Pol. Sci. A 2, 4159 (1964).

71. P. Heydemann and H. D. Guicking, Specific Volume of Polymers as a Function of Temperature and Pressure, Kolloid-Z.u.Z.f.Pol. 193, 16 (1963).

72. J. P. Bell, Temporary Increase in the Creep Rate of Polymers During Irradiation, Sc.D. Thesis, Department of Chemical Engineering, M.I.T. (January 1966).

ACKNOWLEDGEMENTS

Professor R. D. Andrews has offered to me the opportunity for the work presented as part of a more encompassing study of cold-drawing of polymers. I am indebted to him also for his advice and for his continued interest after he left M.I.T.

I sincerely appreciate Professor S. Backer's willingness to assume the supervision of this report after Professor Andrews' departure, and his active support in the final stages. I would also like to thank Professor A. S. Argon and Professor A. S. Hoffman for the opportunities to discuss this work on several occasions.

During the preparation of the final report I benefitted from many discussions with Professor I. V. Yannas, which I gratefully acknowledge.

On casual and frequent occasions throughout this work I have had profitable exchanges of ideas on the report subject with other students in the Fibers and Polymers Division, in particular, Ted J. Hammack and Robert M. Kimmel.

Thanks are also due to Professor Breedis, who brought to my attention the replication method for polymer surfaces and helped to put it into practice. Dr. Gwen Stewart of Boston University microtomed PMMA samples for me and has provided much help in the search for internal shear bands in PMMA by electron microscopy. Though this search remained futile, her help is very much appreciated.

The final document has been typed by Miss Dorothy Eastman. She has taken on this task in spite of her many other duties and brought it to an end with admirable efficiency. I am very grateful to her.

The work on this project has been fully supported by the U. S. Army Natick Laboratories, under M.I.T. DSR Nos. 5043 and 76289. This support is greatly appreciated.

Abstract

13. (cont)

incremental stress changes. The influence of stress on strain rate is reversible. The stress shift factor is predicted correctly from a free volume theory assuming that Poisson's expansion caused by drawing stress changes contributes entirely to the free volume.

The important contribution to the increase in strain rate under constant load is caused by a true strain softening. The conclusion is drawn that it is a consequence of the disturbance of the annealed positions of the polymer segments. In this picture strain causes the breaking up of the relative order that is brought about in annealing; thus leaving the polymer in a far-from-equilibrium state.

Unclassified

Security Classification

DOCUMENT CONTROL DATA - R&D

(Security classification of title, body of abstract and indexing annotation must be entered when the overall report is classified)

1. ORIGINATING ACTIVITY (Corporate author) Massachusetts Institute of Technology Department of Mechanical Engineering Cambridge, Massachusetts 02139	2a. REPORT SECURITY CLASSIFICATION Unclassified 2b. GROUP

3. REPORT TITLE

STUDY OF YIELDING PHENOMENA

4. DESCRIPTIVE NOTES (Type of report and inclusive dates)

Final Report February 1966 - April 1967

5. AUTHOR(S) (Last name, first name, initial)

Ender, D. H.

6. REPORT DATE	7a. TOTAL NO. OF PAGES	7b. NO. OF REFS
July 1967	226	72

8a. CONTRACT OR GRANT NO. DA19-129-AMC-930(N) b. PROJECT NO. 1C024401A329 c. d.	9a. ORIGINATOR'S REPORT NUMBER(S) 9b. OTHER REPORT NO(S) (Any other numbers that may be assigned this report) 68-7-CM C&CM-36

10 AVAILABILITY/LIMITATION NOTICES

Distribution of this document is unlimited. Release to CFSTI is authorized.

11. SUPPLEMENTARY NOTES	12. SPONSORING MILITARY ACTIVITY
	U. S. Army Natick Laboratories Natick, Massachusetts 01760

13 ABSTRACT

In yielding under constant tensile load, glassy polymethyl methacrylate (PMMA) and glassy polystyrene (PS) exhibit work softening at small strains, followed by strain hardening at higher strains. In this work the initial softening has been of most interest. In the constant load experiment, the yield point shows up as a minimum of the deformation velocity vs elongation curve.

Measurements have been made of the variation of delay time (the time for accelerated elongation to occur under load) with stress and temperature (measured on PS and PMMA) with preorientation birefringence (PS), and with thermal history and water absorption (PMMA). The logarithm of the delay time decreases linearly with increasing stress and temperature. The temperature interval systematically investigated is $T_g - 40 \leq T \leq T - 5(^{\circ}C)$. Several experiments with PMMA were made for $T > T_g$. The polymer response to constant load divides the temperature-stress plane into two regions; one where creep is observed and another in which cold drawing takes place. Specimens deforming by creep do not contain deformation bands.

The stress influence on strain rate under constant load is expressible as a stress shift factor. The same stress shift factor governs the stress influence on delay time and deformation rate changes associated with

DD FORM 1 JAN 64 1473

Unclassified

Security Classification

Unclassified

Security Classification

14. KEY WORDS	LINK A		LINK B		LINK C	
	ROLE	WT	ROLE	WT	ROLE	WT
Yield strength	8					
Stress-strain measurements	8					
Tensile properties	8					
Birefringence	8					
Polystyrene	8,9		6,7			
Polymethyl methacrylate	8,9		6,7			
Loading (mechanics)			6			
Strains			6			
Temperature			6			
Equilibrium			7			
Cold drawing			7			
Necking			7			
Delay time			7			

INSTRUCTIONS

1. ORIGINATING ACTIVITY: Enter the name and address of the contractor, subcontractor, grantee, Department of Defense activity or other organization *(corporate author)* issuing the report.

2a. REPORT SECURITY CLASSIFICATION: Enter the overall security classification of the report. Indicate whether "Restricted Data" is included. Marking is to be in accordance with appropriate security regulations.

2b. GROUP: Automatic downgrading is specified in DoD Directive 5200.10 and Armed Forces Industrial Manual. Enter the group number. Also, when applicable, show that optional markings have been used for Group 3 and Group 4 as authorized.

3. REPORT TITLE: Enter the complete report title in all capital letters. Titles in all cases should be unclassified. If a meaningful title cannot be selected without classification, show title classification in all capitals in parenthesis immediately following the title.

4. DESCRIPTIVE NOTES: If appropriate, enter the type of report, e.g., interim, progress, summary, annual, or final. Give the inclusive dates when a specific reporting period is covered.

5. AUTHOR(S): Enter the name(s) of author(s) as shown on or in the report. Enter last name, first name, middle initial. If military, show rank and branch of service. The name of the principal author is an absolute minimum requirement.

6. REPORT DATE: Enter the date of the report as day, month, year; or month, year. If more than one date appears on the report, use date of publication.

7a. TOTAL NUMBER OF PAGES: The total page count should follow normal pagination procedures, i.e., enter the number of pages containing information.

7b. NUMBER OF REFERENCES: Enter the total number of references cited in the report.

8a. CONTRACT OR GRANT NUMBER: If appropriate, enter the applicable number of the contract or grant under which the report was written.

8b, 8c, & 8d. PROJECT NUMBER: Enter the appropriate military department identification, such as project number, subproject number, system numbers, task number, etc.

9a. ORIGINATOR'S REPORT NUMBER(S): Enter the official report number by which the document will be identified and controlled by the originating activity. This number must be unique to this report.

9b. OTHER REPORT NUMBER(S): If the report has been assigned any other report numbers *(either by the originator or by the sponsor)*, also enter this number(s).

10. AVAILABILITY/LIMITATION NOTICES: Enter any limitations on further dissemination of the report, other than those imposed by security classification, using standard statements such as:

(1) "Qualified requesters may obtain copies of this report from DDC."

(2) "Foreign announcement and dissemination of this report by DDC is not authorized."

(3) "U. S. Government agencies may obtain copies of this report directly from DDC. Other qualified DDC users shall request through _____."

(4) "U. S. military agencies may obtain copies of this report directly from DDC. Other qualified users shall request through _____."

(5) "All distribution of this report is controlled. Qualified DDC users shall request through _____."

If the report has been furnished to the Office of Technical Services, Department of Commerce, for sale to the public, indicate this fact and enter the price, if known.

11. SUPPLEMENTARY NOTES: Use for additional explanatory notes.

12. SPONSORING MILITARY ACTIVITY: Enter the name of the departmental project office or laboratory sponsoring *(paying for)* the research and development. Include address.

13. ABSTRACT: Enter an abstract giving a brief and factual summary of the document indicative of the report, even though it may also appear elsewhere in the body of the technical report. If additional space is required, a continuation sheet shall be attached.

It is highly desirable that the abstract of classified reports be unclassified. Each paragraph of the abstract shall end with an indication of the military security classification of the information in the paragraph, represented as *(TS)*, *(S)*, *(C)*, or *(U)*.

There is no limitation on the length of the abstract. However, the suggested length is from 150 to 225 words.

14. KEY WORDS: Key words are technically meaningful terms or short phrases that characterize a report and may be used as index entries for cataloging the report. Key words must be selected so that no security classification is required. Identifiers, such as equipment model designation, trade name, military project code name, geographic location, may be used as key words but will be followed by an indication of technical context. The assignment of links, rules, and weights is optional.

Unclassified

Security Classification